DOCTOR OF PHILOSOPHY

The antimicrobial action of pseudin-2

Husam Hebaishi

2013

Aston University

The antimicrobial action of pseudin-2

Husam Radhi Merza Khalil Hebaishi

Doctor of Philosophy

Aston University

August 2013

Aston University

The antimicrobial action of pseudin-2

Husam Radhi Merza Khalil Hebaishi

Doctor of Philosophy

2013

Thesis summary

The amphibian antimicrobial peptide pseudin-2 is a peptide derived from the skin of the South-American frog *Pseudis paradoxa* (Olson *et al.,* 2001). This peptide possesses tremendous potential as a therapeutic lead since it has been shown to possess both antimicrobial as well insulin-releasing properties (Olson *et al.,* 2001; Abdel-Wahab *et al.,* 2008). This study aimed to develop pseudin-2's potential by understanding and improving its properties as an antimicrobial agent. The structure-function relationships of pseudin-2 were explored using a combination of *in-vitro* and *in-silico* techniques, with an aim to predict how the structure of the peptide may be altered in order to improve its efficacy.

A library of pseudin-2 mutants was generated by randomizing codons at positions 10, 14 and 18 of a synthetic gene, using NNK saturation mutagenesis. Analysis of these novel peptides broadly confirmed, in line with literature precedent, that anti-microbial activity increases with increased positive charge. Specifically, 2 positively-charged residues at positions 10 and 14 and a hydrophobic at position 18 are preferred. However, substitution at position 14 with some polar, non-charged residues also created peptides with antimicrobial activity. Interestingly, the pseudin-2 analogue [10-E, 14-Q, 18-L] which is identical to pseudin-2, except that the residues at positions 10 and 14 are switched, showed no anti-microbial activity at all.

Molecular dynamics simulations of pseudin-2 showed that the peptide possesses two equilibrium structures in a membrane environment: a linear and a kinked α-helix which both embed into the membrane at an angle. Biophysical characterization using circular dichroism spectroscopy confirmed that the peptide is helical within the membrane environment whilst linear dichroism established that the peptide has no defined orientation within the membrane. Collectively, these data indicate that Pseudin-2 exerts its antimicrobial activity via the carpet model.

Keywords: amphibian, peptide, frog

Acknowledgements

Firstly, I would like to thank my supervisor, Dr. Anna Hine, whose support has been instrumental to the successful completion of this project. I would also like to thank my associate supervisors Prof. Cliff Bailey and Dr. Sotos Generalis for their help and support throughout the project.

I would like to thank Dr. Behfar Mogaddam and Prof. Yvonne Perrie for their generous donation of liposomes, Mr. Karan Rana for assistance with the haemolysis testing and Dr. Raul Pacheco Gómez for access to their circular and linear dichroism facilities at the University of Birmingham. Finally, I would like to thank Mr. Alex Brulo for help with building and running CHARMM and NAMD, the two molecular dynamics software packages used in this project. I would also like to thank Ben Stone for his extremely helpful feedback on the molecular dynamics work.

Finally, I would like to thank my parents, my brother, and my lovely partner Anne for everything they've done to help me complete this project. I could not have accomplished this without them.

List of Contents

List of tables

List of Figures

Abbreviations

CHARMM	Chemistry at Harvard Molecular Mechanics
GBSW	Generalised Born with a Switching function
LPS	Lipopolysaccharide
MBP	Maltose Binding Protein
NAMD	Not Just Another Molecular Dynamics program
SUMO	Small Ubiquitin-like Modifier
GST	Glutathione S-transferase
TRX	Thioredoxin

1 Introduction

The amphibian antimicrobial peptide pseudin-2 is a peptide derived from the skin of the South-American frog *Pseudis paradoxa* (Olson *et al.,* 2001). This peptide possesses tremendous potential as a therapeutic lead since it has been shown to possess both antimicrobial as well insulin-releasing properties (Olson *et al.,* 2001; Abdel-Wahab *et al.,* 2008). The main aim of this study is to develop this peptide's potential by understanding and improving its properties as an antimicrobial agent. The structure-function relationships of pseudin-2 have been explored using a combination of *in-vitro* and *in-silico* techniques, with an aim to predict how the structure of the peptide may be altered in order to improve its efficacy.

The last decade has seen an increase in research into antimicrobial peptides derived from frog skin. This trend may be attributed to the increase in the number of pathogenic strains becoming resistant to traditional antibiotics. It can also be argued that the use of these novel antimicrobial agents also gives us the potential to learn valuable lessons from nature. It shows us how these amphibians have managed to effectively protect themselves despite living in environments where these pathogens thrive. This research trend is illustrated below.

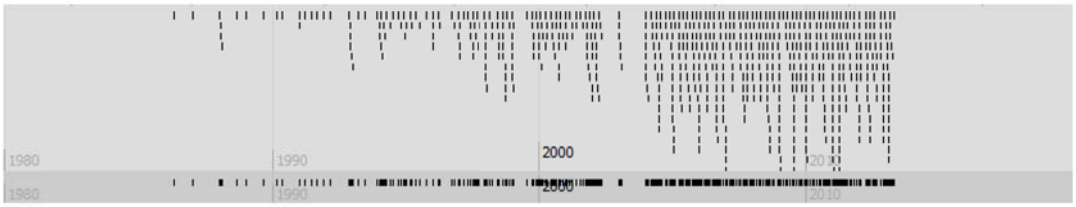

Figure 1.1 A timeline showing the number of research papers on amphibian peptides with interesting biological properties. Each black vertical line in the image is a single published paper.

Figure 1.1 above clearly illustrates the increase in awareness within the worldwide research community of the potential that lies within the study of these molecules. These peptides may not only be developed into novel therapeutics, but can also be used to gain insights into the processes that they mediate.

Since these peptides are large in number, a description of these molecules must incorporate a method of categorisation. The method used herein separates the peptides into families depending on the frog from which these peptides were first isolated, starting with the main focus of this project, pseudin-2. The naturally-occurring members of each family of peptides are listed and briefly described and the structure-function features of each family are discussed in detail. It is important to note since this project focuses on the antimicrobial properties of pseudin-2, other biological features of amphibian peptides other than antimicrobial properties have been omitted.

Prior to describing the available data on amphibian antimicrobial peptides, however, it is important to discuss the clinical need for peptide therapeutics. Since pseudin-2 has been shown to be both an antimicrobial (Olson *et al.*, 2001) as well as an insulin-releasing molecule (Abdel-Wahab, Power & Ng, 2008), the clinical importance of both these biological properties will be elaborated on. Finally, the challenges that may be anticipated in the development of a peptide into a viable therapeutic are also described. This is discussed in further detail in the following section.

1.1 Peptide antimicrobials: clinical need and challenges

There is a large number of pathogens that are resistant to traditional antibiotics,: the antibiotic resistance genes database lists 1737 organisms with antibiotic resistance genes (Liu & Pop, 2009). This problem may be attributed to both misuse of traditional antibiotics, as well as the mechanism of action of these molecules. The improper use of traditional antibiotics increases the exposure of pathogenic strains to these molecules, and this hastens the evolution of resistant strains from susceptible ones. On the other hand, the mechanism of action of traditional antibiotics also impacts the ease with which a pathogen may develop resistance. For example, an antibiotic that elicits its action by interaction with a specific intracellular/extracellular component may be rendered ineffective when that component is altered, as in the case of DNA mutation.

The development of peptide antimicrobials would address the issue of resistance, particularly in the case of amphibian peptides. The majority of antimicrobial peptides have been shown to elicit their antimicrobial action by interacting with liposomes, as in the case of maculatin 1.1 (Chia *et al.*, 2002), gramicidin (Hicks *et al.*, 2009), magainin-2 (Tamba & Yamazaki, 2009) and temporin L (Mangoni *et al.*, 2004). Since the majority of amphibian antimicrobial peptides are cationic (Wang *et al.*, 2009) while biological membranes (both bacterial (Dickson & Koohmaraie, 1989) as well as eukaryotic (Dodge & Phillips, 1967)) are negatively charged, it follows that electrostatics are the driving factor for these interactions. In order to better understand the utility of antimicrobial peptides, it is necessary to describe the selectivity of these peptides, particularly with regards to differences in membrane structure of these pathogens, since it is these biological membranes that the peptides directly interact with.

Microbial pathogens may be broadly classified into three categories: gram-positive bacteria, gram-negative bacteria and fungi. These three classes of pathogens differ considerably in membrane structure. Gram-positive bacteria such as *E. coli* possess an outer peptidoglycan mesh and an inner plasma membrane, which are separated by a periplasmic space. In order for a peptide to be active against a gram-negative pathogen, the peptide needs to be able to get through the outer peptidoglycan in order to disrupt the underlying plasma membrane.

On the other hand, gram-negative bacteria possess an outer layer of lipopolysaccharide, a middle layer of peptidoglycan, and finally an innermost plasma membrane, with periplasmic space in between adjacent layers. In this case, the cell effectively possesses two lipid membranes, the outer lipopolysaccharide layer and the inner plasma membrane, and the peptide must effectively disrupt both layers in order to exhibit toxicity.

In the final category are fungal pathogens, organisms which are very different from bacteria since they are eukaryotic organisms and are very similar in biology to mammalian cells and significantly different from that of the prokaryotic pathogens discussed above. However, these cells also differ

from mammalian cells since they possess an outer cell wall. This cell wall would act as a barrier to toxic molecules such as peptides. The development of an antifungal carries with it the additional challenge of the specificity required to develop an antifungal agent. Such a molecule would need to be highly specific, and specifically target fungal pathogens whilst not showing toxicity towards mammalian cells. The three different membrane structures discussed here are illustrated in Figure 1.1.1 below.

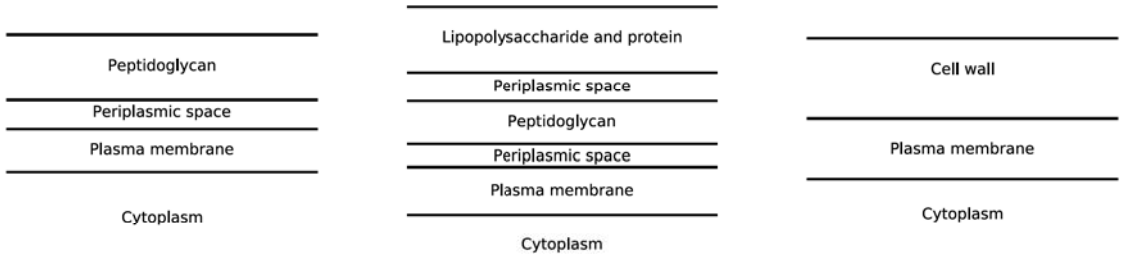

Figure 1.1.1 Illustration showing membrane structure of (a) Gram positive bacteria, (b) Gram negative bacteria and (c) fungi

The final challenge in the development of a peptide therapeutic would be the choice of delivery method to be used. Since the mammalian digestive system is very efficient in the enzymatic breakdown of protein molecules, oral delivery would not be a viable option. Parenteral delivery may be considered, but the half-life of the peptide in plasma must be estimated, particularly relative to the peptide's toxicity. The molecule would need to effectively inhibit the growth of the pathogen in question before its enzymatic breakdown occurred. Strategies such as substitution residues susceptible to proteolytic degradation (Marx *et al.*, 2004), modifications of the N-terminus (Green *et al.*, 2004), and incorporation of a poly(ethyleneglycol) polymer at the termini (Lee *et al.*, 2003) may be employed to increase the plasma half-life of the molecule. It is, however, important, to determine the effects of these modifications on the toxicity of the peptide in question.

There are a large number of peptides with known antimicrobial peptides that possess potential for development into therapeutics as described above. The history of antimicrobial peptides, their modes of action and their structure-function relationships are discussed in the sections that follow.

1.2 History of antimicrobial peptides

The first antimicrobial peptides to be discovered were temporins and magainins, both in the early 1980s. This was rapidly followed by the discovery of a number of peptides from a variety of amphibians worldwide.

Initially, the isolation of antimicrobial peptides was only accompanied by the characterization of the primary structure of the peptides along with preliminary antimicrobial testing. Testing of these peptides for haemolytic activity subsequently became more common, but does not completely cover the spectrum of peptides derived from frog skin. To date, amphibian peptides have been shown to possess antiviral (Belaid *et al.*, 2002), anticancer (Baker *et al.*, 1993) as well as myotropic properties (Meng *et al.*, 2012). A number of amphibian peptides have also been shown to possess the ability to stimulate the release of insulin (Ojo *et al.*, 2011; Kim *et al.*, 2010).

Interestingly, thus, there is significant variation in the availability of published data between the peptide families in relation to the range of properties associated with different families of peptides. This observation may be explained as being due to both historical reasons as well as prevalence. For example, the magainin family of peptides was among the first amphibian antimicrobial peptide family to be discovered, whilst peptides belonging to the brevinin and temporin families may be described as being 'ubiquitous' since they have been isolated from a large number of frog species following their initial discovery. In each of these three families, a large amount data is available on their structural and functional properties. In contrast, more recently discovered peptide families such as the pseudin family, the amount of structural and functional data available is sparse.

1.3 Properties and analysis of known antimicrobial peptides

The antimicrobial database (Wang *et al.,* 2009b) contains a comprehensive list of all peptides with known activities against microbes and includes 2233 individual entries to date. As such, it is a key resource for the broad classification of peptides from natural sources.

Antimicrobial peptides can be described using a number of features including structure, overall charge, percentage hydrophobicity, biological function, biological source and biosynthetic origin. The following paragraphs address the key properties of such peptides: namely secondary structure, hydrophobicity, overall charge and their spectra of activity. Since this body of work focuses on amphibian peptides, each classification system will include a comparison of trends and features of all peptides within the database compared to those of just the amphibian peptides, which comprise a large proportion (16.6% - 372 entries) of all antimuicrobial peptides within the database.

1.3.1 Secondary structure

Antimicrobial peptides with known structures may be classified into one of the following four categories: alpha helical, beta sheet, alpha-beta, non-alpha-beta. The representative peptides for each of these are: magainin-2 (alpha-helix), lactoferrin B (beta sheet), plant defensin Psd1 (combined alpha-beta structure) and bovine indolicidin (non alpha-beta) (Figure 1.3.1.1).

(a)

(b)

(c)

(d)

Figure 1.3.1.1 3D NMR structures of representative antimicrobial peptides: (a) magainin-2 (Gesell *et al.,* 1997), (b) lactoferrin (Hwang *et al.,* 1998) (b) Pisum sativum defensin (Almeida *et al.,* 2002) and (d) bovine indolicidin (Rozek *et al.,* 2000). Images were taken from the Protein Data Bank (Bernstein *et al.,*1977).

However, the above classification only encompasses peptides for which structural data is available. The majority of peptides in the antimicrobial peptide database do not have any structural data associated with them. The distribution of different types of structures for amphibian peptides as well as all peptides within the database is given in Figure 1.3.1.2 below.

Figure 1.3.1.2 Frequency of different structural types for all peptides and amphibian peptides in the antimicrobial peptide database (Wang *et al.,* 2009a).

The above statistics may be explained based on the length of the peptides in question. The average length of all peptides in the database is ~ 33 residues, which suggests that the majority of listed peptides are short. The presence of a beta-sheet structure creates strain within the molecule, which would be more pronounced in smaller molecules. It is, therefore, energetically unfavourable for a short peptide to adopt a beta-sheet structure, which is evident in the statistics presented. The percentage of peptides with a beta-sheet structure is, therefore small, reflective of the number of peptides with a relatively large number of residues.

Amphibian peptides are considerably shorter, with an average length of 24.5 residues. All available structural data concerning frog antimicrobial peptides show helical structure. It is important to note, however, that of the majority of amphibian peptides isolated to date have not been structurally characterized. Therefore, there might still be peptides either undiscovered or uncharacterized with other secondary structures.

Extrapolation of available data might suggest that all amphibian peptides are helical. However, such interpretation would not account for other structural features found within amphibian peptides. Examples include disulfide bridges, present as an intermolecular bridge in the peptide distinctin (Verardi *et al.,* 2011) and intramolecularly in the brevinin peptides (Simmaco *et al.,*

1993) and the presence of turns within helices, as in the case of ranatuerin-2CSa (Subasinghage *et al.,* 2008).

1.3.2 Physical properties: overall charge and percentage hydrophobicity

Overall charge and percentage hydrophobicity are gross physical parameters that do not truly reflect the structure of a peptide, since it is possible for two peptides to have the same values for these two quantities and still have vastly different structures. Nevertheless, simplistic though they may seem, these properties have been linked to the biological activity of peptides. The importance of charge has been demonstrated in the case of pseudin-2, where increasing the positive charge of the peptide increases its toxicity to bacterial cells (Pál *et al.,* 2005). Similarly, increasing the hydrophobicity of temporin A has been shown to increase its toxicity to enterococcus bacteria (Wade *et al.,* 2000).

It is therefore clear that the discussion of the distribution of overall charge and percentage hydrophobicity is relevant to the current study. These distributions have been analysed below for all peptides (including amphibian peptides) in the antimicrobial peptides database (Figure 1.3.2.1).

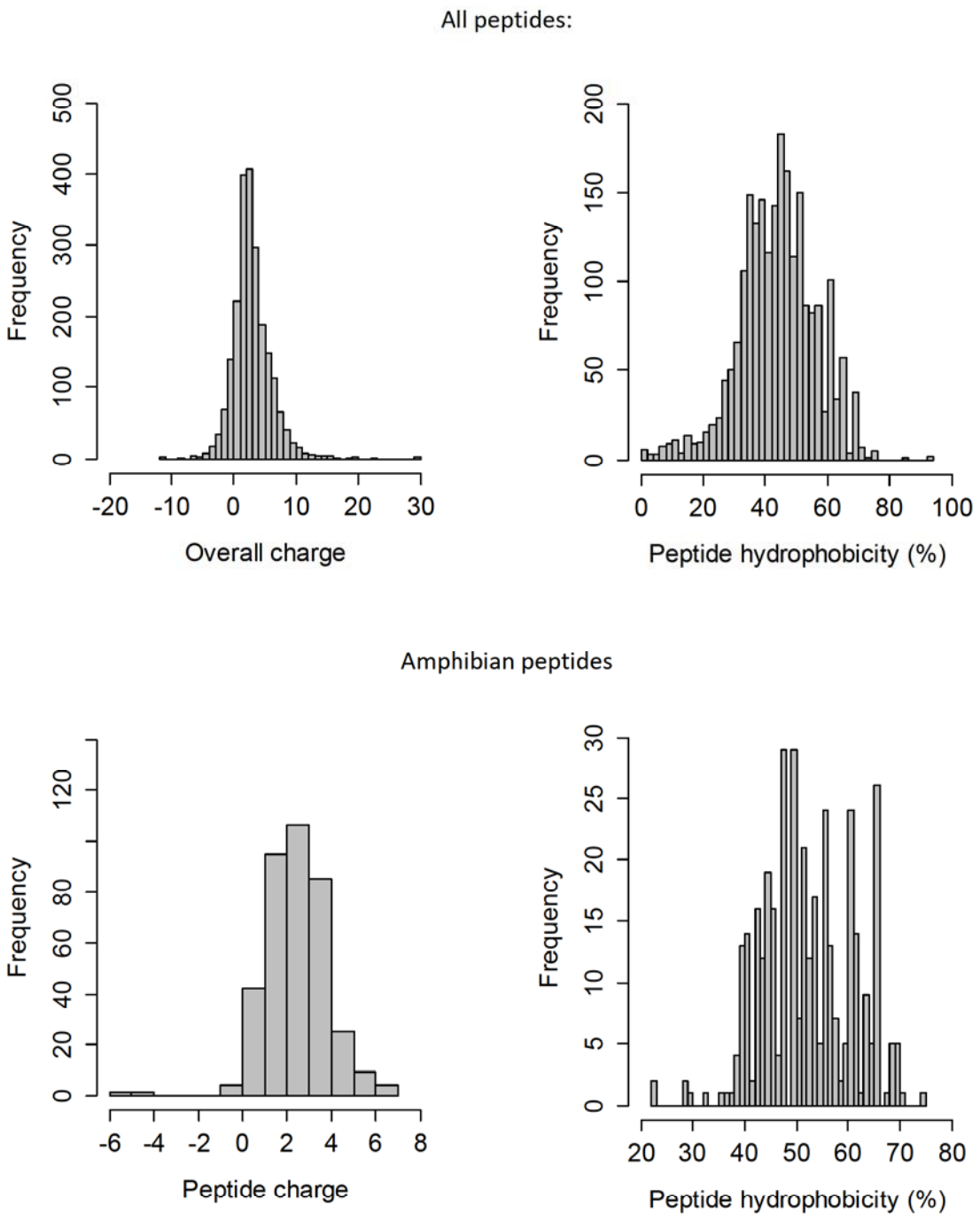

Figure 1.3.2.1 Overall charge and percentage hydrophobicity statistics for all peptides and amphibian peptides in the antimicrobial peptide database.

The data in the figure above shows some notable features. In the case of both the amphibian peptides as well as overall, the peptides in the database have an overall positive charge. The average values of charge are also similar in both cases, with an average overall charge of +3 for all peptides as well as the amphibian peptides alone. On the other hand, the average hydrophobicities show some variation between the two groups. Amphibian peptides have a

higher average hydrophobicity compared to the hydrophobicity of all peptides. Additionally, the hydrophobicity distribution of amphibian peptides is more irregular, with a large number of peptides having a percentage hydrophobicity between 50% and 70%.

These properties can be related to the structural data discussed in the previous section. Since the majority of peptides have helical structures, is it logical that they would have relatively high hydrophobicities. It is generally accepted that hydrophobic residues are helix-promoting residues, which is why the high helicity correlates well with the hydrophobicity. The positive average charge of these peptides has implications with regards to the antimicrobial toxicities of these peptides. This is discussed in further detail the following section.

1.3.3 Biological activities

The peptides listed in the antimicrobial peptide database have been shown to possess a wide range of biological properties. The biological activities of these peptides are summarized in Figure 1.3.3.1 below, with percentages shown for all peptides as well as amphibian peptides alone.

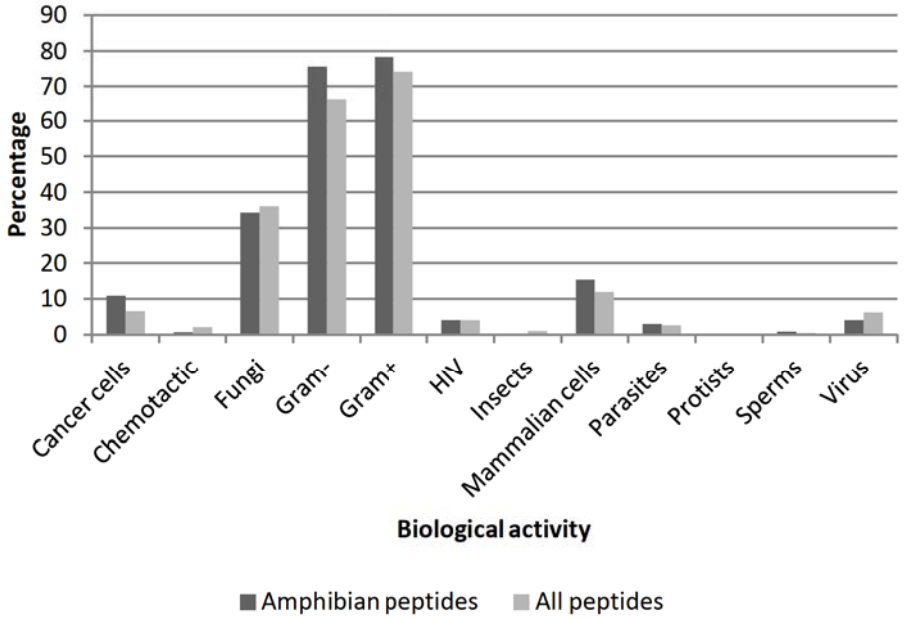

Figure 1.3.3.1 Percentages of all peptides and amphibian peptides in the antimicrobial peptide database with different biological activities. Note that with the exception of chemotaxis, each biological activity refers to toxicity to the organism specified.

The data above shows that the biological activity statistics for both categories of peptides are very similar. The major contributors in both categories are Gram-negative and Gram-positive toxicity, showing that the majority of peptides have been shown to be toxic to bacteria. This is followed by fungal toxicity, which is also a large component of the biological activity of these peptides. Other properties such as chemotaxis and toxicity to mammalian cells, and viruses are considerably smaller contributors.

These features of the biological activity statistics are indicative of the complexity of the underlying processes in each case. Gram-negative and gram-positive bacteria both possess a negatively-charged cellular surface (Dickson & Koohmaraie, 1989). This means that a positively-charged peptide would be attracted to such a surface and by a physical mechanism, the peptide may bring about a disruption of the cellular membrane, translating to toxicity. Fungal membranes are more zwitterionic in nature and have a smaller overall charge (Suomalainen & Nurminen, 1970). This is reflected in the smaller contribution of fungal toxicity to the activity of antimicrobial peptides.

As opposed to bacterial and fungal cellular surfaces which are charged, human erythrocytes (which may be considered a model for mammalian cells) are rich in neutral lipids (Dodge & Phillips, 1967). Additionally, the negatively charged lipids in erythrocytes are located in the inner leaflet of the membrane (Verkleij *et al.*, 1973). Charge effects are less important in this case, and hydrophobicity becomes a deciding factor. It is also possible that the peptide has a more specific mode of action and binds to a receptor on the surface of the cell, as in the case of chemotaxis.

What follows is a detailed analysis of the modes of action of antimicrobial peptides, with regards to their interaction with membranes. Since the majority of peptide biological properties have an underlying biophysical mechanism, only the interactions of peptides with a lipid membrane will be discussed in the following section. Specific interactions of antimicrobial peptides (i.e. interaction with a receptor or other cellular components) are very rarely reported since these types of interactions require a very specific 3D structure of the peptide in question.

1.4 Modes of action of antimicrobial peptides

Since the majority of antimicrobial peptides are cationic, and bacterial membranes rich in negatively charged lipids (Macholz, 1990), the driving force for the antimicrobial action of amphibian peptides is electrostatic attraction. This applies to mammalian cells as well, albeit to a smaller extent. Although these cells also possess a negatively-charged membrane surface, the inner leaflet of the membrane is richer in negatively charged lipids (Verkleij *et al.*, 1973). This accounts for the selectivity seen in amphibian antimicrobial peptides, a number of which show antimicrobial activity towards microbial pathogens whilst showing low toxicity towards mammalian cells. Examples of these peptides include pseudin-2 (Pal *et al.*, 2005), temporins A + B (Simmaco & Mignogna, 1996) and esculentin-1 (Simmaco *et al.*, 1993).

The antimicrobial activities of frog peptides can be explained using a number of molecular models. Since the only cellular component accessible to an external peptide is the membrane, all these models are peptide-membrane models. They describe the change in the structure and

properties of lipid membranes when interacting with an antimicrobial peptide. These have been divided into three sub-sections depending on the nature of the interaction and membrane structure formed. The three models are the toriodal pore, barrel stave and carpet models.

1.4.1 Toroidal pore (Ludtke *et al.*,1996)

In this membrane model, the peptide molecules initially adsorb to the surface of the membrane, and gradually 'push' into the membrane, causing strain on the membrane. This strain gradually builds as more peptides insert into the membrane until a transmembrane pore is formed. It is important to note that in this mechanism, the peptide only interacts with the head groups of the lipid molecules. The lipid tails remain embedded within the membrane and are not exposed to either the peptide or the external environment. A schematic demonstrating this mechanism is given in Figure 1.4.1.1 below:

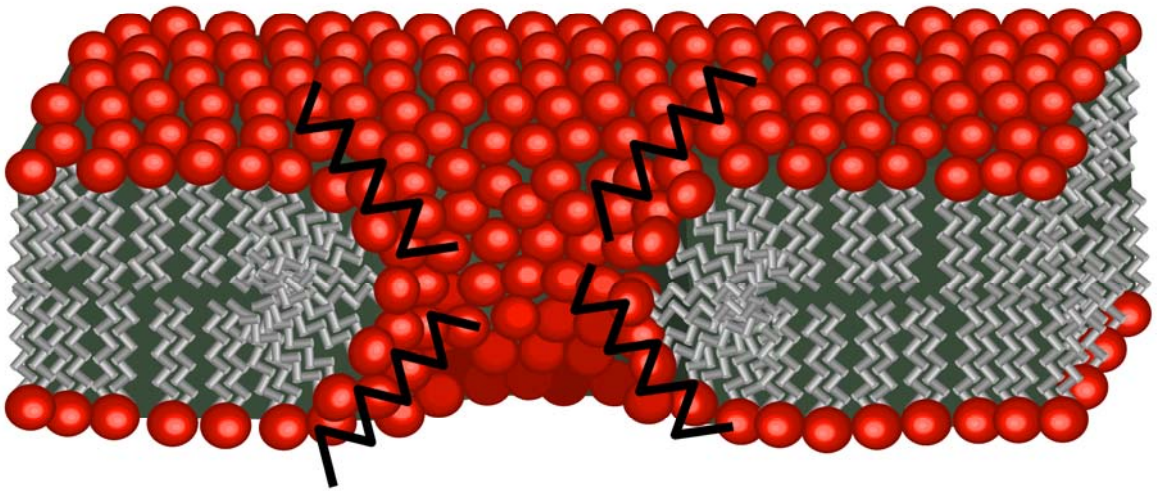

Figure 1.4.1.1 Illustration showing a toroidal pore created in a lipid membrane. The lipid heads are shown as red spheres and the lipid tails as grey lines. The peptide is denoted by black wavy lines. In this illustration, the external environment (containing the peptide) is above the membrane and the cytoplasm is below.

Structurally, the toroidal pore mechanism has been described using a number of techniques. In the case of the peptide maculatin 1.1, electron microscopy and NMR spectroscopy showed rippled cell surfaces, and a lipid phase respectively, both of which are consistent with pore formation (Sani *et al.*, 2013). By observing the leakage of fluorophores of different molecular dimensions from liposomes, the size of the pore was also estimated. Peptide-induced pores have

also been structurally characterised using X-ray diffraction in the case of the peptide melittin (Lee *et al.*, 2013) and Atomic Force microscopy. NMR spectroscopy has also been used to characterise toroidal pores formed by the peptide novicidin (Bertelsen *et al.*, 2012). In all these studies, spectroscopic data was used to determine the orientation of the lipid molecules within the membranes in question, which in this case are 'curved', with their headgroups facing outwards.

This mode of action can lead to rapid cell death by leakage of cell contents and by bulk inflow of water molecules. The parameter that decides the killing rate of the pathogen is the diameter of the pore. It is this parameter which dictates the dimensions of molecules that can flow into or out of the pore. The diameter of the pore consequently determines the rate at which the peptide lyses cells/vesicles. Other important parameters are the number of peptides required to create the pore and the peptide/lipid ratio.

It follows from the above description that the toroidal pore mechanism generally occurs at low peptide/lipid ratios, since only a small number of peptide molecules are required for pore formation to occur. Once this minimum has been reached, a further increase of peptide concentration will not have a large effect on the lysing/antimicrobial effect of the peptide. Additionally, this mechanism only causes a local destabilization of the membrane structure, so overall membrane integrity is preserved.

1.4.2 **Barrel-stave model** (Laver, 1994)

This mode of action is similar to the toroidal pore model since this mode of action also leads to the formation of an opening within the membrane. However, in this case the lipid tails interact with the peptide to form the pore. This is illustrated in Figure 1.4.2.1 below:

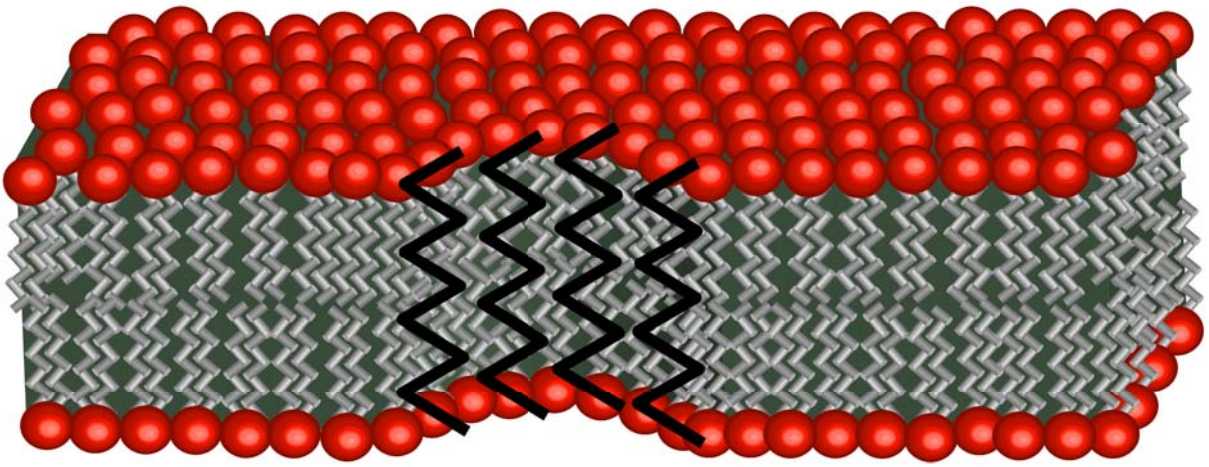

Figure 1.4.2.1 Schematic illustrating the structure of the membrane structure in the barrel-stave model. The lipid heads are shown as red spheres and the lipid tails as grey lines. The peptide is denoted by black wavy lines. In this illustration, the external environment (containing the peptide) is above the membrane and the cytoplasm is below.

The key difference between this model and the toroidal pore model is the position of the lipid tails lining the pore. Generally speaking, the lipid tails interact with the hydrophobic segment of the peptide in order to be shielded from the solvent.

Structurally, barrel-stave pores formed by antimicrobial peptides have been described using NMR spectroscopy in the case of alamethicin (Mihajlovic & Lazaridis, 2012) as well as paradaxin (Ramamoorthy *et al.*, 2010). These studies are comparable to the studies cited in the previous section describing toroidal pores. By using NMR spectroscopy to determine the orientation of lipid molecules within the membrane, it is possible to differentiate between the toroidal pore and barrel stave mechanisms. In the barrel stave model, the lipid molecules remain linear in orientation, contrary to the curved orientation seen in the toroidal pore model. It is interesting to note that this model is less common than the toroidal pore model.

This mechanism shares the same parameters as the toroidal pore model of pore diameter, minimum number of peptides required for pore formation, and minimum peptide concentration necessary for peptide aggregates to form. The barrel-stave model requires the peptide to have a length greater than 20 residues in order to facilitate insertion. This model is also one of local disruption of membrane structure with simultaneous preservation of membrane integrity. Cell

death in mechanism, like in the toroidal pore mechanism, occurs by leakage of cellular contents or bulk water inflow.

1.4.3 'Carpet' model (Pouny *et al.*,1992)

The carpet model is considerably different from the two pore-forming models discussed above. In the 'carpet' model, the peptide molecules simply adsorb to and then coat the membrane surface. As the concentration of peptide increases, the integrity of the membrane is gradually lost. It is important to note that in this model, no structured pores are formed in the membrane. It is simply a generic descriptor for a membrane disruption mechanism in which the peptide completely disrupts membranes by interacting with the membrane surface. Therefore, there is no consensus within the literature for the mechanism of the carpet model of toxicity. This model is the suggested mode of action for the frog antimicrobial peptides aurein 1.2 (Fernandez *et al.,* 2012) and gomesin (Domingues *et al.*, 2010). In both cases, complete membrane lysis is observed.

1.5 Antimicrobial peptide nomenclature and classification

Amphibian peptides are always classified based on their amino acid sequence. Since peptides have been associated with a number of biological properties (such as the ability to release insulin or inhibit the growth of cancerous cells), it is not possible to classify peptides based on their function.

Similarly, amphibian peptides are not generally classified according to their three-dimensional structure, owing to the flexibility engendered by the variable environments of the molecules. Moreover, structural classification would present problems for larger peptide families, since peptides are generally short molecules, and a difference of even a single amino acid can have a significant impact on the peptide's structure.

With regards to the nomenclature of peptides, a number of nomenclature schemes have been proposed (Amiche *et al.,* 2008; Conlon 2008a; Conlon 2008b; Thomas *et al.,* 2012). All these nomenclature systems may be summarized as follows:

- Peptides are classified into families based on their structure
- For analogous peptides from different frogs, the root name of the peptide is the name of the original unique peptide
- This is followed by either one or two uppercase letters of the frog or genus name
- Finally, paralogs are serialized either numerically or alphabetically

Although the scheme mentioned above is the most common, there are a number of notable exceptions. These include the aurein, caerin, maculatin and citropin peptides, all of which use a hierarchical numbering system to denote the relationship between analogues.

1.6 Structure-function relationships of amphibian antimicrobial peptides

Since this study focuses on the structure-activity relationship of pseudin-2, it is necessary to closely examine the data available on the structure-activity relationships of other families of amphibian antimicrobial peptides. This allows us to examine the similarities between pseudin-2 and the structure-activity relationships of other peptides. A detailed, comprehensive review of the available data on amphibian antimicrobial peptides is, therefore, crucial to this study.

The following section lists the major families of antimicrobial peptides, and reviews the studies investigating their antimicrobial properties. The parent peptides of each of the peptide families in the following discussion are given in **Table 1.6.1 Details of the parent peptides of** the families **covered** in the following discussion

, along with their antimicrobial and haemolytic properties, where this information is available. Note that this table only contains the parent peptides of each of the peptide families reviewed.

Peptide	Sequence	MIC			HC_{50}	Reference, amphibian
		E. Coli	*S. Aureus*	*C. Albicans*		
Aurein 1.1	GLFDIIKKIAESI	-	-	-	-	(Rozek *et al.*, 2000), *Litoria aurea*
Aurein 1.2	GLFDIIKKIAESF	-	50 µM	-	-	
Aurein 2.1	GLLDIVKKVVGAFGSL	-	-	-	-	
Aurein 2.2	GLFDIVKKVVGALGSL	-	25 µM	-	-	
Aurein 2.3	GLFDIVKKVVGAIGSL	-	100 µM	-	-	
Aurein 2.4	GLFDIVKKVVGTIAGL	-	25 µM	-	-	
Aurein 2.5	GLFDIVKKVVGAFGSL	-	50 µM	-	-	
Aurein 2.6	GLFDIAKKVIGVIGSL	-	50 µM	-	-	
Aurein 3.1	GLFDIVKKIAGHIAGSI	-	50 µM	-	-	
Aurein 3.2	GLFDIVKKIAGHIASSI	-	50 µM	-	-	
Aurein 3.3	GLFDIVKKIAGHIVSSI	-	100 µM	-	-	
Aurein 5.2	GLMSSIGKALGGLIVDVLKPKTPAS	-	-	-	-	
Caerin 1.1	GLLSVLGSVAKHVLPHVVPVIAEHL	>100 µg/ml	3 µg/ml	-	-	(Wegener *et al.*, 1999), *Litoria citropa*
Citropin 1.1	GLFDVIKKVASVIGL	>100 µg/ml	25 µg/ml	-	-	(Wegener *et al.*, 1999), *Litoria citropa*
Citropin 1.1 sm1	GLFAVIKKVASVIGGL	100 µg/ml	25 µg/ml	-	-	
Citropin 1.1 sm2	GLFDVIAKVASVIGGL	>100 µg/ml	100 µg/ml	-	-	
Citropin 1.1.3	GLFDVIKKVASVIGLASP	>100 µg/ml	>100 µg/ml	-	-	
Citropin 1.2	GLDFIIKKVASVVGGL	>100 µg/ml	25 µg/ml	-	-	
Citropin 1.3	GLFDIIKKVASVIGGL	>100 µg/ml	25 µg/ml	-	-	
Citropin 2.1	GLIGSIGKALGGLLVDVLKPKL	>100 µg/ml	>100 µg/ml	-	-	
Citropin 2.1.3	GLIGSIGKALGGLLVDVLKPKLQAAS	>100 µg/ml	>100 µg/ml	-	-	
Maculatin 1.1	GLFGVLAKVAAHVVPAIAEHF	>100 µg/ml	6 µg/ml	-	-	(Wegener *et al.*, 1999), *Litoria citropa*
Temporin A	FLPLIGRVLSGIL	11.9 µM	2.3 µM	3.4 µM	>120 µM	(Simmaco & Mignogna, 1996), *Rana temporaria*
Temporin B	LLPIVGNLLKSLL	21 µM	6 µM	4 µM	>120 µM	

Brevinin 1	FLPVLAGIAAKVVPALF**C**KITKK**C**	-	-	-	-	(Morikawa *et al.*, 1992), *Rana brevipoda porsa*
Brevinin 2	GLLDSLKGFAATAGKGVLQSLLSTAS**C**KLAKT**C**	-	-	-	-	
Magainin 1	GIGKFLHSAGKFGKAFVGEIMKS	-	-	-	-	(Zasloff, 1987), *Xenopus laevis*
Magainin 2	GIGKFLHSAKKFGKAFVGEIMNS	5 µg/ml	50 µg/ml	80 µg/ml	-	
Distinctin	ENREVPPGFTALIKTLRKCKII | NLVSGLIEARKYLEQLHRKLKNCKV	14.5 µM	28 µM			(Batista *et al.*, 2001), *Phyllomedusa distincta*
Dermadistinctin K	GLWSKIKAAGKEAAKAAAKAAGKAALNAVSEAV	0.6 µM	4.7 µM			(Batista *et al.*, 1999), *Phyllomedusa distincta*
PGLa	GMASKAGAIAGKIAKVALKAL	-	-	-	-	(Andreu *et al.*, 1985), *Xenopus laevis*
Esculentin 1	GIFSKLGRKKIKNLLISGLKNVGKEVGMDVVRTGIDIAGCKIKGEC	0.2 µM	0.4 µM	-	>100 µM	(Simmaco *et al.*, 1993), *Rana esculenta*
Ranatuerin-1	SMLSVLKNLGKVGLGFVA**C**KINKQ**C**	2 µg/ml	50 µg/ml	70 µg/ml	>20 µg/ml	(Goraya *et al.*, 1998), *Rana catesbeiana*
Ranatuerin-2	GLFDTLKGAAKDVAGKLEGLK**C**KITG**C**KLP	-	60 µg/ml	-	>20 µg/ml	
Ranatuerin-3	GFLDIIKNLGKTFAGHMLDKIK**C**TIGT**C**PPSP	-	60 µg/ml	-	>20 µg/ml	
Ranatuerin-4	FLPFIARLAAKVFPSII**C**SVTKK**C**	-	55 µg/ml	-	>20 µg/ml	
Ranatuerin-5	FLIPASLLGKYL	-	>200 µg/ml	-	>20 µg/ml	
Ranatuerin-6	FISAIASMLGKFL	-	100 µg/ml	-	>20 µg/ml	
Ranatuerin-7	FLSAIASMLGKFL	-	200 µg/ml	--	>20 µg/ml	
Ranatuerin-8	FISAIASFLGKFL	-	130 µg/ml	-	>20 µg/ml	
Ranatuerin-9	FLFPLITSFLSKVL	-	130 µg/ml	-	>20 µg/ml	
Gaegurin 1	SLFSLIKAGAKFLGKNLLKQGACYAACKASKQC	25 µg/ml	-	>200 µg/ml	>100 µg/ml	(Park *et al.*, 1994), *Rana rugosa*
Gaegurin 2	GIMSIVKDVAKNAAKEAAKGALSTLSCKLAKTC	75 µg/ml	-	150 µg/ml	>100 µg/ml	
Gaegurin 3	GIMSIVKDVAKTAAKEAAKGALSTLSCKLAKTC	75 µg/ml	-	>200 µg/ml	>100 µg/ml	

Gaegurin 4	GILDTLKQFAKGVGKDLVKGAAQGVLSTVSCK LALTC	75 µg/ml	-	200 µg/ml	>100 µg/ml	
Gaegurin 5	FLGALFKVASKVLPSVKCAITKKC	50 µg/ml	-	50 µg/ml	>100 µg/ml	
Gaegurin 6	FLPLLAGLAANFLPTIICKISYKC	100 µg/ml	-	50 µg/ml	>100 µg/ml	

Table 1.6.1 Details of the parent peptides of the families covered in the following discussion

1.6.1 Aureins

Aureins are a small family of antimicrobial peptides, of varying lengths (13-25 residues), isolated from the frog *Litoria aurea*. In addition to their antimicrobial properties, aureins have been shown to possess anticancer properties (Bowie, *et al.,* 2000). Aureins are among the best characterised families of amphibian antimicrobial peptides. The 3D structure of micelle-bound aurein 1.2 is present in the Protein Data Bank (Bernstein *et al.,* 1977), and is known to be a perfect alpha helix (Wang & Li, 2004). Later NMR studies have confirmed this structure, showing that aurein 1.2 becomes helical in a membrane environment (Sani *et al.,* 2013) and that it prefers anionic membranes, which it disrupts via a concentration-dependent carpet mechanism (Sani *et al.,* 2012). The structure of aurein 2.3 has also been linked to membrane binding and disruption by a combination of molecular dynamics and circular dichroism experiments (Mura & Dennison, 2012). The same study also showed that aurein 2.5 forms an oblique helix in the presence of lipid vesicles.

The structure-function relationships of aureins have also been probed by the generation of aurein analogues. The naturally-occuring amidated form of aurein 2.5 was de-amidated to study the importance of amidation on the function of the peptide as an antimicrobial (Dennison, 2012). The amidation of this peptide was found to increase its helical content and stabilise the alpha helices formed at the surface of membranes. Similarly, C-terminus truncated analogues of aurein 2.2 have also been synthesized to study the importance of the C-terminus residues with regards to its antimicrobial activity (Cheng *et al.,* 2010). It was shown that the removal of C-terminus residues reduced the ability of the peptide to insert into vesicles. A more potent analog of aurein 1.2 (G1->R, F3->W) has also been characterised (Soufian & Hassani, 2011). The dimerization aurein 1.2 has been investigated as a method for improving its biological properties, but does not appear to affect the helical structure of the peptide in a membrane environment (Lorenzón *et al.,* 2013). However, both C- and N-terminus dimers of the peptide were shown to have lower haemolytic activity than the naturally-occuring monomer and to be able to bring about the aggregation of *C.*

Albicans cells. Finally, the antimicrobial effect of aurein 2.5 has been shown to be amphipathicity driven, with no apparent change in membrane interaction associated with change in membrane surface charge.

A number of studies have also been conducted studying the nature of the interaction between aureins and lipid membranes. Aurein 2.2 has been shown to be more helical/disruptive in the presence of a membrane mimicking that of Gram-positive bacteria (Cheng *et al.,* 2011). The direct observation of lipid membranes in the presence of aurein 1.2 has revealed that the peptide interacts with the surface at low concentrations (5 µM) and gradually causes loss of membrane integrity as the concentration increases to 10 µM (Lee *et al.,* 2010). Similarly, aurein 2.2 and aurein 2.3 have been shown to bind to membrane surfaces at low concentrations and insert at high concentrations (Cheng *et al.,* 2009).

In conclusion, aureins interact preferentially with anionic membranes, predominantly forming helices and using a carpet mechanism to disrupt membrane structure. The natural amidation of the peptide is important for its function. The amphipathicity of these peptides is the driving factor for toxicity.

1.6.2 Caerins

Caerins are a family of moderately long peptides (22-25 residues) isolated from the frog *Litoria citropa*. Their structure-function relationships are described below. The majority of data available on caerin peptides is structural and involves the use of spectroscopic techniques such as NMR, CD or surface Plasmon resonance.

Early NMR studies have shown that caerin 1.1 does not form a complete helix on binding with neutral liposomes (David, 1992), but rather forms two smaller helices with a loop segment in between them (Wong *et al.,* 1997). Caerin 1.1 has also been shown to disrupt the membranes of Gram positive bacteria (Chia *et al.,* 2000). More recent studies have described the relationship between membrane binding of caerin 1.1 and membrane curvature, showing that a long

membrane curvature is required for caerin 1.1 interaction due to the length of the peptide (Fernandez *et al.,* 2013; Gehman *et al.,* 2008; Chen & Mark 2011).

An atomic force microscopy study of the interaction of caerin 1.1 with membranes showed that the peptide inserts into membranes regardless of their lipid composition (Mechler *et al.,* 2007), whilst preceding oriented circular dichroism studies revelaed that caerin 1.1 inserts into membranes at an angle of 50° (Marcotte *et al.,* 2003). Although NMR studies of caerin 1.4 has showed that it has a similar structure to caerin 1.1 caerin 1.4 has different amtimicrobial properties which are attributed to differences in hydrophobicity and helix angle between the two peptides (Wegener *et al.,* 2003; Chia *et al.,* 2000).

Caerin 1.1 (GLLSVLGSVAKHVLPHVVPVIAEHL) possesses a 'hinged' helical structure, with two alpha helical segments, with a hinge region between the proline residues at positions 15 and 19. The importance of the flexible hinge of caerin 1.1 has also been investigated (Pukala *et al.,* 2004). It was shown using NMR and molecular dynamics experiments that the replacement of the proline residue at position 15 of the peptide with alanine or glycine residues decreased the 'hinge angle' of the peptide and decreased its antimicrobial activity.

In conclusion, caerins are relatively long antimicrobial peptides which disrupt membranes by a carpet mechanism. This mechanism is strongly affected by the presence of a 'hinge' at position 15 of the peptide. Increased rigidity of this molecular 'hinge' is associated with decreased antimicrobial activity.

1.6.3 Citropins

Citropins are a large family of antimicrobial peptides isolated from the frog *Litoria citropa*. Although the members of this family vary in length, the majority are short peptides. In addition to the antimicrobial properties of this family of peptides, citropins have as been shown to be protective against oxidative damage (Ghiselli *et al.,* 2011) and to show synergistic effects with

certain antimicrobials (Giacometti & Cirioni, 2005). The peptide citropin 1.1 has been best characterized and will be discussed below.

NMR studies of citropin 1.1 have shown that it causes total membrane disruption of uncharged liposomes (Gehman *et al.,* 2008; Ambroggio *et al.,* 2005) and does so via a detergent-like mechanism (Balla *et al.,* 2004). A study of the interaction of citropin 1.1 with membranes has shown that the peptide is most miscible with anionic vesicles (Ambroggio *et al.,* 2004) which it perturbs more strongly than zwitterionic vesicles (Seto *et al.,* 2007). Oriented circular dichroism data has shown that it forms an alpha helix when interacting with the surface of a membrane (Marcotte *et al.,* 2003).

A molecular dynamics study of citropin 1.1 using restraints from NMR data describes the structure of citropin 1.1 in a membrane environment (Sikorska & Greber, 2009). It has been shown that the peptide forms two short alpha helices at positions (4-7) and (10-16) separated by a flexible loop. The truncated (1-13) citropin 1.1 has been shown to be completely helical while the analogue (1-13) Ala4 citropin 1.1 has been shown to contain a short helical portion in its middle segment. The substitution of aspartate for lysine in citropin 1.1 is associated with an increase in hydrophobic moment as well as antimicrobial activity (Chia *et al.,* 2011). Additionally, it has been shown that the terminal residues of citropin 1.1 are important for maintaining the overall positive charge of the peptide while increasing its amphipathicitiy increases its toxicity to gram-negative bacteria (Doyle *et al.,* 2003).

In conclusion, citropins are a class of short antimicrobial peptides that disrupt microbial membranes using a carpet mechanism. The 'hinge' or flexibility of these peptides (brought about in some peptides by the presence of a proline residue) plays a crucial role in their toxicity to microbial pathogens. Additionally, their overall positive charge, hydrophobic moment and amphipathicity are also important structural parameters.

1.6.4 Maculatins

Maculatins are a class of moderately long peptides (21 residues) isolated from the frog *Litoria citropa*. The length of these peptides plays an important role in shaping their antimicrobial properties, as discussed below.

Maculatin peptides, particularly maculatin 1.1, have been well characterised by a number of studies, including their interaction with membranes, pure structural studies using spectroscopic techniques, as well as studies involving the production of analogues of naturally-occuring peptides. Resulting data are reviewed below.

Studies of the interaction of maculatin 1.1 with membranes have showed that the peptide interacts most strongly and preferentially disrupts anionic membranes rather than zwitterionic ones (Fernandez *et al.,* 2013; Seto *et al.,* 2007; Ambroggio *et al.,* 2004; Marcotte *et al.,* 2003; Chia *et al.,* 2002; Sani *et al.,* 2012; Parton *et al.,* 2012). The accepted mechanism of action of maculatin 1.1 is the formation of structured and stable pores within the membrane (Bond *et al.,* 2008; Gehman *et al.,* 2008; Mechler *et al.,* 2007; Ambroggio *et al.,* 2005; X. Han & W. J. Kang 2004). Membrane curvature has also been shown to be an important factor to stabilise the membrane pores formed by the peptide (Chen & Mark, 2011).

The middle proline residue has been shown to be an important part of the structure of maculatin 1.1 (GLFVGVLAKVAAHVVPAIAEHF), both in aqueous as well as membrane environments (Chia *et al.,* 2000). This residue causes a 'kink' in the peptide which has been shown to be crucial to its activity as an antimicrobial (Chia *et al.,* 2011). Finally, the removal of N-terminus residues of maculatin 1.1 completely eliminates its activity as an antimicrobial, while increasing its positive charge makes the peptide more toxic to both prokaryotic as well as eukaryotic cells (Niidome *et al.,* 2004).

In conclusion, maculatin 1.1 is a long cationic peptide which lyses microbial cells by forming pores in their membranes. The N-terminal residues of this peptide are crucial to its activity as an

antimicrobial. The middle proline residue in the peptide is also key to its function as it leads to the formation of a 'kink'in its helical structure.

1.6.5 Temporins

Temporins are a family of very short (10-13 resdiues) antimicrobial peptides initially isolated from the skin of the European frog *Rana temporaria* (Simmaco & Mignogna, 1996). A number of temporin peptides possess antimicrobial activity against both gram-negative and gram-positive bacteria and yeast (Abbassi, *et al.* 2008). It is important to note that a large number of temporin peptides have been isolated from a number of amphibians, and the structure-function relationships of these peptides are also included in the following section.

Structural studies conducted on temporins demonstrate that their helical and hydrophobic structure is crucial to both their antimicrobial and haemolytic properties. A combined experimental/molecular dynamics study on temporins A and L has shown that temporin L forms the more stable helix, and that in both peptides residues 7-13 are the most helical (D'Abramo *et al.,* 2006). Additionally, the anti-enterococcal properties of temporin A have been enhanced by the introduction of bulky, hydrophobic side chains at positions 5 and 12 and a positive residue at position 7 (Wade *et al.,* 2000). Replacing the residues on the hydrophilic face of the amphipathic peptide temporin-1CEb with lysine residues has been shown to lead to a substantial improvement in its antimicrobial properties (Shang *et al.,* 2012). The helicity of temporins also determines their toxicity to mammalian cells (Mangoni *et al.,* 2011)..

An increase in the positive charge increases the antimicrobial activity of temporins, but only when combined with an increase in the amphipathic nature of the peptide. An alanine-scan study has led to the discovery of a potent analogue of temporin-1b with increased toxicity towards *E. Coli* compared to the parent peptide (Avitabile *et al.,* 2013). This analogue contains two additional lysine residues at the N-terminus and a glycine -> alanine substitution at position 6 of the peptide. These changes are consistent with other studies as they show that the maintenance of the

amphipathic nature of these peptides while increasing their charge leads to an increase in antimicrobial toxicity.

Chirality has no effect on the antimicrobial toxicity of temporins, although it does affect their haemolytic activity. The toxicity of temporin A to eneterococcus is non-chiral, since the substitution of all the residues of the peptide with their D-enantiomers does not affect its toxicity (Wade *et al.,* 2000). A similar observation was made recently in the case of temporin L, where a single D->L amino acid substitution has been shown to considerable reduce its haemolytic activity while having no effect on its toxicity to *C. Albicans*. Finally, the substitution of the helix-disrupting aminobutyric acid at positions 9, 14 and 18 of temporin-1DRa lowers the cytotixicity of the peptide to eukaryotic cells while preserving its antimicrobial activity (Conlon *et al.,* 2007).

The interaction of temporins and their analogues with cellular membranes is crucial to an understanding of both their antimicrobial and haemolytic properties. Temporin L, for instance, loses its antimicrobial effects in the presence of purified LPS from *E. Coli* (Giacometti *et al.,* 2006), whilst Temporins A and B cause leakage of large molecules from bacterial cells (Mangoni & Rinaldi, 2000). These peptides also disrupt membrane structure locally (as opposed to a detergent-like disruption of membranes) and increase hydrocarbon chain mobility (Rinaldi *et al.,* 2001). Temporins A and L interact differently with SDS and DPC micelles (model micelle systems for bacterial and eukaryotic membranes, respectively) (Carotenuto *et al.,* 2008). The two peptides orient parallel to SDS micelles while being perpendicular to the surface of DPC micelles. It is, therefore clear, that both the antimicrobial as well as haemolytic properties of these peptides are mediated by membrane interaction.

In summary, the antimicrobial and haemolytic properties are the result of interplay between a number of contributing factors. These peptides are largely helical and cationic in nature. Their antimicrobial properties may be improved by enhancing their helicity nature and overall positive charge. It is also evident that these peptides exert their antimicrobial action using a 'carpet' or

detergent-like mechanism. Their haemolytic properties, on the other hand, seem to depend on their ability to form a stable helix and the chirality of the residues constituting the peptide.

1.6.6 Brevinins

Brevinins are a class of antimicrobial peptides of varying lengths (23-37 residues) originally isolated from the frog *Rana brevipoda* porsa. Since the isolation of Brevinin-1 and -2 from this frog, sturcutrally-related Brevinins have been discovered in a number of other frogs. An interesting feature of these peptides is the intramolecular disulphide bridge between the two cysteine residues at the C-terminus end of the peptides. The role of this bridge, as well as the other structural features of this family of peptides, is discussed below.

Structurally, brevinins possess a helical structure in membrane-mimetic environments while being disordered in aqueous environments. A study using combined CD/NMR spectroscopy has demonstrated that Brevinin-1ED has an amphipathic alpha-helical structure stabilized in membrane-mimetic environments (Won *et al.,* 2004). Similar results were found in the case of brevinin-1E, with CD/NMR spectroscopy results showing that while the peptide is disordered in water, it is alpha-helical in membrane-mimetic environments (Son *et al.,* 2003).

The intramolecular disulfide bridge in brevinins promotes toxicity towards both mammalian cells as well as pathogens. A dicarba derivative of Brevinin-1BYa was synthesized by replacing the natural disulfide bond in the molecule with a dicarba bond, which is non-reducible (Hossain & Guilhaudis, 2011). The dicarba derivative was significantly more toxic to *E. Coli*, *S. Aureus* and *C. Albicans* as well as being more toxic to mammalian cells. In the case of brevinin-1E, the removal of the disulfide bridge completely eliminates the haemolytic activity of the peptide (Kumari & Nagaraj, 2001).

In conclusion, the structure-function relationships of brevinins indicate that the peptides form an amphipathic helix in membrane environments while being disordered in aqueous systems. The disulfide bridge in these peptides also plays an important role in both the antimicrobial toxicity as

well as haemolytic activity of this family of peptides. It confers antimicrobial toxicity to these peptides, and its removal can reduce haemolytic activity.

1.6.7 Magainins

Magainins are a class of short (21-23 amino acids in length) peptides originally isolated from the frog *Xenopus Laevis* and shown to possess broad-spectrum antimicrobial activity. Structure-activity studies conducted on magainins focus on the peptide magainin-2, and these are discussed below.

Structurally, magainin-2 is helical in membrane environments, with positional hydrophobicity being important for toxicity. Magainin-2 forms an amphipathic helix in the membrane-mimic TFE/water (Marion *et al.,* 1988). With regards to positional hydrophobicity, only the hydrophobic residues within the helical segment of the peptide are to be considered in hydrophobicity calculations (Tachi *et al.,* 2002; Guerrero & Saugar 2004).

A number of studies have been conducted investigating the mechanism of antimicrobial action of magainin-2. A confocal laser-scanning microscopy study has shown that magainin-2 exhibits two transition states in combination with membranes: a binding state and a pore-forming state, with the concentration of the peptide at the interface being an important factor in the formation of pores (Tamba & Yamazaki, 2009). This toroidal pore mechanism is further supported by an X-ray diffraction study showing that magainin-2 disrupts the order of lipid tails in membranes (Münster *et al.,* 2002). *In-silico* studies of magainin-2 also support the toroidal pore mechanism, showing a stable configuration at the membrane surface as well as within the membrane (Maddox & Longo 2002; Leontiadou *et al.,* 2006; Shental-Bechor *et al.,* 2007). Finally, magainin-2 also disrupts the electrical potential of lipid membranes (Westerhoff, 1989)

In conclusion, the literature suggests that magainins (specifically magainin-2) interact with biological membranes by the formation of an amphipathic helix. The peptide has a stable conformation parallel to the membrane surface but also forms pores depending on the

concentration at the surface. Finally, the position of hydrophobic residues in the peptide play an important role in the specificity of its toxic properties and its preferential binding to bacterial membranes.

1.6.8 Distinctins

Distinctins are a class of peptides that were recently isolated from the skin of the frog *Phyllomedusa distincta*. The characterization of distinctin revealed that the peptide was a heterodimer consisting of a long and short peptide connected by a disulfide bridge (Batista *et al.,* 2001).

Structurally, distinctin is helical in structure both in aqueous and membrane environments. A CD study of distinctin has shown that the peptide possesses helical structure in the presence of POPC/POPG liposomes which is stabilized by peptide-peptide and peptide-helix interactions (Resende, 2009). The ordered structure of distinctin in aqueous solution has also been described (Verardi *et al.,* 2011).

The unique disulfide-bridged-heterodimeric structure of distinctin has been shown to be crucial to maintaining the structure and stability of the peptide. Both peptide chains as well as the disulfide bond of distinctin are necessary for the quartenary structure and stability of the peptide (Serra *et al.,* 2008).

Finally, evidence indicates that a concentration-dependent toroidal pore mechanism is the most likely mechanism for the antimicrobial action of distinctins. In the case of distinctin, a high concentration of peptide is required for pore formation to occur (Verardi *et al.,* 2011). The pores formed by distinctin form channels for inorganic cations, with peptide clusters on opposite sides of the membrane combining to form the pore (Becucci *et al.,* 2011). Additionally, the peptide dermadistinctin K has independently been shown to disrupt lipid packing (Verly *et al.,* 2009).

In conclusion, distinctin presents an interesting case with regards to antimicrobial peptides: one that is not only helical in the absence of a lipid interface, but one that is also resitanct towards the activity of proteases. At high concentrations, distinctin binds to membranes and creates pores that allow the flow of inorganic cations.

1.6.9 PGLa

PGLa is a short peptide of simple amino acid composition which, like magainin-2, was isolated from the skin of the frog *Xenopus Laevis*. As shown in Table 1.6.1, the peptide is moderately antimicrobial, with low haemolytic activity. It is, therefore, an interesting candidate as a therapeutic. The majority of structural studies conducted on PGLa examine its synergistic effects when combined with the peptide magainin-2, isolated from the skin of the same frog. These are discussed below.

PGLa has an alpha-helical structure in membrane environments. An early NMR study showed that the peptide has a helical structure with the helix spanning residues 6-21 and that the axis of the helix is parallel to the surface of the membrane (Bechinger *et al.,* 1998).

An NMR study on the interaction of PGLa with membrane-mimetics showed that the peptide has a higher affinity for prokaryotic membranes, which it binds at the surface (Lohner & Prossnigg, 2009).

In the presence of magainin-2, PGLa binds to the surface of prokaryotic membranes and forms pores, with membrane curvature being an important parameter for pore formation. The activity of PGLa in the presence of magainin-2 depends on the curvature of the lipid membrane in question (Strandberg *et al.,* 2013). In membranes with positive curvature, PGLa and magainin-2 both bind parallel to the membrane surface whereas in the case of negative curvature, PGLa adopts a tilted conformation, inserting into the membrane while magainin-2 remains on the surface. This synergy between the two peptides leads to a conformation that forms a 'wormhole' pore (Tremouilhac & Strandberg, 2006). Finally, single mutations have been shown to alter the

synergistic effects observed in the activities of the peptides PGLa and magainin-2 peptides (Matsuzaki *et al.,* 1998).

In conclusion, the peptide PGLa is a part of a binary defense system of the frog *Xenopus Laevis*. This binary system is based on the precise three-dimensional structure of its two components. This configuration allows the two peptides PGLa and magainin-2 to create pores in the membranes of bacterial cells without damaging mammalian cells.

1.6.10 Esculentins

Esculentins are a family of relatively long antimicrobial peptides isolated from the skin of the frog *Rana esculenta*. Like brevinins, esculentins also contain an intramolecular disulfide bridge. Since the number of esculentins isolated from other frogs is considerably smaller than in the cases of other families such as temporins and brevinins, the number of structural studies on esculentin peptides is also smaller.

Available structural data on esculentins shows that they form three helical segments in a membrane environment. A combined NMR/CD study of esculentin-1c showed that in 70% TFE/water, the peptide possesses three helical segments with flexible loops in between (Kang *et al.,* 2010).

The N-terminus residues of esculentins are more important for antimicrobial activity than C-terminus residues, as demonstrated using studies conducted on esculentins with C-terminus truncations. Esculentin-1b[1-18] has activity against drug-resistant *S. Aureus* (Mangoni *et al.,* 2008) while Esculentin-1a[1-21] has activity against *E. Coli* and *S. Aureus* (Islas-Rodriguez *et al.,* 2009). Additionally, Esculentin-1b[1-18] shows synergistic bactericidal effects with antibiotics (Maisetta *et al.,* 2009).

The disulfide bridge present in esculentins enhances antimicrobial activity, but its removal does not eliminate activity completely. In the case of esculentin-1, the peptide retains its antimicrobial

activity when its disulfide bridge was removed but its presence accelerated the killing effect of the peptide(Ponti *et al.,* 1999).

In conclusion, esculentins are disulfide-containing peptides that are alpha-helical in membrane environments. Their N-terminus residues are crucial to their antimicrobial activity, while the disulfide bridge present in these molecules only enhances their toxicity to pathogens.

1.6.11 Ranatuerins

Ranatuerins are a family of antimicrobial peptides of varying lengths (12-26 residues) from the frog *Rana catesbeiana*. Like brevinins, Ranatuerins also belong to the class of peptides containing the 'Rana box' – an intramolecular disulfide bridge. Although a large number of ranatuerin analogues have been isolated from a number of different of frogs, only a small number of structural studies have been conducted on ranatuerins. These are discussed below.

Available data on ranatuerins suggests a helical structure for these peptides in a membrane environment, while being disordered in aqueous solution. A combined NMR/molecular modelling study of the structure of Ranatuerin-2CSa showed that the peptide adopts an ordered helical structure in TFE/water but is disordered in aqueous solution (Subasinghage *et al.,* 2008). The peptide adopted a helix-turn-helix structure with the helical segments spanning residues 2-21 and 26-30.

The helical structure and cationicity of ranatuerins determine their antimicrobial action. The substitution Asn8->Lys within ranatuerin-1 gives an analogue that was more toxic to against *S. Aureus* and *E. Coli*, which was attributed to the increased cationicity and helical content of the peptide (Sonnevend *et al.,* 2004).

The intramolecular disulfide bridge as well as N-terminus residues play an important role in the antimicrobial action of ranatuerins. In the case of ranatuerin-1, deletion of either the cyclic region

(19-25) or 8 N-terminus residues completely eliminated the antimicrobial activity of the peptide (Sonnevend *et al.,* 2004).

In conclusion, the available structural data on ranatuerins suggests that these peptides are disordered in water but adopt a largely helical structure in a membrane environment. Not only are helicity and cationicity important for antimicrobial action, but also the intramolecular disulfide bridge as well as the N-terminus residues. Finally, it is important to note the inherent heterogeneity in this family of peptides. The large difference in length and primary structure of the members of the ranatuerin family suggests that it is likely that these peptides have very different mechanisms underlying their antimicrobial properties.

1.6.12 Gaegurins

Gaegurins are a small family of relatively long (24-37 residues) antimicrobial peptides. There follows a discussion of the structure-function relationships of the gaegurin family of peptides.

Structural studies have only been conducted on gaegurin-4, and suggest a helical structure for gaegurin peptides. Gaegurin-4 has a helical structure in hydrophobic conditions (80% methanol/water) (Chi *et al.,* 2007), SDS micelles (Park *et al.,* 2007) as well as TFE/water (Park *et al.,* 2000). NMR spectroscopy studies have also described a structure with two helical segments connected by a flexible loop (Chi *et al.*, 2007; Park *et al.*, 2007; Park *et al.*, 2000). Finally, gaegurin-4 has been shown to undergo a coil->helix transition in membrane-mimetic environments (Eun *et al.,* 2006).

The N-terminus residues of gaegurins are crucial to their activity as antimicrobials. The 13 N-terminus residues of gaegurin-5 have been identified as the minimum requirement to maintain its toxicity to bacterial cells (Won *et al.,* 2004). Earlier studies have also revealed important features of the function of this peptide. This finding is supported by an earlier study which showed that the deletion of 9 residues from the C-terminus of gaegurin-4 did not have a large effect on its antimicrobial acitivity (Kim *et al.,* 2004).

The disulfide bridge present in gaegurins is important for both structure as well as antimicrobial action. In the case of gaegurin-6, the disulfide bridge it stabilises its helical structure and its removal leads to complete loss of antimicrobial activity (Lee *et al.,* 1998).

The antimicrobial activity of gaegurins involves an alteration of the conductance of cellular membranes via pore formation. Gaegurin4 selectively increases K^+ ion conductance in concentration-dependent manner (Kim *et al.,* 1999). A more recent study has linked its selective bacterial toxicity to ion conductance effects (Kim *et al.,* 2009). In this study, it was demonstrated that gaegurin-4-induced K^+ efflux is higher in bacterial cells than in erythrocytes. Transmission electron microscopy of *E. Coli* cells in the same study showed that the peptide forms pores on the surface of cells.

In conclusion, gaegurins (particularly gaegurin-4 and gaegurin-6) are alpha helical peptides which show selective toxicity to bacterial cells. Structural data suggests that these peptides form two helical loops and that their toxicity is mediated by increasing membrane permeability to K^+ ions. The N-terminus of these peptides and well as the intramolecular disulfide bridge are crucial to their bacterial toxicity.

1.6.13 Peptides with insulin-releasing properties

As well as antimicrobial activity, a number of peptides belonging to different families are able to stimulate the release of insulin. This is particularly relevant, since the subject of the current study, pseudin-2, also stimulates insulin release (Abdel-Wahab *et al.,* 2008).

Before reviewing amphibian peptides with known insulin-releasing properties, it is important to discuss the clinical need for such a therapeutic and the physiological effect of using a therapeutic with insulin-releasing properties, as well as combined insulin-releasing and anti-infective properties. Firstly, however, it is relevant to note the difference between type 1 and type 2 diabetes. Type 1 diabetes is a disorder which results from the autoimmune destruction of the insulin-producing beta-cells of the pancreas. Therefore, individuals suffering from type ii diabetes

require constant insulin injection into the bloodstream since they suffer from a complete lack of insulin (due to the destruction of the insulin-producing cells in the pancreas). This is currently the only treatment that may be used for type 1 diabetes. Type 2 diabetes, on the other hand, is characterised by insulin resistance (cells failing to respond to insulin) or relative insulin deficiency. In this case, therapeutics which possess insulin-releasing properties (such as peptides) would be useful.

There is a number of drugs currently in clinical use for stimulating the release of insulin, such as the drugs glipizide, glimepiride and nateglinide (Brunton *et al.*, 2005). These drugs bring about the closure of K^+ channels on the surface of insulin-producing beta-cells in the pancreas, inhibiting the downstream enzyme cascade that leads to the release of insulin. Since there are already a number of drugs in clinical use for the treatment of type 2 diabetes, there is no clear clinical need for an insulin-releasing peptide.

However, it has recently been shown that individuals suffering from both type 1 and type 2 diabetes suffer from increased risk of lower respiratory tract infection, urinary tract infection, and skin and mucous membrane infection compared to healthy individuals (Muller *et al.*, 2005). Therefore, an insulin-releasing peptide with broad-spectrum antimicrobial activity would potentially be clinically useful, as it would stimulate insulin release whilst also reducing the risk of infection. Nevertheless, there might not be any benefit associated with the clinical use of such a peptide when compared with simply combining an antibiotic and an antidiabetic compound. Additionally, there would be considerable challenges to developing a peptide into an antidiabetic drug since the mechanism of action of the drug would need to be described in detail so its physiological effects are fully understood.

It is also important to note that the use of a peptide with both antimicrobial and antidiabetic properties is if the peptide is used with diabetic individuals, since the peptide could be used as an antidiabetic with its antimicrobial property as a secondary effect. The use of a combined

antidiabetic/antimicrobial as an antibiotic in an individual not suffering from diabetes would be problematic since the peptide would increase the risk of hypoglycaemia in such an individual by stimulating insulin release.

The stimulation of insulin release is a complex process which can be initiated at various steps in the insulin-release pathway. This complexity is evident in the available data on insulin-releasing peptides, in which a variety of mechanisms of action are suggested. Table 1.6.2 below lists all frog peptides with insulin-releasing properties along with their mechanism of action, where known.

Peptide(s)	Cell line, Mechanism	Reference
None (peptide with 75% homology with C-terminus of dermaseptin-BIV precursor)	BRIN-BD11, mechanism unknown	(Marenah *et al.*, 2004)
Five bombesin-related peptides	BRIN-BD11, possible involvement of a cAMP-dependent, G protein-insensitive pathway	(Marenah *et al.*, 2004)
Brevinin-1, Palustrin-1c (48% homology with brevinin-1)	BRIN-BD11, mechanism unknown	(Marenah *et al.*, 2004)
Frog skin insulinotropic peptide (novel)	BRIN-BD11, mechanism unknown	(Marenah *et al.*, 2004)
Pipinin-1	BRIN-BD11, mechanism unknown	(Marenah *et al.*, 2005)
Temporin-1Vb Temporin-1Oe Temporin-1DRb Temporin-1TGb	BRIN-BD11 cells, release occurred via a mechanism of the ATP-dependent K^+ channel pathway	(Abdel-Wahab & Marenah, 2007)
Brevinin-1CBb Ranatuerin-2CBd	BRIN-BD11, mechanism unknown	(Mechkarska *et al.*, 2011)
Tigerinin-1R	BRIN-BD11, possible mechanism involves membrane depolarisation and increase in intracellular calcium	(Ojo *et al.*, 2011)
Brevinin-1E Brevinin-2EC Esculentin-1 Esculentin-1B	BRIN-BD11, in the case of esculentins, possible involvement of both cyclic AMP-protein kinase A and -C-dependent G-protein sensitive pathways	(Marenah *et al.*, 2006)
Rugosin-A-like peptide	BRIN-BD11, mechanism unknown	(Marenah *et al.*, 2005)
Brevinin-2GUb	BRIN-BD11, calcium-independent mechanism	(Conlon *et al.*, 2008)
Phylloseptin-L2	BRIN-BD11 cells, mechanism	(Abdel-Wahab *et al.*, 2008)

	independent of calcium influx and closure of ATP-sensitive K^+ channels	
Brevinin-2-related peptide **Brevinin-2-related peptide-[D4-<K] analogue**	BRIN-BD11 cells, mechanism unknown	(Abdel-Wahab *et al.*, 2010)
Gaegurin 6	Pancreatic β Rin5mf cells, calcium influx	(Kim *et al.*, 2010)
Caerulein-B1 **Xenopsin** **Xenopsin-AM2**	BRIN-BD11 cells, mechanism unknown	(Zahid *et al.*, 2011)

Table 1.6.2 Peptides with known insulin-releasin properties along with the cell lines used in the study and the relevant reference for each peptide/group of peptides.

It is clear that frog skin is a rich source of insulin-releasing peptides, all of which may potentially qualify as candidate therapeutics for the treatment of type-2 diabetes, although the mechanism of action differs considerably between peptides. The data reviewed above shows that in the majority of cases, the mechanism of insulin release of amphibian peptides is not known. Therefore, a considerable amount of study would be required to firstly understand the insulin-releasing mechanism of these peptides in order to test them for clinical use.

1.7 Clinical status of amphibian antimicrobial peptides

Although there are a number of amphibian antimicrobial peptides (as reviewed above), there are currently no peptides in clinical use as a registered product. Of the amphibian peptides mentioned previously, only the peptide magainin-2 reached the stage of advanced (phase III) clinical trials (for use as a topical antibiotic), at which point the clinical study of the peptide was abandoned (Hancock, 1997). Therefore, there is no clear evidence demonstrating the use of amphibian peptide in a clinical setting.

Taking that into consideration, this work aims to demonstrate how pseudin-2 may be used as a antimicrobial by studying the structure of the peptide using spectroscopy as well as *in-silico* methods, and using mutagenesis to improve its antimicrobial properties. It is important to note that although pseudin-2 possesses both antimicrobial (Kim *et al.*, 2007) as well as insulin-releasing

properties, this study deals only with the antimicrobial properties of the peptide. This is described in further detail in the following section.

1.8 The Pseudins

Pseudin-2 (the subject of the current study) is a 24-residue antimicrobial peptide first isolated from the skin of the skin of the South American frog *Pseudis paradoxa* (also commonly known as the 'paradoxical frog') (Olson *et al.,* 2001). It was isolated along with three other members of a new family of amphibian antimicrobial peptides termed 'pseudins'. The primary sequences of the four members of this family of peptides are given in Table 1.8.1 below, along with the MIC values of pseudin-2 against *E. Coli* and *S. Aureus*:

Table 1.8.1 Primary sequences, MIC and HC_{50} values of the pseudin family of peptides, from study by Olson and co-workers (Olson *et al.*, 2001). All data reported in the study is shown.

Table 1.8.1 shows that upon its initial discovery, pseudin-2 was shown to possess broad-spectrum antimicrobial activity (against representative Gram negative, Gram positive and fungal pathogens) whilst only having low haemolytic activity. Naturally-occurring pseudin-2 is active against three microbes, representing the three major classes of microbial pathogens: Escherichia coli (Gram-negative bacterium), Staphylococcus aureus (Gram-positive bacterium) and Candida Albicans (yeast). Moreover, the parental sequence of pseudin-2 can be modified to improve its antimicrobial activity, since the incorporation of lysine residues at positions 8, 10 and 14 produces pseudin-2 analogues that are more potent as antimicrobials (Pal *et al.*, 2005). The same study also showed that this increase of positive charge can also increase the haemolytic activity of the peptide, depending on the position of the substituted lysine residues. Substitutions of L-lysine at

those positions were associated with a two-fold increase in hemolysis relative to D-Lysine at the three positions mentioned.

The mechanism of action of pseudin-2 has also been partially described (Park *et al.,* 2010). Park and co-workers have shown that pseudin-2 has a bactericidal effect on *E. Coli* which is partially inhibited by the presence of LPS. They have shown that pseudin-2 aggregates to form a helical structure and causes the leakage of fluorescent molecules from liposomes. They also present data that they claim shows that pseudin-2 binds to RNA, although that data is questionable. Finally, they suggest a model for the antimicrobial activity of pseudin-2 in which the peptide initially coats the membrane. The peptide then aggregates and creates toroidal pores in the membrane.

Not only is pseudin-2 a broad-spectrum antimicrobial, but it also stimulates insulin release in rat clonal (BRIN-BD11) pancreatic cells (Abdel-Wahab *et al.,* 2008). The lysine-18 analogue of pseudin-2 is even more potent than the parental peptide, stimulating insulin release (Abdel-Wahab *et al.*, 2008), at a level 46% higher than the parental peptide. Additionally, there was no release of lactate dehydrogenase, a marker of cellular damage. This indicates that the insulin release is not accompanied by any damage to the cells. Finally, the insulin-releasing ability of both pseudin-2 and its lys-18 analogue were independent of calcium concentration. Glucose at a concentration of 5.6 mM was used as a negative control in the study.

Therefore, pseudin-2 was chosen as the subject of this study since it has been independently shown that both the antimicrobial (Pal *et al.*, 2005) as well as insulin-releasing (Abdel-Wahab, Power & Ng, 2008) properties of the peptide may be improved by simply altering the primary sequence of the peptide (as discussed above). In this study, however, only the antimicrobial properties of pseudin-2 will be considered. This is because there is a greater clinical need for novel antimicrobials due to the prevalence of antibiotic resistance (as discussed in Section 1.1) relative to insulin release for which effective drugs already exist (Section 1.6.13).

Therefore, the therapeutic utility of pseudin-2 (proposed in this study) would be as a topical antibiotic, similar to the peptide magainin-2 (1.6.13), since the parental peptide possesses broad-spectrum antimicrobial activity. As a result of this proposal, since the peptide would only come into contact with dead cells (on the skin surface), the haemolytic activity of the peptide as well as its insulin-releasing properties become less important, since the peptide does not come into direct contact with the circulation. However, it is important to note that (as discussed in Section 1.6.13), it is not desirable to use an antimicrobial with insulin-releasing properties since the risk of hypoglycaemia would simply be an additional complication in a non-diabetic individual with a bacterial or fungal infection. Nevertheless, the insulin-stimulating property of pseudin-2 may represent an avenue that may be pursued independently to develop a novel antidiabetic drug, but not without significant challenges. The major challenge in such an endeavour would be the need to completely understand the physiological effect of the use of the peptide to stimulate insulin release.

1.9 Hypothesis and aims

Therefore, the hypothesis for this study is as follows:

Pseudin-2 may be developed into an antimicrobial compound for clinical use by:

a) Structural understanding of its antimicrobial action

b) Altering its primary structure

In order to test this hypothesis, the aims of this thesis are as follows:

- To produce a library of pseudin-2 analogues by mutagenesis and screen this library for suitable candidates based on antimicrobial activity.
- To establish a method for the production of pseudin-2 and its analogues.
- To determine the antimicrobial potency of these analogues.

- To use molecular dynamics and biophysical characterization to determine the equilibrium structure of pseudin-2 in a membrane environment.
- To use the combined information from mutagenesis, antimicrobial toxicity testing, molecular modelling and biophysical characterisation, alongside published knowledge concerning pseudin-2 to better understand its mechanism of antimicrobial action.

2 Materials and methods

2.1 DNA Methods:

2.1.1 List of chemicals/reagents

Table 2.1.1.1 below contains the details of chemicals/reagents used in the methods described below:

Chemical/Reagent	Manufacturer	Catalog Number
XmnI Restriction Endonuclease	New England Biolabs	R0194S
HindIII Restriction Endonuclease	New England Biolabs	R0104S
AflII Restriction Endonuclease	New England Biolabs	R0520S
BamHI Restriction Endonuclease	New England Biolabs	R0136S
PmlI Restriction Endoluclease	New England Biolabs	R0532S
T4 DNA Ligase	New England Biolabs	M0202S
T4 DNA Ligase Reaction Buffer	New England Biolabs	B0202S
NEBuffer Set (1, 2, 3, 4 & BSA)	New England Biolabs	B7000S
Antarctic Phosphatase	New England Biolabs	M0289S
Antarctic Phosphatase Reaction Buffer	New England Biolabs	B0289S
Hi-Res Standard Agarose	AGTC Bioproducts	AGD1-500gm
Luria Broth Base, powder	Invitrogen	12795-084
Difco Agar, Granulated	Difco Microbiology	214530
Calcium Chloride, hexahydrate	Fisher Scientific	C/1240/60

Table 2.1.1.1. List of chemicals and reagents used in the subsequent methods.

2.2 Oligonucleotide sequences

Table **2.2.1** below lists all the oligonucleotide sequences used in this thesis. All oligonucleotides were ordered from Eurofins MWG Operon.

Name	Sequence (5'-3')
Pseudin2-top	GGC CTG AAT GCG CTT AAG AAA GTG TTT CAG GGA ATT CAT GAA GCG ATT AAA CTG ATT AAT AAT CAT GTA CAG TA
pseudin-2-bottom	AGCTTA CTG TAC ATG ATT ATT AAT CAG TTT AAT CGC TTC ATG AAT TCC CTG AAA CAC TTT CTT AAG CGC ATT CAG GCC
pMAL-forward	GGTCGTCAGACTGTCGATGAAGCC
pMAL-reverse	TGTCCTACTCAGGAGAGCGTTCAC
ps2_pet45b_top	GGC CTG AAT GCG CTT AAG AAA GTG TTT CAG GGA ATT CAT GAA GCG ATT AAA CTG ATT AAT AAT CAT GTA CAG TAA
ps2_pet45b_bottom	CCG GAC TTA CGC GAA TTC TTT CAC AAA GTC CCT TAA GTA CTT CGC TAA TTT GAC TAA TTA TTA GTA CAT GTC ATTC
mut_top	TTAAG AAA GTG TTT NNK GGT ATT CAT NNK GCG ATT AAA NNK ATT AAT AAT CAT GTA CAG TA
mut_bottom	C TTT CAC AAA NNM CCA TAA GTA NNM CGC TAA TTT NNM TAA TTA TTA GTA CAT GTC ATTCGA
pET45b_PCR_forward	ATGCGTCCGGCGTAGA
pET45b_PCR_reverse	CTTGTCGTCGTCATCAT

Table 2.2.1. Oligonucleotide sequences used for cloning and mutagenesis of pseudin-2.

2.3 Media preparation

2.3.1 Liquid Growth medium

Invitrogen's Luria Broth Base powder was dissolved in distilled water to a concentration of 2% (w/v) and sterilized by autoclaving. When ampicillin was required in the medium, filter sterilized ampicillin was added to a final concentration of 50 µg/ml.

2.3.2 Solid growth medium

Difco agar and Invitrogen's Luria Broth Base were dissolved in distilled water to final concentration of 2% (w/v) and sterilized by autoclaving. When required, filter-sterilized ampicillin was added to a final concentration of 50 µg/ml just before pouring. When IPTG was required, filter-sterilized IPTG was added to a final concentration of 0.3 mM to the cool medium just before pouring. After making any necessary additions, the solution was poured into sterile 100mm Petri-dishes and allowed to set.

2.4 DNA Manipulation

2.4.1 Oligonucleotide phosphorylation

Unless otherwise specified, the reaction was set up as follows: 100 pmol oligonucleotide, T4 DNA Ligase Buffer [1×] , 1 unit of T4 Polynucleotide Kinase and sterile distilled water in a total volume of 10 µl. The reaction mix was then incubated at 37 °C for 60 minutes and 65 °C for 20 minutes. T4 DNA Ligase Buffer was used since it contains the right concentration of ATP and because T4 PNK exhibits 100% activity in this buffer. The two oligonucleotides corresponding to the top and bottom strand were first phosphorylated separately and then the solutions were mixed and annealed.

2.4.2 Oligonucleotide annealing

Unless otherwise specified, the following temperature profile was used to anneal oligonucleotides: 95 °C for 5 minutes, 94 °C-4 °C at 1 °C per minute.

2.4.3 Restriction digest

Unless otherwise specified, the reactions were set up as follows: NeBuffer (1/2/3/4) [1X], enzyme [1U], 1000ng substrate DNA and sterile distilled water in a total reaction volume of 50 µl. The digest mix was incubated at 37 °C for 60 minutes and 65 °C for 20 minutes. When dephosphorylation was required, Antarctic Phosphatase Buffer was added to the digest mix to a final concentration of 1X, and 5U of the Antarctic Phosphatase Enzyme were added. The thermal profile used for dephosphorylation was 15 minutes at 37 °C and 5 minutes at 65 °C.

2.4.4 Ligation

Unless otherwise specified, the reactions were set up as follows: 6 U of enzyme, 100 ng of substrate DNA, DNA Ligase Buffer [1×] and where appropriate, 0.1 pmol/µl of insert in a total volume of 20 µl. The ligation mix was incubated at 16 °C for 18 hours and 65 °C for 20 minutes.

2.4.5 DNA sequencing

Unless otherwise specified, the DNA sequencing mix was set up as follows: 3.2 pmol of sequencing primer and 200-500 ng of template DNA in a total volume of 10 µl. This mix was then taken to Birmingham University where the sequencing reaction was carried out on an ABI 3730 capillary sequencer. The traces were then manually analyzed using Chromas Lite version 2.01. All analyzed sequences were exported to FASTA format.

2.4.6 DNA Alignment

Two types of DNA alignment were used: DNA-DNA and protein-translated nucleotide. In the second type of alignment, the subject DNA sequences are translated into amino acid sequences in all frames and aligned against the query amino acid sequence. BLAST (Altschul *et al.,* 1997) was used for both types of alignments. Default options were used in all cases. For the DNA-DNA alignments, the sense strand of the pseudin-2 cloning sequence was set as the query sequence, and for the protein-translated nucleotide alignment, the amino acid of pseudin-2 was set as the query sequence. In all cases, the subject sequences were the FASTA sequences exported from Chromas Lite.

2.4.7 PCR protocol

Unless otherwise specified, PCR reactions were set as follows: 0.5U Taq polymerase, PCR Buffer [1×], dNTPs [100 µM] , $MgCl_2$ [2 mM], forward + reverse primers [5 pmol each] in a total reaction volume of 25 µl. The thermal profile used was as follows:

95 °C for 5 minutes

95 °C for 30 seconds
55 °C for 30 seconds } `30 cycles
72 °C for 60 seconds

Colony PCR was performed by first streaking each colony inside a sterile PCR tube, followed by streaking on an ampicillin plate (2.3.2). The PCR mix containing all the components was then added to the tube and the reaction was carried out using the thermal profile shown above.

2.4.8 Agarose gel Electrophoresis

Unless otherwise specified, agarose gels were prepared by dissolving agarose in 1× TAE buffer to a final concentration 1% w/v for plasmid DNA and 2% w/v for smaller DNA species. The gel solution was heated in the microwave to dissolve the agarose completely and Ethidium bromide was added to the gel to a final concentration of 0.5µg/ml just before pouring. The appropriate gel volume was selected based on the dimensions of the casting tray. 1X TAE buffer was also used as the running buffer. The 1X TAE Buffer contained 40mM Tris-acetate (pH8.0), 1 mM EDTA, and 20 mM glacial acetic acid. Gels were electrophoresed at 7 V/cm length of gel and visualized on a UV-transilluminator.

2.5 Cell culture protocols

2.5.1 Protocol for producing competent cells

A volume of 30ml of liquid broth (2.3.1) in a 250 ml conical flask was inoculated with a single colony of cells grown on Nutrient Agar (2.3.2). The culture was incubated at 37°C for 16 hours with shaking at 200 rpm. A volume of 30 ml of fresh broth (2.3.1) was then inoculated with 0.3ml of the overnight culture, and incubated at 37 °C for 2 hours with shaking at 200 rpm. The cells were harvested by centrifuging at 4000 rpm for 5 minutes at 4°C. The supernatant was discarded and the pellet resuspended by vortexing in 6 ml of ice-cold 50 mM $CaCl_2$. The cells were then left on ice for 10 minutes. The cells were once again centrifuged at 4000 rpm for 5 minutes at 4°C, resuspended by vortexing in 6 ml of ice-cold 50 mM $CaCl_2$, and left on ice for another 10 minutes. Finally, the cells were centrifuged at 4000 rpm for 5 minutes at 4°C, resuspended by vortexing in 1.2 ml of ice-cold 50 mM $CaCl_2$, and left on ice for 20 minutes. A volume of 100 µl of the cells were

then aliquoted into sterile 0.5ml eppendorf tubes. The plasmid DNA was then added, the suspension was mixed gently by shaking, and was left to stand on ice for 30 minutes. The cells were then heat-shocked by placing in a 37°C water bath for 60 seconds and were then transferred back to the ice for 2 minutes. A volume of 500 µl of broth (2.3.1) was added to each tube, and the tubes were placed in a 37°C water bath for 40 minutes. After this final incubation, 200 µl of each suspension was spread onto an agar plate containing ampicillin (2.3.2).

2.5.2 Small-scale plasmid DNA isolation

Small-scale plasmid DNA isolation was performed using the 'QIAprep Spin Miniprep Kit' made by Qiagen. A single colony was picked from an ampicillin plate and used inoculate a culture of 7 ml LB medium containing ampicillin. The culture was grown for at 37 °C for 16 hours with shaking at 200 rpm. The cells were harvested by centrifugation at 3000 × g for 15 min at 4 °C. The pelleted bacterial cells were resuspended in 250 µl Buffer P1 containing RNAse A and LyseBlue. A volume of 250 µl of Buffer P2 was added and the tube was gently inverted tube 4–6 times to mix. A volume of 350 µl of Buffer N3 was added and the tube was inverted immediately but gently 4–6 times. The cells were then centrifuged at 13,000 × g for 10 min. The supernatant from the previous step was added to the QIAprep Spin Column by pipetting. The column was then centrifuged at 13,000 × g for 60 seconds and the flow-through was discarded. The QIAprep Spin Column was washed by adding 0.75 ml Buffer PB, centrifuging at 13,000 × g for 60 seconds and discarding the flow-through. The column was then centrifuged at 13,000 × g for an additional 1 min to remove residual wash buffer. Finally, the QIAprep Spin Column was placed in a clean 1.5 ml microcentrifuge tube and 50 µl of sterile distilled water was added to the center of the column to elute the plasmid DNA. The column was left to stand for 1 minute and then centrifuged at 13,000 × g for 1 minute. The flow-through contained the plasmid.

2.5.3 Large scale plasmid DNA isolation

The reagents and column used in this protocol were obtained from the 'Genopure Plasmid Maxi Kit' produced by Fischer Scientific. A 200ml volume of ampicillin broth (2.3.1) was inoculated with a single colony from a selective plate containing ampicillin. The bacterial cells from 200 ml *E. Coli* culture for 10 minutes at 4,000 rpm at 4 °C.. The supernatant was discarded and the pellet was resuspended in 12 ml suspension buffer containing RNase and mixed well by gentle shaking. A volume of 12 ml of Lysis Buffer was added to the suspension which was then mixed gently by inverting the tube 6 to 8 times. The suspension was then incubated for 2 minutes at 20 °C. A volume of 12 ml chilled Neutralization Buffer (at 4 °C) was added to the suspension which was then immediately mixed gently by inverting the tube 6 to 8 times until a homogenous suspension is formed. The tube was incubated for 5 minutes on ice. The lysate was cleared by filtration through a paper filter and the flow-through was collected. A fresh column was equilibrated using 6 ml Equilibration Buffer. The column was allowed to empty by gravitational flow and the flow-through was discarded. The cleared lysate from the previous step was loaded onto the equilibrated column. The column was allowed to empty by gravitational flow and the flow-through was discarded. The column was washed twice with 16 ml Wash Buffer, allowed to empty by gravitational flow and the flow-through was discarded. The column was then eluted using 15ml Elution Buffer (pre-warmed to 50 °C), and the flow-through (containing the plasmid) was collected. The eluted plasmid DNA was precipitated with 11ml isopropanol (equilibrated to 20°C) and immediately centrifuged at 15,500 × g for 30 minutes. Finally, the plasmid DNA was washed with 70% Ethanol and centrifuged at 15,500 × g, 4 °C for 10 minutes. The supernatant was then removed carefully using a pipette tip, and the plasmid DNA pellet was air-dried for 10 minutes. Finally, the plasmid DNA pellet was dissolved in 200 µl sterile distilled water.

2.6 Protein purification

2.6.1 Buffers used for protein purification (pET45b construct)

The final concentrations of the components of each buffer are given below:

Lysis Buffer	Wash Buffer	Elution buffer
50 mM NaH_2PO_4	50 mM NaH_2PO_4	50 mM NaH_2PO_4
300 mM NaCl	300 mM NaCl	300 mM NaCl
10 mM Imidazole	20 mM Imidazole	250 mM Imidazole
pH 8.0	pH 8.0	pH 8.0

In each case, all the required components were dissolved in 75% of the volume of distilled water needed to give the final concentrations required. The pH of the buffer was then adjusted to 8.0 using 5 M NaOH, and finally the remaining volume of distilled water was added to give the final concentration required.

2.7 Buffers used for protein purification (pMAL-c5x constructs)

Initially, 20 mM Tris-HCl (pH 7.4) was prepared by dissolving Tris base in 75% of the required volume of distilled water, adjusting the pH to 7.4 using 3 M HCl and adding the remaining volume of distilled water to give the required concentration. This solution was then used as a component in the column buffer containing 20 mM Tris-HCl, 200 mM NaCl and 1 mM EDTA.

This column buffer was then used in affinity purification of expression of the pMAL-c5x constructs. The elution buffer was prepared by adding free maltose to the column buffer to a concentration of 10 mM.

2.7.1 Protein expression

Competent Tuner DE3 cells (reference) were transformed using the construct and 30ml of sterile broth containing ampicillin was inoculated with a single transformed colony. The culture was grown for 18 hours at 37 °C. A volume of 2ml of the overnight culture were diluted 100-fold in 200 ml of sterile broth containing ampicillin. This culture was grown at 37 degrees Celsius to an OD of 0.4-0.6 at 600nm (approximately 2 hours). Sterile IPTG was added to a final concentration of 0.3 mM and the culture was grown at 30 degrees for 18 hours. The cells were then harvested by

centrifugation at 4000 × g for 20 minutes and the supernatant was discarded. For pmal-c5x purification, the pellet was resupended in 6ml column buffer and frozen at -20 °C. For pET45b-constructs, the dry pellet was frozen at -20 °C.

2.7.2 Protein purification of pMAL-c5x constructs

The cells in 200ml of culture were harvested by centrifugation at 4000 × g for 20 minutes and the supernatant was discarded. The pellet was resuspended in 10ml of column buffer and frozen at -20 °C overnight. The cells were then thawed for 10 minutes on ice and the cells were lysed by sonication (6 × 15 second bursts with, pausing for 5 seconds in between). The suspension was then centrifuged at 9000 × g for 30 minutes to obtain the supernatant (cleared lysate) was saved. A volume of 3 ml of the amylose resin was poured into a 5 ml chromatography column and the flow-through was discarded. The column was washed with 24 ml of column buffer. The cleared lysate was then loaded on the column. The column was then washed with 36ml of column buffer. The protein was eluted in 10 fractions of 0.6 ml with column buffer containing 10 mM maltose. The fractions were tested for protein by mixing 10 µL of each fraction with 490 µL of Bradford reagent. The protein-containing fractions were then pooled and stored at 4 degrees Celsius.

2.7.3 Protein expression and purification of pET45b-constructs

The dry pellet was thawed on ice for 10 minutes and the cells were resuspended in 4 ml cell lysis buffer. Lysozyme was added (concentration needed) and the suspended cells were incubated on ice for 30 minutes. The suspension was then sonicated on ice to lyse the cells (6 × 10 second bursts with a 10 second cooling period in between). The cell suspension was centrifuged at 10,000 × g for 30 minutes and the supernatant (cleared lysate) was saved. A volume of 1ml of Ni-NTA Superflow slurry was mixed with 4ml of the cleared lysate and the resultant mixture was placed on a shaker at 200 rpm and incubated at 4 °C for 60 minutes. The lysate-resin mixture was loaded on a chromatography column and the flow-through was collected. The column was washed twice with 4ml wash buffer. The flowthrough from each of the two washes was collected. The proteins were eluted 4 times with 0.5 ml elution buffer.

2.7.4 Factor Xa cleavage of MBP fusions

Factor Xa protease from New England Biolabs (UK) was added to the protein solution to a final solution of 200 ng/µL and the solution was incubated at 25 °C for 24 hours.

2.8 SDS PAGE

2.8.1 Sample preparation

The peptide/protein sample was prepared by mixing the sample with 4× SDS reducing buffer to dilute the concentration of the buffer to 1×. The resultant solution was then incubated at 95°C for 5 minutes after which it was loaded onto the polyacrylamide gel. The recipe for the concentrated (4×) SDS reducing buffer is was prepared to contain 0.0625 M Tris-HCl, pH 6.8, 10% glycerol, 2% SDS , 5% 2-mercaptoethanol and 0.05% bromophenol blue. The Tris-HCl solution used to make the buffer was initially prepared separately by dissolving Tris base in distilled water to a concentration of 0.5 M, and adjusting the pH of the buffer to 6.8. This buffer was then diluted to give the concentration shown above.

2.8.2 Two-phase polyacrylamide gel preparation

In order to prepare the stacking and resolving gels, it is necessary to make two Tris-HCl buffer solutions: 0.5 M Tris-HCl, with pH set to 6.8, and 1.5 M Tris-HCl, with pH set to 8.8. In both cases the pH was set using 6 N HCl. These buffers were then appropriately diluted to give the required concentrations in the stacking and resolving gels, respectively. The gels were prepared by initially preparing the resolving gel solution (adding the TEMED last), pouring the gel between the casting plates, overlaying the gel with a thin layer of isopropanol, and allowing the polymerization to occur. Upon complete polymerization, the isopropanol was removed using filter paper. The stacking gel solution was then prepared (once again adding the TEMED last) and poured on top of the polymerized resolving gel. The comb was then inserted and the stacking gel was allowed to polymerise. The recipes for the stacking and resolving gel solutions are given below. The samples

were prepared as per the method previously described (2.8.1) and run using the Tris-Glycine buffer system (0).

Stacking gel	Resolving gel
0.25 M Tris-HCl pH 6.8	0.0375 M Tris-HCl pH 8.8
0.1% SDS	0.1% SDS
0.1% Ammonium persulfate	0.1% Ammonium persulfate
5-10% Acrylamide solution (37.5:1 acrylamide:bisacrylamide)	15-20% Acrylamide solution (37.5:1 acrylamide:bisacrylamide)
0.08% TEMED	0.08% TEMED

2.8.3 Three-phase polyacrylamide gel preparation

In order to prepare a three-phase gel, the resolving gel solution was prepared as per the recipes shown below (adding TEMED last), poured between the casting plates, and overlaid with 0.5ml of isopropanol. Upon complete polymerization, the isopropanol was removed by absorption with filter paper. The spacer and stacking gel mixtures were then prepared. The spacer gel was poured to a height of 1cm above the resolving gel. Finally, the stacking gel was poured and the comb was inserted. The stacking and spacer gels were then allowed to simultaneously polymerise. Finally, removal of the comb gave the final gel. The peptide/protein sample was prepared as per the method previously described (2.8.1) and electrophoresed using the Tris-tricine buffer system (2.8.5).

Stacking gel	Spacer Gel	Resolving gel
5% Polyacrylamide (37.5:1 acrylamide:bisacrylamide)	5% Polyacrylamide (19:1 acrylamide:bisacrylamide)	5% Polyacrylamide (19:1 acrylamide:bisacrylamide
0.75M Tris-HCl pH 8.5	10% glycerol	1M Tris-HCl, pH 8.5
0.1% APS	1.66M Tris-HCl pH 8.5	0.1% APS
0.1% SDS	1M Tris-HCl pH 8.5	0.1% SDS
0.08% TEMED	0.1% APS	0.04% TEMED
	0.1% SDS	
	0.08% TEMED	

The final layout of the polyacrylamide gel following polymerization is shown in Figure 2.8.3.1 below.

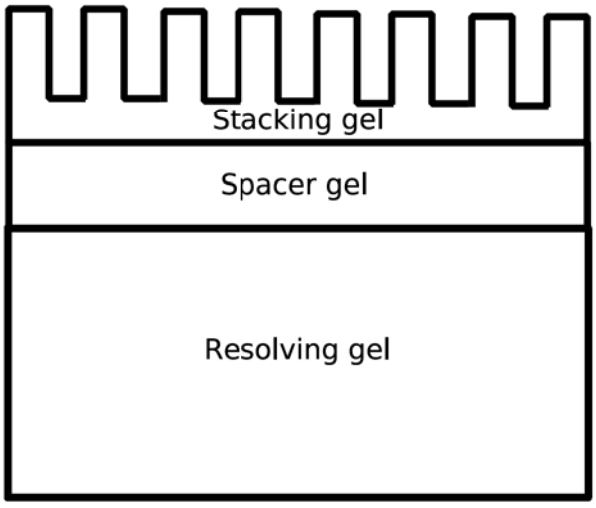

Figure 2.8.3.1 Illustration showing the layout of the three-phase gel used in SDS-PAGE

2.8.4 SDS-PAGE using the Tris-Glycine buffer system

In the case of the Tris-Glycine buffer system, the same running buffer was used in both the anode and cathode compartments of the gel chamber. This buffer is prepared to contain 0.2M Glycine, 0.1% SDS, and 0.01M Tris-base. The pH of the buffer is not adjusted.

2.8.5 SDS-PAGE using the Tris-Tricine buffer system

In the case of the tris-tricine buffer system, two different buffers were used in the anode and cathode compartments of the gel chamber. The recipes for the cathode and anode buffers are given below:

Cathode buffer	Anode buffer
0.1 M Tris	0.2 M Tris-HCl, adjusted to pH 8.5 using concentrated HCl
0.1 M Tricine	
and 0.1% SDS	

2.8.6 Coomassie blue staining

Firstly, the staining and destaining solutions were prepared as follows:

Staining solution	Destaining Solution
10% (v/v) acetic acid	10% (v/v) acetic acid
0.25% (w/v) Coomassie blue G-250	in ddH2O:Methanol (1:1)
in ddH2O:Methanol (1:1)	

The gel was rinsed using distilled water and placed in a small plastic tray. A volume of 50ml of the staining solution was then added to the gel and the gel was incubated with the staining solution for 20 minutes at 25°C with gentle rocking. The staining solution was then discarded and the

destaining solution was added. The gel was then incubated with the destaining solution at 25°C with gentle rocking until the background staining of the gel was completely removed. The gel was then imaged under white light.

2.8.7 Oriole fluorescent gel staining

The gel is placed in a small plastic container and mixed with 25ml of the Oriole fluorescent gel stain from Bio-Rad (#161-0496) so that the gel is completely submerged within the staining solution. The gel was then incubated with the gel at room temperature for 90 minutes with gentle agitation. Finally, the staining solution was discarded, and the gel was imaged on a UV-transilluminator.

2.9 Peptide toxicity testing

2.9.1 Preparation of media for toxicity testing

Both Mueller-Hinton broth and Mueller-Hinton agar were ordered from Oxoid (catalog numbers CM0405 and CM0337) and prepared by dissolving the dehydrated media in distilled water as per the instructions provided. The media were then sterilised by autoclaving and the agar was poured into sterile petri dishes and allowed to set.

2.9.2 Determination of Minimum Inhibitory Concentration (MIC)

The pathogen strains used in the MIC tests were as follows: *E. Coli* NCTC 10536, *S. Aureus* ATCC 6538 and *C. Albicans* ATCC 76615.

In order to determine the MIC of the peptide, the broth microdilution method was carried out in accordance with CLSI standards (Clinical and Laboratory Standards Institute). An overnight culture of the organism was grown on a Mueller Hinton agar (MHA) plate at 37°C. A loopful of the organism was suspended in sterile saline and the optical density adjusted to 1.0 at 470nm. This gave a cell concentration of approximately 10^8 cfu/ml. This suspension was then diluted 1:100 in sterile Mueller Hinton broth (MHB) to give a cell density of 10^6 cfu/ml. A volume of 50 µl of sterile MHB was dispensed into each well on the plate. Peptides were diluted in PBS at the highest concentration possible while maintaining solubility. A volume of 50 µl of the first compound was dispensed into the wells of the first column and mixed thoroughly. A 50µl aliquot was then removed from the wells of the first column and dispensed into the wells of the second column. This process was repeated across the wells of the plate. Each well was then inoculated with a volume of 50 µL of the test organism, with each well inoculated with 10^5 cfu/ml. The microtitre plates were sealed with adhesive plastic film and incubated for 18/24 hours at 37 ºC. Growth of the test organism was seen as a "button" of cells at the bottom of the well. The MIC was recorded as the lowest concentration of the test compound that inhibited growth.

2.9.3 Determination of HC_{50} value of a peptide

The red blood cells are first separated from the plasma and other blood components by centrifugation (1800 rcf for 10 minutes) and resuspended in a volume of PBS as that of the whole blood sample. The blood cells are then diluted 100-fold in PBS to give ~5 x 10^7 cells. A series of eppendorf tubes are prepared with 50 µL of PBS. A volume of 100 µL of the peptide is transferred into an empty eppendorf tube. A volume of 50 µL of this solution is taken and mixed with 50µL PBS in the second tube. This process is repeated to generate 10 dilutions and the last tube is discarded. An additional two tubes are prepared: one with 50µL of PBS and one with 50 µL of 1% Tween-20 dissolved in PBS. These are the negative and positive control, respectively. A volume of 50 µL of the diluted red blood cells are added to each tube (this includes all peptide tubes as well as the positive and negative controls) and mixed thoroughly. The peptide solutions as well as the negative and positive controls are incubated at 37 °C for one hour. All tubes are centrifuged at 12,000 × g for 30 seconds to pellet the cells and any cellular debris. A volume of 90 µL of the supernatant is transferred to a 96-well plate with a flat bottom used for taking optical density measurements. The optical density of each solution is measured at 450nm. Taking the positive control measurement as 100% and the negative as 0%, the haemolysis percentage of the peptide at different concentrations is calculated. The HC_{50} value of the peptide is the concentration of peptide that brings about 50% haemolysis.

2.10 Molecular dynamics

2.10.1 CHARMM Implicit membrane simulation

The WALP16 peptide was generated as a linear peptide using an acetylated N-terminus and a 3-methyl C-terminus. The peptide was initially centered by mass at x=0, y=0, z=0 and then placed at a position of 45 Å on the Z-axis so as to be 17 Å above the implicit membrane. The simulation box was defined as a cube with a side of 110 Å.

The non-bonding parameters were then set up using a smoothing function to gradually reduce an interacting atom pair's contribution with to the energy calculation as distance increases and a switching function to gradually eliminate this contribution. These functions were used for both electrostatic and van-der-waals interactions using the following parameters: 20 Å cutoff for generating interacting atom pairs, a 16 Å cutoff for both the smoothing and switching functions.

Following that, the Born-radii were read from the 'stream_gbsw.inp' file provided with the CHARMM package and the GBSW model was setup using 38 angular integration points, 24 radial integration points with a maximum radial integration distance of 20 Å, a membrane thickness of 28 Å, a membrane switching distance of 2.5 Å and a smoothing distance of 0.3 Å. A solvent dielectric constant of 80 was used and the nonpolar surface tension coefficient of 0.04 was specified.

The heavy atoms of the peptide were constrained harmonically to restrict their movement and then the peptide minimized for 50 steps using steepest descent to remove any bad contacts.

Finally, the molecular dynamics run was initiated using the leapfrog integrator with langevin dynamics using a timestep of 2fs temperature of 310K. The coordinates and energies of the system were saved every 1000 timesteps for further analysis.

2.10.2 Replica-exchange simulations in CHARMM

A linear 3D model of the peptide was constructed in CHARMM (version c35b3) using its primary sequence). The C-terminus and the N-terminus were modelled as acetylated and 3-methyl (designations ACE and CT3) respectively, and all histidine residues were modelled as neutral. The peptide was positioned at 45Å along the Z-axis and minimised for 300 steps using the steepest descent method. The simulation parameters used during the minimization are identical to those used in the replica exchange simulations, with the exception of the non-bonding parameters. In both cases, smoothing and switching functions were used to initially reduce and finally eliminate

the energy contribution of each atom pair. The difference between the minimization and the simulation run was the cutoff parameters used.

The peptide was initially minimized using a 24 Å cutoff for generating interacting atom pairs and a 20 Å cutoff for both the smoothing and switching functions. The minimized peptide was then used in the replica exchange simulations. Each replica-exchange simulation was setup using a 24 Å cutoff for generating interacting atom pairs and a 20 Å cutoff for both the smoothing and switching functions.

Each simulation was run as a GBSW simulation using 38 angular integration points, 24 radial integration points with a maximum radial integration distance of 20 Å, a membrane thickness of 28 Å, a membrane switching distance of 2.5 Å and a smoothing distance of 0.3 Å. A solvent dielectric constant of 80 was used and the nonpolar surface tension coefficient of 0.04 was specified.

Finally, the simulation was run for 1000 steps of 2 fs each using the leapfrog integrator function with langevin dynamics and the temperature at that particular replica. The temperature of the simulation varied depending on the temperature of the replica at the time. The simulations were run and controlled using the MMTSB replica-exchange toolkit (Feig *et al.,*2004). The setup was as follows: 32 identical simulations were set up with starting temperatures ranging from 300K – 800K or 300K-1000K, depending on the length of the peptide. The temperatures chosen for each range are given in Table 2.10.2.1 below

Replica	300-800K range	300-1000K range	Replica	300-800K range	300-1000K range
1	300.00	300.00	**17**	497.71	558.46
2	309.64	311.88	**18**	513.71	580.58
3	319.60	324.23	**19**	530.22	603.57
4	329.87	337.07	**20**	547.27	627.47
5	340.47	350.42	**21**	564.86	652.32
6	351.42	364.30	**22**	583.02	678.16
7	362.72	378.72	**23**	601.76	705.01
8	374.38	393.72	**24**	621.10	732.93
9	386.41	409.32	**25**	641.07	761.96

10	398.83	425.52	**26**	661.67	792.13
11	411.65	442.38	**27**	682.94	823.50
12	424.89	459.90	**28**	704.90	856.11
13	438.54	478.11	**29**	727.56	890.02
14	452.64	497.04	**30**	750.95	925.26
15	467.19	516.73	**31**	775.08	961.91
16	482.21	537.19	**32**	800.00	1000.00

Table 2.10.2.1 Temperatures used in the CHARMM GBSW replica-exchange simulations, both in the 300K-800K and the 300K-1000K temperature ranges. All temperatures are given in degrees Kelvin.

The temperatures chosen were exponentially spaced. Initially, the replicas were initialised using the temperatures given in Table 2.10.2.1. Every 2 ps, an exchange step was attempted in a pairwise manner between the simulations. The Metropolis-Hastings criterion was used to decide whether or not the exchange was successful. The equation for this selection criterion is given below:

$$p = min\left(1, \frac{exp\left(-\frac{E_j}{kT_i} - \frac{E_i}{kT_j}\right)}{exp\left(-\frac{E_i}{kT_i} - \frac{E_j}{kT_j}\right)}\right) = \min\left(1, e^{(E_i - E_j)\left(\frac{1}{kT_i} - \frac{1}{kT_j}\right)}\right)$$

where, E_i = Total potential energy of simulation i

T_i = Temperature (in Kelvin) of simulation i

E_j = Total potential energy of simulation j

T_j = Temperature (in Kelvin) of simulation i

When the criterion was satisfied, the temperatures of the two simulations in question would be exchanged and the atoms in the simulations would be re-initialised at the new temperatures. The atomic coordinates of the peptide and the potential energy of the system were also saved every 2 ps for further analysis.

All simulation snapshots were generated using Visual Molecular Dynamics (University of Illinois) version 1.9.1. Secondary structure assignment was also performed using VMD.

2.10.3 NAMD Simulations

2.10.3.1 Initial setup

First, WALP16 was generated as a linear peptide using an acetylated N-terminus and a 3-methyl C-terminus (designations ACE and CT3 respectively). The peptide was placed at 57 Å along the Z-axis. The lipid membrane was generated using the membrane tool in VMD 1.8.7, using the lipid POPE (phosphatidyl ethanolamine) and using X and Y parameters of 80 Å. The solvate package within VMD was used to generate the water molecules, using the dimensions of the box containing both the peptide and the lipid membrane, using a boundary parameter of 1.5 Å. With regards to the Z-axis parameters passed to solvate, 2 Å on the top and 15 Å on the bottom were added in order to add enough water molecules between the peptide and membrane on either side of the membrane.

2.10.3.2 Minimization of lipid tails

The heads of the lipid molecules within the simulation, the water molecules, as well as the WALP16 peptide were all selected and fixed. A minimization was then run for 1000 steps using the default conjugate gradients minimization algorithm within NAMD to minimize the lipid tails only. Finally, the simulation was run for 0.5 ns to allow the lipid tails to relax further. The simulation parameters used here were identical to those used for the final molecular dynamics run, and are described later.

2.10.3.3 Second minimization

The second minimization was carried out by applying harmonic constrains to all atoms of the WALP16 peptide only. Finally, a minimization was then run for 1000 steps using the default conjugate gradients minimization algorithm within NAMD to minimize the water and lipid molecules around the peptide. Finally, the simulation was run for 0.5ns to allow further relaxation of the system. The simulation parameters used here were identical to those used for the final molecular dynamics run, and are described in the following section.

2.10.3.4 Final simulation setup

The simulation was set up using a temperature of 310K using the all_27 CHARMM force-field. Periodic boundary conditions were set up to match the dimensions of the cubic simulation box used, with the 'cellOrigin' parameter set to the exact center of the box and were applied to all molecules within the system. The force-field and integrator parameters used were a 1-4 scaling parameter of 1.0, and a cutoff of 12 Å. A switching function was used to calculate non-bonded interactions using a switching distance of 10 Å, and a cutoff distance of 13.5 Å to be used to determine non-bonding atom pairs. A timestep of 2fs was used for the default leapfrog integrator function. Particle-Mesh Ewald electrostatics was setup to calculate electrostatic interactions. The parameters used were 80 Å for the X and Y grid sizes and 120 Å for the Z grid size.

Langevin dynamics and constant pressure (variable volume) control were setup using the following parameters:

Parameter	Value	Parameter	Value
Group Pressure	On	Langevin Piston Target (Bar)	1.01325
Flexible Cell	On	Langevin Piston Period (steps)	200
Constant Area	On	Langevin Piston Decay (steps)	50
Langevin Piston	On	Langevin Piston Temperature (K)	310

Finally, the simulation was run for a total time of 108ns. The atomic coordinates were saved every 2ps and the energies were saved every 0.1ps for further analysis.

2.10.4 RMSD Calculation

The backbone RMSD of the peptide was calculated using the RMSD trajectory tool in VMD version 1.8.7. Only the alpha carbon atoms were used for this calculation, and the molecule was centered and aligned in order to eliminate translational changes so only structural changes would be observed. The first frame of the simulation was used as the reference frame. The equation used to calculate the RMSD is given below:

$$RMSD\ (a,b) = \sqrt{\frac{1}{N}\sum_{i=1}^{N}\left((a_{ix}-b_{ix})^2+(a_{iy}-b_{iy})^2+(a_{iz}-b_{iz})^2\right)}$$

where, N = Number of particles

a, b = The two points being compared

a_{ix},a_{iy},a_{iz} = The x, y, and z coordinates of the first point

b_{ix}, b_{iy}, b_{iz} = The x, y, and z coordinates of the second point

2.10.5 Radius of gyration

The radius of gyration of the peptide was calculated for all atoms in the peptide using the following equation:

$$R_g = \sqrt{\frac{1}{N}\sum_{i=1}^{N}(r_i - r_{cm})^2}$$

where, N = Number of atoms

r_i = x, y and z coordinates of the atom in question

r_{cm} = x, y and z coordinates representing the centre of mass of the molecule

2.11 Biophysical characterization

2.11.1 Liposome preparation

The liposomes were prepared using Egg-Phosphatidylcholine from Sigma-Aldrich (P3556). The lipids were dissolved in a chloroform:methanol (9:1) solvent mixture and the solvent was evaporated to yield a dry film. The film was resuspended in distilled water to give a concentration of 10 mg/ml of lipid in water. This protocol is based on a previously described method (Ali *et al.*,2013).

2.11.2 Circular Dichroism

The circular dichroism measurements were carried out using a Jasco J-715 spectropolarimeter with optical density measurements taken in a range of 190 nm-320 nm at a temperature of 25 °C.

The measurements were taken at 0.5 nm intervals. A volume of 80 µL of sample was loaded into a quartz cell with a path length of 1mm. The peptide was mixed with phosphate buffer at pH 7 and in the presence and absence of liposomes. In all cases, the peptide concentration used was 0.1 mg/ml and the liposome concentration was 10 mg/ml. The peptide's structure was determined in the presence and absence of liposomes by measuring background spectra in the absence of peptide, following which a second spectrum was measured in the presence of the peptide. The first spectrum was then subtracted from the first to determine the contribution of the peptide alone. This is described in more detail below:

	Peptide structure in aqueous environment	**Peptide structure in lipid environment**
Spectra measured:	Peptide in buffer (**Spectrum A**) Buffer alone (**Spectrum B**)	Peptide in buffer in the presence of liposomes (**Spectrum A**) Liposomes in buffer (**Spectrum B**)

In both cases, the final spectrum was calculated as follows:

Final spectrum = **Spectrum A** – **Spectrum B**

2.11.3 Linear Dichroism

The linear dichroism measurements were also carried out using a Jasco J-715 spectropolarimeter. Like the circular dichroism measurements, optical density measurements were taken in a range of 190 nm-320 nm at 25 °C with measurements taken at 0.5nm intervals. The linear dichroism setup used is shown below (Figure 2.11.3.1), and is based on the previously published Couette-flow method (Marrington *et al.*,2005).

Figure 2.11.3.1 Diagrams showing (a) the structure of the Couette-flow LD cell and (b) the capillary and rod assembly in the cell. Image taken from paper by Marrington and co-workers (Marrington *et al.*,2005).

A volume of 50 µL of solution was loaded into the quartz tube shown in Figure 2.11.3.1 above and the rod was set to rotate at 3,000 rpm. Background spectra were measured in the absence of the peptide followed by test spectra in the presence of peptide in order to isolate the signal of the peptide. This is described below:

	Peptide structure in aqueous environment	**Peptide structure in lipid environment**
Spectra measured	Peptide in buffer (**Spectrum A**) Buffer alone (**Spectrum B**)	Peptide in buffer in the presence of liposomes (**Spectrum A**) Liposomes in buffer (**Spectrum B**)

In both cases, the final spectrum was calculated as follows:

Final spectrum = **Spectrum A** – **Spectrum B**

2.12 Calculation of peptide properties

2.12.1 Helical potential

Helical potential was calculated using the agadir algorithm (Muñoz & Serrano 1997; Lacroix *et al.*, 1998; Muñoz & Serrano 1995b; Muñoz & Serrano 1995a; Muñoz & Serrano 1994)

2.12.2 Peptide hydrophobicity

Peptide hydrophobicity was calculated using the values published by Kyte and Doolittle (Kyte & Doolittle, 1982). The values for each residue in the peptide were added to give the overall hydrophobicity.

2.12.3 Amino acid distribution in mutagenesis data

First, the amino acids were divided into four groups depending on chemical classification of their side groups, the codons within each group were counted, and the ratio of the total was calculated. The results are shown below:

Group	Amino acids within group	Total number of codons	Ratio of total
Positively charged	K + R + H	1 + 3 + 1 = 5	0.16
Negatively charged	D + E	1 + 1 = 2	0.06
Polar, uncharged	W + Y + S + T + N + Q	1 + 1 + 3 + 2 + 1 + 1 = 9	0.29
Hydrophobic	G + A + V + I + L + C + M + P + F	2 + 2 + 2 + 1 + 3 + 1 + 1 + 2 + 1 = 15	0.48
	Total	31	0.99

The ratios shown above were multiplied by the number of mutant peptides to give the theoretical codon distribution for each group. The number of occurrences of each amino acid were then counted and classified into the groups shown above. This is the observed codon distribution. The percentage variance between the actual and observed codon distributions is then calculated as follows:

Percentage variance = (Observed codon distribution – Theoretical codon distribution) / Number of peptides x 100

For example, taking 10 mutant peptides with one mutated residue, with 2 positively charged, 2 negatively charged and 6 hydrophobic residues found at the mutated position, the calculation is carried out as follows:

Group	Ratio of total	Theoretical codon distribution	Observed codon distribution	Percentage variance
Positively charged	0.16	0.16 × 10 = 1.6	2	(2 – 1.6) / 10 × 100 = 4%
Negatively charged	0.06	0.06 × 10 = 0.6	2	(2 – 0.6) / 10 × 100 = 14%
Polar, uncharged	0.29	0.29 × 10 = 2.9	0	(0 – 2.9) / 10 × 100 = -29%
Hydrophobic	0.48	0.48 × 10 = 4.8	6	(6 – 4.8) / 10 × 100 = 12%

It is important to note that the method described above only applies to mutant peptides produced using NNK mutagenesis.

3 Results – Cloning and mutagenesis

3.1 Introduction

3.1.1 Production of antimicrobial peptides

The study of antimicrobial peptides creates a demand for a method for the production of these molecules in sufficient quantities and in pure form. The two main approaches for achieving this goal are chemical synthesis and bacterial expression. Both approaches are associated with advantages and disadvantages. While chemical synthesis can be used to produce peptides of very high purity and in large amounts, this method becomes expensive when a large number of peptides is involved. This makes expression a more attractive option as it allows for the cost-effective production of a large number of different, but related peptides which may be used in high-throughput screening methods. However, the isolation and purification of peptides using such a method is not trivial. This is due to challenges in visualizing these molecules and separating them from other proteins normally produced by bacterial cells. Additionally, these small peptides are also prone to degradation by bacterial proteases, which further complicates their efficient production. Finally, the successful generation of toxic peptides within the cells might lead to cell death, and this forms the final hurdle production of a large number of peptides in a cost-effective manner. Strategies have, nevertheless, been developed that help overcome these hurdles. Peptides can be successfully produced in bacterial cells by expressing them as concatemers (Morin *et al.*,2006; Kim *et al.*,2008), or by choosing a suitable protein to reduce the toxicity of the peptide and prevent its proteolysis (Skosyrev *et al.*,2003; Xu *et al.*,2007; Yu *et al.*,2010). The data available on such methods suggests that these techniques should be evaluated for each peptide that is to be produced as there is no single method that works for all peptides.

In order to probe the structure-function relationships of antimicrobial peptides, it is necessary to produce mutants that differ from the parent peptide in either one or several residues. These mutants are then tested for activity to find ones that are more potent than the parent peptide.

The expression of peptides in a suitable host system allows for the use of a molecular biology technique known as saturation mutagenesis to generate peptide mutants. This technique and its applications are described below.

3.1.2 Saturation mutagenesis

Saturation mutagenesis or codon randomization is a molecular biology technique which relies on the randomization of codons at a particular position in a peptide/protein in order to mutate the amino acid residue at that particular position. The coding DNA is randomized in order to generate a collection of proteins which vary in the positions selected for mutagenesis. Codon randomization allows for the understanding of the structure-function relationship of a protein/peptide using an unbiased approach. This is generally performed by the generation of a mutagenesis 'cassette': a DNA fragment which is inserted into the gene of interest in order to alter the amino acid sequence of the expressed protein. The discussion that follows will be restricted to codon randomization approaches that use standard molecular biology techniques. Methods that are based on novel chemistry will be excluded. For the sake of simplicity, the three main randomization approaches will be explained using an sample case in which only one codon is randomized.

3.1.2.1 NNN Randomisation

In this method, the mutagenesis cassette contains all the possible codons at the mutated positions (N = A/G/C/T). This is a simple method to generate a gene library with all 20 amino acids at the mutated position. However, due to the redundancy of the genetic code, 64 codons are required to encode all 20 amino acids. This introduces a large disparity between the number of genes and the number of encoded proteins, one which increases exponentially with the increase in the number of randomized codons. This may be reduced by using NNK randomization, which is described below.

3.1.2.2 NNK Randomisation

In the case of NNK randomization, the codon at the randomized position is replaced with NNK (where N=A/G/C/T and K = G/T). Like NNN randomization, this generates a gene library with all 20 amino acids at the randomized position but it considerably reduces the redundancy found in NNN randomization. Using this method, 32 genes are required to encode all 20 amino acids at the randomized position.

In order to apply saturation mutagenesis (either NNN or NNK randomisation) to peptides, a number of residues are selected for mutagenesis. Mutants are generated by substituting the residues at those positions for all 20 amino acids. The entire sequence (consisting of both the conserved as well as the mutated residues) may then be synthesized either as a DNA cassette for insertion into an expression vector or directly as a peptide using chemical synthesis. The peptide mutants may then be tested in order to determine the effect of the mutated residues in question. This is illustrated in Figure **3.1.2.2.1** below using a random peptide sequence:

H-C-C-D-E-R-X-F-S-E-X-R-K-L-I-X-A

Figure 3.1.2.2.1. Illustration of NNK randomisation using a random peptide sequence. Amino acid residues in red denote the residues selected for mutagenesis while amino acids in black show the conserved residues.

3.1.3 Applications of saturation mutagenesis

Saturation mutagenesis has been heavily used to probe the activity of a number of enzymes, such as proteases (Vojcic *et al.*,2013; Varadarajan *et al.*,2005), lipases (Peng, 2013; Yedavalli & Madhusudhana Rao, 2013), tyrosine kinases (Williams *et al.*,2013), tyrosine hydroxylases (Daubner *et al.*,2013), as well as carbonyl reductases (Jakoblinnert *et al.*,2013). The application of saturation mutagenesis to the study of enzyme activity is a logical one, since most enzymes possess an active site consisting of a small number of amino acids. This active site is crucial in determining the activity and properties of the enzyme, and therefore its utility. Therefore, by the

mutation of the small number of residues, it is possible to generate enzyme mutants greatly improved characteristics.

Although the use of saturation mutagenesis in the study of enzymes is well-established, the utility of this technique is not limited to the study of large proteins. Saturation mutagenesis has recently been applied to the study of peptides. In the case of the antimicrobial peptide Nisin A, where the substitution K12 -> A gave a peptide with a two-fold increase in toxicity (Molloy *et al.*, 2013). An extensive mutagenesis study was also conducted using the lantibiotic actagardine A, where all amino acids except those forming the thioester bridge were mutated (Boakes *et al.*,2012). The large number of mutant peptides obtained were screened for antimicrobial activity, which led to the identification of the mutant [V15 -> F] with improved activity against Gram positive pathogens. Additionally, although saturation mutagenesis has not been applied directly to pseudin-2, substitution of lysine at positions 3, 10, 14 of the peptide gives rise to mutants that are four times more toxic to *E. Coli* and eight times more toxic to *S. Aureus*. It is therefore, clear, that this approach has been successfully applied to antimicrobial peptides to yield mutants with improved antimicrobial activities.

It is important to note that although mutagenesis leads to the identification of peptides with improved properties (as discussed above), it does not lead to an understanding of the structure-function properties of these peptides. This is since the residues to be mutated are either randomly selected or all residues of the peptide are substituted simultaneously. Structural data obtained from spectroscopic techniques such as NMR and LD and CD spectroscopy, as well as *in-silico* approaches such as molecular dynamics can help understand the underlying mechanism for the mechanism of the antimicrobial action of these peptides. In addition to saturation mutagenesis, the structural study of pseudin-2 (using LD/CD spectroscopy as well as molecular dynamics) has also been carried out.

3.1.4 Aims

This work aimed to create a synthetic gene to encode pseudin-2, suitably designed for subsequent expression and saturation mutagenesis (to create a library of pseudin-2 variants). This relates to the second component of the hypothesis, altering the primary structure of the peptide. The hypothesis is given below:

Pseudin-2 may be developed into an antimicrobial compound for clinical use by:

a) Structural understanding of its antimicrobial action

b) Altering its primary structure

The pseudin-2 gene was to be cloned in three expression vectors: pMAL-c5x, pMAL-p5x (Chapter 3) and pET45b (Chapter 4). Both pMAL vectors express the peptide as an N-terminal fusion to Maltose Binding Protein (MBP) a large fusion partner, which should prevent degradation and facilitates purification. Proteins expressed from pMAL-c5x are retained in the cytoplasm of the cell whereas those expressed from pMAL-p5x are shuttled to the periplasm of the cell. In contrast, the pET45b vector expresses the peptide as a C-terminal fusion to a small 6xHis tag which simply facilitates purification. The selection of these three expression vectors allowed for three different expression strategies: expression with a large fusion partner both cytoplasmically and periplasmically, as well as the expression with a small fusion partner.

3.2 Pseudin-2 cloning

The sequence of pseudin-2 was obtained from a study on the isolation and properties of pseudin-2 (Olson *et al.,* 2001). A termination codon was added to the amino acid sequence, which was then reverse-translated for the preferred codons of *E. Coli* using the Codon Usage Database (Nakamura *et al.,* 2000). A *Hind*III overhang was incorporated (5'-AGCT-3'), to facilitate cloning in the pMAL-p5x and pMAL-c5x expression vectors by double digestion with *Xmn*I and *Hind*III. The *Xmn*I site was chosen since it allowed for the expressed peptide to be cleaved using a protease, Factor Xa, without leaving any vector-derived amino acids on the peptide. The sequence was also

designed to contain *Afl*II, *Eco*RI restriction sites for subsequent saturation mutagenesis and colony screening. The DNA was ordered as two oligonucleotides, one corresponding to each of the top and bottom strands (

Figure **3.2.1**).

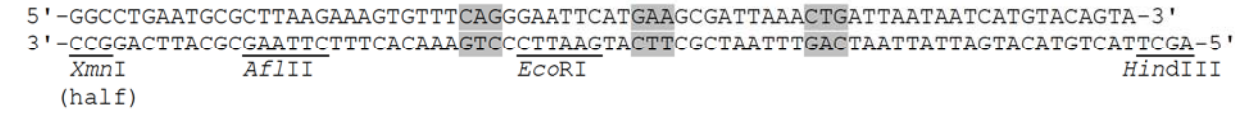

Figure 3.2.1. Oligonucleotides sequences used to construct a synthetic pseudin-2 gene. Positions to be randomised during saturation mutagenesis are highlighted with gray shading.

3.3 Cloning of pseudin-2

Plasmids pMAL-c5x and pMAL-p5x were both obtained from New England Biolabs and a plasmid Maxi-prep (0) was prepared of each. Each plasmid (5 µg) was double-digested using 15 units each of *Xmn*I and *Hind*III and dephosphorylated (2.4.3). Meanwhile, the two pseudin-2 oligonucleotides were phosphorylated (2.4.1) and annealed (2.4.2), to form the double-stranded insert.

3.3.1 Insertion into vector pMAL-c5x

The prepared pseudin-2 gene was ligated with 100ng *Xmn*I/*Hind*III-digested pMAL-c5x vector using T4 DNA Ligase (2.4.4) in 5-fold molar excess. Competent *E. Coli* DH5α cells were prepared and transformed (2.5.1) with 10ng of the uncut vector, digested vector, self ligated vector (as transformation controls) and the fragment-ligated vector. The resulting colony counts are given in Table 3.3.1.1:

pMAL-c5x uncut	632
Cut pMAL-c5x (*Xmn*I + *Hind*III digested)	95
Self-ligated pMAL-c5x	27
Fragment-ligated pMAL-c5x	24

Table 3.3.1.1. Colony counts for the c5x pseudn-2 cloning experiment.

The data above shows a number of features. Firstly, the large number of colonies obtained with the intact plasmid show that the parental vector was of high purity and the transformation method used was appropriate. The relatively large number of colonies of the double-digested

plasmid shows that the digest was not completely successful. The large number of colonies obtained with the digested plasmid since there is a relatively large number of plasmid molecules not linearised by either restriction endonuclease. Finally, in comparing the self and the fragment ligation transformations, it is clear that the ligation with the pseudin-2 gene is only marginally favoured compared to the simple re-ligation of the linearised vector in the absence of insert.

Since the size of the pseudin-2 insert was comparable to the size of the fragment removed from the vector by double-digest, colony screening was performed by PCR amplification (2.4.7) followed by a *Bam*HI digest of the PCR product (2.4.3), since successful insertion of pseudin-2 eliminates the *Bam*HI restriction site from the vector. The pMAL-forward and pMAL-reverse PCR primers (2.2) were used in this amplification.

Twenty colonies from the fragment ligation plate were selected and the multiple cloning site of the plasmid was then amplified by colony PCR (2.4.7) using the standard PCR protocol except for the amount of Taq polymerase used (0.5U per reaction) and amount of the forward and reverse primers (12.5 pmol of each primer). Following PCR amplification, 1U of *Bam*HI was added to each 25 µl reaction, as well as NeBuffer 2 to a final concentration of 1X in a total volume of 100 µl. The resultant digest mix was then incubated at 37°C for 1 hour and 65°C for 20 minutes. Samples of each reaction were then electrophoresed on an agarose gel (2.4.8) in order to determine whether or not a *Bam*HI restriction site was present.

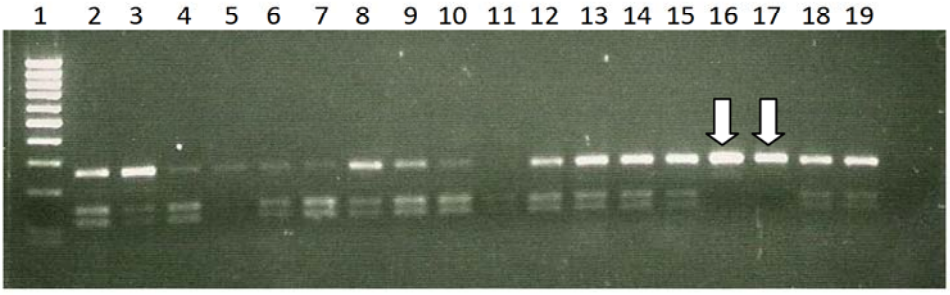

Figure 3.3.1. Gel image showing digested PCR products from pseudin-2 c5x cloning experiment. The gel (2% agarose) was loaded as follows: Lane 1: 1000ng of MassRuler Low Range DNA Ladder, Lanes 2-19: 50% of colony-screen PCR reaction. PCR products containing the pseudin-2 insert, indicated by the absence of a *Bam*HI digest product, have been indicated (lanes 16 and 17).

The gel image (Figure 3.3.1) shows that two colonies did not digest with *Bam*HI (as indicated by the missing double bands corresponding to the digest). Plasmid DNA from these colonies was then isolated on a small scale (2.5.2), and a sequencing solution was prepared using the pMAL-forward primer. DNA sequencing (2.4.5) and alignment (2.4.6) confirmed the presence of the pseudin-2 insert in both colonies. Large-scale plasmid isolation (0) was then performed on one of the colonies.

3.3.2 Cloning of pseudin-2 in pMAL-p5x

Plasmid pMAL-p5x was ligated with the prepared pseudin-2 gene using T4 DNA ligase (**2.4.4**). Owing to the high background of non-recombinant colonies in section **3.3.1**, the self and fragment ligation reactions were re-digested with by adding 3 units of *Bam*HI and NeBuffer 2 [1X] in order to reduce the amount of uncut/self-ligated vector (**2.4.3**). These digests were incubated at 37°C for 3 hours and 65°C for 20 minutes. Finally, competent cells were produced and transformed (**2.5.1**) with 10ng of uncut, digested, self-ligated and fragment-ligated vector. The colony counts are given in Table **3.3.2.1** below:

pMAL-p5x uncut	2400
Digested pMAL-p5x (*Xmn*I + *Hind*III digested)	3
Self-ligated pMAL-p5x	9
Fragment-ligated pMAL-p5x	18

Table 3.3.2.1. Colony counts for the p5x pseudin-2 cloning experiment.

Seventeen colonies were screened by colony-PCR under standard conditions except for the amount of forward and reverse primers used [10 pmol of each primer per reaction] (2.4.7). Each PCR reaction was then digested by adding 1 unit of *Bam*HI and NeBuffer 2 [1x] in a total volume of 100 µl (2.4.3). Samples of this digest were then loaded onto a 2% standard agarose gel and electrophoresed (2.4.8). Figure 3.3.2.1 below shows the result of this screen.

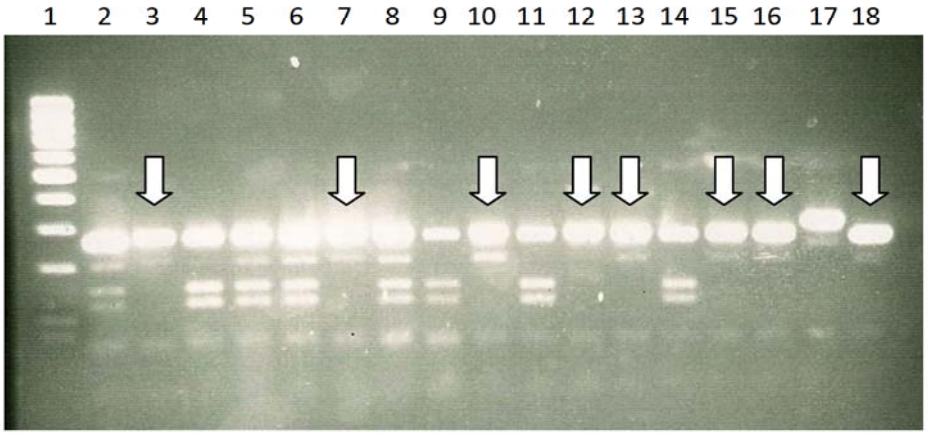

Figure 3.3.2.1. Gel image showing digested PCR products from pseudin-2 p5x cloning experiment. The gel (2% agarose) was loaded as follows: Lane 1: 1000ng of MassRuler Low Ranger DNA Ladder, Lanes 2-18: 10% of the final mixture (PCR reaction digested with *Bam*HI). PCR products containing the pseudin-2 insert, indicated by the absence of a *Bam*HI digest product, have been indicated (Lanes 3, 7, 10, 12, 13, 15, 16 and 18).

Eight colonies (highlighted) contained no *Bam*HI restriction site. Small scale plasmid isolation was performed on these sequences, and the plasmid solutions were sequenced using the pMAL-forward primer (2.4.5). One colony containing the correct sequence was selected and used to perform large-scale plasmid DNA isolation (0).

3.4 Saturation mutagenesis of pseudin-2 in pMAL-c5x

Positions 10 and 14 of pseudin-2 were selected for mutagenesis since it has previously been shown that positions 10 and 14 of pseudin-2 can be mutated to alter the antimicrobial activity of pseudin-2 against *E. Coli*, *S. Aureus* and *C. Albicans* and its haemolytic activity (Pál *et al.*,2005). Additionally, it has been shown using CD spectroscopy that pseudin-2 is helical in structure (Park *et al.*, 2011). Assuming a helical structure for pseudin-2, with 3.6 residues per turn of an alpha helix, residues 10 and 14 would be located roughly on the same 'face' of the helical structure. Position 18 of pseudin-2 was additionally selected for mutagenesis in order that all three mutated residues occur on the same side of the helical structure. Position 18 has been shown to be crucial to the insulin-releasing ability of pseudin-2, with the Lys-18 analogue showing a 100% increase insulin release compared to native pseudin-2 (Abdel-Wahab, Power & Ng, 2008). However, the

role of this residue in the antimicrobial action of pseudin-2 has not been investigated. Therefore, NNK saturation mutagenesis of positions 10, 14 and 18 was undertaken. This should produce a theoretical library of 8000 unique peptides. Two oligonucleotides were designed to have two 5'overhangs in order that the insert could be incorporated into the vector by cassette mutagenesis following double digestion with AflII and *Hind*III.

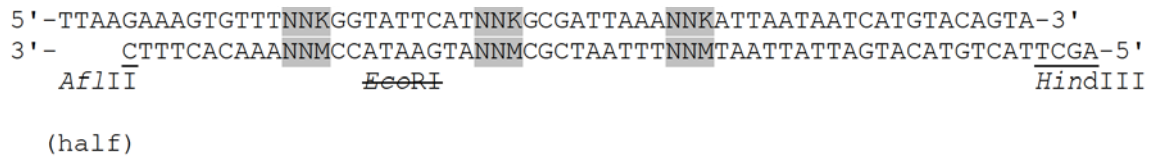

Figure 3.4.1. Oligonucleotides sequences used in NNK mutagenesis of pseudin-2

A single-base silent mutation was also incorporated to eliminate the *Eco*RI restriction site, so that *Eco*RI digestion can be used to linearize any vectors containing the original pseudin-2, thereby eliminating them from the subsequent transformation. The mutagenesis cassette was ordered as two oligonucleotides, one corresponding to each of the top and bottom strands (

Figure **3.4.1**).

In order to produce novel pseudins, 1 µg of the pMAL-c5x pseudin-2 construct was double-digested using one unit each of AflII and *Hind*III (2.4.3). The digest was incubated at 37°C for 3 hours and 65°C for 20 minutes. The two oligonucleotides, were phosphorylated (2.4.1) and annealed (2.4.2) to form a double stranded mutagenesis cassette. One hundred ng of the digested c5x_pseudin-2 was ligated with 0.1 pmol of the insert using 6 units of T4 DNA Ligase (2.4.4). Resulting colony counts are given in Table 3.4.1. Multiple fragment ligation plates were produced in order to produce a large number of pseudin-2 analogues.

Transformation	Intact Vector	Digested vector	Self Ligation	Fragment Ligation[a]
Colonies	2160	5	43	**145**, **124**, 208, 129, 162, 246, 144, 190

Table 3.4.1. Colony counts from the mutagenesis experiment. Numbers in bold indicate plates from which colonies were picked for sequencing. [a]Each number refers to the colony count on a separate plate of clones.

3.5 Screening for novel Pseudins with antibacterial activity

A high-throughput replica plating method was created to screen the novel mutants.

Fragment ligation plates highlighted in bold in Table 3.4.1 were replica plated onto one plate containing ampicillin only and another containing ampicillin plus IPTG. IPTG induces expression of the cloned gene. Thus, it was reasoned that if the encoded peptide is toxic to the cells when expressed in the cytoplasm, the replica-plated colony should not grow in the presence of IPTG. The corresponding colony could then be identified and sub-cultured from the uninduced (ampicillin-only) plate. Therefore, colonies that were missing from the IPTG plate were picked from the ampicillin plate and used to perform small-scale plasmid isolation (2.5.2). The isolated plasmid DNA (1 µg) was then digested with *Eco*RI (2.4.3) and electrophoresed (2.4.8) in order to determine the presence/absence of the mutagenised segment, since *Eco*RI digests only parental DNA. The gel images following electrophoresis are shown in Figure 3.5.1.

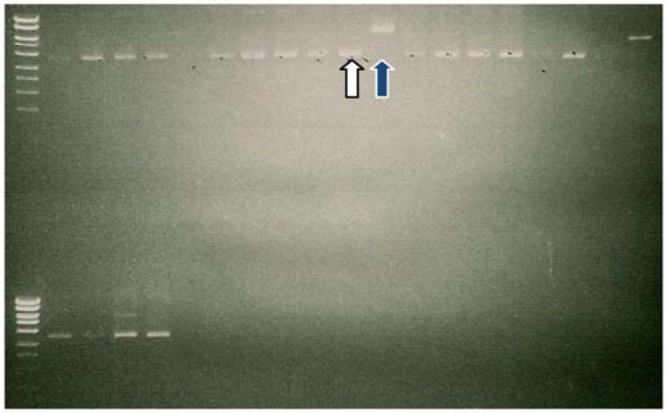

Figure 3.5.1. Gel image showing sample screening of plasmids for the presence of a mutated insert. Absence of a linearized plasmid band (white arrow: indicating the absence of an *Eco*RI restriction site) indicates the presence of the mutated insert. Digestion with *Eco*RI (blue arrow) indicates the presence of the original pseudin-2 insert. Samples were electrophoresed on a 1% agarose and 1000 ng MassRuler High Range DNA Ladder.

All positive plasmids isolated were sequenced (2.4.5) and a sequence alignment was performed (2.4.6) in order to determine the amino acid sequence of the expressed Pseudins. The coupled mutagenesis and screening procedure is illustrated in Figure **3.5.2** below. Sequence data is shown in Table 3.5.1.

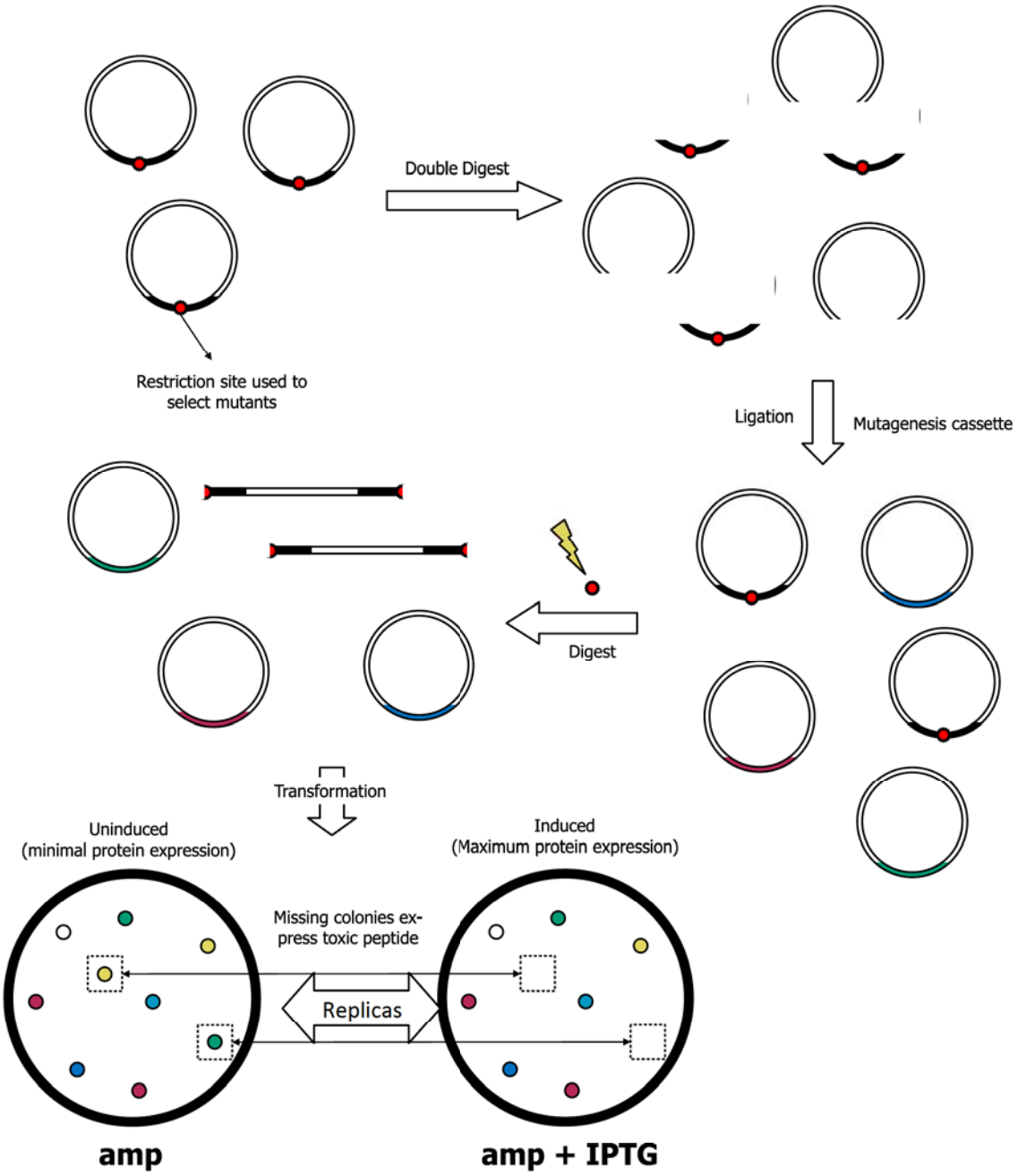

Figure 3.5.2. Mutagenesis workflow. The figure shows subcloning of the mutagenesis cassette and the additional digest step used to eliminate the original plasmid. *E. Coli* cells were transformed and replica plating onto the induction medium revealed which colonies expressed a toxic peptide. These colonies were then picked to isolate the plasmid which was then sequenced to determine the sequence of the peptide.

Table 3.5.1 below contains the sequences of novel toxic and non-toxic pseudin-2 analogues as determined by replica plating analysis. A few non-toxic mutants were also selected to facilitate future analysis.

Sequence	Charge	Helical potential	Activity
GLNALKKVF**C**GIH**T**AIK**H**INNHVQ	3	0.93	Toxic
GLNALKKVF**S**GIH**H**AIK**I**INNHVQ	3	0.76	Toxic
GLNALKKVF**D**GIH**S**AIK**Y**INNHVQ	2	0.95	Toxic
GLNALKKVF**L**GIH**M**AIK**P**INNHVQ	3	1.77	Toxic
GLNALKKVF**Y**GIH**K**AIK**I**INNHVQ	4	1.35	Toxic
GLNALKKVF**T**GIH**S**AIK**L**INNHVQ	3	0.78	Toxic
GLNALKKVF**W**GIH**V**AIK**D**INNHVQ	2	1.15	Toxic
GLNALKKVF**V**GIH**S**AIK**C**INNHVQ	3	1	Toxic
GLNALKKVF**W**GIH**T**AIK**M**INNHVQ	3	1.34	Toxic
GLNALKKVF**C**GIH**K**AIK	4	1.21	Toxic
GLNALKKVF**H**GIH**S**AIK**R**INNHVQ	4	0.94	Toxic
GLNALKKVF**S**GIH**G**AIK**M**INNHVQ	3	0.8	Toxic
GLNALKKVF**L**GIH**L**AIK**M**INNHVQ	3	2.55	Toxic
GLNALKKVF**K**GIH**L**AIK**L**INNHVQ	4	1.41	Toxic
GLNALKKVF**W**GIH**G**AIK**S**INNHVQ	3	1.07	Toxic
GLNALKKVF**H**GIH**R**AIK**V**INNHVQ	4	0.77	Toxic
GLNALKKVF**G**GIH**V**AIK**S**INNHVQ	3	0.75	Toxic
GLNALKKVF**C**GIH**F**AIK**G**INNHVQ	3	0.9	Toxic
GLNALKKVF**D**GIH**L**AIK**N**INNHVQ	2	1.06	Toxic
GLNALKKVF**S**GIH**L**AIK**G**INNHVQ	3	0.89	Toxic
GLNALKKVF**Y**GIH**T**AIK**G**INNHVQ	3	1.23	Toxic
GLNALKKVF**I**GIH**W**AIK**W**INNHVQ	3	1.29	Toxic
GLNALKKVF**V**GIH**S**AIK**T**INNHVQ	3	0.96	Toxic
GLNALKKVF**L**GIH**M**AIK	3	2.26	Toxic
GLNALKKVF**S**GIH**L**AIK**G**INNHVQ	3	0.89	Toxic
GLNALKKVF**P**GIH**T**AIK**L**INNHVQ	3	1.23	Toxic
GLNALKKVF**G**GIH**W**AIK**M**INNHVQ	3	0.93	Toxic
GLNALKKVF**K**GIH**T**AIK**N**INNHVQ	4	1.09	Toxic
GLNALKKVF**R**GIH**W**AIK**W**INNHVQ	4	1.17	Toxic
GLNALKKVF**L**GIH**L**AIK**A**INNHVQ	3	2.47	Toxic
GLNALKKVF**F**GIH**N**AIK**F**INNHVQ	3	1.24	Toxic
GLNALKKVF**R**GIH**P**AIK**L**INNHVQ	4	0.98	Toxic
GLNALKKVF**K**GIH**T**AIK**N**INNHVQ	4	1.09	Toxic
GLNALKKVF**I**GIH**Q**AIK**I**INNHVQ	3	1.16	Toxic
GLNALKKVF**S**GIH**G**AIK**I**INNHVQ	3	0.76	Toxic
GLNALKKVF**T**GIH**R**AIK**I**INNHVQ	4	0.81	Toxic
GLNALKKVF**F**GIH**G**AIK**A**INNHVQ	3	1.12	Non-toxic
GLNALKKVF**N**GIH**P**AIK**L**INNHVQ	3	0.91	Non-toxic
GLNALKKVF**F**GIH**P**AIK**I**INNHVQ	3	1.05	Non-toxic
GLNALKKVF**T**GIH**W**AIK**P**INNHVQ	3	0.58	Non-toxic
GLNALKKVF**T**GIH**V**AIK**A**INNHVQ	3	0.83	Non-toxic

Table 3.5.1. Active and Inactive pseudin-2 analogues generated by conventional codon randomization, along with calculated values of hydrophobic moment, mean residue hydrophobicity, molecular mass, charge and helical potential. Substituted residues have been highlighted in bold font.

3.6 Saturation mutagenesis of pseudin-2 in pMAL-p5x

Experiments detailed in sections 3.4 and 3.5 were repeated with plasmid pMAL-p5x (periplasmic expression). Interestingly however, the sequence data obtained using the replica method in the pMAL-p5x constructs revealed a large number of deletions and point mutations. This may be explained based on the periplasmic expression system of this vector. Since pseudin-2 exerts its effects by membrane interaction, shuttling of a pseudin-2 fusion would, in theory, lead to high toxicity since the peptide would be exposed to both membranes of the bacterial cell. In light of the mutations observed when using this vector, it was decided that further study of the peptide be attempted using only the pMAL-c5x constructs.

3.7 Discussion

The residue distribution of the toxic peptides generated in plasmid pMAL-c5x was analysed and compared to the expected values if the distribution of residues at each position was completely random. Taking into account the redundancy in the genetic code, the expected random occurrence of a residue at a particular position was compared with the residue distribution at each of the mutated position: 10, 14 and 18. This analysis is shown in Figure **3.7.1** below.

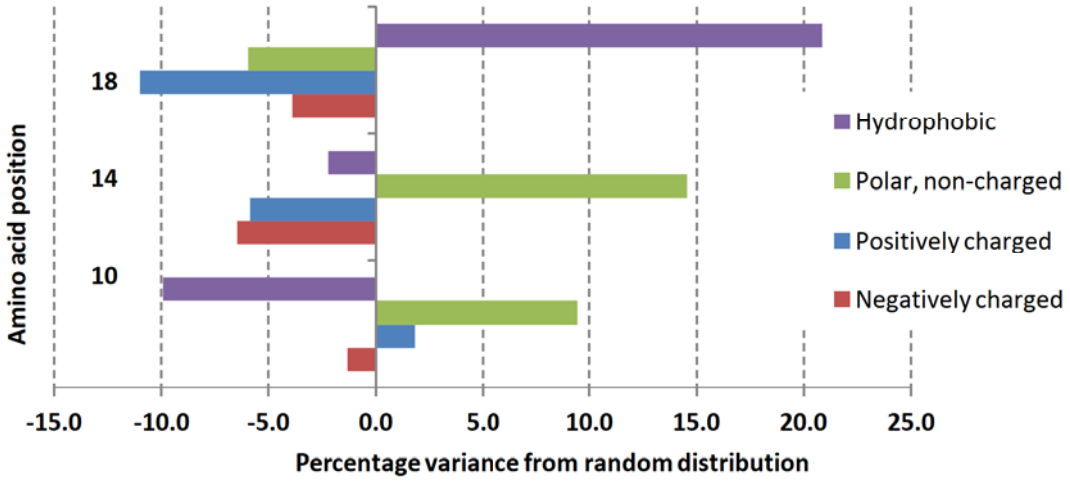

Figure 3.7.1. Occurrence of different classes of amino acids at the mutated positions compared to the values expected given a random distribution.

Assuming all toxic peptides generated using the replica-plating method are genuine toxic mutants, the data presented above shows a number of interesting features. At position 18, hydrophobic residues are favoured. With regards to positions 14 and 10, however, it is the polar, non-charged residues that are favoured. This is an interesting finding since previous studies suggest that positive charges are required at these positions (Pal *et al.*, 2005).

3.8 Conclusion

Since the peptides shown in Table 3.5.1 were screened by toxicity following cytoplasmic expression, it not possibly to determine the relative toxicity of the mutants to native pseudin-2. It is also not possible to determine the toxicity of the mutants relative to one another since the cytoplasmic concentration of the expressed fusion could not be determined. Finally, one may speculate that this apparent toxicity is due to the peptide fusions being cleaved by cellular proteases within the bacterial cell, releasing the toxic peptide into the cytoplasm of the cell. However, the extent of this cleavage was also not determined. Finally, literature data always pertains to the testing of purified peptides. Since the cytoplasmic concentration of the toxic pseudin-2 mutants obtained by replica-plating is not known, this data cannot be directly compared to published toxicity data. Therefore, it is necessary to attempt to synthesise purified pseudin-2 mutants, either by expression or by chemical synthesis. These two methods are described in Chapters 4 and 5, respectively.

4 Expression and attempted isolation of pseudin-2

4.1 Aims

The aim of this work is to establish a protocol for the expression of pseudin-2 and pseudin-2 mutants in *E. Coli* and its subsequent isolation and purification. Once purified, it becomes possible to determine the antimicrobial activity of the isolated peptides against representative pathogens as well as their haemolytic activity. This work relates to the second element of the hypothesis, since successful expression of purified pseudin-2 would enable testing of the antimicrobial properties of pseudin-2 mutants, as in the second component of the hypothesis, which is given below.

Pseudin-2 may be developed into an antimicrobial compound for clinical use by:

a) Structural understanding of its antimicrobial action

b) Altering its primary structure

4.2 Protein expression in protein pMAL-c5x

In order to establish a working protocol for the production of recombinant pseudin-2, *E. Coli* Tuner DE3 cells were transformed with pMAL-c5x-pseudin-2 (2.5.1) and grown using standard conditions (2.7.1). The same process was followed for the parental construct pMAL-c5x. The standard protocol was followed for the purification of MBP fusion proteins in both cases (0). Following the column purification of the MBP (pMAL-c5x) and MBP-pseudin-2 fusion were analysed using SDS-PAGE. The protein samples were prepared (2.8.1), a two-phase gel prepared (2.8.2), and the samples were electrophoresed using a Tris-Glycine buffer system (0). Finally, the gel was stained using Coomassie Blue (2.8.6). Figure 4.2.1 shows the resulting gel image.

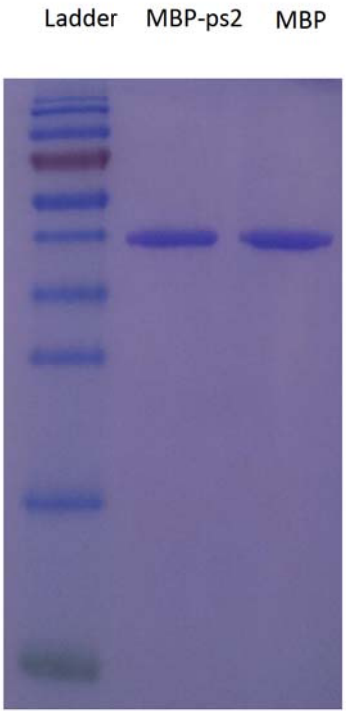

Figure 4.2.1 SDS-polyacrylamide gel (15%) loaded with 5uL Pageruler Prestained Protein Ladder, and 1.5µg each of MBP-pseudin-2 and parental MBP. Gel was stained using coomassie blue. (Gel was run using a Tris-Glycine buffer system [0])

Figure 4.2.1 shows that in both cases, the fusion protein is of high purity, since no additional protein bands are visible. However, it can also be seen from Figure 4.2.1 that there is no apparent difference between the sizes of the two protein bands. This may be due the inability of the gel to resolve the small difference in size between the two bands (~2.5kDa), or else may result from post-translational cleavage.

To enable visualisation of the pseudin-2 peptide, various PAGE formats were examined to give the best resolution of a low MW protein marker. A tricine SDS-PAGE buffer system was examined, since this is reputed to be optimal for the efficient separation of smaller molecules. Additionally, a three-phase gel was used to further enhance resolution (Schägger, 2006). Tricine (as opposed to glycine), a 3-stage gel (as opposed to a conventional stack/resolve PAGE) gave the best resolution of low MW species.

To attempt to isolate pseudin-2 from the pseudin-2-MBP fusion protein (Figure 4.2.1) was cleaved using Factor Xa to liberate the free peptide (0). The resulting products were separated using an

Amicon filtration device with a 10kDa cutoff, which should capture the larger MBP fragment while allowing the peptide to flow through. An alternative purification regime was also followed, involving on-column cleavage of the fusion partner using Factor Xa (0), to compare efficacy.

These products were then all examined using a 3-phase tricine PAGE gel. The samples (2.8.1) and three-phase gel (2.8.3) were prepared and electrophoresed using a Tris-Tricine buffer system 2.8.5) and the gel was stained with the Oriole fluorescent gel stain (2.8.7), since its manufacturers claim it has a higher sensitivity to small peptides. The resulting products of purification, visualised in this manner, are illustrated in Figure 4.2.2 alongside the chemically-synthesised peptide Bombesin (1.6 kDa) as a visualisation standard.

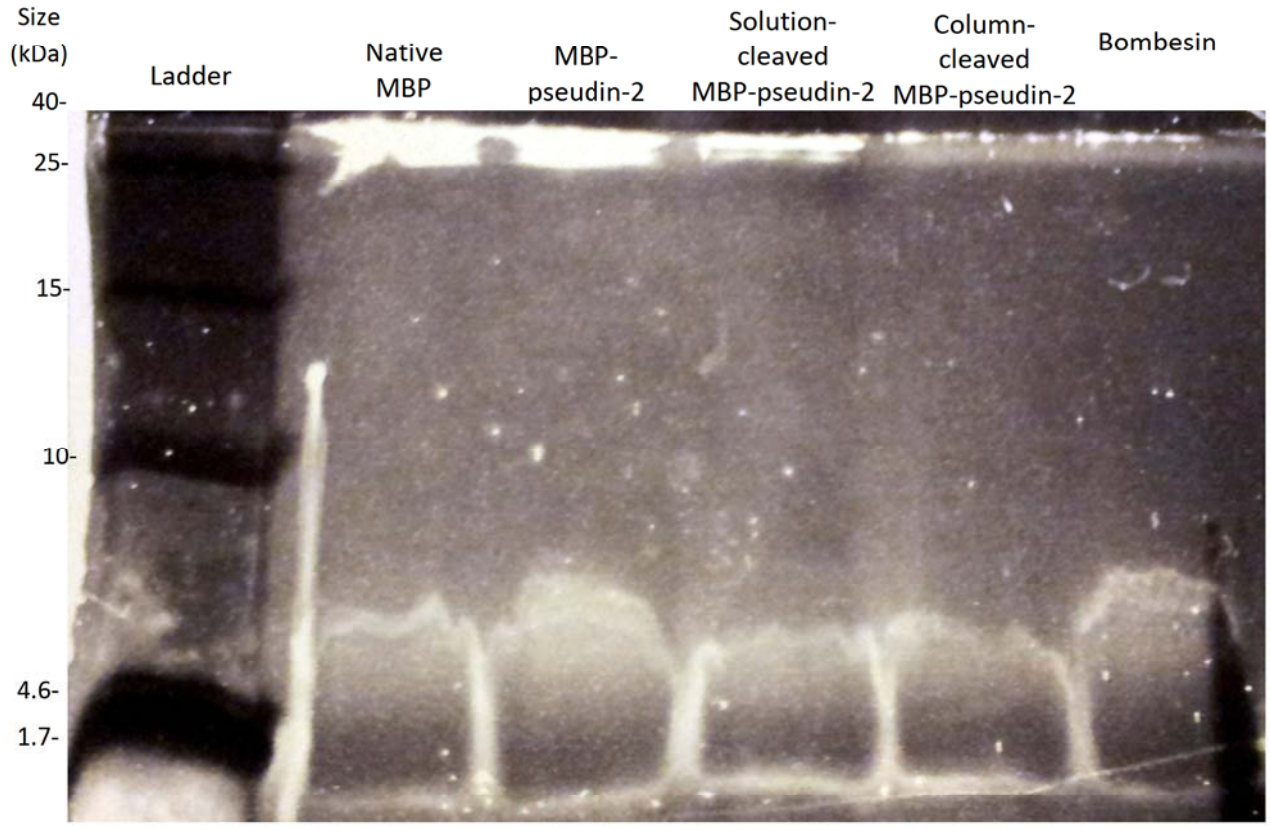

Figure 4.2.2. SDS-PAGE gel (three-phase gel) loaded as follows: Lane 1: 5 µL of the Spectra LR Protein Ladder, Lane 2: native MBP, Lane 3: MBP-pseudin-2 fusion, Lane 4: Factor Xa cleaved MBP pseudin-2 (solution cleavage), Lane 5: cleaned up MBP-pseudin-2 (following column cleavage). Lane 6: 0.6 µg of chemically synthesised Bombesin. Lanes 2-5 were each loaded with 15 µL of the respective solutions and the gel was stained using the oriole gel stain (**2.8.7**)

The gel in Figure 4.2.2 above shows a low-molecular-weight band in all lanes, suggesting that all fractions contain a peptide fragment. The large band in lane 6 shows chemically synthesised bombesin, which is a purified peptide. The fact that this peptide appears as a 'smear' instead of a distinct band shows that it is not possible to correctly resolve peptide fragments on the gel, despite the use of a triple-phase gel system. Both lanes 1 and 2 contain a 'smear' at the bottom corresponding to a peptide fragment, which would be expected. It is important to note here that even the expression of MBP using the parental vector yields a peptide fragment as MBP is fused to a small peptide within the native expression vector. There is no clear difference between the peptide bands in lanes 3 and 4, suggesting that cleavage using Factor Xa does not make a significant difference to the peptide yield. However, as above, this is difficult to ascertain due to the large size of the peptide bands. A comparison of the protein bands in lanes 4 and 5 shows that the large molecular-weight band at the top of the gel (most likely corresponding to MBP) is present in lane 4 but absent in lane 5. This suggests that the column purification of the Factor Xa-cleaved protein solution was at least partially successful, since the high-molecular-weight protein was almost completely removed. However, ESI-MS analysis of the protein solution loaded corresponding to Lane 5 showed no trace of pseudin-2.

Since it was inconclusive as to whether any of samples 3-5 (Figure 4.2.2) actually contained intact pseudin-2, all were tested for toxicity against *E. Coli*. Neither the pseudin-2-MBP fusion protein, nor the concentrated, purified cleaved pseudin-2 peptide, nor the Psudin-2 peptide that resulted from on-column cleavage/concentration showed any detectable antibacterial activity. It could not be established whether this lack of pseudin-2 toxicity was due to its absence (possibly owing to cellular cleavage prior to purification) or whether in fact the peptide had been purified successfully, but somehow inactivated during that purification. An alternative expression regime was clearly required.

4.2.1 Cloning of pseudin-2 into pET45b

Since the expression of pseudin-2 with the large fusion partner MBP was unsuccessful, an alternative expression regime was examined in which the peptide was expressed with a small fusion partner, namely a His_6 tag. Firstly, the Psudin-2 gene was cloned in an appropriate vector.

Plasmid pET45b (2 µg) was digested using the restriction enzyme *Pml*I in the presence of BSA for 2 hours at 37°C and dephosphorylated (2.4.3). The two oligonucleotides carrying the gene sequence of pseudin-2 (2.2: ps2_pET45b_top, ps2_pET45b_bottom) were phosphorylated separately (2.4.1) and then annealed (2.4.2) to make the insert. The dephosphorylated vector and the insert were mixed in a 5:1 molar ratio of insert to vector and ligated using standard conditions (2.4.4). A parallel ligation was set up in exactly the same way but without the insert. Competent *E. Coli* DH5α cells were made and transformed using 20ng each of self and fragment ligated vector (2.5.1). The colony counts for each are given below:

Fragment-ligated pET45b	144
Self-ligated pET45b	26

27 colonies were selected and screened for the presence of the insert using colony PCR (2.4.7). The colonies were also streaked on ampicillin agar plates and grown overnight at 37°C in order to be able to recover the transformants after the PCR screen. pET45 forward and reverse PCR primers were used for the screen (2.2).

The PCR reactions (50%) were then electrophoresed on an agarose gel (2.4.8). The remaining 50% of the PCR reaction was diluted 10-fold in distilled water to be sent for sequencing (2.4.5).

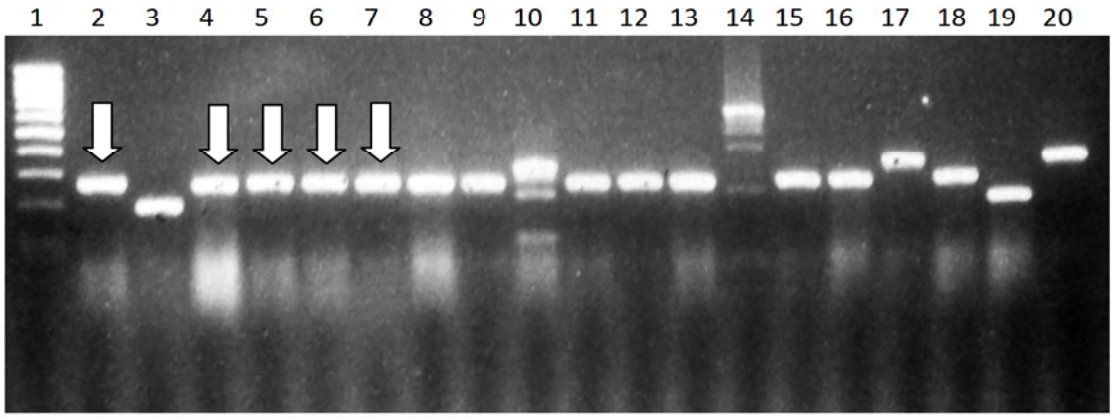

Figure 4.2.3. Gel showing the results of the colony PCR screen of the pET45b cloning experiment to determine successful insertion of the pseudin-2 gene into the vector. The gel (2% agarose) was loaded as follows: Lane 1: 1000ng MassRuler DNA Ladder, Low Range, Lanes 2-20: 50% of the single-colony PCR reaction. The gel shows that most transformants contained the insert as they showed a PCR product of the right size (265bp in the presence of the insert, 190bp otherwise). A few of the PCR products containing the insert have been indicated using arrows (Lanes 2, 4, 5, 6 and 7).

Figure **4.2.3** shows that the majority of the colonies screened gave a PCR product at 265bp, which is the PCR product expected after successful insertion of the pseudin-2 gene into the vector. The figure also shows colonies with the parental vector without the insert (Lanes 2 and 19), evidenced by the smaller size (190bp) of the product. A few colonies showing larger PCR products were also observed. These are most likely where two copies of the gene had been incorporated into the vector (Lanes 17 and 20).

The diluted PCR reactions containing the correct length product in indicated lanes (lanes 2, 4, 5, and 6) were mixed with 3.2pmol of the forward PCR primer previously shown to make a 10 µL sequencing reaction (2.4.5), which was sent for sequencing. The sequencing data confirmed the presence of the gene for pseudin-2 in the right orientation and position, with no mutations. Small-scale plasmid isolation was then performed on one of the colonies containing the correct gene sequence to obtain the plasmid DNA (2.5.2).

4.3 Protein expression of His_6-tagged pseudin-2

Competent *E. Coli* Tuner DE3 cells were made (2.5.1) and transformed using 20 ng of the pET45b-pseudin-2 construct. These cells were then grown using the standard protocol for protein expression (2.7.1). The overnight culture was diluted into 200ml of fresh ampicillin broth which

was induced using 1mm IPGT at the exponential phase of growth. The cells were then allowed to express the peptide overnight at 30°C.

Qiagen Nickel resin was used to purify the his-tagged peptide according to the manufacturer's instructions (2.7.3). The resulting protein samples were prepared, (2.8.1) and a three-phase gel prepared (2.8.3) and electrophoresed (2.8.5) using a Tris-Tricine buffer system. The gel was stained using the Oriole fluorescent gel stain (2.8.7). Figure 4.3.1 shows the resulting gel image.

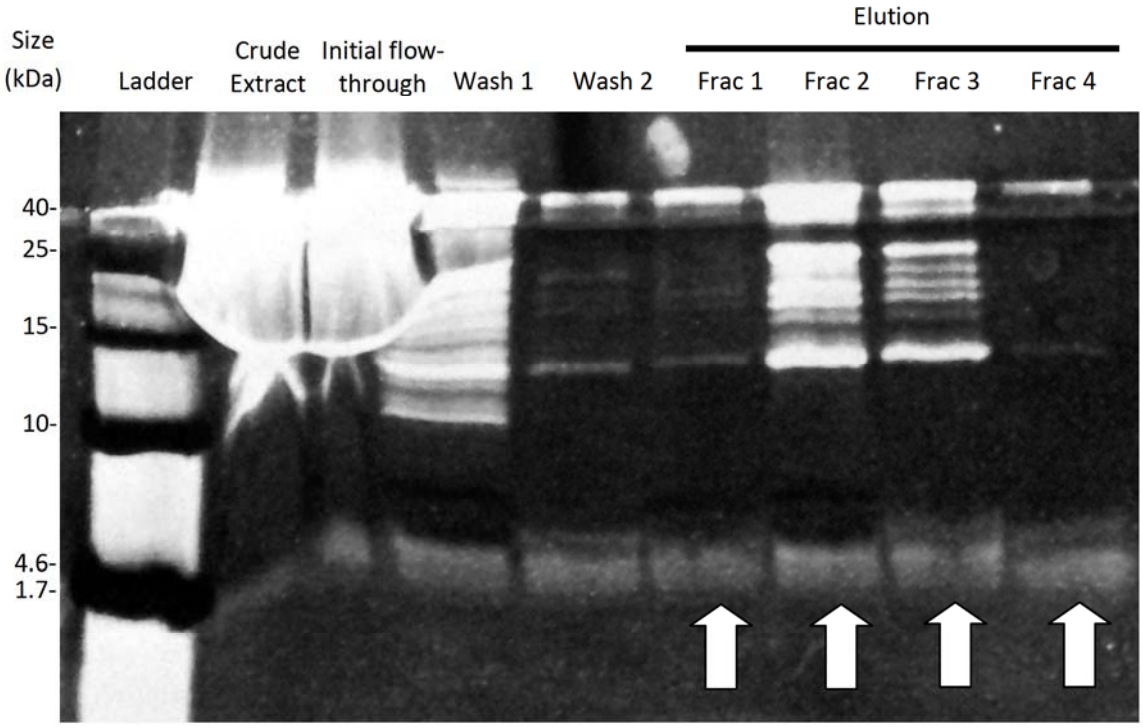

Figure 4.3.1 Three-phase gel loaded with 15 µL each of the solutions indicated. The Spectra Multicolor Low Range Protein Ladder (5ul) was loaded as a marker. The swelling observed in lanes 2 and 3 is due to the large amount of protein in the crude extract and initial flow-through. The potential band thought to correspond to pseudin-2 and the molecular weights of the ladder bands have been indicated.

The gel in Figure 4.3.1 shows a number of interesting features. The crude extract of the cells contains a large amount of protein and this is observed in the wash-through as well. It is this concentration of protein in both lanes that causes the overloading artefact observed in the figure. The comparable amount of protein in both bands shows that the majority of cellular proteins do not bind to the nickel-containing purification resin, but simply flow through. The lanes corresponding to the two washes show that a large amount of non-specific binding proteins are

separated from the resin. This is particularly true in the case of the first wash, where a large amount of protein is observed. Finally, the four elution fractions, in addition to the previous fractions, all seem to contain a low-molecular-weight peptide which could correspond to the his-tagged-pseudin-2. Although this low-molecular-weight fraction is observed in all four of the elution fractions, larger proteins are also seen, particularly in fractions 2 and 3. Since these bands occur at the same positions as in the wash samples, they show non-specific binding proteins.

The four fractions corresponding to the gel bands shown above were tested for antibacterial activity on *E. Coli* Tuner DE3 cells. Initial results were encouraging, but the control experiments showed that the peptide elution buffer (containing 250 mM imidazole) was itself toxic to the bacteria. Additionally, the use of imidazole as the eluting agent was not compatible with the BCA Assay, which is used as a standard method for measuring peptide concentration. This method was, therefore, deemed unsuitable for the purposes of this study.

Expression and isolation of His_6-pseudin-2 were repeated, but using a low pH buffer (pH = 4.5) to elute the peptide from the nickel resin. Control tests showed that this buffer was not toxic to the *E. Coli* cells but unfortunately, none of the eluted His_6-pseudin-2 showed any antibacterial activity either.

Finally, the experiment was repeated using an elution buffer in which the amino acid histidine replaced imidazole at the same concentration, since the two are structurally similar. Histidine is not toxic to *E. Coli* cells at this concentration. Unfortunately, it transpired that histidine has a higher affinity for nickel than does imidazole. Thus this elution buffer stripped the nickel ions from the purification resin. This was observed as a colour change in the resin as the blue colour of the resin was transferred to the protein solution. Since Nickel ions are known to be toxic to microorganisms (Babich & Stotzky, 1983) , this method was deemed unsuitable for the purposes of this experiment.

In conclusion, none of the purification strategies for pseudin-2 had proved successful, and visualisation had proved problematic. Additionally, pseudin-2 is sufficiently small to permit affordable chemical synthesis, which would solve the problems encountered during the expression experiments. Therefore, expression of pseudin-2 and its mutants was abandoned in favour of chemical synthesis.

5 Antimicrobial activity of native and variant, chemically-synthesised, pseudin-2 peptides

5.1 Aims

Given the difficulties in testing expressed Psuedin-2, the key initial experiment was to test the antimicrobial activity of chemically-synthesised pseudin-2. Thereafter it was aimed to test the activity of the peptides identified in Chapter 2, to give a clearer idea of their true anti-microbial activity. Additionally, while testing for toxicity by expression only allows the testing against one microbe, the isolation of peptides allows for the testing of the peptides for toxicity against a number of different pathogenic strains. This relates to the second component of the hypothesis, development of pseudin-2 into an antimicrobial by altering its primary structure. The hypothesis is given below.

Pseudin-2 may be developed into an antimicrobial compound for clinical use by:

a) Structural understanding of its antimicrobial action

b) Altering its primary structure

5.2 Choice of pathogens

The organisms chosen for antimicrobial activity testing were *E. Coli*, *S. Aureus* and *C. Albicans* since they represent the three main classes of pathogens: Gram negative bacteria, Gram positive bacteria and fungi respectively. Additionally, these three organisms have been used in a large number of studies of antimicrobial peptides such as magainins (Mechkarska *et al.*, 2010), brevinins (Iwakoshi-Ukena *et al.*, 2011), esculentins (Wang *et al.*, 2010) and temporin-1Ta(Grieco *et al.*, 2011).

5.3 Chemically-synthesised pseudin-2

Chemically synthesized, high-purity pseudin-2 was obtained from United Biosystems (UK). Meanwhile, to further examine the lack of efficacy of His-tagged psuedin-2 peptide (Chapter 4), MA-His_6-pseudin-2 was obtained from Alta Biosciences. Minimum Inhibitory Concentration (MIC)

values (2.9.2) and haemolysis (HC_{50}) values (2.9.3) of these chemically synthesised pseudin-2 and His-tagged-pseudin-2 peptides were then determined and compared with known, published values, where relevant (Table 5.3.1).

	MIC (μM)			HC_{50} (μM)	Reference
Peptide	*E. Coli*	*S. Aureus*	*C. Albicans*		
pseudin-2	**20**	**160**	**-**	**360**	(Pál *et al.*,2005)
pseudin-2	**2.5**	**80**	**130**	**-** *(300)*	(Olson *et al.*,2001)
pseudin-2	**7.5** *(30)*	**30** *(30)*	**-** *(30)*	**-** *(200)*	This study
MA-His_6-pseudin-2	**-** *(48.6)*	**-** *(48.6)*	**-** *(48.6)*	**-** *(97)*	This study

Table 5.3.1 Minimum inhibitory concentration values of pseudin-2 against *E. Coli*, *S. Aureus* and *C. Albicans* in the literature compared to values obtained in this study. Values in brackets show the highest concentration tested. Test organisms were incubated with the peptide at the highest concentration followed by 11 successive two-fold dilutions of the highest concentration (2-fold diluted, 4-fold diluted, 8-fold diluted etc.). All concentrations were calculated taking peptide purity into account (Appendix D). A dash indicates no toxicity detected at the highest concentration tested.

The data in Table 5.3.1 above show good correlation between the chemically-synthesised pseudin-2 employed in this study and previously published values. Differences between MIC values for the same organism in different studies are likely due to the difference in the pathogen strain used in each test. It is unlikely that these differences can be attributed to differences in the impurities present in the peptides as in all cases the peptides are of high purity. This data is not compared to any common positive controls since this work was carried out in order to directly reproduce previous data (Olson *et al.*, 2001) and to confirm the antimicrobial activity of naturally-occuring pseudin-2. The purification was carried out by the supplier of the purified peptides since the lack of RP-HPLC equipment made it impossible for the peptide purification to be carried out in-house.

In contrast, the His-tagged pseudin-2 does not show any antimicrobial activity (a > symbol indicates that there was no activity at the highest concentration tested), particularly against *E. Coli*, which is the pathogen most sensitive to native pseudin-2. One may postulate that the

addition of the histidine residues alters the electrostatic interaction between pseudin-2 molecules at the surface of cells, and/or may hinder helix formation leading to a loss in antimicrobial activity. It is also important to note that His-tagged-pseudin-2 (much like native pseudin-2) has low haemolytic activity. This is in good agreement with previously published data on the structure-function relationships of haemolytic peptides which suggests that it is the hydrophobic nature of the peptide, and not its charge that determine its haemolytic activity (Conlon *et al.*, 2009).

Finally, the lack of antimicrobial activity of His-tagged-pseudin-2 confirms the findings in Chapter 4, that addition of an N-terminal His_6 tag effectively eliminates anti-microbial activity. Any future use of a His-tag would therefore necessitate its proteolytic removal, after expression/purification.

5.4 Activities of selected mutant peptides

Having confirmed the activity of chemically-synthesised pseudin-2, 5 further peptides were selected from the toxic mutants identified in chapter 3. Three peptides complied with the conclusions to Chapter 3 that positions 10, 14 and 18 should be polar non-charged, polar non-charged and hydrophobic respectively (in this instance tryptophan is treated as polar non-charged since it can make a hydrogen bond from its side group). An example of a peptide containing hydrophobic residues at all three positions and one containing positively charged, hydrophobic, hydrophobic at positions 10, 14 and 18 respectively was also selected. Finally, a peptide was designed in which the polar, non-charged residue at position 10 (Q) was substituted with a positively charged residue (R) to test the theory that increased positive charge correlates with increased antimicrobial activity. All six peptides were obtained from Alta Biosciences, synthesised to high purity. The pure peptides were supplied with Mass-spectroscopy and HPLC traces to confirm their purity. These traces can be found in Appendix C. In the case of the purified peptides, the mass spectroscopy traces showed a peak corresponding to the exact mass of the synthesized peptide. The HPLC traces of these peptides showed one large peak corresponding to the pure

peptide and another smaller impurity peak. In all six of the purified peptides, the final purity was above 80%.

5.4.1 Resuspension and solubility of synthesized peptides

All synthesized peptides were dissolved in phosphate-buffered saline, which is the buffer required for MIC assays. In some cases, the peptides exhibited poor solubility and thus larger volumes of buffer were required. Even then, these solutions appeared cloudy. The situation was resolved by adding acetic acid to a final concentration of 0.03% v/v, having confirmed that this concentration of acetic acid was non-toxic in standard MIC tests (data not shown) for all strains tested. The final concentrations of the peptides are given in Table 5.4.1.1 below:

Peptide sequence	Concentration (μM)
GLNALKKVFWGIHTAIKMINNHVQ	55.8
GLNALKKVFYGIHTAIKGINNHVQ	105.6
GLNALKKVFRGIHEAIKLINNHVQ	111.6
GLNALKKVFRGIHPAIKLINNHVQ	208.8
GLNALKKVFLGIHMAIKPINNHVQ	225.6
GLNALKKVFTGIHSAIKLINNHVQ	116.4

Table 5.4.1.1. Concentrations of the purified peptides after dissolution in PBS. The low concentration of peptide M2608-F1 is due to extremely low solubility in the buffer. The concentrations have been calculated taking into account the purity of each peptide (Appendix D)

5.4.2 Note on pH

Although the addition of the acetic acid lowered the pH of the solutions to 5.0, the final working pH of the peptide solution (within MIC test wells) was 7.0. This was due to the successive dilution of the peptide solution by the growth medium used for the MIC testing of the peptides. The pH in this experiment was estimated using universal pH paper.

5.4.3 MIC values of purified peptides

The MIC values of the purified peptides were determined (**2.9.2**) for three representative pathogenic strains of *Escherichia Coli*, *Staphylococcus Aureus* and *Candida Albicans*, and compared to peptide controls (Table **5.4.3.1**). The peptides magainin-2 and indolidicin were

chosen since both peptides are clinically relevant since both peptides reached Phase III clinical trials (testing on a large number of human patients) (Gordon *et al.*, 2005).

Code/peptide name	Peptide sequence	MIC (µM)		
		E. Coli	*S. Aureus*	*C. Albicans*
F1	GLNALKKVF**W**GIH**T**AIK**M**INNHVQ	- *(14)*	- *(14)*	- *(14)*
F2	GLNALKKVF**Y**GIH**T**AIK**G**INNHVQ	- *(26.4)*	- *(26.4)*	- *(26.4)*
F3	GLNALKKVF**R**GIH**E**AIK**L**INNHVQ	- *(28)*	- *(28)*	- *(28)*
F4	GLNALKKVF**R**GIH**P**AIK**L**INNHVQ	**6.5** *(52.2)*	- *(52.2)*	- *(52.2)*
F5	GLNALKKVF**L**GIH**M**AIK**P**INNHVQ	- *(56.4)*	- *(56.4)*	- *(56.4)*
E8	GLNALKKVF**T**GIH**S**AIK**L**INNHVQ	- *(29.1)*	- *(29.1)*	- *(29.1)*
Pseudin-2	GLNALKKVFQGIHEAIKLINNHVQ	**7.5** *(30)*	**30** *(30)*	- *(30)*
Magainin-2	GIGKFLHSAGKFGKAFVGEIMKS	**21**	**21**	**33**
Indolicidin	ILPWKWPWWPWRR	**1**	**1**	**3**

Table 5.4.3.1. MIC values of the purified pseudin-2 mutants compared to pseudin-2 (this study), magainin-2 (Zasloff, 1987) and indolicidin (Morin *et al.*, 2006). Values in brackets show the highest concentration tested. Test organisms were incubated with the peptide at the highest concentration followed by 11 successive two-fold dilutions of the highest concentration (2-fold diluted, 4-fold diluted, 8-fold diluted etc.). *It is important to note that after 24 hours, the MIC of the active peptide increases to 26 µM. The randomized positions in the mutants have are shown in bold font. The concentrations have been calculated taking into account the purity of each peptide (Appendix D).

Of the 6 peptides tested (at the concentrations tested), only the analogue [10-R, 14-P, 18-L] showed antimicrobial activity. Although the antimicrobial activity of this peptide against *E. Coli* is comparable to that of magainin-2, no toxicity was detected against *S. Aureus* or *C. Albicans*. This may be due to the low concentration [30 µM] used as a result of the low solubility of the peptide. Taking the above data into consideration, it is unclear whether this peptide would be a suitable candidate for therapeutic development. It is, however, clear that it is considerably less potent than indolicidin (a peptide which reached phase III clinical trials), which suggests that it is unlikely to be a candidate for development into an antibiotic.

The HC_{50} of the active peptide M2608-F4 was determined to be 200 µM (2.9.3). This gives a therapeutic window of 26.67 when calculated based on the MIC against *E. Coli* of 7.5 µM. This is identical to the MIC of chemically-synthesised pseudin-2 determined earlier. The haemolytic activity of this peptide, is, however, higher than native pseudin-2.

It is important to note that although all the chemically synthesized peptides showed toxicity in the previous replica-plating test, only one of the seven purified peptides showed any activity. It is

likely that the replica-plating screen excluded peptides with high toxicity towards *E. Coli*, since expression of these peptides (i.e. leaky expression from the uninduced promoter) would lead to cell death. For peptides with more moderate MICs, it is possible that the concentrations at which peptide toxicity was tested were simply too low for any activity to be detected (particularly for peptides F1-F3 and E8). It is therefore clear that replica-plating must at the very least, be supplemented by MIC analysis of the peptides at sufficiently high concentrations.

5.5 Crude peptide toxicity testing

To further investigate the data from mutagenesis / replica plating, a further 44 peptides were ordered for chemical synthesis as crude peptides (Alta Biosciences, Episcan synthesis, typically 60%-70% pure). These peptides were synthesized chemically by successive addition of one amino acid at a time to form the full-length peptide chain. The impurities are, therefore, likely to be truncations of the full sequence, where one of the addition steps failed. Since RP-HPLC equipment was not available in-house and financial constrains prevented the purification of all peptides, no chromatography data was obtained for these peptides and they were simply tested as crude peptides.

A total of fourteen were selected at random from the original replica plating screen, five were designed to contain a single negatively-charged residue at position 10, ten were selected to contain polar, non-charged residues at positions 10 & 14 and a hydrophobic residue at position 18 (as identified by the analysis of the replica plating experiments in chapter 3) and nine were selected to contain positive charge at positions 10 & 14 and a hydrophobic residue at position 18, in line with published literature. These crude peptides were tested for antimicrobial activity against representative strains of *E. Coli*, *S. Aureus* and *C. Albicans*. The MIC's of these peptides at 37°C was measured after 18 hours (2.9.2 – the accepted, literature standard) and also 24 hrs to investigate whether effects were more long-lived.

Amino acid identity			MIC (μM) 18 hrs			MIC (μM) 24 hrs			Other parameters			Code
10	14	18	*E. Coli*	*S. Aureus*	*C. Albicans*	*E. Coli*	*S. Aureus*	*C. Albicans*	Charge	Helical potential	Hydro-phobicity	
T	W	P	2	25	51	2	51	51	5	0.37	-0.2	B1
R	R	A	3	6	3	13	6	13	7	0.63	-4.2	D4
H	R	V	3	-	-	3	-	-	7	0.47	-0.5	A6
R	H	L	6	-	-	6	-	-	7	0.56	-0.9	D7
H	K	V	6	-	-	13	-	-	7	0.46	0.1	D5
K	R	I	6	-	-	13	-	-	7	0.66	-0.9	D6
H	S	W	6	-	-		-	-	6	0.49	-1.9	C7
K	H	F	13	-	-	13	-	-	7	0.63	-1.3	D8
R	S	A	13	-	-		-	-	6	0.66	-0.5	C1
K	S	F	25	-	-	51	-	-	6	0.66	1.1	C10
K	T	N	25	-	-		-	-	6	0.67	-5.1	A7
D	S	F	25	-	-	51	-	-	4	0.53	1.5	D3
K	T	A	51	-	-	51	-	-	6	0.75	0.2	C9
R	N	V	51	-	-		-	-	6	0.56	-0.8	C4
K	T	F	51	-	-		-	-	6	0.67	1.2	C5
Y	K	I	51	-	-	51	-	-	6	0.78	2.3	A2
S	N	A	51	-	-	51	-	-	5	0.6	0.5	B12
W	G	S	51	-	-	-	-	-	5	0.67	0.9	A5
F	P	I	51	-	-	-	-	-	5	0.65	8.7	A12
C	T	H	-	25	-	-	51	-	6	0.59	1.6	A1
R	N	I	-	-	-	-	-	-	6	0.59	-0.5	C8
H	Q	V	-	-	-	-	-	-	6	0.47	0.5	C6
H	Q	L	-	-	-	-	-	-	6	0.54	0.1	C2
K	T	I	-	-	-	-	-	-	6	0.68	2.9	C3
T	R	I	-	-	-	-	-	-	6	0.49	2.3	A9
S	S	W	-	-	-	-	-	-	5	0.52	0.5	B8
N	Q	F	-	-	-	-	-	-	5	0.6	-1.2	B7
Q	T	F	-	-	-	-	-	-	5	0.61	1.6	B10
N	Q	I	-	-	-	-	-	-	5	0.57	0.5	B5
S	N	V	-	-	-	-	-	-	5	0.49	2.9	B4
T	N	F	-	-	-	-	-	-	5	0.45	1.6	B9
T	Q	I	-	-	-	-	-	-	5	0.45	3.3	B11
T	S	A	-	-	-	-	-	-	5	0.52	3.3	B3
Q	T	L	-	-	-	-	-	-	5	0.68	2.6	B6
S	G	I	-	-	-	-	-	-	5	0.47	6.3	A8
S	G	M	-	-	-	-	-	-	5	0.5	3.7	A4
N	P	L	-	-	-	-	-	-	5	0.56	1.7	A11
T	V	A	-	-	-	-	-	-	5	0.52	8.3	B2
F	G	A	-	-	-	-	-	-	5	0.7	7.2	A10
W	V	D	-	-	-	-	-	-	4	0.71	2.8	A3
D	S	A	-	-	-	-	-	-	4	0.62	0.5	C11
E	N	V	-	-	-	-	-	-	4	0.67	0.2	C12
E	Q	L	-	-	-	-	-	-	4	0.73	-0.2	D2
D	T	I	-	-	-	-	-	-	4	0.56	3.3	D1

Table 5.5.1. Minimum Inhibitory concentrations of crude pseudin-2 analogues. The three amino acids shown indicate the residues at positions 10, 14 and 18 of pseudin-2 (GLNALKKVFQGIHEAIKLINNHVQ). The MIC values were calculated using an average molecular weight of 2662.78, assuming 65% purity, with values rounded off to the nearest integer. Colours indicate amino acid classification: blue = basic (H, R, K), red = acidic (D, E), green = polar non-charged (S, T, N, Q, Y), yellow = hydrophobic (F, G, A, V, L, I, P, C). Tryptophan is coded as polar non-charged in positions 10 and 14 due to hydrogen bonding characteristics and hydrophobic in position 18 due to hydrophobic characteristics.The peptides are sorted in ascending order of MIC against *E. Coli* at 18 hours. In all cases, 51 μM was the highest concentration tested and 11 successive two-fold dilutions of the highest concentration were used.

5.5.1 Antimicrobial activity - *E. Coli*

Table **5.5.1** demonstrates that for antimicrobial activity against *E. Coli*, there is a preference for positively charged residues at position 10 of pseudin-2 (68%) whilst at position 14, polar uncharged residues are preferred (47%). Nearly all residues at position 18 are hydrophobic.

The notable outliers with respect to the residue preferences shown above are the pseudin-2 analogues [10-T, 14-W, 18-P] and [10-D, 14-S, 18-F]. In the case of the pseudin-2 analogue [10-T, 14-W, 18-P], none of the mutated residues are positively charged. Additionally, this peptide contains a proline residue at position 19, which is likely to contribute to flexibility at that position within the peptide since proline residues (unlike other amino acids) contain a secondary amine. This can be expected to reduce helicity at that position by introducing a 'turn' or 'kink'. Tryptophan is a residue that contains a large planar side group which might be expected to remain at the surface of a membrane. It is possible that these two hypothetical structural features: the turn at position 18 and the surface-stability at position 14 contribute to the mechanism of toxicity of this pseudin-2 mutant.

The pseudin-2 analogue [10-D, 14-S, 18-F] mutant on the other hand differs considerably from the others since it is the only mutant with a negatively-charged residue at position 10. This disagrees strongly with both the trends seen in the other peptides, as well as with literature data suggesting that more positively-charged peptides show toxicity to *E. Coli* (Pal *et al.*, 2005). There are two possible explanations for this observation. Since this peptide is only moderately toxic, one may theorise that the presence of the negatively-charged aspartic residue only decreases the peptide's toxicity but doesn't eliminate it completely. An alternative explanation is that the toxicity of this peptide is dependent on a different, unknown mechanism of action for which the presence of a negatively-charged residue at position 10, is preferred.

Since there are 19 peptides toxic to *E. Coli* at 18 hours, it is possible to look for correlation between the MIC values of the toxic peptides as a function of their hydrophobicity and helical

potential. The relationship between toxicity and overall charge is not shown below since the distribution of charge values in the toxic peptides is small, which makes it difficult to look for a statistical relationship. The plots of MIC against *E. Coli* against hydrophobicity and helical potential are shown in Figure **5.5.1.1** below.

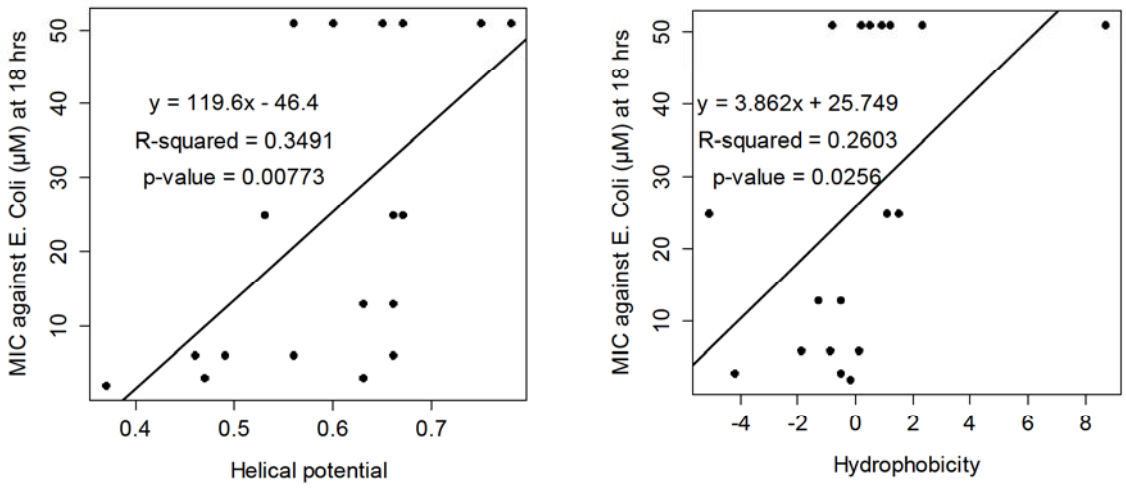

Figure 5.5.1.1. Values of MIC against *E. Coli* (μM) at 18 hours as a function of hydrophobicity and helical potential, along with the results of simple linear regression analysis (R-squared and p-values) carried out on the data.

The plots above show that there is little or no correlation between helical potential (as shown by the small R-squared values and relatively large p-values) and *E. Coli* toxicity, whereas overall peptide hydrophobicity cannot be linked to its toxicity to *E. Coli* at all.

In conclusion, with the exception the two mutants discussed earlier, toxicity to *E. Coli* is dependent on the presence of a positively-charged residue at position 10, either a positively-charged or polar uncharged residue at position 14 and a hydrophobic residue at position 18. This data is, therefore, in good agreement with published pseudin-2 mutagenesis data (Pal *et al.*, 2005). This data can also be explained in the light of the membrane structure of the gram-negative bacterium. The outer membrane of *E. Coli* contains lipololysaccharide; it does not contain a barrier that would prevent peptide interactions at the surface. Therefore, simple electrostatic interactions are going to be the driving force for toxicity of small peptides to *E. Coli*.

5.5.2 *S. Aureus* toxicity

The number of peptides toxic to *S. Aureus* is considerably smaller compared to those toxic to *E. Coli*. Of the 50 peptides tested, only three showed toxicity to *S. Aureus*. These are the pseudin-2 analogues [10-T, 14-W, 18-P], [10-R, 14-R, 18-A], and [10-C, 14-T, 18-H]. Since only 3 data points (corresponding to the three peptides) exist for overall charge and helicity, it is not possible to look for a statistical correlation between these properties and antimicrobial activity. It is, however, possible to simply interpret the data and speculate as to the possible mechanism of toxicity against this pathogen.

In the case of the pseudin-2 analogue [10-R, 14-R, 18-A], the toxicity may be simply explained as an increase in the overall positivity of the peptide. With positively-charged arginine residues at positions 10 and 14, the positive charge is likely the driving force behind the toxicity of these mutants since *S. Aureus*, like *E. Coli*, also possesses a negatively-charged membrane surface (Dickson & Koohmaraie, 1989). The pseudin-2 analogue [10-C, 14-T, 18-H] also contains a positively charged residue: a histidine residue at position 18. It is therefore, likely that this peptide also interacts electrostatically with the cell membrane of *S. Aureus*. Finally, in the case of the pseudin-2 analogue [10-T, 14-W, 18-P], there are no positively-charged residues, which suggests that this peptide elicits its toxicity using a mechanism different from that of the other two toxic mutants.

In conclusion, peptides with a large positive charge are likely to be toxic to *S. Aureus*, but the toxicity of the pseudin-2 analogue [10-R, 14-R, 18-A] suggests that the presence of a positive charge at positions 10 and 14 of pseudin-2 analogues that are toxic to *S. Aureus*. With regards to the other two toxic peptides, they are less positive than the analogue [10-R, 14-R, 18-A] and both only moderately toxic, which supports the notion that electrostatic interactions are important for toxicity to *S. Aureus*, a pathogen that possesses a negatively-charged membrane surface.

The smaller number of peptides toxic to *S. Aureus* may also be explained on the basis of the membrane structure of the pathogen. *S. Aureus* cells, like *E. Coli* cells, have a negative membrane surface but the cells also have a peptidoglycan 'mesh'. It is, therefore, more difficult for a peptide to interact with the membrane of the cells since it has to fold to a size smaller than the pores of this molecular 'mesh'. This explains the smaller number of mutant peptides toxic to *S. Aureus* relative to *E. Coli*, even though both pathogens possess a negative membrane surface.

5.5.3 *C. Albicans* toxicity

The number of toxic peptides is smallest in the case of *C. Albicans*, with only two analogues [10-R, 14-R, 18-A] and [10-T, 14-W, 18-P] showing toxicity. Due to the extremely small number of toxic peptides and the complexity of the eukaryotic pathogen *C. Albicans*, it is difficult to determine the basis for the toxicity of the two mutant peptides with activity against *C. Albicans*. This may be explained based on the membrane structure of the pathogen. *C. Albicans* possess a cell wall which acts a semi-permeable membrane. Additionally, it has been suggested that peptide transport in yeast is under the control of cell-surface proteins, and the activity of these proteins is crucial to the development of antifungal agents (Wakiec *et al.*, 2008). Therefore, this eukaryotic pathogen presents two additional challenges to the development of an antifungal agent which are not present in the case of prokaryotic pathogens. It is, therefore, possible that the analogues toxic to *C. Albicans* [10-R, 14-R, 18-A] and [10-T, 14-W, 18-P] do so by a combination of biophysical interaction as well as a more specific interaction involving cell surface proteins. This explains the difference in the primary structure between the two mutants, since the analogue [10-R, 14-R, 18-A] possesses two positively charged arginine residues and a hydrophobic alanine residue, while [10-T, 14-W, 18-P] possesses a polar threonine residue, a tryptophan residue, and a helix-bending proline residue.

5.5.4 Peptide stability: 18 vs. 24 hours

The data in Table 5.5.1 shows that in the case of *E. Coli*, 6 of the 19 toxic peptides show a decrease in toxicity between the 18 and 24-hour incubation periods. In the case of *C. Albicans*, one of the two toxic peptides shows a similar trend, while two of the three toxic peptides in the case of *S. Aureus* show the same decrease in toxicity. One may speculate that this is attributed to the simple hydrolysis of the peptide following the long incubation at 37°C. This is the most likely process to lead to the degradation of the peptides over long incubation periods since the peptides interact predominantly with the membranes of the cells in question. However, it is also possible that this process is mediated by cellular proteases which are released into the growth medium following the lysis of the cells by the toxic peptides. Due to the difficulties in visualization and purification of the peptides (described in detail in Chapter 4), it was not possible to look for peptide degradation. This is further complicated by the fact that the peptides used in these tests were of low purity. Additionally, the lack of in-house equipment combined with financial restraints made it impossible to determine whether peptide degradation occurred after 24 hours.

5.5.5 Therapeutic leads

The data shows only one potential therapeutic lead worth of further investigation: the analogues [10-T, 14-W, 18-P]. The MIC values of this analogue compared to those of pseudin-2 and well as magainin-2 and indolicidin, are given in **Table 5.5.5.1** below:

Peptide	Sequence	MIC (μM)		
		E. Coli	*S. Aureus*	*C. Albicans*
$T_{10}W_{14}P_{18}$	GLNALKKVF**T**GIH**W**AIK**P**INNHVQ	**2** *(51)*	**25** *(51)*	**51** *(51)*
Pseudin-2	GLNALKKVFQGIHEAIKLINNHVQ	**7.5** *(30)*	**30** *(30)*	**-** *(30)*
Magainin-2	GIGKFLHSAGKFGKAFVGEIMKS	**21**	**21**	**33**
Indolicidin	ILPWKWPWWPWRR	**1**	**1**	**3**

Table 5.5.5.1. MIC values of the purified pseudin-2 mutants compared to parental pseudin-2 (this study), magainin-2 (Zasloff, 1987) and indolicidin (Morin *et al.*, 2006). Values in brackets show the highest concentration tested. Test organisms were incubated with the peptide at the highest concentration followed by 11 successive two-fold dilutions of the highest concentration (2-fold diluted, 4-fold diluted, 8-fold diluted etc.). Peptide concentrations were calculated taking into account the purity of each peptide.

The pseudin-2 analogue [10-T, 14-W, 18-P] shows some potential as a therapeutic lead since the peptide possesses broad-spectrum activity (for the three major classes of pathogens) comparable to magainin-2, a peptide which reached phase III clinical trials for use as a topical antibiotic (Gordon *et al.*, 2005). This analogue could, therefore, be similarly developed. Interestingly, however, magainin-2 has not been developed into a registered product for clinical use since it does not offer any benefit compared to the use of conventional antibiotics (Gordon *et al.*, 2005). It is likely that similar challenges are to be expected if this peptide is to be developed into an antibiotic. Additionally, since the peptide was tested in crude form, the antimicrobial activity observed may not represent the true antimicrobial activity of the peptide. It would, therefore, be necessary to purify the peptide to >95% purity in order to assess its true antimicrobial activity.

5.5.6 A note on the use of crude peptides

It is important to note that the molar MIC values shown in Table 5.5.1 are calculated based on the assumption that the crude peptides are 65% pure. Due to financial constraints, and due to the lack of in-house RP-HPLC equipment, it was not possible to have such a large number of peptides synthesized with high purity. The synthesis method used for the crude peptides (Episcan) typically provides peptideds of this length of 60-70% pure. Therefore average purities of 65% were assumed.

6 Molecular dynamics study of pseudin-2

Although the mutagenesis data offers useful clues as to the structure-function relationships, a different approach is required to determine the 3D equilibrium structure of pseudin-2 in a membrane environment. *De-novo* modeling using molecular dynamics allows us to determine the structure of a peptide knowing only its primary structure. It is, therefore, a powerful approach for understanding the molecular mechanism of the antimicrobial action of pseudin-2. This work relates to the first component of the hypothesis, since the molecular dynamics simulations would describe the structure of pseudin-2 in a membrane environment, and help offer clues as to its mechanism of action. The hypothesis is given below.

Pseudin-2 may be developed into an antimicrobial compound for clinical use by:

a) Structural understanding of its antimicrobial action

b) Altering its primary structure

6.1 Aims

The aims of this work are as follows:

- Using a suitable control peptide to find a suitable molecular dynamics setup to describe the equilibrium structure of peptides in a water/membrane environment
- To use this setup to determine the equilibrium structure of pseudin-2 in this environment

6.2 Molecular dynamics - an introduction

Molecular dynamics is a computational approach that combines three very different disciplines: biology, physics and computer science. It is a computational technique that calculates the trajectory of atoms in 3D space by evaluating the forces that the atoms exert on one another. This information of what takes place at the atomic level allows us to better understand the macroscopic features of the system in question. This makes it a very useful tool to study antimicrobial peptides, as it provides us with data that can be used to aid in the design of these

molecules, and their conversion into viable therapeutics by aiding in the selection of interesting peptide candidates for further investigation. Additionally, the input required for molecular dynamics studies is minimal, which also makes it ideal for the study of novel molecules. Starting with only the primary sequence of the peptide, a large amount of useful information can be obtained regarding its properties.

There are a number of molecular dynamics packages available for the study of protein structure and these differ in ease of use, types of simulations they are capable of running and data analysis features. The two molecular dynamics packages used in this report are CHARMM and NAMD, and these are discussed below. This is followed by a description of replica-exchange molecular dynamics, its use and applications.

6.2.1 CHARMM

The molecular dynamics package CHARMM (Chemistry at HARvard Macromolecular Mechanics) is one of the first molecular dynamics packages to be used in research. The first version of CHARMM was written in 1983 (Brooks *et al.*,1983) but is still under active development (Brooks *et al.*,2009). The software offers a large number of modules which can be used for running various types of simulations, both implicit and explicit with different types of biological and organic molecules of varying sizes. Since the simulations are setup and run using the programming language FORTRAN, this allows for a large degree of flexibility in the choice of parameters used in these simulations. CHARMM includes a suite of data analysis tools which allows the simulations to be setup, run and the resulting data to be analysed without requiring additional software tools. Finally, CHARMM has recently had a new module added that allows the user to carry out Monte Carlo simulations (Hu *et al.*,2006).

In the literature, CHARMM has been used to run simulations of different types of systems, such as simulations of zinc ions in water (Obst & Bradaczek, 1997), peptides (Andersson *et al.*,2013; Yeh & Hummer 2002; Ma *et al.*,2013), nucleic acids (Prabhu *et al.*,2008; Sarzyńska *et al.*,2008).

Additionally, the use of CHARMM to study the structure of large proteins is well-established (Ma & Nussinov 2003; Eleftheriou *et al.,*2006; Ferber *et al.,*2012; Chaudhury *et al.,*2012). The use of CHARMM in the studies mentioned illustrates the flexibility and modular nature of the CHARMM program. Its application to study peptide structure will be utilised in this work.

6.2.2 NAMD

NAMD is a relatively recent molecular dynamics package developed by the Theoretical and Computational Biophysics group in the University of Illinois (Phillips *et al.,*2005). NAMD is available as an open-source package, alongside VMD (Visual Molecular Dynamics), which was developed by the same research group (Humphrey *et al.,*1996). The main advantage of using NAMD is its scalability as the package can be set up to work within a compute cluster, utilising a large number of cores to carry out a simulation. This type of parallel computation has the potential to considerably reduce the time required to run a simulation, and this is especially true when the simulation box consists of thousands of atoms. The free availability of the NAMD software package makes it an interesting option for molecular dynamics simulations. Additionally, there is a considerable amount of documentation readily available which describes the use of NAMD for carrying out various types of simulations.

In the literature, NAMD has been used extensively in understanding the structure and function of aquaporins, water channel proteins found in mammalian cells (Törnroth-Horsefield *et al.,*2006; Chakrabarti *et al.,*2004; Wang & Tajkhorshid 2010; Wang & Tajkhorshid 2007). It has also been used to simulate the glutamate transporter (Huang & Tajkhorshid, 2008; Huang & Tajkhorshid, 2010) as well as to understand blood clotting (Morrissey *et al.,*2008; Morrissey *et al.,*2010; Tavoosi *et al.,*2011). A common feature of these simulations is that they all contain a lipid membrane. This hints at the ease at which membrane/water simulations can be run using NAMD. It is also interesting to note that in a large number of studies using NAMD, an explicit membrane and solvent are used. Although this considerably increases the computational load required to run the simulation, the scalable nature of the NAMD package makes it feasible to run these

simulations. It is these reasons that make NAMD a useful package for an initial simulation setup of our peptide of interest, pseudin-2 in a lipid/water environment.

6.2.3 Replica-exchange molecular dynamics

Replica exchange is a specialised type of molecular dynamics simulation which is used for rapid folding of proteins and peptides or to quickly determine the lowest energy state of a molecular system. In replica exchange, several identical simulations are set up in parallel, initialised with different starting temperatures. Each of these simulations is run for a short interval and then an update step is carried out. Simulations with adjacent temperatures are then compared in a pairwise manner using the Metropolis-hastings criterion (2.10.2).This calculates the probability of the structure in one simulation existing in a different simulation. If this condition is satisfied, the temperatures of the two simulations in question are exchanged. All the simulations are then initialised at their new temperatures, run for a short interval, and the process is repeated. The whole process is summarised in Figure 6.2.3.1 below.

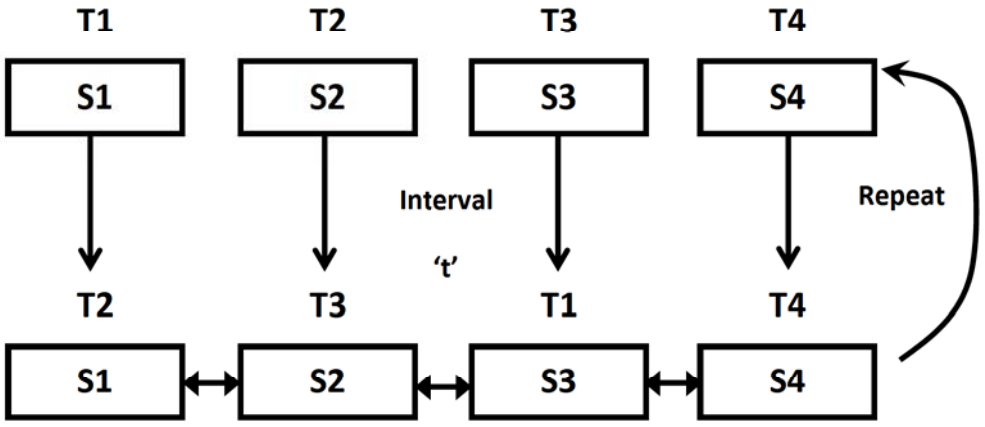

Figure 6.2.3.1 Diagram showing the various steps in a replica-exchange molecular dynamics simulation. Simulations are set up in parallel and at regular intervals; the Metropolis-Hastings criterion is evaluated for adjacent simulations. If the criterion is met, the temperatures are swapped and the simulations are run for another short interval, and the process is repeated. The vertical single-headed arrows show the running of the simulation between the before the exchange is attempted. The double-headed horizontal arrows between the replicas show the exchange that is attempted after each simulation has run for an interval 't'.

There are a number of features that must be noted when using setting up and running replica-exchange simulations. Firstly, the temperature range and number of replicas must be chosen carefully for the system in question. Larger molecules are likely to require a larger temperature range in order to achieve folding. Additionally, if the number of replicas is too small the exchange rate will be low but if they are too high it increases computational load. There needs to be a balance between the temperature range and number of replicas in order to obtain a high exchange rate between the replicas (>40%). Secondly, the temperatures chosen must be exponentially spaced, as this increases the likelihood of exchange attempts being successful.

The application of replica-exchange simulations to peptides is logical for two reasons. Firstly, the small size of these molecules reduces the computational load per replica since the number of atoms, and hence calculable interactions, is small. Additionally, the number of replicas required to achieve a high exchange rate would be small since the changes in potential energy are small for a system with a small number of atoms, such as a peptide. Therefore, it is not surprising that a large number of replica exchange studies have been conducted that study the structure of peptides (Im & Brooks, 2005; Jas & Kuczera, 2004; Ohkubo & Brooks, 2003). It is the small size of these molecules that allows replica exchange simulations to be carried out that meets the required criteria. Although the studies cited above were carried out in CHARMM, it is important to note that replica exchange is a general approach that can be carried out using other molecular dynamics packages as well, such as NAMD (Menz *et al.*,2010) as well as the AMBER package (Jani *et al.*,2011).

6.3 Molecular dynamics simulations and the use of control peptides

In order to determine the molecular mechanism of the antimicrobial action of pseudin-2 and its analogues, molecular dynamics simulations needed to be carried out using both control peptides as well as pseudin-2. Initially, an all-atom system was used as this approach fully describes the

interactions between all atoms and molecules in the system and is the most likely to offer useful insights into the structure-function relationships of pseudin-2 since the movement of not only the peptide but also the water and lipid molecules would be modelled in full atomic detail. However, in order to assess the suitability of this as well as others molecular dynamics simulation setups, a suitable control peptide was required. The peptide chosen as the insertion control is WALP16 (Figure 6.3.1). This peptide was chosen for its simple hydrophobic structure and the availability of both in vitro as well as *in-silico* data that clearly shows that the peptide folds into a helix and inserts into biological membranes. The use of the term 'folding' with regards to peptide simulations is common in published data, since considerable molecular rearrangement is required for peptide to adopt a particular secondary structure (Balaraman *et al.*, 2011; Jas & Kuczera, 2004; Im & Brooks, 2005). Finally, the small size of the molecule (16 residues) reduces the computational load required to run simulations on this molecule.

WALP16 GWWLALALALALAWWA

Figure 6.3.1. Primary structure of WALP16

The peptide was initially modelled using in a fully explicit water-membrane system as such a system, despite being computationally intensive, has the potential to be the most informative. Following that, modelling was attempted using an implicit water-membrane system run both as a normal simulation and using replica exchange. The exploration of these three simulation setups allowed for the selection of the most suitable system by looking for the degree of folding of the control peptide WALP16.

6.4 Full-atom molecular dynamics simulation of WALP16 using NAMD

The molecular dynamics package NAMD was chosen as an initial system to describe the folding of the control peptide WALP16 for a number of reasons. The main reason for the use of this package is the ability to model peptides and lipid membranes in full atomic detail. The use of full-atom

models, although computationally intensive, carries with it the potential to be very structurally detailed. Finally, the availability of literature on the use of NAMD to run molecular dynamics simulations means the package can be easily applied to the problem of peptide folding.

6.4.1 Langevin Dynamics

Langevin dynamics was chosen as the simulation method since this technique has been shown to accurately describe the folding of peptides in an aqueous membrane environment (Im & Brooks, 2005). Langevin dynamics is an extension of molecular dynamics, with mathematical equations that account for frictional effects caused by high-speed collisions of solvent molecules. This makes it well-suited to the study of peptide insertion since these effects are likely to be important in membrane interaction and insertion. This is because the peptide interacts with both the solvent and the lipid molecules in the system. The additional mathematical terms present in langevin dynamics simulations that account for these effects are, therefore, likely to play an important role.

6.4.2 Force-field

The force-field chosen in both this simulation as well as subsequent ones is the CHARMM22 force field. This force-field contains corrections relating to energy calculations of the protein backbone which have been shown to improve agreement with structural NMR data of the peptide gramicidin A (Mustafa & Busath, 2009). This force-field has been chosen as it has successfully been used to model peptide-membrane interactions (Im & Brooks, 2005) as well as determine peptide structure (Abbassi *et al.*,2010; Abbassi *et al.*,2008).

6.4.3 Water model

The water model used in this explicit solvent simulation was the TIP3P model. This model assumes that the water molecules are rigid molecules, and that there are three interaction sites on each water molecule. Compared to the flexible SPC model, the TIP3P model is simpler, and allows for

more efficient computation during molecular dynamics. This especially true in cases such as this, where simulations contain a large number of water molecules.

6.4.4 Geometry and dimensions of simulation box, and periodic boundary conditions

A cubic simulation box was used with x, y and z dimensions as follows: [x=68, y=68, z=122]. The box was made to be longer along the z direction in order to accommodate the water molecules above the below the membrane, where the peptide was also located. Periodic boundary conditions were applied to all molecules in the system in all three directions. This meant that no molecule could 'drift away' or escape the system as movement of a molecule close to one edge of the box would make it reappear in the opposite edge.

6.4.5 Generation and placement of molecules

The peptide was generated as a linear molecule and placed in the centre of the water box ~25 Å above the lipid membrane. POPE was used as the lipid in this simulation as the ethanolamine in the head group is non-charged which simplifies of the data resulting from the simulation as charge effects are not present. The lipid membrane was centred at Z=0. The temperature used in the simulation was the physiological temperature of 37 degrees (310K). PME were used to calculate long-range electrostatics. Langevin dynamics were used with a coefficient of 5 pa/s for the heavy atoms to model the viscosity of the solvent phase. Ions are usually added to NAMD simulations to neutralise the effects of charged residues so the resulting system has no overall charge. However, since the system was already electrically neutral overall, no ions were added to the system. Figure 6.4.5.1 below shows the initial state of the water box used in the simulation. The final simulation box contained 48,281 atoms.

It is important to note that the membrane used in this simulation is a less-detailed representation of a bacterial membrane, which is of interest here since pseudin-2 is most active against bacteria (Olson *et al.*, 2001). There are two key differences between the membrane used here and a bacterial membrane. Firstly, the membrane is made up entirely of one lipid molecule. Biological

membranes generally comprise a variety of lipid species with proteins embedded within them. Secondly, since this membrane only contains neutral lipids, it is completely uncharged. This is not true of bacterial membranes, which are negatively charged (Dickson & Koohmaraie, 1989). Taking these points into consideration, one may still consider the membrane used in this setup a simplified version of a bacterial membrane.

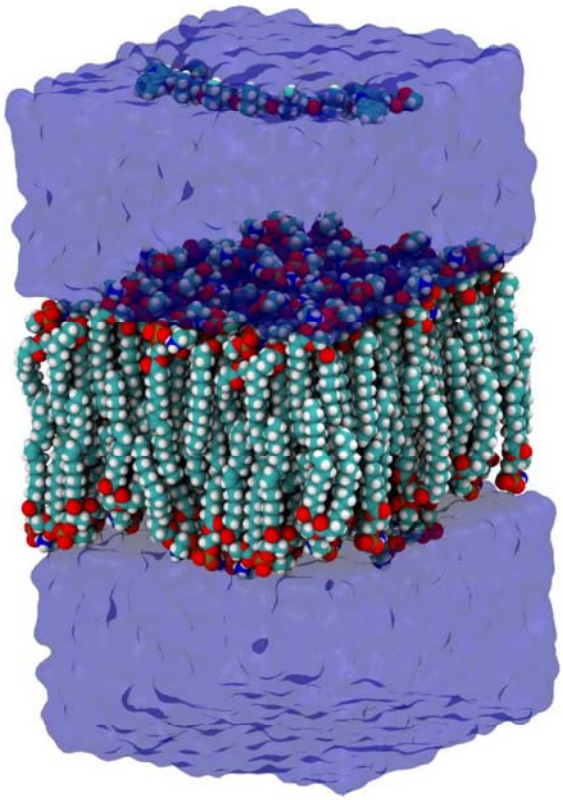

Figure 6.4.5.1. Image showing the initial setup of the simulation box. The water box is shown as a transparent blue cube. The peptide as well as the lipid molecules are shown in sphere representations, coloured by atom.

6.4.6 Minimization and equilibration

An initial minimization was performed (1000 minimisation steps followed by a 0.5ns run) fixing all atoms except the lipid tails in order to allow them to relax and remove any bad contacts that may have arisen during initial setup [2.10.3.2]. A second minimization was carried out with the peptide atoms constrained harmonically. Both minimization steps were carried out using the default minimization function in NAMD, which uses a conjugate-gradient algorithm. The constrained

movement of the peptide molecule combined with the free movement of the surrounding water and lipid atoms allows further equilibration of the system. In this system, it allows the water and lipid atoms to adjust to the spatial arrangement of the peptide molecule. Figure 6.4.6.1 below shows the result of the two minimization steps.

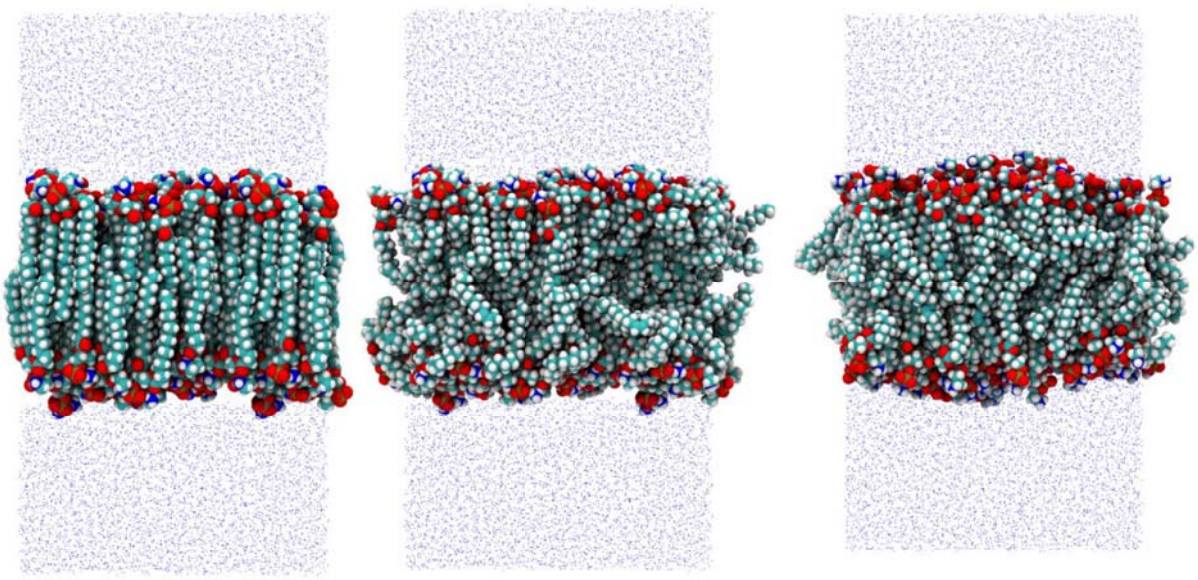

Figure 6.4.6.1. Simulation box showing (a) the initial state of the system, (b) the relaxed lipid tails after the first equilibration step and (b) the completely relaxed system after the second equilibration. The lipid molecules are shown composed of atomic spheres coloured by atom and the water molecules are shown as points for clarity.

It is important to note that this explicit solvent setup described here has been used to describe a both proteins as well as peptides. Explicit solvent simulations have been used to study the unfolding of beta-2 microglobulin, a transmembrane protein displayed on all nucleated mammalian cells identifying them to immune cells (Ma & Nussinov, 2003). Explicit solvent simulations have also been used to show that two temporin-L analogues (Pro3 and Phe1) have different effects on the structure of micelles (Saviello *et al.*, 2010). Explicit solvent simulations have also been used to show the formation of toroidal pores in micelles by the antimicrobial peptide magainin-2 (Leontiadou *et al.*, 2006). Finally, although the general use of explicit solvent/membrane setups such as the one described is fairly common, there are considerable

differences in the methods the simulation setups used. These include the length of the simulation trajectory, temperature, use of replica-exchange and langevin dynamics, as well as the software packages and modules used to carry out the simulations.

6.4.7 Simulation results

The simulation was run using NAMD on 16 cores for a total simulation time of 108ns (0).

Figure 6.4.7.1 below shows the potential energy changes during the course of the simulation.

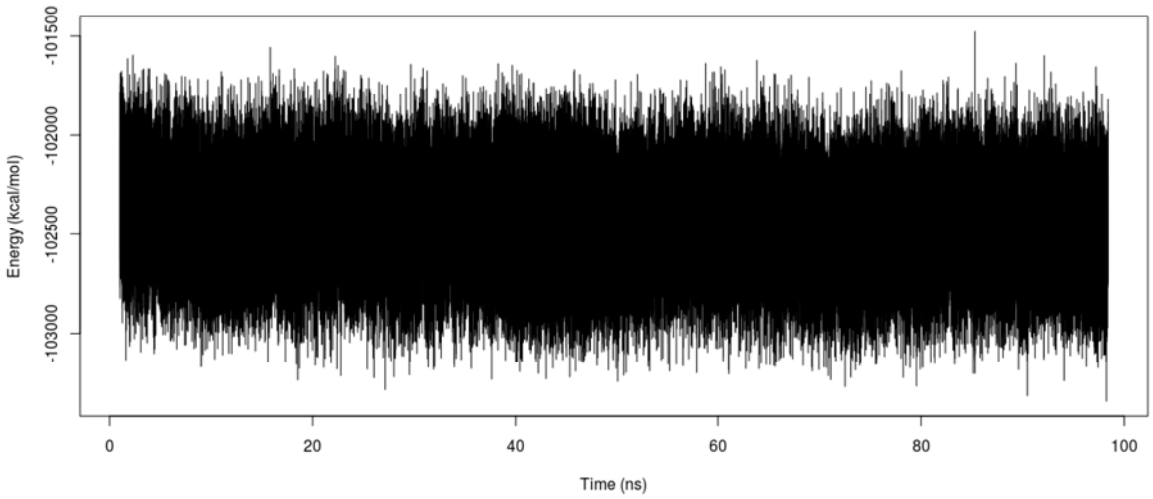

Figure 6.4.7.1. Plot showing the change in potential energy during the course of the NAMD simulation

The image above shows that there is no decrease in the potential energy of the system. This suggests that the system is not moving towards total equilibrium. Additionally, the peptide remains unstructured at the end of the simulation (Figure 6.4.7.2) and does not show the helical character this peptide has previously been shown to possess. Finally, although the peptide moves closer to the membrane, no insertion event can be seen in the simulation. This is illustrated in Figure 6.4.7.2 below.

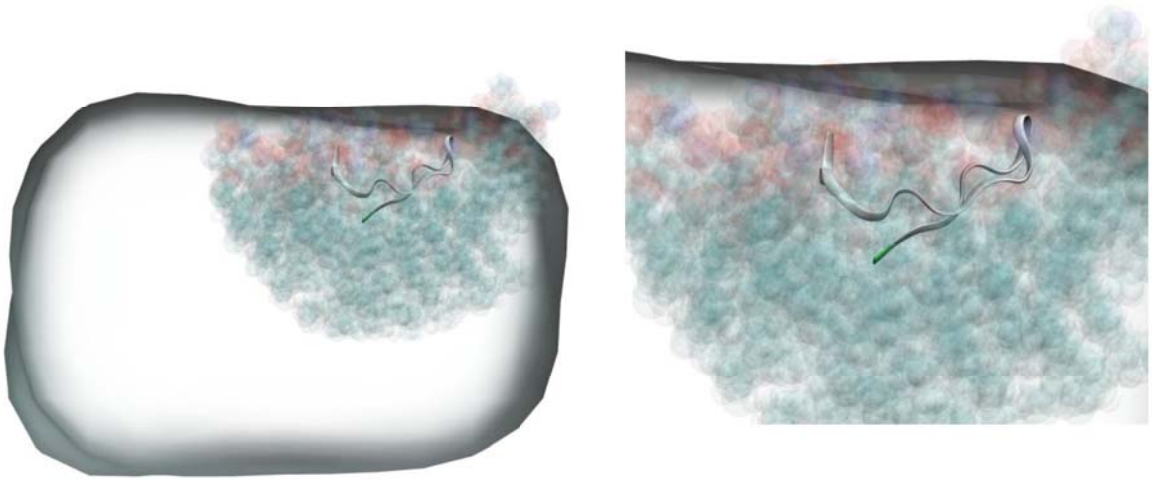

Figure 6.4.7.2. The structure of WALP16 at the end of the NAMD simulation. The peptide is shown as a silver ribbon and the lipid molecules within 15 Å of the peptide are shown with spheres representing the atoms. The lipid molecules shown have been made partially transparent in order that the structure of the peptide may be clearly visible. The box in both pictures shows the boundaries of the lipid membrane. For the sake of clarity, the water molecules in the simulation are not shown.

Figure 6.4.7.2 above shows that the peptide does interact with the lipid heads but neither completely inserts into the membrane nor folds into the alpha helical structure characteristic of this peptide.

The RMSD (2.10.4) and radius of gyration plots for this simulation are shown in Figure 6.4.7.3 below with the two major rearrangement events indicated using arrows. Both RMSD and radius of gyration were calculated using the alpha carbon atoms of the peptide. Analysis of the structure of the peptide using STRIDE within VMD showed no helical structure at any point during the simulation

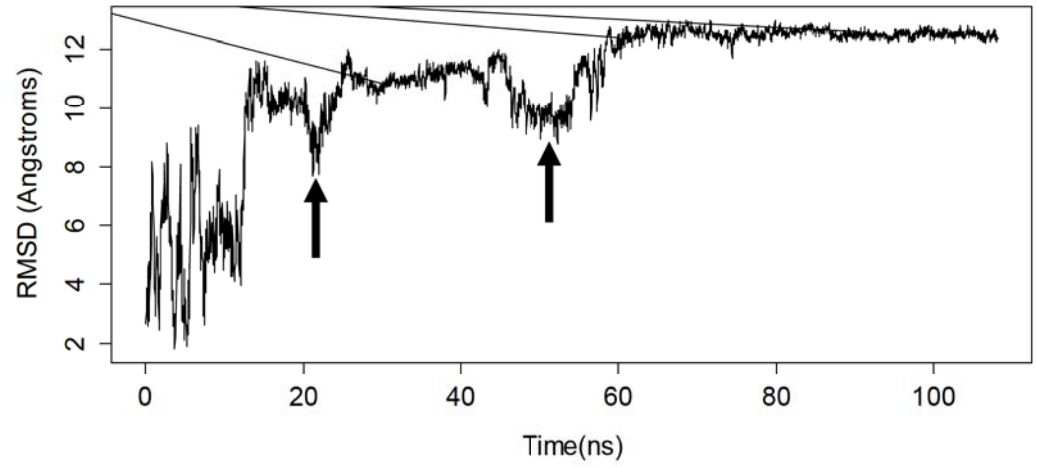

.

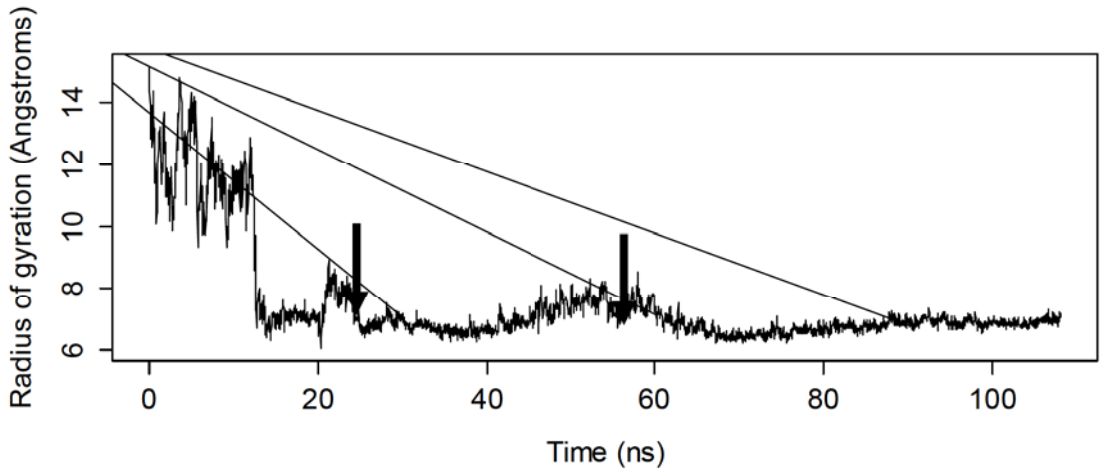

Figure 6.4.7.3. Changes in RMSD and radius of gyration of the alpha carbon atoms of WALP16 during the NAMD simulation. Structures corresponding to the timepoints highlighted are shown in the following figure.

The arrows in Figure 6.4.7.3 indicate two main rearrangement events: one at ~24ns and another at ~54 ns. The first corresponds to the peptide partially folding into a coil and the second to its rearrangement following binding to the lipid heads. These two rearrangement events are shown in Figure 6.4.7.4 below.

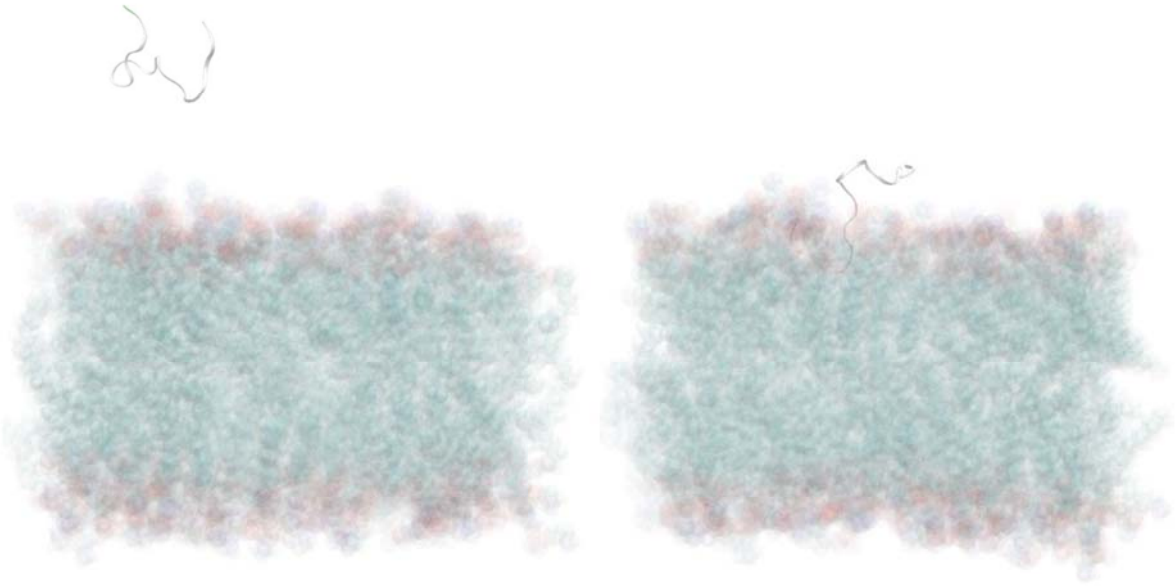

(a) (b)

Figure 6.4.7.4 (a,b). The two rearrangement events observed in the NAMD simulation. The two snapshots correspond to 24 ns (a) and 54 ns (b) respectively.

Therefore, it is clear that despite the long simulation time, the complete folding of the peptide does not occur. This highlights one of the main drawbacks of full-atom simulations. These simulations are computationally expensive as they take all atomic interactions into account but a normal full-atom simulation is incapable of showing peptide folding unless long trajectories (of the orders of microseconds) are considered.

Since the complete folding of WALP16 did not occur during the course of the NAMD simulation despite a relatively long trajectory, an alternative to all-atom simulations was sought. The two alternatives to these types of simulations are to either use an implicit solvent/membrane model (part of the CHARMM software package) or to use a coarse-grain simulation model.

Coarse-grain simulations offer reduced computational cost at the cost of detail, since groups of atoms are modelled as a single 'bead'. Implicit membrane models also reduce computational load considerably but the cost in these simulations is the loss of detail with regards to lipid and water

interaction. Both the aqueous and lipid components of the system are modelled as 'phases', so the detail in the interaction of the peptide with either the water or lipid molecules would be lost. The peptide, however, may be modelled in full atomic detail and the movement and folding of the peptide can be described in detail.

Of these two methods, the CHARMM GBSW implicit membrane/solvent model was chosen since the modelling of the equilibrium structure of the peptide in full atomic detail is relevant to this study of pseudin-2. Therefore, loss of detail with regards to the solvent/membrane molecules was chosen over loss of overall detail in coarse-grain simulation systems.

6.5 CHARMM GBSW Implicit solvent/membrane model

In order to overcome the large computational load associated with full-atom simulations, CHARMM's GBSW model was adopted. The reduced computational load associated with this model allows the user to run longer trajectories with relatively little computational power. It was, therefore, decided that this model would overcome the problem of partial folding observed in the NAMD simulation described earlier. This system uses a Generalised-Born model to model two phases and also contains a switching function between the aqueous and hydrophobic phases. It is an implicit solvent/membrane model which allows the modelling of both the solvent (water) and lipid phases implicitly, i.e. without using atoms to represent these phases. In this model, the peptide was represented with full atomic detail and placed in the implicit water/solvent model and allowed to fold. In all simulations, the peptide (in linear form) was positioned 25 Å above the implicit membrane, in the aqueous phase. The simulation setup is illustrated in Figure **6.5.1** below:

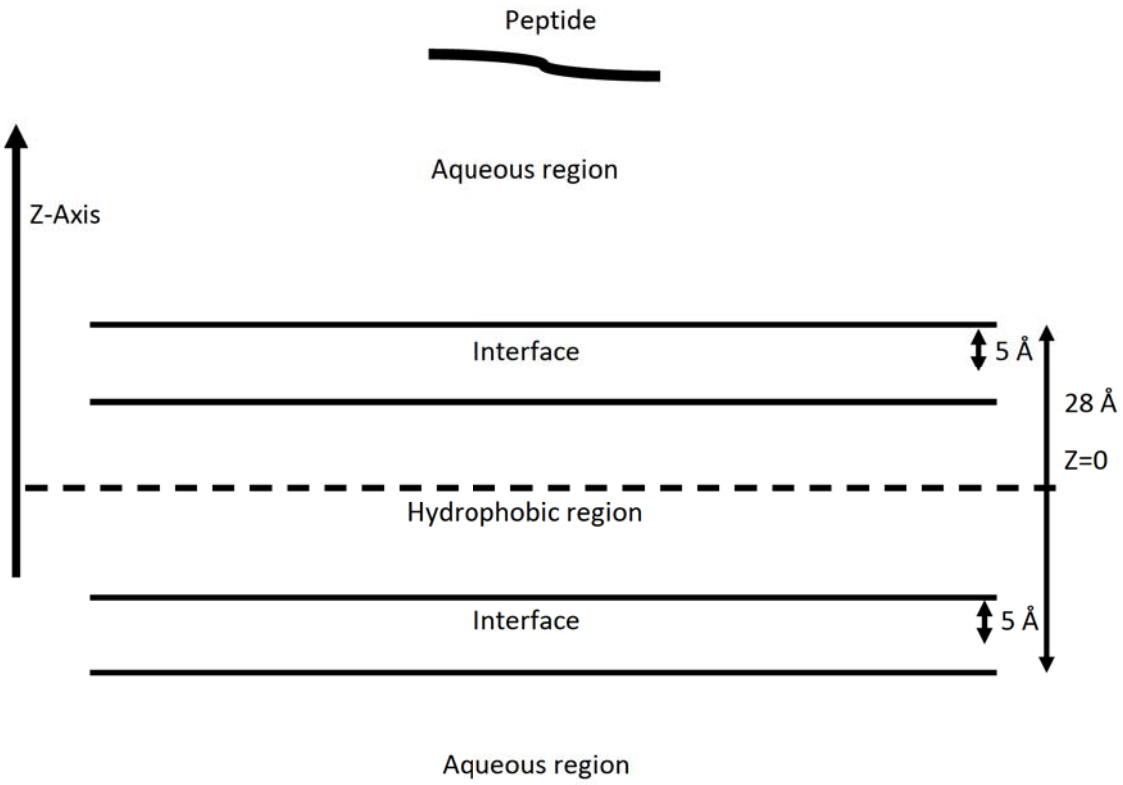

Figure 6.5.1. Illustration showing the GBSW Solvent/Membrane model in CHARMM. The centre of the hydrophobic region is at Z=0 and the regions change along the Z-axis. The approximate position of the peptide is also shown.

In this model, both the lipid membrane and the solvent are replaced by two distinct regions: an aqueous and a hydrophobic phase. The setup included a hydrophobic region 28 Å in length with an interfacial region 5 Å in length with a smoothing function to create transition between the hydrophobic and aqueous regions. Note that the entire layout is symmetrical along the Z-axis.

The simulation was setup using WALP16 and standard conditions (2.10.1). Like the NAMD simulation, Langevin dynamics were used. Langevin dynamics were restricted to the heavy atoms and a coefficient of friction of 5pa/s was used. The simulation was run for 72ns. The potential energy plot during the course of the simulation is shown in Figure 6.5.2 below.

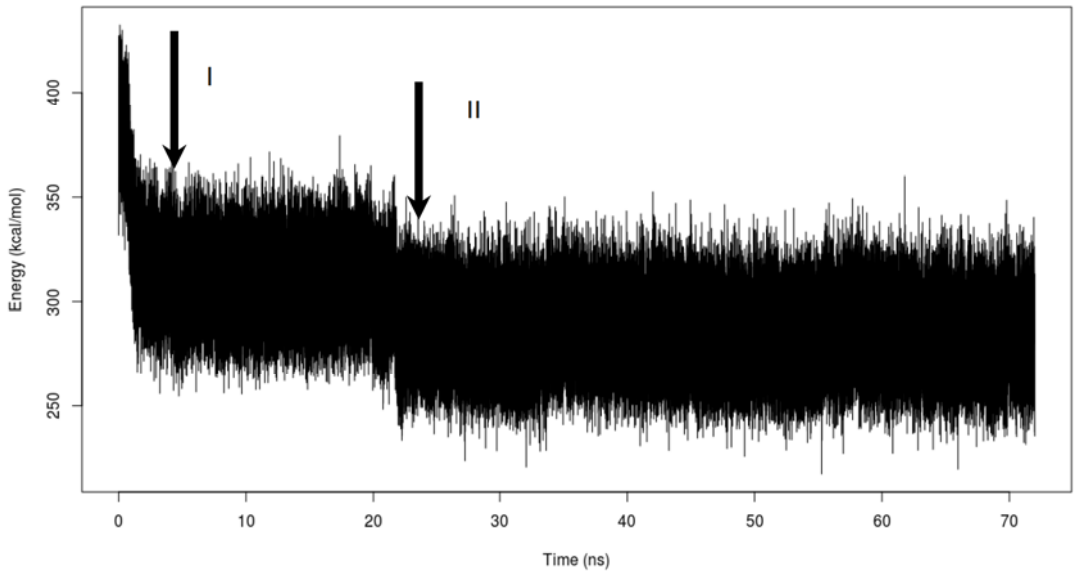

Figure 6.5.2. Potential energy of the system during the CHARMM GBSW simulation of WALP16. The two arrows indicate the two events associated with an abrupt decrease in potential energy

The two events associated with a sharp decrease in potential energy occur at ~3 ns and ~22 ns. These are the time points at which the peptide inserts into a membrane, and partially folds into an alpha helical structure. The structures at these two timepoints are given in Figure 6.5.3 below. This structure is only partly consistent with *in-vitro* structural data of WALP16 (obtained by infrared spectroscopy and circular dichroism) since the peptide is known to form a membrane-spanning perfect helix (de Planque *et al.*, 2001).

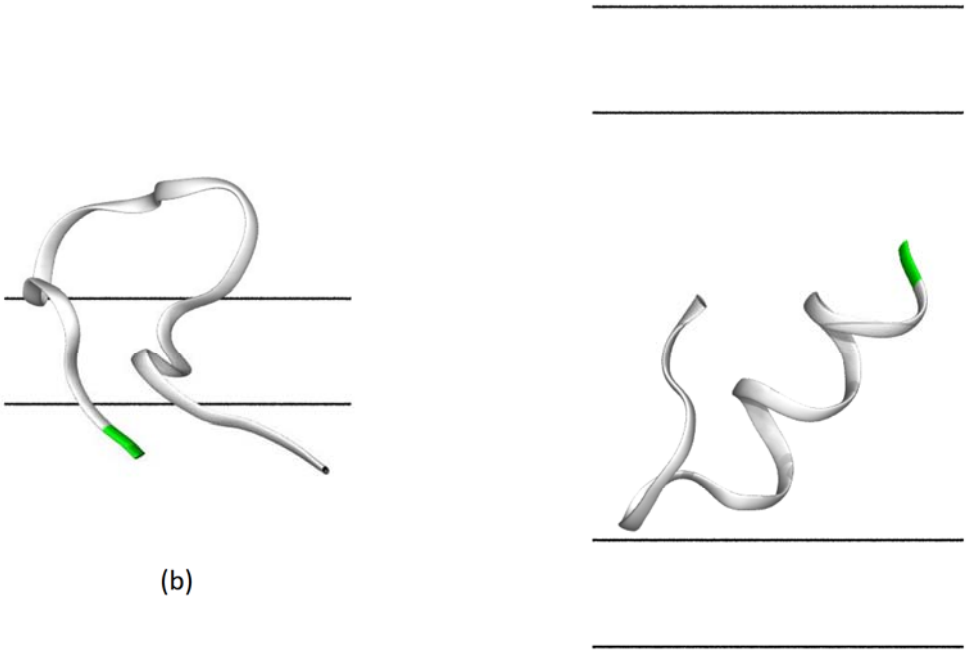

(b)

(c)

Figure 6.5.3. The structure of the peptide during (a) insertion into the implicit membrane and (b) partial folding into an alpha helix

The above structures show that the simulation data is consistent with what is to be expected, i.e. that the peptide inserts into the membrane and forms a helix (Im & Brooks, 2005). However, the folding of the peptide is incomplete. An examination of the position of the peptide with respect to the implicit membrane (Figure 6.5.4) also supports this observation.

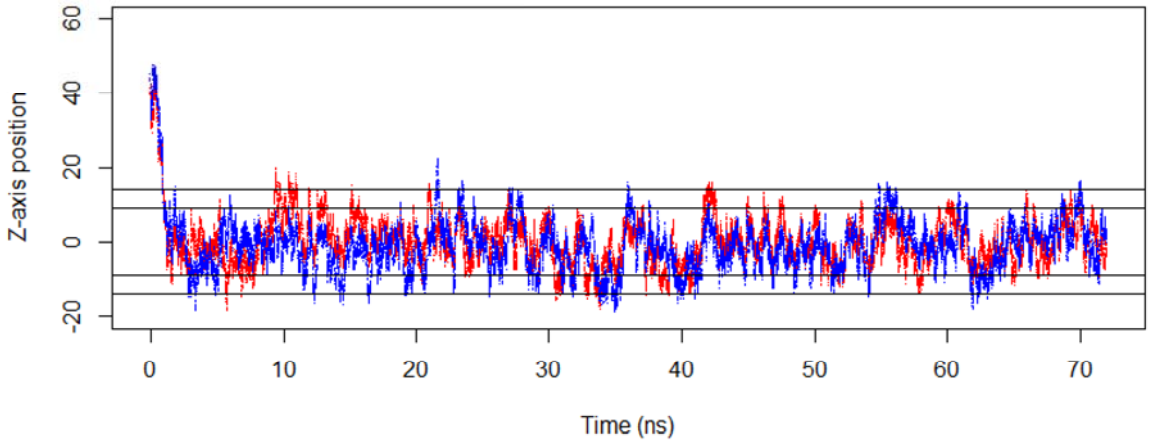

Figure 6.5.4. Positions of the N-terminus (red) and C-terminus (blue) of WALP16 during the CHARMM GBSW simulation. The horizontal lines indicate the positions of the hydrophobic, aqueous, and interface regions as previously described.

The figure above shows that throughout the entire simulation, the N-terminus and C-terminus of the peptide remain close to one another, again illustrating that the peptide is not a completely-formed helix. This partial folding of the peptide may be explained on the basis that the peptide is simply trapped within a local energy minimum, since the peptide is known to form a membrane-spanning perfect helix (de Planque *et al.*, 2001). The simulation setup has not allowed the peptide to find its global energy minimum during the course of the simulation. This is supported by both the RMSD and radius of gyration plots of this trajectory shown in Figure 6.5.5 below.

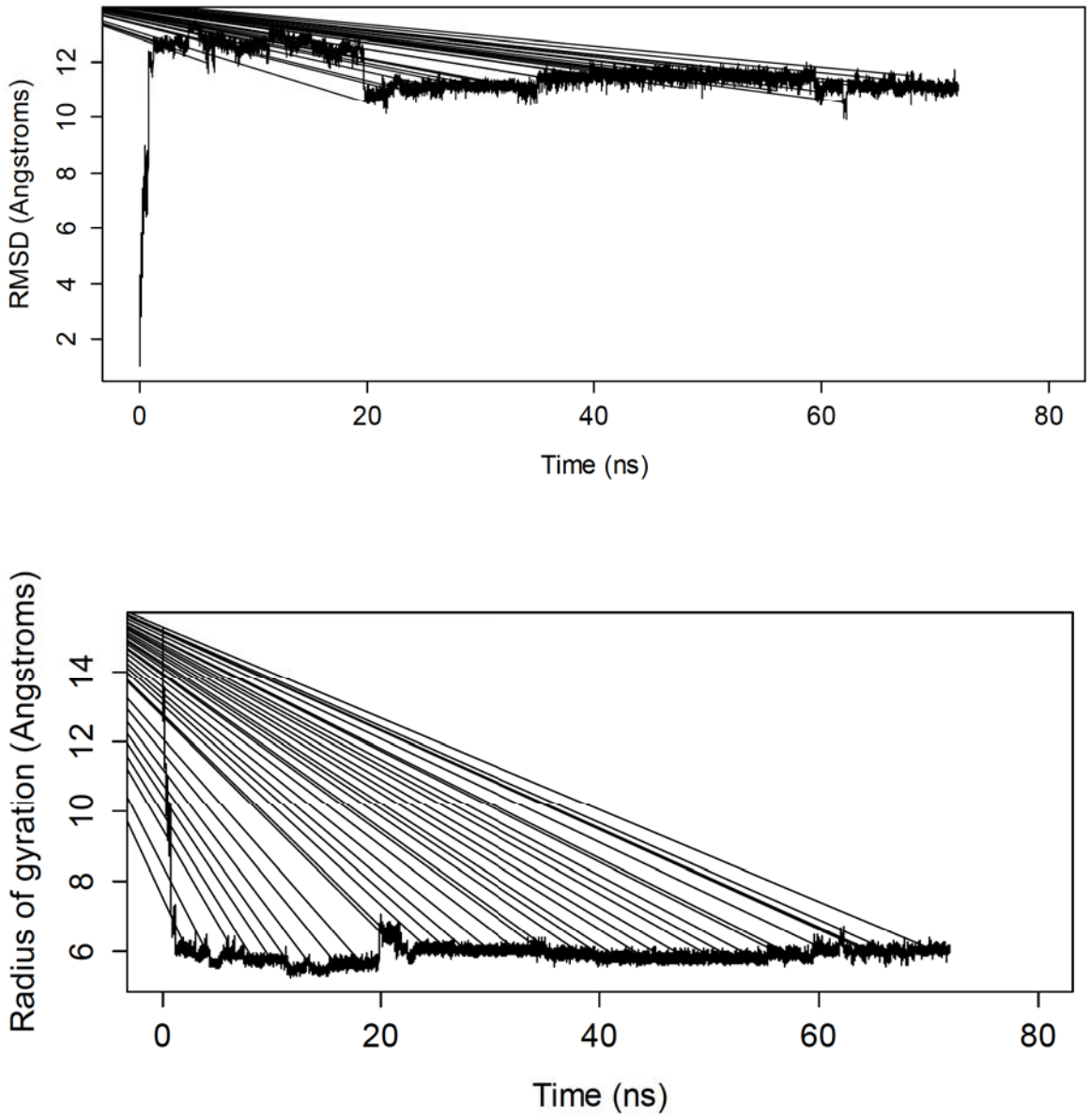

Figure 6.5.5. The RMSD (a) and radius of gyration of WALP16 during the CHARMM GBSW simulation

The RMSD plot shows an initial fluctuation of the peptide, an abrupt change at ~20 ns, followed by little change in the peptide's structure. This is mirrored in the radius of gyration of the peptide, where only a single large change is observed, also at ~20 ns, followed by little change in the radius of gyration of the peptide.

Therefore, despite the relatively long trajectory of this simulation , the complete folding of WALP16 was not observed. The simulation was, therefore, terminated at 72ns, at which point WALP16 retained its partially folded structure (Figure 6.5.6).

Figure 6.5.6. Structure of WALP16 at the end of the 72 ns simulation.

Therefore, although the implicit membrane simulation was associated with a reduced computational cost, the complete folding of WALP16 was not obtained.

6.6 Replica exchange simulations

Since both the full-atom and implicit membrane/solvent simulations at a single temperature (300K) were unsuccessful in folding WALP16, replica exchange simulations were attempted as these have been shown to be able to rapidly fold small peptides in a very efficient manner (Im & Brooks, 2005). All simulations were run using 32 replicas with 32 exponentially-spaced temperatures ranging between 300K and 1000K for TMX-3 (see below) and 300K -800K for all other peptides. The temperature chosen for folding the peptides is 300K in all cases as this temperature is commonly used as the lowest temperature in replica exchange studies. The initial setup of the peptides was identical to that used in the single-temperature simulation described earlier, except in this case replicas at different temperatures were used.

6.6.1 A note on the presentation of replica-exchange simulation data

Replica exchange data may be considered as matrix in which each conformation has both a replica value as well as a temperature value. In other words, each replica will contain conformations at various temperatures and each temperature will contain conformations from various replicas. Therefore, in order to find the lowest energy conformation of the system, one must analyse at the lowest temperature 'ensemble'. This is illustrated in Figure 6.6.1.1 below. In this illustration, Temp1 is the lowest temperature

	Temp1	Temp2	Temp3	Temp4
Replica 1	$N_{(T1,R1)}$	$N_{(T2,R1)}$	$N_{(T3,R1)}$	$N_{(T4,R1)}$
Replica 2	$N_{(T1,R2)}$	$N_{(T2,R2)}$	$N_{(T3,R2)}$	$N_{(T4,R2)}$
Replica 3	$N_{(T1,R3)}$	$N_{(T2,R3)}$	$N_{(T3,R3)}$	$N_{(T4,R3)}$
Replica 4	$N_{(T1,R4)}$	$N_{(T2,R4)}$	$N_{(T3,R4)}$	$N_{(T4,R4)}$
Replica 5	$N_{(T1,R5)}$	$N_{(T2,R5)}$	$N_{(T3,R5)}$	$N_{(T4,R5)}$

Figure 6.6.1.1. Diagram showing the data generated by a replica exchange. The highlighted cells show the trajectory for the lowest temperature ensemble.

In order to simplify the analysis of the replica simulation data, the lowest temperature ensemble was selected (300K) and a trajectory was generated using the replicas within that ensemble. The data was then analysed using similar methods to those used in previous simulations: using RMSD and radius of gyration values and secondary structure classification.

6.6.2 Selection of control peptides

Since the aim of this molecular dynamics study was to look for folding and membrane insertion in pseudin-2, WALP16 was once again selected as an initial control to assess the ability of the replica-exchange setup to correctly predict the folding and insertion of the peptide. Following the successful folding of WALP16, various other control simulations were also carried

out. This was in order to thoroughly assess the ability of the simulation setup used to handle different molecular features. A summary of all the control peptide simulations is given in

Table **6.6.2.1** below:

Name	Sequence	Function
WALP16	GWWLALALALALAWWA	Initial insertion control
WALP23	GWWLALALALALALALALWWA	Second, larger insertion control
TMX-3	GGWAALAAHAAPALAAALAHAAASRSRSRSR	Control for non-insertion

Table 6.6.2.1. The amino acid sequence and the function of the various peptides used in the control simulations.

All simulations were run as replica-exchange simulations for 30ns.

Replica exchange simulations were set up for the three control peptides shown above. The temperature range used for WALP16 and WALP23 was [300K-800K] and a higher temperature range was used for the large TMX-3 peptide [300K-1000K]. The ends were blocked in all simulations using an acetylated N-terminus (CHARMM designation: AC3) and a 3-methyl C-terminus (CHARMM designation: CT3). Each of the three control simulations is described in the following section.

6.6.3 WALP16 replica-exchange simulation

A replica-exchange simulation was run with WALP16 using standard conditions (2.10.2). The potential energy diagram shows a gradual decrease in energy followed by a plateau when the global energy minimum of the peptide is reached (Figure 6.6.3.1 (a)). The representative low-energy structure of the peptide is shown in Figure 6.6.3.1 (b). This structure is that of a perfect helix and is consistent with data published by Im and co-workers (Im & Brooks, 2005).

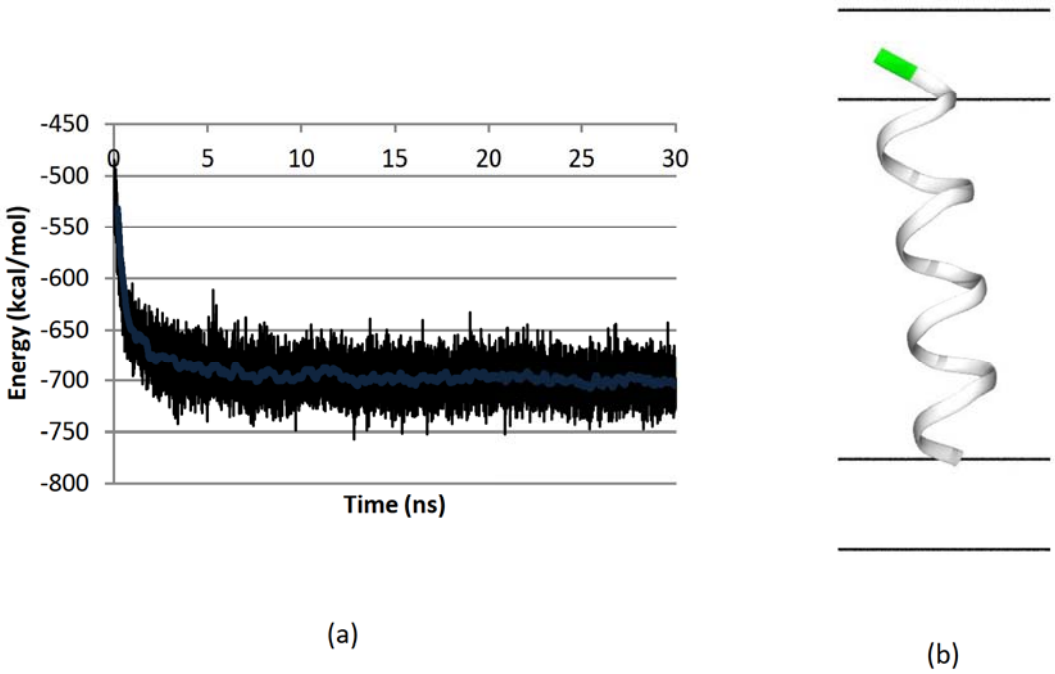

(a) (b)

Figure 6.6.3.1 (a) Potential energy change for the 300K ensemble of the WALP16 replica exchange simulation and (b) the equilibrium structure of the peptide

RMSD and radius of gyration analysis shows results that are consistent with the trend seen in the potential energy (Figure 6.6.3.2). Both the backbone RMSD as well as the radius of gyration of the peptide fluctuate considerably during the initial part of the simulation. Once the peptide is helical, the structure only shows minor changes during the course of the simulation. Additionally, it is interesting to note that the final radius of gyration of the peptide is close to 6.66 Å, which is the expected value for a perfect helix (assuming a helix has 3.6 residues per turn with a translation of 1.5 Å).

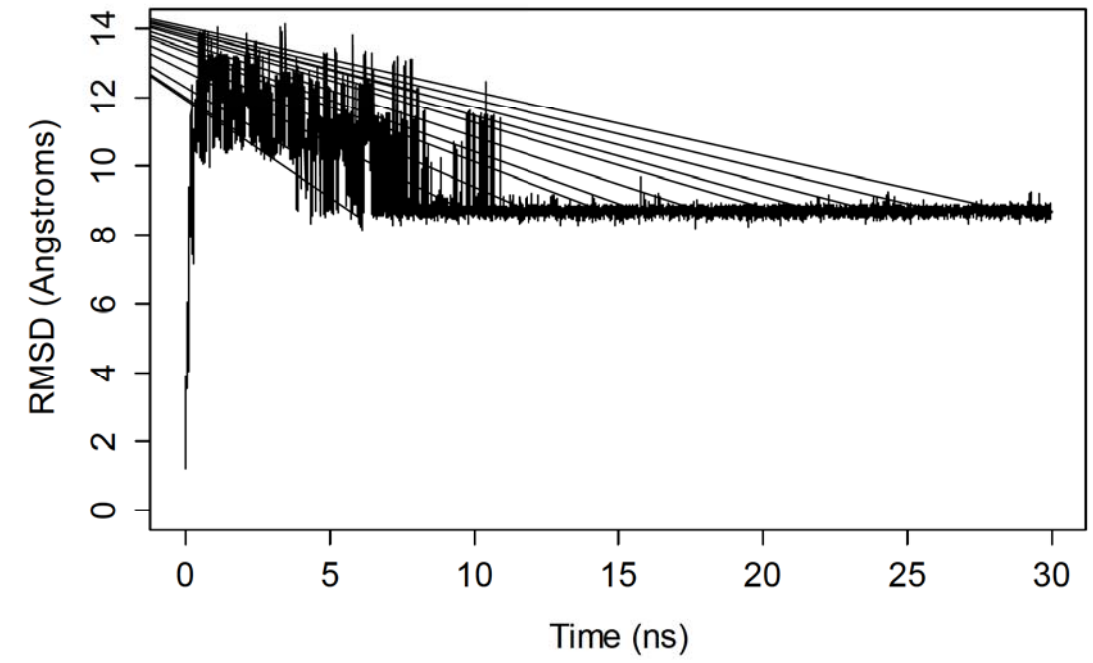

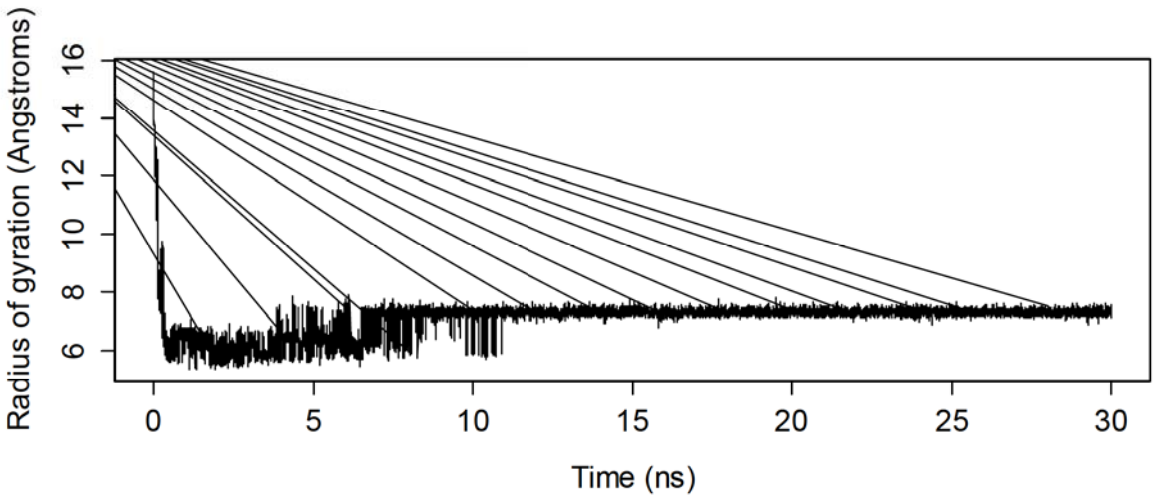

Figure 6.6.3.2. Backbone RMSD and radius of gyration of the replica exchange simulation of WALP16.

The position of the peptide during the simulation (Figure 6.6.3.3) shows that following folding, the peptide inserts into the membrane completely, with its N-terminus and C-terminus on opposite ends of the membrane. The data shown below appears noisy due to the constant swapping of replicas but a comparison of this data with the backbone and RMSD data for the same trajectory shows that the peptide forms a straight, stable helix within the membrane.

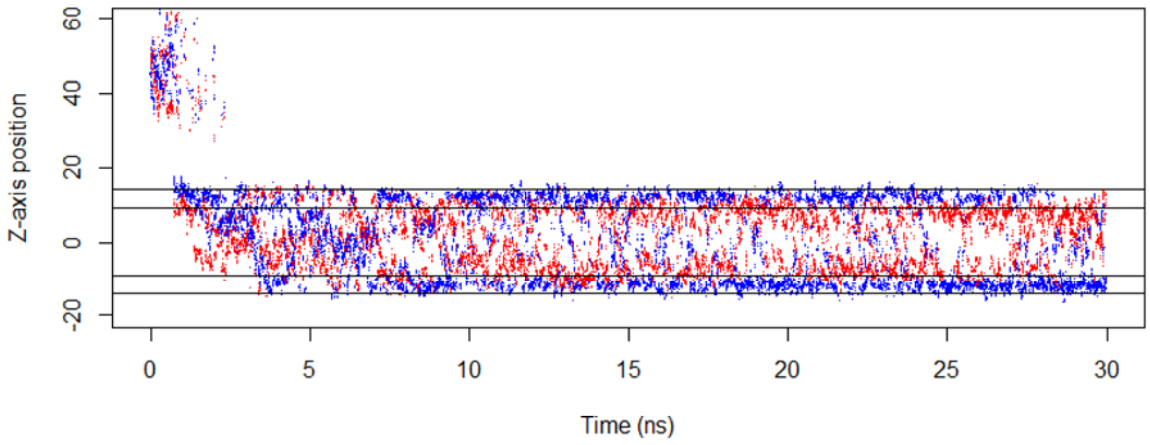

Figure 6.6.3.3. Z-axis positions of the N-terminus (red) and C-terminus (blue) of WALP16 during the CHARMM GBSW simulation. The horizontal lines indicate the positions of the hydrophobic, aqueous, and interface regions as previously described.

Finally, an analysis of the equilibrium secondary structure of the peptide was carried out using the built-in STRIDE function in VMD 1.8.7. The secondary structure of each residue of the peptide was assigned during the final 1ns of the 300K trajectory. The percentage of frames during which each residue was helical is shown below (Figure 6.6.3.4).

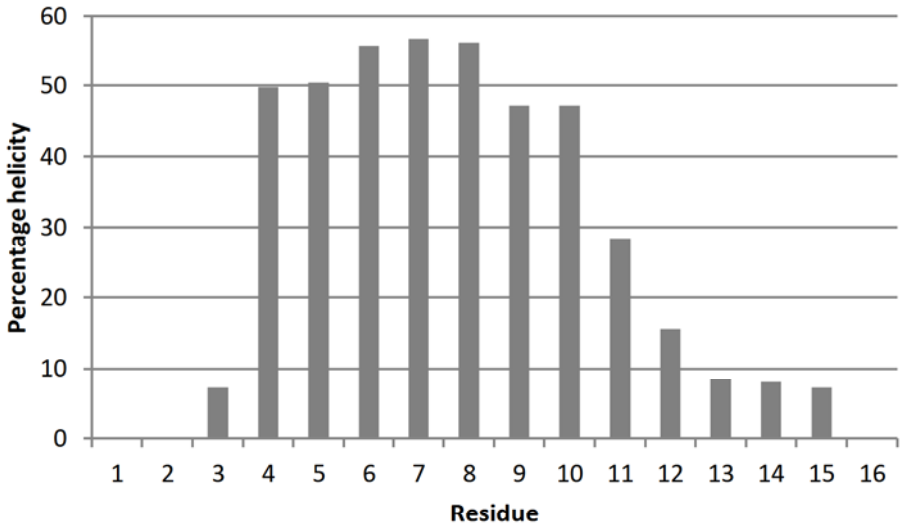

Figure 6.6.3.4. Percentage time spent in a helical structure for each of the 16 residues of WALP16 in the 300K trajectory.

`

The data above shows that the first three residues and the last four residues do not possess a helical character at equilibrium, whereas the middle residues (4-11) have a high helical character. One could argue that the percentage helicity shown disagrees with the known equilibrium structure of the peptide, which is that of a perfect helix. This could be due to the inability of the STRIDE algorithm to properly assign secondary structure to such a small molecule. It is, however, important to note that the peptide folds correctly and (as demonstrated by the RMSD and radius of gyration plots) its structure does not change after it has folded. As seen in Figure 6.6.3.4, the peptide is also helical along its entire length.

6.6.4 WALP23 replica-exchange simulation

A replica-exchange simulation was run with WALP23 using standard conditions (2.10.2). Although the WALP16 control demonstrates that the modelling setup used can fold small peptides effectively, it does not establish its ability to deal with slightly larger peptides. It is for this reason that the WALP23 control was chosen. The peptide possesses a very similar primary acid sequence to that of WALP16 but is comparable in size to pseudin-2. This peptide has also been shown to insert into membranes and fold into an alpha helical structure (Im & Brooks, 2005). The folding of this peptide would, therefore, confirm the ability of the simulation system to cope with larger molecules.

The potential energy plot of WALP23 is similar to that of WALP16, but the energy decrease is slower to reach a plateau (Figure 6.6.4.1 (a)). Since WALP23 is a larger molecule, a longer time is required before the molecule is completely folded. The final structure is also completely helical, as expected, with the peptide completely inside the hydrophobic region of the membrane. Additionally, the peptide positions itself at an angle of 45 degrees, which is also to be expected. The completely helical equilibrium structure of the peptide is also shown below (Figure 6.6.4.1 (b)).

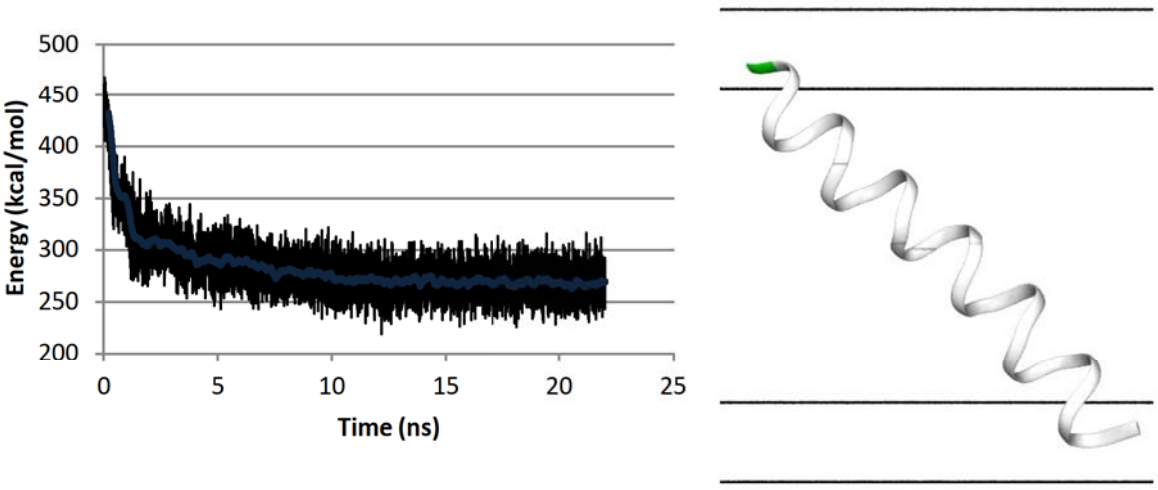

(c)

(d)

Figure 6.6.4.1. Potential energy change and equilibrium structure of the 300K ensemble of the WALP23 replica exchange simulation. The residue highlighted in green is the N-terminal glycine residue.

The backbone RMSD and radius of gyration changes during the trajectory are shown in Figure 6.6.4.2 below.

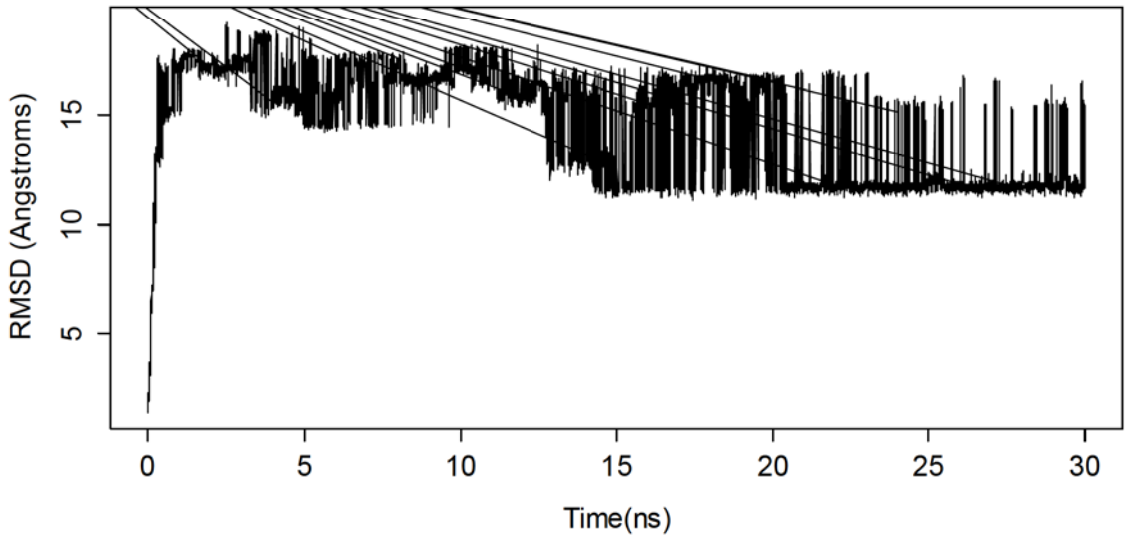

(a)

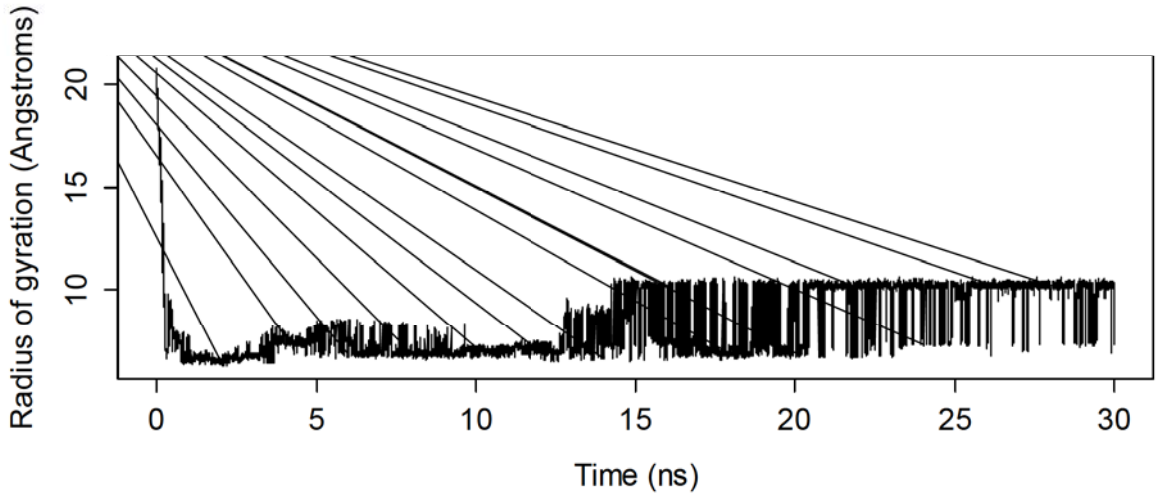

(b)

Figure 6.6.4.2. Backbone RMSD and radius of gyration values during the 300K trajectory of the WALP23 replica exchange simulation.

Both the backbone RMSD and radius of gyration plots of the WALP23 300K trajectory show an interesting feature. After the initial rearrangement (~13ns), there is rapid switching between two structures. Additionally, the frequency of this switching decreases towards the end of the simulation. An analysis of the trajectory reveals that this peptide possesses a second meta-stable

structure. This meta-stable structure is that of a 'kinked' helix. This structure is seen with decreasing frequency towards the end of the simulation. It is likely that a slightly longer trajectory is required to eliminate this meta-stable state and show the true equilibrium structure of the peptide. This structure is shown in Figure 6.6.4.3 below.

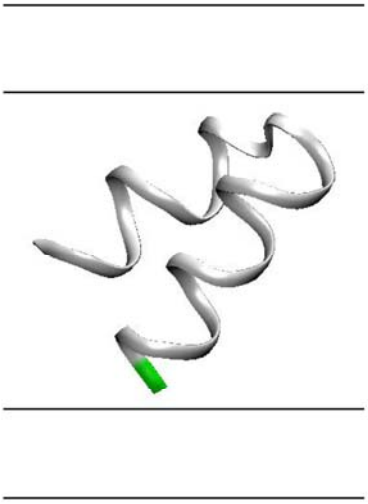

Figure 6.6.4.3. Meta-stable structure observed towards the end of the WALP23 replica exchange simulation. The horizontal lines indicate the aqueous, hydrophobic, and interface regions as previously described. The residue highlighted in green is the N-terminal glycine residue.

The Z-axis position of WALP23 shows a similar pattern to that seen in the case of WALP16. Taking the rapid swapping characteristic of replica-exchange simulations into account, the peptide adopts a conformation with its N-terminus and C-terminus at opposite ends of the membrane. This is shown below (Figure 6.6.4.4).

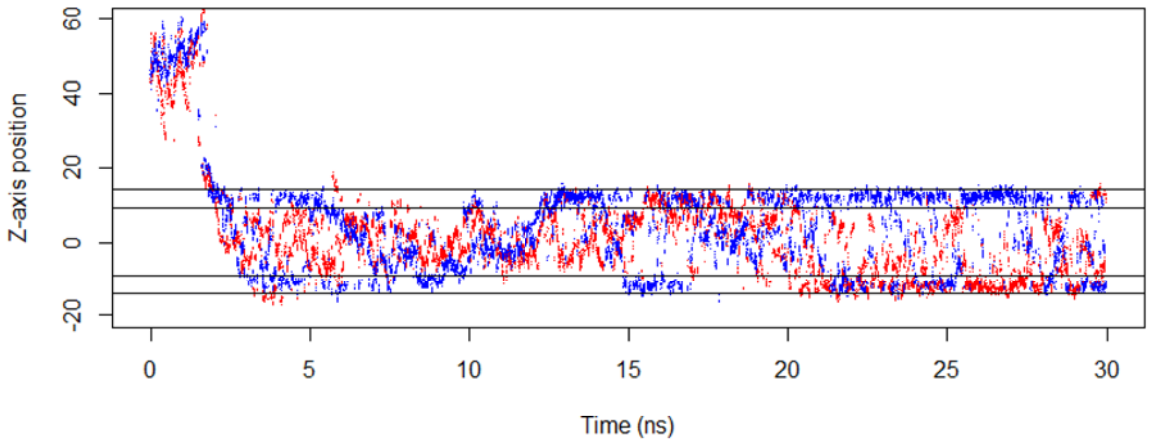

Figure 6.6.4.4. Z-axis positions of the N-terminus (red) and C-terminus (blue) of WALP16 during the CHARMM GBSW simulation. The horizontal lines indicate the positions of the hydrophobic, aqueous, and interface regions as previously described.

With regards to the secondary structure classification of the peptide at equilibrium, STRIDE analysis of the last 1ns of the simulation shows that the peptide is completely helical all along its length. This data is in good agreement with the perfect helical structure observed in the simulation. The percentage helicity of the peptide during the last 1ns of the simulation is shown below (Figure 6.6.4.5).

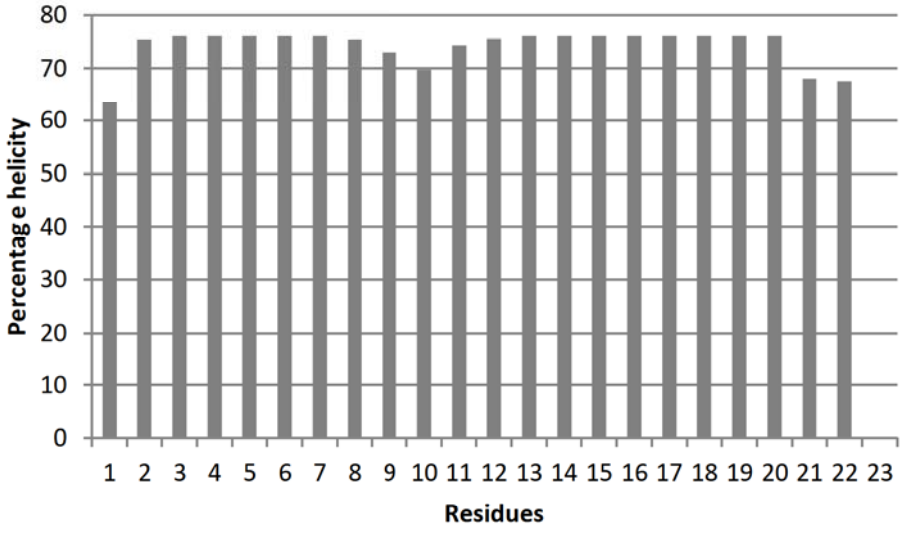

Figure 6.6.4.5. Percentage time spent in a helical structure for each of the 23 residues of WALP23 in the last 1ns of the300K trajectory.

6.6.5 TMX-3 replica-exchange simulation

The final simulation was chosen for two main reasons. Firstly, this peptide has a more diverse primary structure which includes hydrophobic, polar non-charged as well as positively charged residues. Additionally, this peptide is known to remain at the surface of membranes without inserting into them. TMX-3 is, therefore, a suitable peptide to demonstrate that the simulation setup used can adequately describe peptides that do not insert into membranes and possess a diverse primary structure.

A replica-exchange simulation was run with TMX-3 using standard conditions (2.10.2).The potential energy plot of TMX-3 is similar to that of WALP16 and WALP23 as it shows a rapid decrease in potential energy (Figure 6.6.5.1). This is may be associated with the fact that this peptide does not completely insert into the membrane. Additionally, due to the relatively large size of this molecule the higher temperatures used are likely to allow for the more efficient crossing of energy barriers. The equilibrium structure of TMX-3 consists of two helical segments with a 'kink' at the proline residue at position 12.

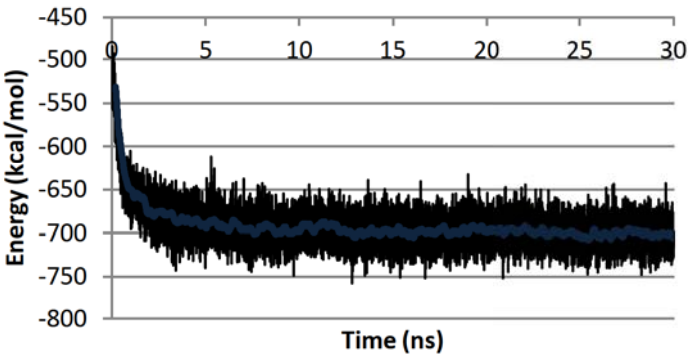

(e)

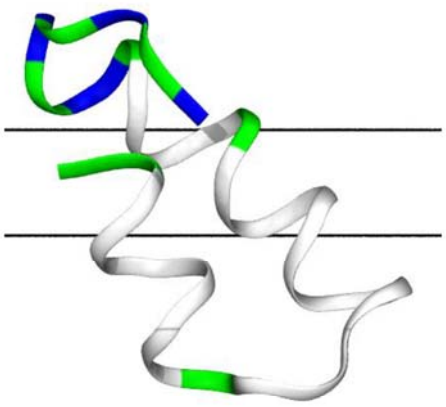

(f)

Figure 6.6.5.1. (a) Potential energy plot of TMX-3 during the 300K trajectory and (b) the equilibrium structure of the peptide at the end of the simulation

Both the backbone RMSD and radius of gyration plots of TMX-3 (Figure 6.6.5.2) are reflective of its flexible structure. Both show an initial rearrangement followed by constant change in structure which starts at ~3ns and continues till the end of the simulation. This is considerably different from the RMSD and radius of gyration values seen in the case of the WALP peptides. Both WALP16 and WALP23 formed rigid helices and this is clearly evident in the examination of the RMSD and radius of gyration values of their respective trajectories.

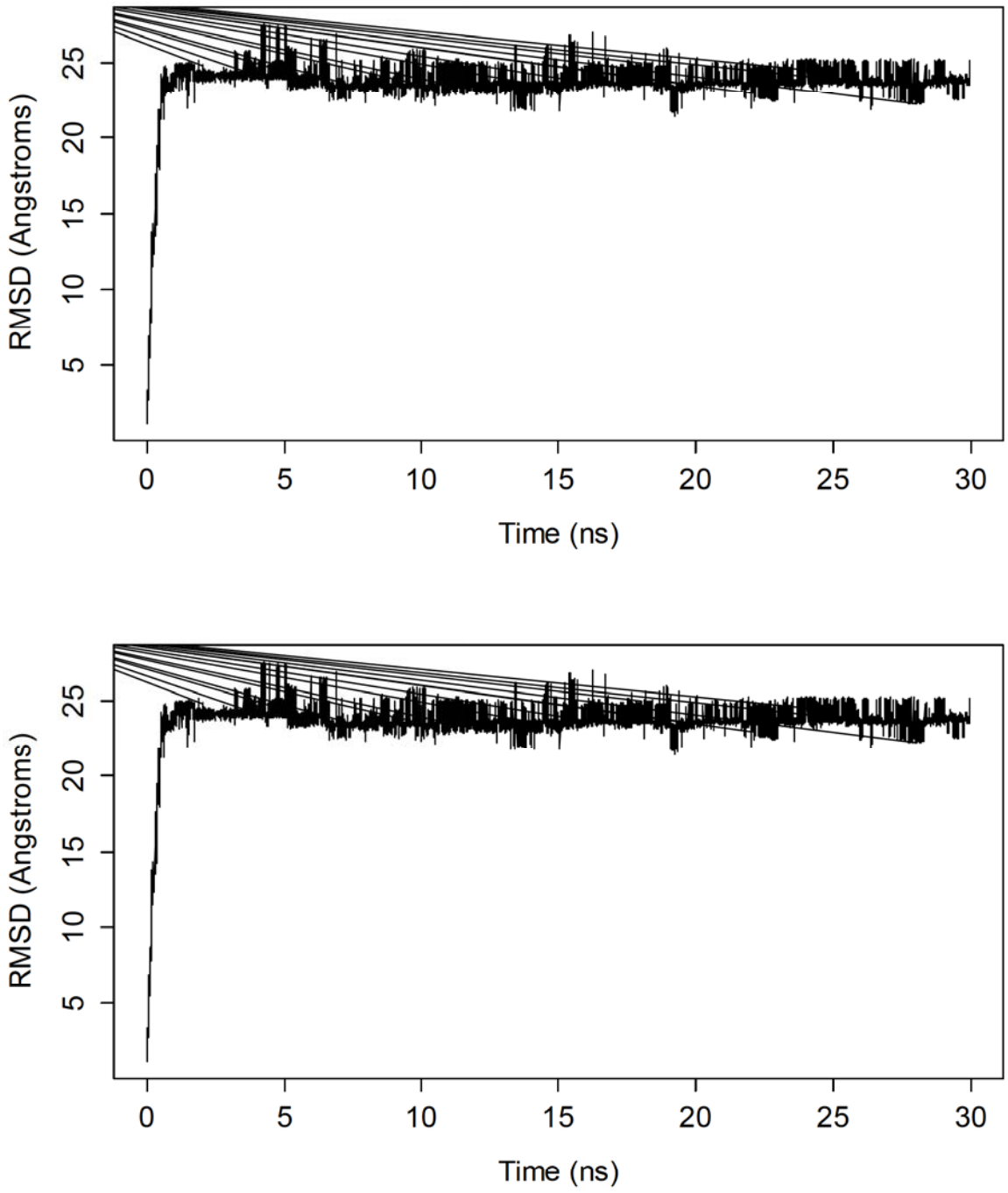

Figure 6.6.5.2. Backbone RMSD and radius of gyration values during the 300K trajectory of the TMX-3 replica exchange simulation.

The Z-axis position of the peptide during the simulation (Figure 6.6.5.3) also strongly reinforces the equilibrium structure shown earlier in Figure 6.6.5.1. The peptide remains partially embedded into the membrane with its N-terminus just below and its C-terminus just above the interfacial region.

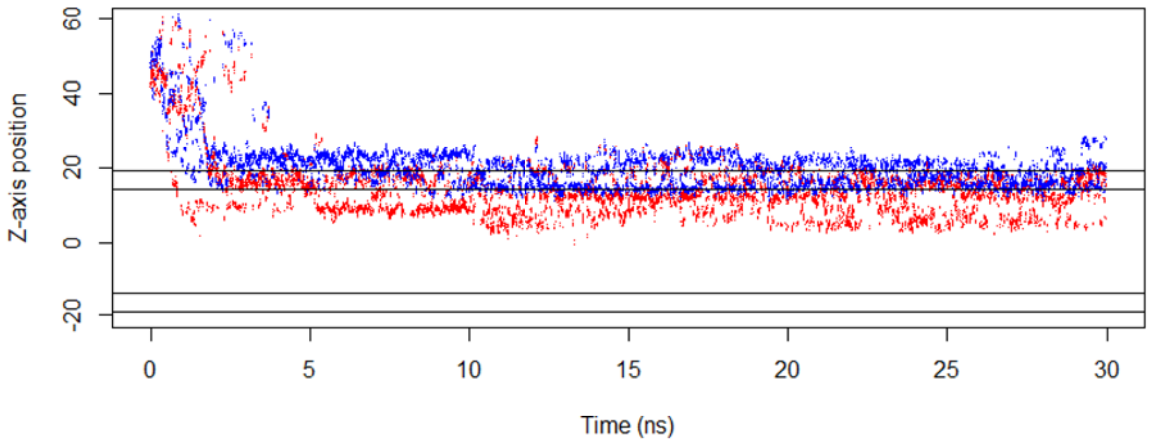

Figure 6.6.5.3. Z-axis positions of the N-terminus (red) and C-terminus (blue) of TMX-3 during the replica-exchange simulation. The horizontal lines indicate the positions of the hydrophobic, aqueous, and interface regions as previously described.

Finally, the secondary structure classification of the peptide more clearly illustrates the flexible and rigid segments within the peptide (Figure 6.6.5.4). At equilibrium, the peptide consists of two helical segments, spanning residues 2-7 and 12-22. Between these segments is a flexible region. Additionally, the C-terminus of the peptide showed little helical character and was highly variable.

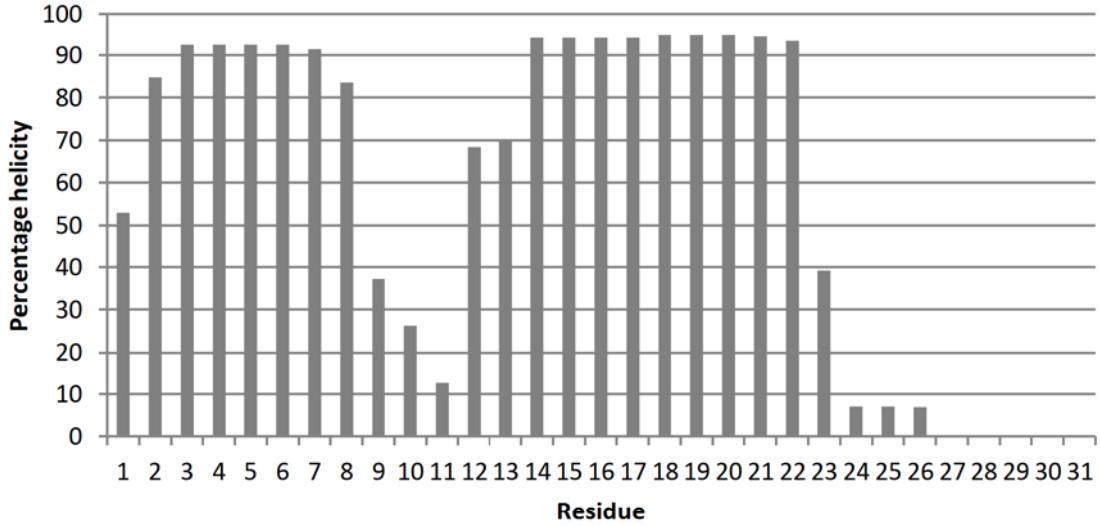

Figure 6.6.5.4. Percentage time spent in a helical structure for each of the 23 residues of TMX-3 in the last 1ns of the300K trajectory.

6.6.6 Effect of charged ends on membrane insertion

Finally, prior to modelling pseudin-2, the effect of charge on the adopted replica exchange simulation setup was examined, both to assess the effect of charged ends and to assess the effect of charge within the molecule. In the first simulation, the WALP16 simulation was repeated using normal charged ends instead of the blocked ends (2.10.2). Figure 6.6.6.1 below shows the potential energy change and the equilibrium structure of the peptide in the simulation.

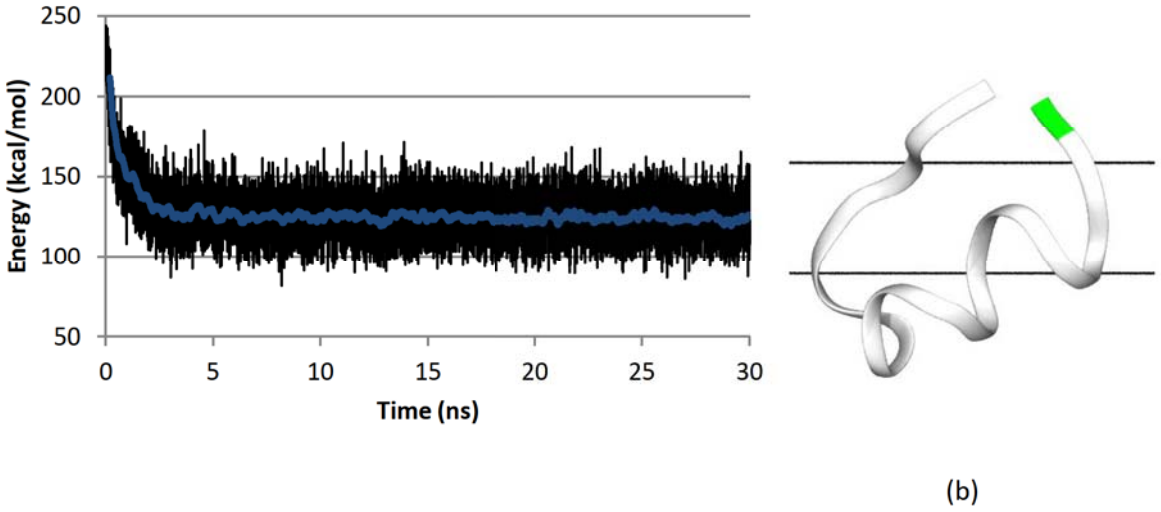

Figure 6.6.6.1. (a) Plot showing change in potential energy during the WALP16 simulation carried out with charged ends and (b) the structure of the peptide at the end of the 30ns simulation

The backbone RMSD and radius of gyration plots of the WALP16 peptide with charged ends are shown in Figure 6.6.6.2 below.

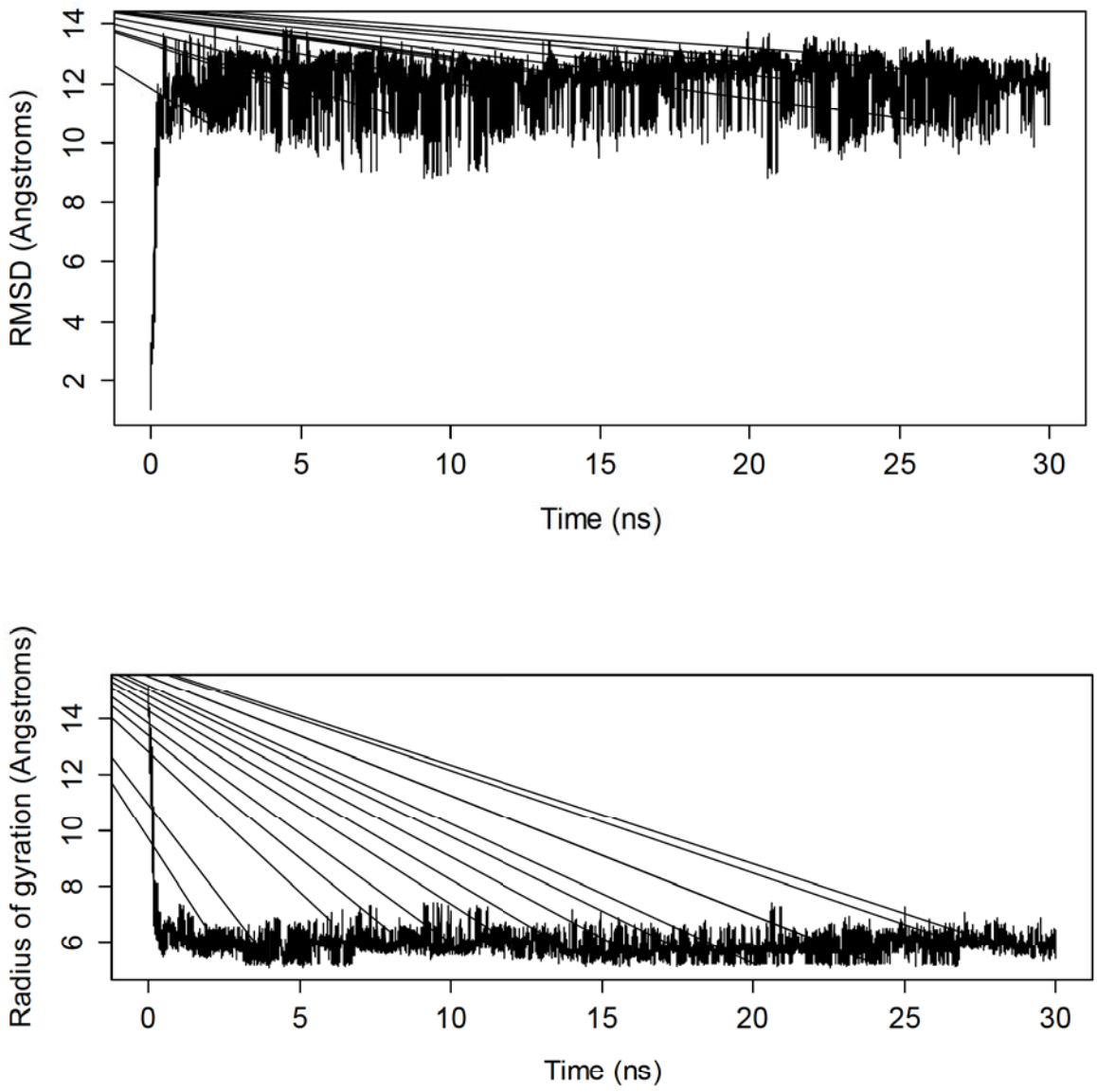

Figure 6.6.6.2. Backbone RMSD and radius of gyration values during the 300K trajectory of the TMX-3 replica exchange simulation.

The backbone RMSD and radius of gyration plots of the charged WALP16 simulation show features that are very different from those observed in the case of the WALP16 simulation carried out with blocked ends. Both plots show a peptide with a highly variable structure, with no indication that the peptide has folded or reached an equilibrium structure.

This is confirmed by an examination of the Z-axis position of the N-terminus and C-terminus of the peptide (Figure 6.6.6.3). Both ends of the peptide remain above the membrane throughout the 30ns simulation. This data suggests that the charged ends 'repel' the membrane completely.

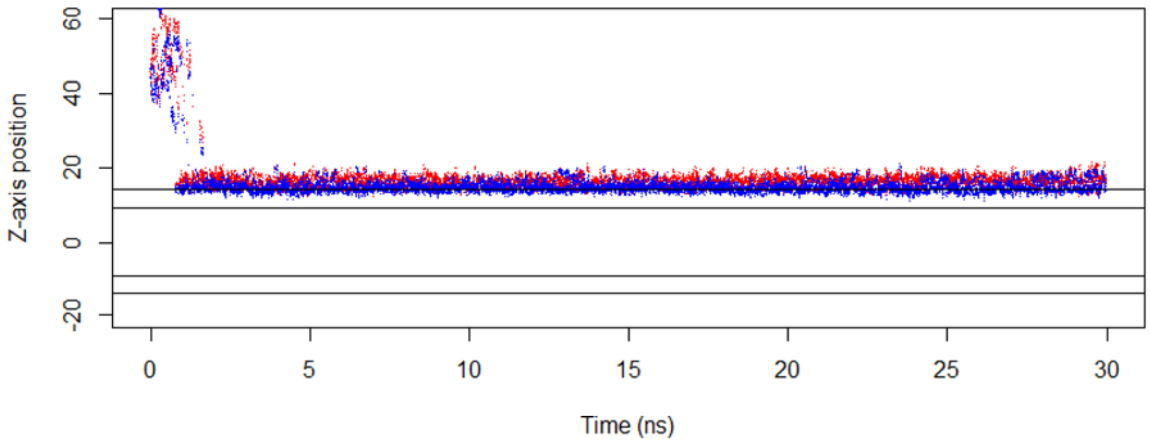

Figure 6.6.6.3. Z-axis positions of the N-terminus (red) and C-terminus (blue) of WALP16 with charged ends during the replica-exchange simulation. The horizontal lines indicate the positions of the hydrophobic, aqueous, and interface regions as previously described.

A similar pattern is observed when examining the charged arginine residue at position 25 of the TMX-3 peptide. As shown in Figure 6.6.6.4 below, this residue remains above the membrane throughout the entire simulation.

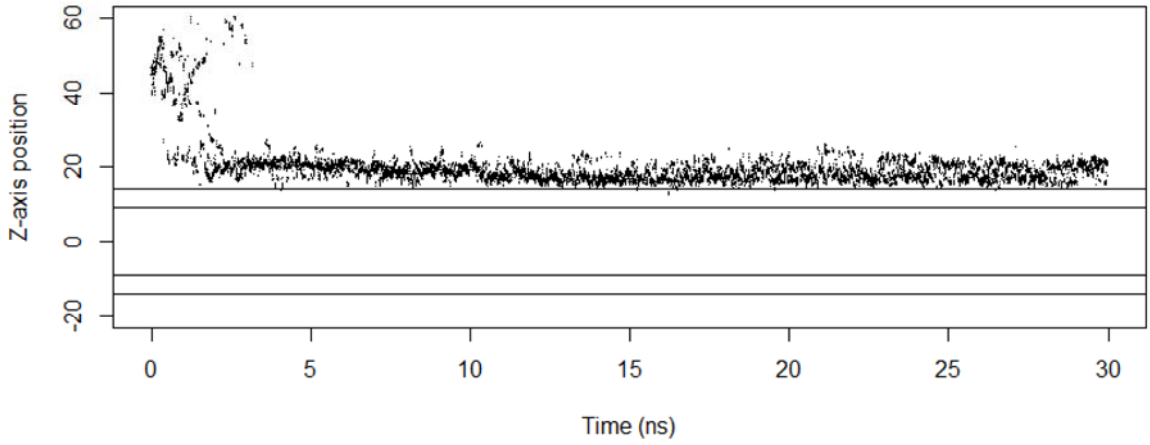

Figure 6.6.6.4. Plot showing the Z-axis position (in Å) of the arginine residue at position 25 in the TMX3 peptide in the simulation previously discussed. The data was taken from the representative replica in the 300K ensemble. The horizontal lines in the plot indicate the position of the implicit membrane.

The above data shows that the charged residues within the peptide remain completely above the membrane/solvent interface. These residues do not cross into the switching region of the

membrane at any point during the 30ns simulation. It may, therefore, be concluded that the presence of charged residues, either at the ends or within the peptide interferes with the simulation setup here. It is, therefore, preferable, to block the ends of the peptides and neutralise any charges present within the molecule.

6.6.7 pseudin-2 simulation

A replica-exchange simulation was set up using the amino acid sequence of pseudin-2 all charged residues within the peptide neutralised (2.10.2). The temperature range used was 300K-800K and the blocked ends ACE and CT3 were used for the N-terminus and C-terminus respectively. The simulation was run for 30ns. The potential energy plot of the simulation shows a similar trend to that seen in previous simulations, with a gradual decrease until a plateau is reached (Figure 6.6.7.1).

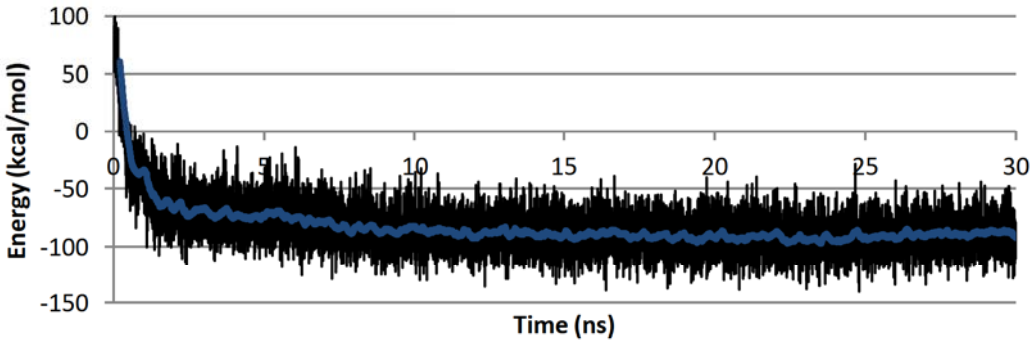

Figure 6.6.7.1. Plot showing the change in potential energy in the 300K ensemble of the pseudin-2 simulation.

The backbone RMSD and radius of gyration plots of the 300K ensemble show similar features to those seen in the case of WALP23 (Figure 6.6.7.2). There is rapid swapping between two conformations of the peptide with considerably different structures but similar energies. Additionally, the frequency of this swapping increases towards the end of the simulation.

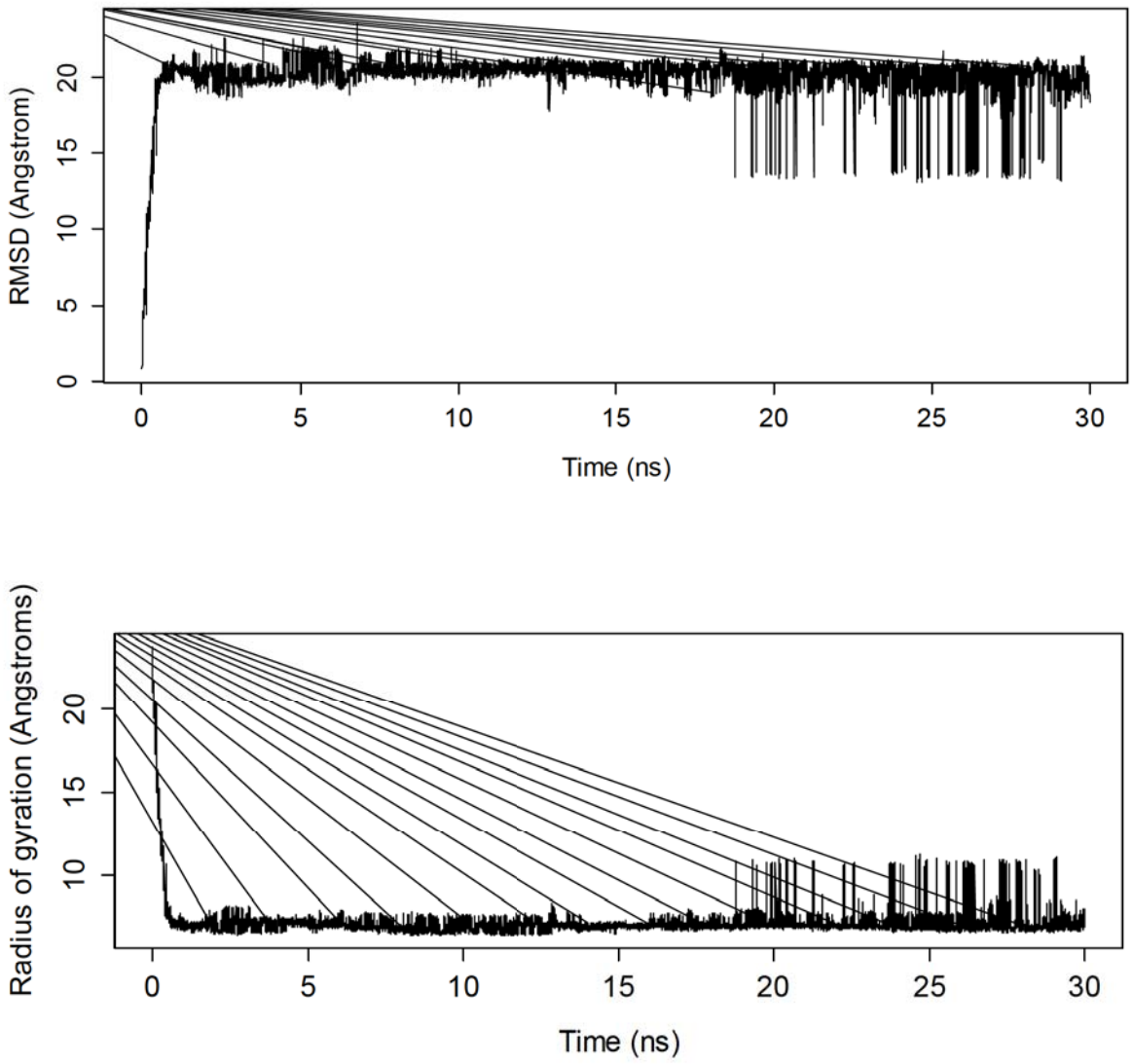

Figure 6.6.7.2. Plots showing backbone RMSD and radius of gyration of pseudin-2 in the 300K trajectory.

An examination of the 300K trajectory shows that these two structures are one of a linear helix and one of a two helix with a flexible region in between (Figure **6.6.7.3** (a) and (b) respectively).

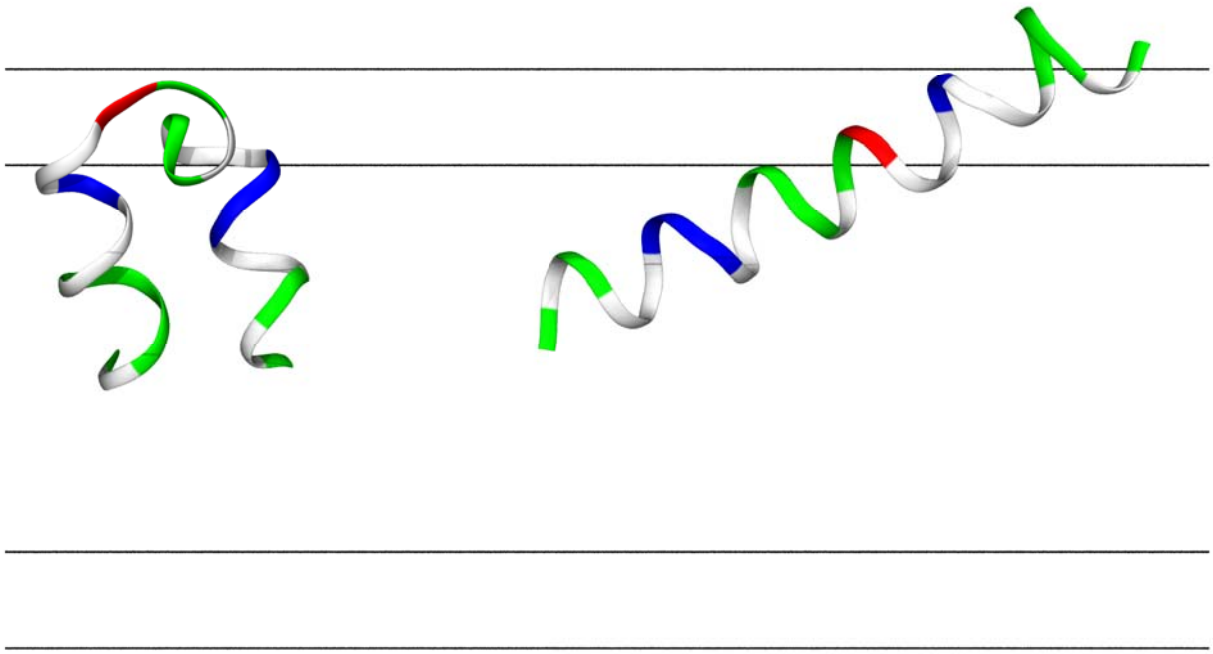

(a) (b)

Figure 6.6.7.3. The two equilibrium structures of pseudin-2 seen in the 300K trajectory: (a) the 'kinked' helix and (b) the linear helix. The residues of the peptide are coloured based on their type. The colours are as follows: white = hydrophobic, green = polar uncharged, blue = positively charged, red = negatively charged. The horizontal lines show the interfacial region between the aqueous and hydrophobic phases, as previously described.

An examination of the Z-axis position of the peptide during the trajectory (Figure 6.6.7.4) shows that the N-terminus remains below the membrane while the C-terminus is almost always above it. Following the initial equilibration period, the peptide embeds itself partially into the membrane in this orientation, regardless of structure.

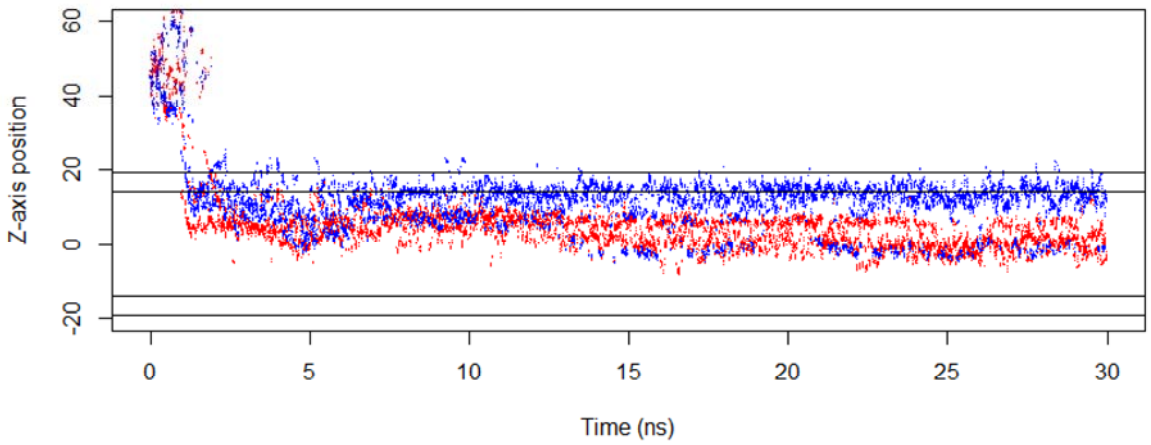

Figure 6.6.7.4. Z-axis positions of the N-terminus (red) and C-terminus (blue) of pseudin-2 during the replica-exchange simulation. The horizontal lines indicate the positions of the hydrophobic, aqueous, and interface regions as previously described.

An examination of the secondary structure during the last 1ns of the 300K trajectory of pseudin-2 (Figure 6.6.7.5) shows that the peptide may be divided into three segments: an N-terminal segment (residues 1-10) that are largely helical in nature, a flexible region spanning residues 11-14, followed by a flexible C-terminus region (residues 15-24) with some helical character.

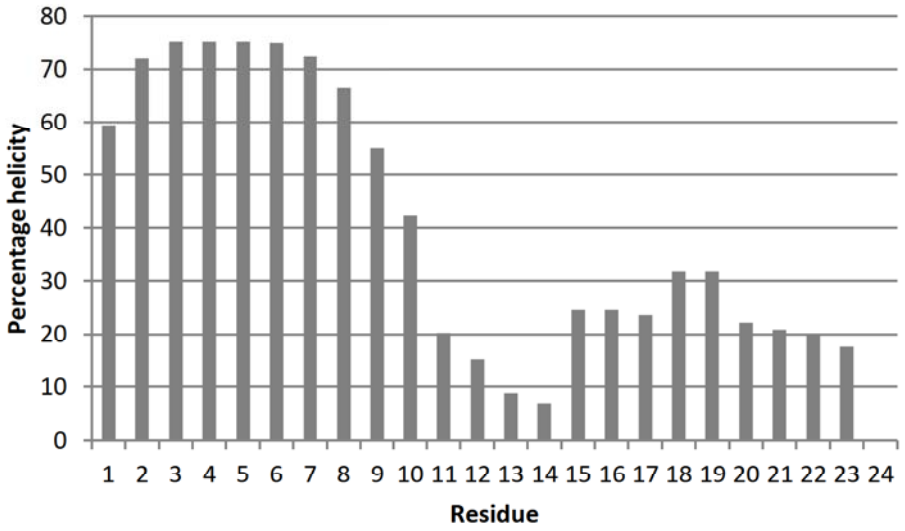

Figure 6.6.7.5. Percentage time spent in a helical structure for each of the 24 residues of pseudin-2 in the last 1ns of the 300K trajectory.

In conclusion, the molecular dynamics study of pseudin-2 suggests that the antimicrobial action of the peptide is mediated by two structures, a linear helix and a 'kinked' helix comprising two

helical segments connected by a flexible 'hinge'. The kinked helical structure described here has also been previously reported: the antimicrobial peptides ranatuerin-2CSa [helical: residues 2-21, 26-30, turn: residues 22-25] (Subasinghage *et al.*, 2008) and gaegurin-4 [helical: residues 2-10, 16-32, loop: residues 12-15] (Park *et al.*, 2007) have both been shown to possess two helical segments with molecular 'hinges' in between them.

It is important to note that it is not possible to deduce the kinetics of the interaction of pseudin-2 with lipid membranes using the data from the replica-exchange simulation. This is a limitation that arises due to the temperature swapping that is carried out during these simulations. Additionally, these types of simulations make it difficult to determine the interplay between the two structures described. It is, however, clear that both structures play a role in the antimicrobial action of the peptide as they are both involved in the interaction of the peptide with membranes. This could occur by one of two mechanisms. The first possible mechanism is that one of the two structures being a transient structure leading to the formation of the other. The second is that both structures are stable, and it is the interaction between these two structures that manifests in the form of antimicrobial action of pseudin-2.

In order to validate the molecular dynamics data, the biophysical characterisation of pseudin-2 was carried out using both circular and linear dichroism. These techniques allow for the determination of the secondary structure and the orientation of the peptides in a membrane environment, respectively. The biophysical characterisation of pseudin-2 is described in more detail in the following chapter.

7 Linear and Circular dichroism study of pseudin-2

An alternative to determine the three-dimensional structure of a protein/peptide involves examining the way in which a solution of the sample interacts with polarised light. The interaction with circularly polarised light (termed circular dichroism) allows for the determination of the secondary structure elements (alpha helix, beta sheet and random coil) present in a peptide sample. In the case of the sample's interaction with linearly polarised light (termed linear dichroism), the resultant spectrum can be used to determine the peptide's orientation relative to a surface. The two techniques may be used to examine the same system, offering information on secondary structure as well as orientation simultaneously. What follows is a detailed description of the two techniques and their applications. This work relates to the first component of the hypothesis, since the determination of the secondary structure and orientation of pseudin-2 in a membrane environment would help understand the mechanism of its antimicrobial action. The hypothesis is given below.

Pseudin-2 may be developed into an antimicrobial compound for clinical use by:

a) Structural understanding of its antimicrobial action

b) Altering its primary structure

7.1 Circular Dichroism

Circular dichroism is a biophysical characterization technique used to determine the secondary structure of proteins and other smaller organic molecules. It has also been shown to estimate changes in the secondary structure of a system, provided the components of the solution are compatible with the spectroscopy technique used. The technique relies on the differential absorption of circularly polarized light when passed through a solution containing the sample (see Figure 7.1.1 for an illustration showing circularly polarized light). Using this technique, relative absorption of right and left circularly-polarized light is measured at different wavelengths to

obtain a CD absorption spectrum. The secondary structure of the protein/peptide of interest can then be determined by examining the features of this spectrum.

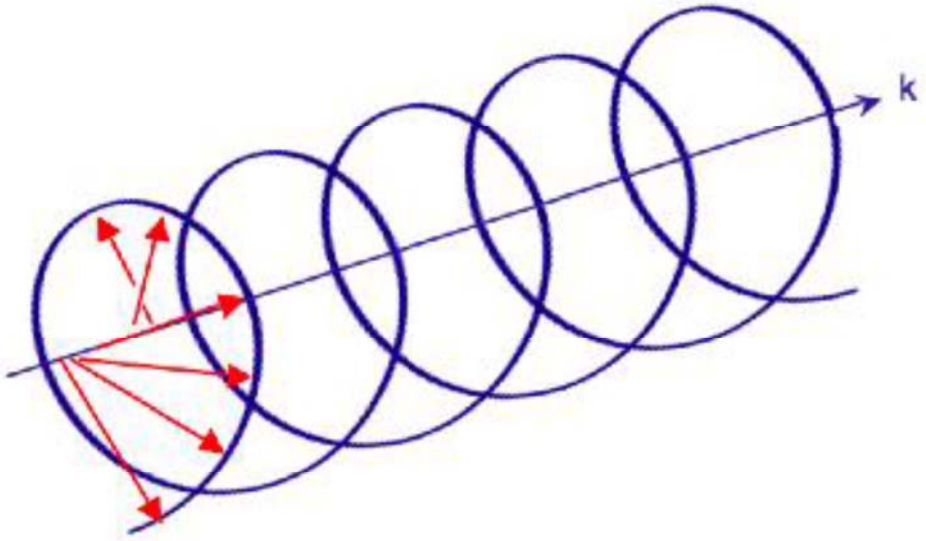

Figure 7.1.1. Illustration showing circularly polarized light. The straight line (k) indicates the axis of propagation of the light and the red arrows show the direction of the electric field vector.

Characteristic absorption minima and maxima are known for different types of secondary structure, and have been described for alpha-helical, antiparallel beta-sheet and random coil conformations (Greenfield & Fasman, 1969). The spectrum shown in Figure 7.1.2 below was taken from the study by Greenfiel and Fasman and shows the characteristic spectra for each configuration. The important features of the spectra shown in Figure 7.1.2 have been listed in Table 7.1.1.

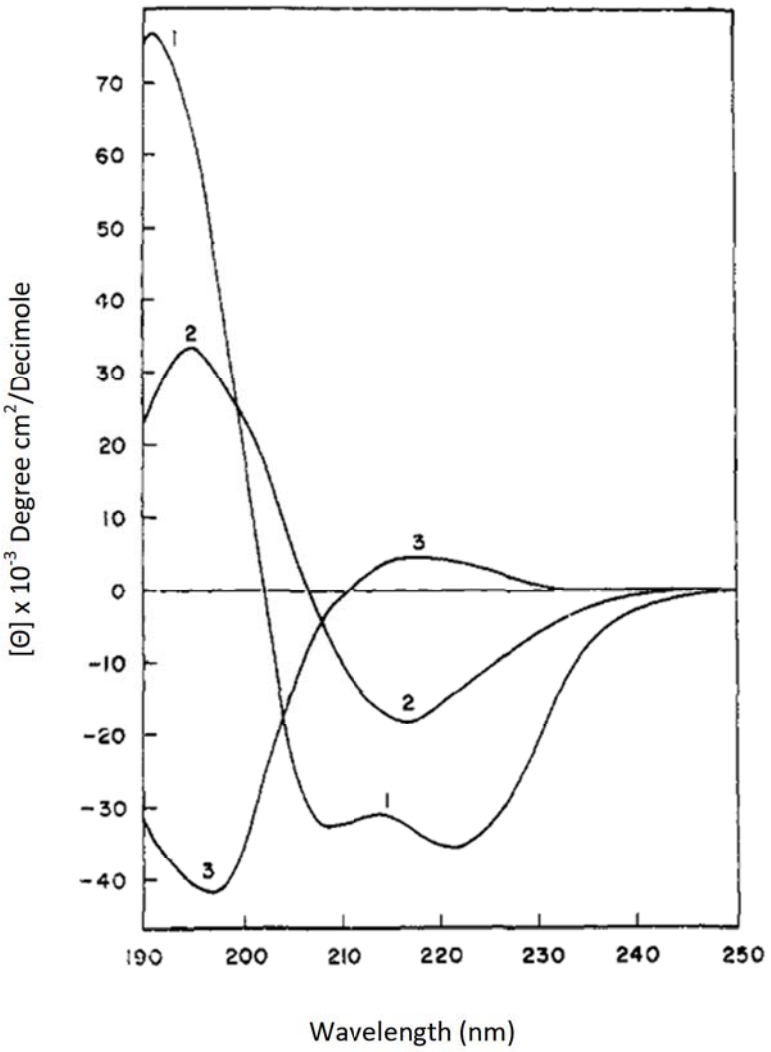

Figure 7.1.2. Circular dichroism spectrum of poly-L-lysine in the alpha-helical (Curve 1), antiparallel beta-sheet (Curve 2) and random coli (Curve 3) configurations.

Secondary structure	Features [Maximum/minimum] and wavelength (nm)		
Alpha-helix	↑193	↓222	↓208
Antiparallel beta sheet	↑195	↓218	
Random coil	↓195		

Table 7.1.1. Important features of spectrum … above. Upward facing arrows indicate maxima and downward facing arrows indicate minima.

In addition to the above features, a number of tools have been developed using reference spectra from a large number of proteins/peptides (Perez-Iratxeta & Andrade-Navarro 2008; Unneberg *et al.*,2001; Lobley *et al.*,2002; Reed & Reed 1997). Given an input spectrum, these tools compare the spectrum to the database and find a 'best-match' which can then be used to predict the structure of the peptide/protein in question.

Circular dichroism has been applied extensively to the study of peptides. The structures of antimicrobial peptides aurein 1.2 (Cheng *et al.*, 2011), aurein 2.3 (Mura & Dennison, 2012), aurein 2.5 (Dennison, 2012), nigrocins 1 and 2 (Park *et al.*, 2001), maculatin 1.1 (Sani *et al.*, 2012) and japonicins 1 and 2 (Isaacson *et al.*, 2002) have been elucidated using circular dichroism. The use of circular dichroism to study the secondary structure of peptides is, therefore, well-established.

7.2 Linear dichroism

Linear dichroism is a spectroscopic technique which is used to determine the orientation of molecules within a system. In a manner similar to circular dichroism, linearly polarized right parallel and perpendicular to the axis of propagation is passed through the sample. This is illustrated in Figure 7.2.1 below. The difference in the absorption of the two light components is measured at different wavelengths to give a linear dichroism spectrum.

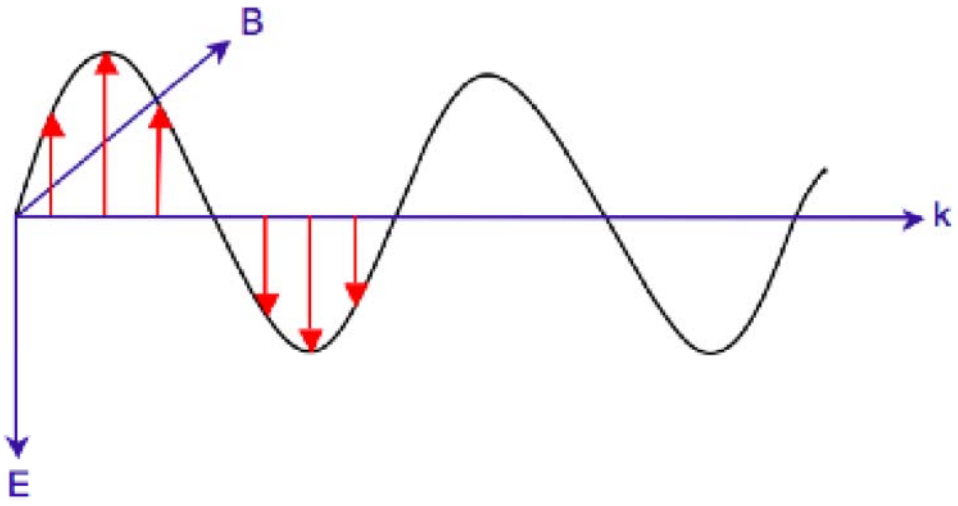

Figure 7.2.1. Illustration showing linearly polarised light perpendicular to the propagation axis. In an LD experiment, there would be a second component, one parallel to the axis of propagation. The line 'k' indicates the axis of propagation and the red arrows show the direction of the electric field vector.

To carry out linear dichroism analysis to obtain the orientation of molecules in a sample, it is necessary to orient the molecules by the application of force. This can be achieved either by using a stretched polymer film or by using coquette flow.

In the stretched film setup, a small drop of the sample is applied to a polymer film made of a polymer such as polyethylene (Falk *et al.*,1986). The film is then stretched to orient the sample along the direction of stretching and the linearly polarised light is passed through. This is illustrated in Figure 7.2.2 below.

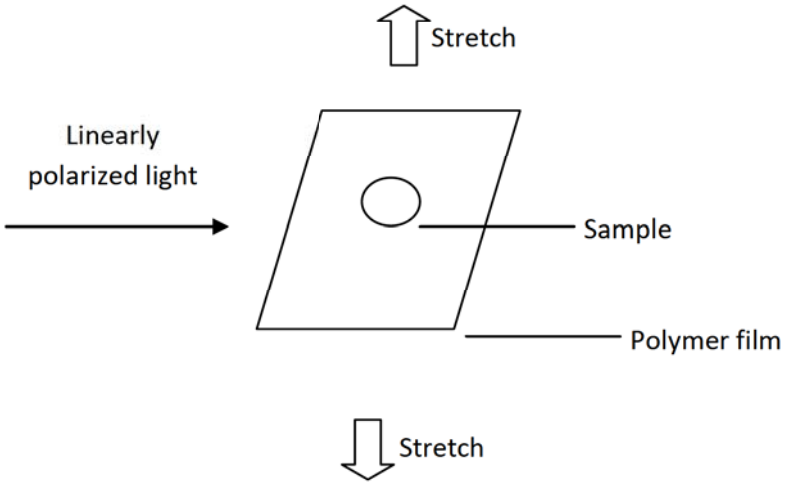

Figure 7.2.2. Diagram illustrating the stretched film method for aligning molecules in order to obtain a linear dichroism spectrum. The molecules are aligned along the axis of stretch of the polymer film.

The couette flow setup consists of two concentric cylinders with a small gap between them. The cylinders are made of quartz which is designed to be completely transparent to the polarized light. The sample is placed in the gap between the two cylinders and the central cylinder is rotated at high speed (~3000 rpm). This generates large shear forces between the two cylinders which orient the molecules in the sample. The linearly polarised light is then passed through both cylinders and an absorption spectrum is measured. The couette flow setup is illustrated in Figure 7.2.3. Couette flow is currently the only reproducible method to align molecules for linear dichroism analysis.

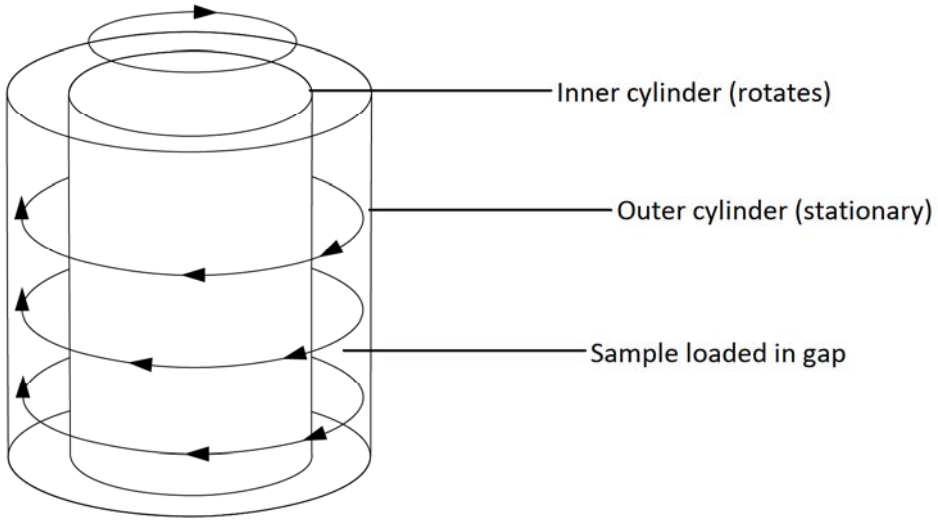

Figure 7.2.3. Diagram illustrating the couette flow setup of aligning molecules to obtain a linear dichroism spectrum. The arrows indicate the direction of rotation of the inner cylinder with respect to the outer cylinder.

In order to determine the orientation of protein/peptide within a sample using linear dichroism, it is necessary to know the secondary structure of the protein/peptide. This is a necessary requirement as the features observed in linear dichroism spectra are dependent on secondary structure. Linear dichroism has been applied to the structural study of the orientation of designed cyclic peptides (Ennaceur *et al.*, 2009), the peptide antibiotic gramicidin (Svensson *et al.*, 2011), melittin (Svensson *et al.*, 2011) and magainin-2 (Bechinger *et al.*, 1999).

In addition to biophysical characterisation, it is possible to use *in-silico* approaches to aid in the determination of the 3D structure of the peptide of interest. The low cost associated with the use of these computational techniques makes them a powerful tool in molecular biology. Additionally, these tools can give useful insights into the structure of the peptide of interest with nothing more than the peptide's amino acid sequence as input. One such technique that has become increasingly popular in recent years is molecular dynamics, and is described below.

7.3 Circular Dichroism and Linear Dichroism analysis of pseudin-2

In order to obtain a reference for the visualisation and biological activity of pseudin-2, the chemically synthesised pseudin-2 (chapter 5; >95% pure) was employed.

The three-dimensional structure of pseudin-2 was examined in both aqueous and lipid environments, using both circular and linear dichroism. Chemically synthesised pseudin-2 was mixed with Egg-PC liposomes (2.11.1) (phosphatidylcholine) in phosphate buffer (phosphate buffer contains no ions that give a strong signal in a CD spectrum, masking the signal correspond to the peptide alone). The Circular Dichroism spectrum of pseudin-2 was obtained 2.11.2)in the presence and absence of liposome (1mg/ml).The concentration of peptide in the experiment was 0.1mg/ml. Although the concentration used is relatively high, it is comparable to the concentration of pseudin-2 used in a previous CD study of the peptide where a concentration of 50 μM (0.13 mg/ml) was used. CD spectra of the liposome and buffer components were measured separately and subtracted from the spectra of the peptide in order to obtain a spectrum that only shows the signal corresponding to the peptide 2.11.2). The spectrum obtained is shown below (Figure 7.3.1).

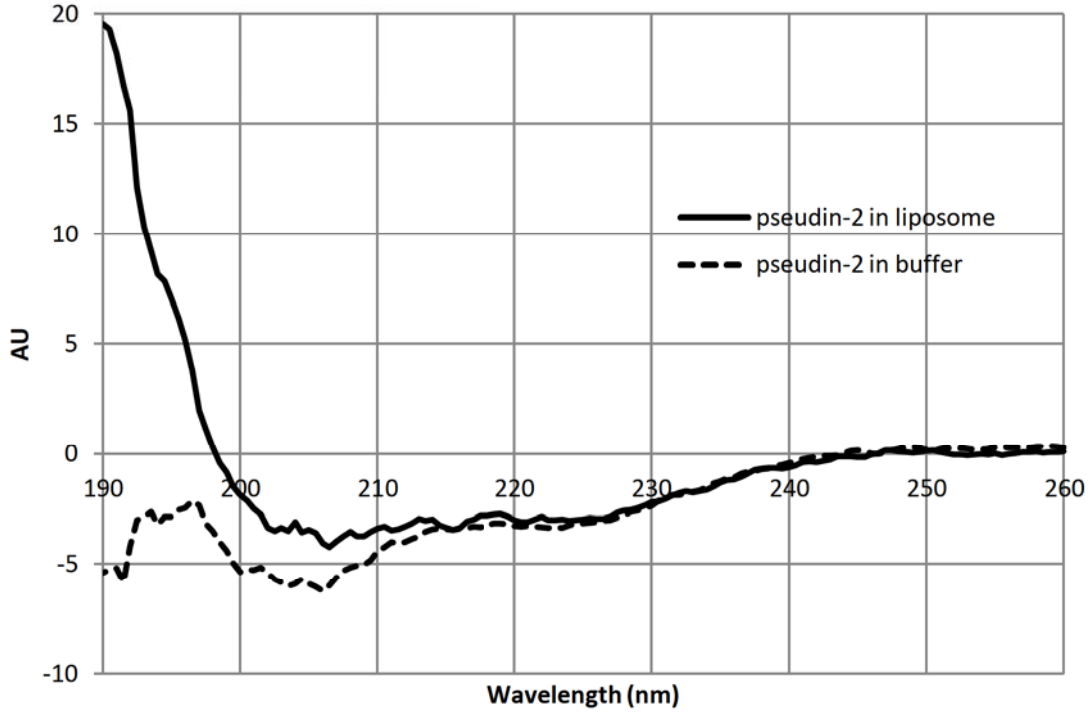

Figure 7.3.1. Circular dichroism spectra of pseudin-2 (0.1mg/ml) in phosphate buffer (0.05M) in the presence and absence of phosphatidylcholine liposomes (1mg/ml)

The spectrum above shows how the structure of pseudin-2 is affected by the presence of liposomes. In aqueous solution, the peptide shows a spectrum characteristic of a disordered peptide. In the presence of liposomes, however, the spectrum changes to one which shows considerable helical character. The three prominent features of a CD spectrum of a helical peptide/protein are a strong maximum at 190nm and two weaker minima at 208 and 220nm. The two minima normally observed in a helical spectrum are also visible in the data shown above. However, the strong maximum at 190 nm is clearly present, which strongly suggests that the peptide possesses considerable helical character at the concentration and conditions used in the experiment. Additionally, this peak is absent in the spectrum taken in the buffer alone, suggesting that the liposomes play a key role in the folding of the peptide. This data is in good agreement with previously published CD data on pseudin-2.

After the conditions for circular dichroism were established, the LD spectrum of pseudin-2 in the presence of PC liposomes was measured (Figure 7.3.2). The same concentrations of peptide and liposome were used as those for the CD experiment (0.1 mg/ml pseudin-2, 1 mg/ml liposomes). A spectrum was measured every hour for 18 hours in order to look for potential changes in the structure of the peptide that might occur over a long timescale. A background spectrum of the liposomes in buffer without the peptide was also measured and subtracted from the peptide spectra in order to isolate the peptide signal 2.11.3). For the sake of clarity, only the first and last LD spectra are shown (Figure 7.3.2).

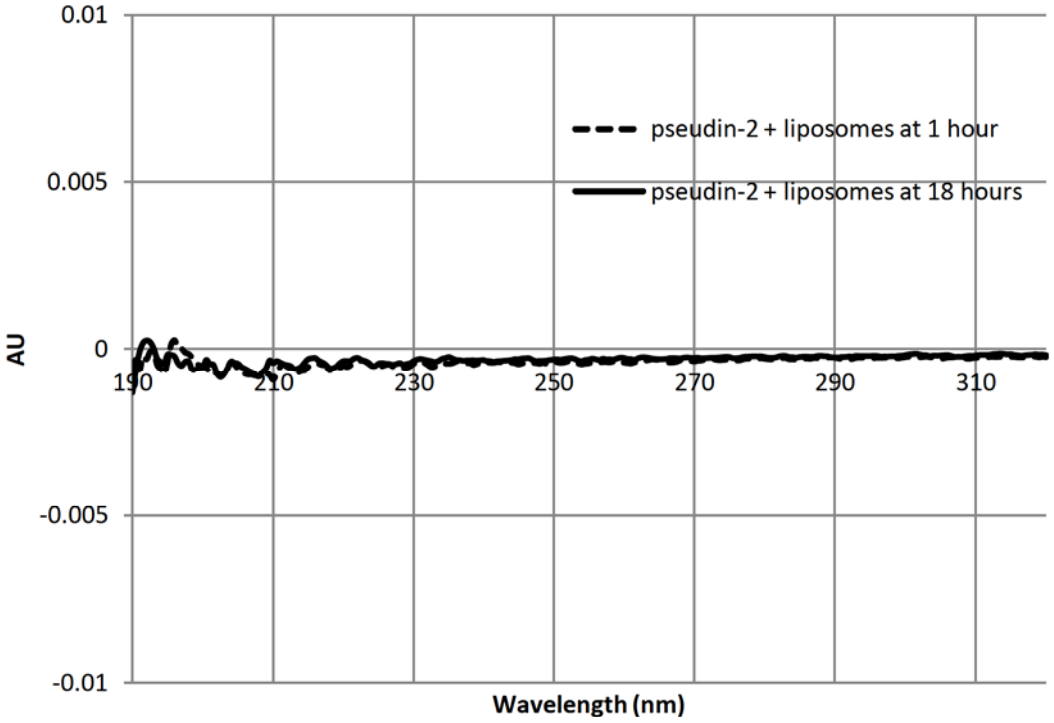

Figure 7.3.2. Linear dichroism spectrum of pseudin-2 (0.1 mg/ml) in the presence of PC liposomes (1 mg/ml)

Figure 7.3.2 above shows no clearly-discernable characteristics, which is consistent with no directionality of the peptide within the liposomes. Additionally, the fact that the spectrum remains the same throughout the duration of the experiment suggests that the system reaches equilibrium rapidly, with no changes occurring over the timescale of 18 hours.

The lack of directionality of the system suggests no clear orientation of the peptide. This could either be due to a completely random arrangement of the peptide that is associated with the liposome or due to an equilibrium that does contain oriented molecules but where there is no overall orientation in one particular direction. This finding suggests that it is unlikely that pseudin-2 cannot act via the toroidal pore or barrel-stave models, since both involve clear orientation of the peptide, perpendicular to the membrane. If the peptide acted via either the toroidal pore or barrel stave models, there would be clear features on the LD spectrum corresponding to transmembrane structure. Both surface and transmembrane binding peptides show clear

absorption maxima and minima corresponding to both surface binding and insertion (Svensson *et al.*, 2011). Thus the data herein indicates that of the three known mechanisms for peptide antimicrobial action, the data here suggests that carpet model is the most likely mechanism for pseudin-2 activity, since this model involves random orientation of peptides. The scenario is supported by the molecular dynamics data, where the linear form of the pseudin-2 molecule positions itself at an angle to the membrane. The second equilibrium structure (kinked helix) is also oriented at an angle to the membrane (Figure **6.6.7.3**) albeit a lesser angle. Thus again, molecular dynamics simulations would predict no clear LD spectrum. The molecular dynamics data, therefore, supports the both the circular dichroism and linear dichroism data since pseudin-2 is largely helical in character but does not orient itself either completely parallel or perpendicular to the membrane.

It is, however, important to acknowledge that the complete lack of an LD signal has never been reported in the literature. Therefore, the linear dichroism data presented here may not be directly linked to the carpet model. The carpet model is simply the most plausible intepretetation of the data.

8 Discussion and future direction

The data presented in this thesis was generated using a variety of experimental techniques, comprising molecular biology, spectroscopy and *in-silico* molecular dynamics studies. It is logical, therefore, to discuss the results of each chapter in turn, making comparisons to published data where appropriate. The main findings of this thesis are listed and their relevance to the hypothesis is clearly indicated. Finally, additional work is suggested so the hypothesis may be tested further.

8.1 Mutagenesis data

Using replica-plating as a screening method, a number of pseudin-2 mutants with observed toxicity to *E. Coli* were identified for purification at a later stage. This toxicity was interpreted as an inhibition of growth following expression of the MBP-fusion of the respective pseudin-2 mutant. Although such an approach allows for the rapid screening of mutant peptides for toxicity, there are fundamental limitations to its utility.

Since the peptides were screened by simply expression the MBP-peptide fusion, the intracellular concentration of the peptide was not known. This made it impossible to estimate the toxicity of the peptide. Additionally, it was not possible to estimate the decrease in growth associated simply with increased protein expression within the bacterial cell, a phenomenon likely to contribute to the inhibition of growth observed. Finally, it was not known whether the peptide was being degraded/cleaved by enzymes within the cell, a process which is key to determining the toxicity of the mutant in question. Logically, therefore, the replica-plating screen was only intended to be used as a method to generate mutants that would be purified and tested for their antimicrobial activity against not only the Gram negative pathogen but also two other representative pathogens: *S. Aureus* (Gram positive pathogen) and *C. Albicans* (fungal pathogen).

It is not possible to compare this data with the literature since there are no published studies where such a method was used to screen mutant peptides. In all published data on amphibian

antimicrobial peptides, the peptides tested were purified to >95% using RP-HLPC (see Table 1.6.1 for examples).

8.2 Protein expression

The expression of pseudin-2 in *E. Coli* proved extremely difficult for a number of reasons. The use of SDS-PAGE to estimate the purity of the expressed pseudin-2 fusion was unsuccessful (both in the case of the MBP as well as His6 fusions). It was also not possible to clearly determine the presence of the peptide in the cytoplasmic extract of the bacterial cells. Finally, testing the peptide fractions (both with and without proteolytic cleavage) for antimicrobial activity also yielded no result.

A comparison of the protein expression data with published data reveals certain similarities, but also key differences between the approach used here and literature data. The expression of the antimicrobial peptides adenoregulin [His_6-tag fusion] (Zhou *et al.*, 2005), palustrin-2CE [GST fusion] (Sun *et al.*, 2012), palustrin-OG1 [SUMO fusion] (Xie *et al.*, 2013), brevinin-2GU [TRX fusion] (Zhou *et al.*, 2009), cecropin [Trx-His_6 fusion] (Xu *et al.*, 2007) and brevinin-2R [Trx fusion] (Mehrnejad *et al.*, 2008) in E. Coli has been reported. It is clear that a variety of expression strategies have been used to express antimicrobial peptides in E. Coli, and in this study, due to time constraints, only two expression strategies were attempted: MBP and His_6 pseudin-2 fusions. Additionally, in all the studies cited above, the expressed peptide was purified using RP-HPLC. Due to the lack of in-house RP-HPLC equipment and financial constrains preventing the purification of a large number of peptides, RP-HPLC was not used to purify the expressed pseudin-2 fusion.

8.3 Antimicrobial activity of chemically-synthesised pseudin-2 analogues

The testing of chemically-synthesised pseudin-2 showed broad-spectrum antimicrobial activity that was consistent with published data (Table 5.3.1). The His_6-pseudin-2 fusion, however, did not show any antimicrobial activity. This may offer an explanation for the lack of antimicrobial activity observed during the expression and attempted purification of His_6-pseudin-2. With regards to the

pseudin-2 mutants, only the analogue [10-T, 14-W, 18-P]-pseudin-2 showed potential for development into a therapeutic, since it showed broad-spectrum antimicrobial activity comparable to that of magainin-2, a peptide which reached phase III clinical trials for use as a topical antibiotic (Gordon *et al.*, 2005). However, in order for this route to be successful, the peptide must offer benefits relative to the simple use of a traditional, more well-established antibiotic. If this requirement is unfulfilled, the development of this molecule into a therapeutic will not be successful. Additionally, this analogue demonstrates that it is not only positive charge that decides the toxicity of pseudin-2 as suggested in the literature.

In comparing the antimicrobial activity of the pseudin-2 analogues described in this study with published data on pseudin-2 analogues, the same issue of purity arises. In the study describing pseudin-2 analogues, all the peptides described were purified to >95% homogeneity using RP-HPLC (Pal *et al.*, 2005). This is a major limitation of the antimicrobial work described here, since the peptides used in the toxicity testing were tested as crude peptides. This fact is particularly important in the case of the analogue [10-T, 14-W, 18-P], the peptide observed to be the most potent against the three representative pathogens: *E. Coli*, *S. Aureus* and *C. Albicans*. There would be significant challenges to developing this peptide into a therapeutic, the most important of which is that the peptide would need to be synthesised and purified so that its true antimicrobial properties may be determined.

8.4 Molecular dynamics

The molecular dynamics setup used (implicit membrane/solvent model) showed that pseudin-2 alternates between a kinked and a straight helix in a membrane environment. The same molecular dynamics model was used to describe the folding of three helical control peptides: the peptides WALP16 and WALP23 which insert into the membrane form a perfect α-helix, and TMX-3, which remains at the membrane surface, forming a kinked helix. This data is perfectly consistent with previously published data on a molecular dynamics study of the three control

peptides mentioned, showing the same structures found here (Im & Brooks, 2005). The structural data in this study describing the kinked helical conformation of pseudin-2 is, therefore, valid.

It is important to note the limintations of the molecular dynamics setup in order to correctly interpret the data. Since the membrane/solvent setup was modelled using implicit phases, it is only a very rough representation of a biological membrane. Since the membrane is modelled as a continuous 'phase', it does not account for the diversity in the types of lipids that constitute a biological membrane. Charge effects that may be present in a biological membrane due to the presence of charged lipid species are absent. Additionally, since the replica-exchange method of temperature swapping was used to hasten the folding process, it is not possible to make deductions regarding the kinetics of the process. Finally, it was observed that the setup does not model charges correctly as they simply 'repel' the membrane, which is why pseudin-2 was modelled as a completely neutral molecule. Taking these limitations into consideration, the results of the molecular dynamics study of pseudin-2 are still accurate since the model accurately describes the folding process of the control peptides.

Finally, the kinked helix described by the molecular dynamics simulations is not unprecedented in the literature. The antimicrobial peptides gaegurin-4 (Park *et al.*, 2000) and ranatuerin-2CSa (Subasinghage *et al.*, 2008) have both been shown by structural NMR spectroscopy to possess two helical segments with a turn between them. The helical segments span residues 2-10, 16-32 in the case of gaegurin-4 (GILDTLKQFAKGVGKDLVKGAAQGVLSTVSCKLAKTC) , and 2-21, 26-30 in the case of ranetuerin-2CSa (GILSSFKGVAKGVAKDLAGKLLETLKCKITGC). Since pseudin-2 forms a kinked helix in the molecular dynamics simulations without inserting into the membrane, this data tends to support the carpet model of antimicrobial peptide action, where the peptide disrupts membrane structure by binding to the surface. Both the barrel stave and toroidal models require the formation of a stable membrane-spanning structure, which is quite different from the surface-binding flexible helix-loop-helix structure observed. However, this conclusion is largely

speculative since the molecular dynamics data does not describe the mode of action with sufficient detail to clearly distinguish between the three possible models.

8.5 Circular and linear dichroism

The circular dichroism data clearly shows that the peptide forms an alpha-helix in the presence of liposomes, while it exhibits a disordered structure in an aqueous environment. This observation takes into account the contribution of the buffer and liposomes to the CD signal, since spectra were independently measured for the two components and subtracted from the final signal to give the signal corresponding to the peptide alone. Finally, this data is consistent with published data on the CD spectrum of pseudin-2, showing that the peptide adopts a helical structure in the presence of liposomes (Park *et al.*, 2011).

The linear dichroism data, on the other hand, is a negative result. Despite subtracting the liposome and buffer signal in order to isolate the peptide signal, there is no signal either in the presence or the absence of liposomes. This indicates that pseudin-2 adopts neither a parallel nor perpendicular orientation with respect to the membrane, since the use of linear dichroism to determine helix orientation in liposomes has been described in the case of magainin-2 (Bechinger *et al.*, 1999), as well as gramicidin (Hicks *et al.*, 2009) and melittin (Svensson *et al.*, 2011). However, since this is a negative result which has never been reported in the literature, it is difficult to draw conclusions based on the data.

Collectively, the circular and linear dichroism data show that pseudin-2 adopts a helical structure in a membrane environment without orienting either parallel or perpendicular to the membrane. In both the toroidal pore and barrel-stave models, the peptide is oriented perpendicular to the membrane. Since the data presented here suggests that the peptide orients neither parallel nor perpendicular to the membrane, it shows that of the three models, the carpet model is the most plausible. However, since the linear dichroism study presented a negative result, this conclusion is

largely speculative. Further analysis would be required to describe the mode of action of pseudin-2 in order to clearly determine the most appropriate model of its antimicrobial action.

8.6 Conclusions relative to hypothesis

Taking into account the previous discussion, the central hypothesis of this study may be reviewed in light of the main findings of this thesis. The hypothesis is as follows:

Pseudin-2 may be developed into an antimicrobial compound for clinical use by:

a) Structural understanding of its antimicrobial action

The structural data in this study may be summarised as follows:

- Molecular dynamics simulations of pseudin-2 show that it adopts a flexible helical structure
- Linear and circular dichroism results show a clear helical structure of the peptide but only hint that the peptide is unoriented (due to the lack of an LD signal)

If it is assumed that the carpet model is the mode of action of pseudin-2, the amphipathicity of the peptide may be modified in order to improve its antimicrobial properties. Peptide amphipathicity has been suggested to be important in the case of peptides caerin 1.1 (Wong *et al.*, 1997) and aurein 1.2 (Fernandez *et al.*, 2012) and the carpet model has been suggested as the mode of action of both peptides. It is important to note here the lack of a linear dichroism signal, which means the carpet model of action of pseudin-2 is only speculative.

With regards to the molecular dynamics data, the kinked helical structure may be altered by producing mutants to deliberately alter the structure in order to determine the aspects of the peptide's structure crucial for its antimicrobial action. This might begin by placing a proline residue in the kinked region, introducing a permanent 'turn' at that position. The analogue can then be tested for its antimicrobial properties.

Therefore, although it is possible to draw a link between the antimicrobial action of pseudin-2 and its structure, further work is required in order to fully understand this relationship, since the data described here is only preliminary. Additionally, it is important to consider the limitations of the methods used to obtain the structural data described in this thesis (discussed in detail in the previous sections).

b) Altering its primary structure

The testing of pseudin-2 mutants revealed that it is possible to improve the properties of the peptide by saturation mutagenesis of positions 10, 14 and 18. If the peptide is only intended for use as a topical antimicrobial, the improvement in antimicrobial activity observed in the pseudin-2 analogue [10-T, 14-W, 18-P] would be sufficient to develop a therapeutic candidate. The haemolytic properties would not be relevant considering use as a topical antibiotic. Therefore, simple mutagenesis may be used to find a therapeutic lead, which may then be taken forward for clinical trials, as in the case of magainin-2 (Gordon *et al.*, 2005). As stated earlier, it is important to consider the fact that the peptides tested were crude peptides, and that the peptides would need to be re-tested in pure form in order to determine their true antimicrobial activities.

In conclusion, both structural work and simple saturation mutagenesis can be used to discover a pseudin-2 mutant with potential for development into a therapeutic. However, given the limitations of the current work (as discussed earlier), this is not completely clear. The following section suggests approaches to overcome the limitations of the work described in this thesis, with an aim to develop a pseudin-2 mutant into a viable antibiotic.

8.7 Future work

Any future work carried out to continue this work needs to address the limitations of each of the approaches employed in this study of pseudin-2. This is discussed in further detail below for each of the three major techniques employed in this thesis.

8.7.1 Protein expression/chemical synthesis

Any future work involving the testing of pseudin-2 needs to address the issue of purity. The ability to produce peptides in sufficient quantity and with high purity is key to the development of a pseudin-2 into an analogue. Since RP-HPLC is the clear standard for peptide purification regardless of source, direct access to RP-HPLC equipment for peptide purification is of utmost importance.

Regarding the choice between synthesis and purification of the mutants, the decision must be made taking into account both the financial cost and the time and effort required. Although expression in *E. Coli* might seem like a cost-effective option, optimisation of the growth conditions may be required in order to obtain a large yield of peptide. Chemical synthesis is considerably more time-efficient since there is less optimisation required: the peptide is simply synthesised as a crude peptide and then purified using RP-HPLC to homogeneity.

If protein expression is to be considered, a number of expression strategies exist such as expressing the peptide as a GST fusion, a SUMO fusion (offering cleavage with the highly specific SUMO protease). Additionally, in order to overcome the problem of expressing a peptide/fusion that is toxic to the cells, cell-free expression systems may also be considered. However, the high cost associated with the use of such systems means they should only be considered as a last resort.

8.7.2 Molecular dynamics

There were two main limitations of the molecular dynamics work described in this thesis. Firstly, the membrame/solvent model used was an implicit model, which makes it impossible to model the molecular features of biological membranes such as charge and the presence of different

types of lipid species. Secondly, since the temperature-swapping replica exchange method was used, it was not possible to determine the kinetics of the folding process of pseudin-2. There are alternative methods which allow the above two limitations to be overcome.

The problem of lack of atomic detail may be overcome by using a completely explicit model, in which all the components of the system (including solvent molecules, lipid molecules and ions) are modelled in full atomic detail. However, the computational cost associated with running such a simulation would be large due to the large number of degrees of freedom in such a system. Depending on the computational resources available, it might be necessary to use a coarse-grain setup in which groups of molecules are represented as beads, thereby decreasing the total degrees of freedom of the system.

8.7.3 Structural characterization using spectroscopic techniques

Although the circular dichroism spectrum of pseudin-2 shown here is consistent with published data (Park *et al.*, 2011), the linear dichroism spectrum showed no signal whatsoever. This negative result makes it difficult to determine the orientation of the peptide with respect to liposomes. This can be overcome by using structural NMR spectroscopy. This technique would allow for the determination of the three-dimensional structure of pseudin-2 in a membrane environment. This structure may then be further investigated using molecular a molecular dynamics approach, as discussed above.

List of References

Abbassi, F., Galanth, C., Amiche, M., Saito, K., Piesse, C., Zargarian, L., Hani, K., Nicolas, P., Lequin, O. & Ladram, A. (2008) Solution structure and model membrane interactions of temporins-SH, antimicrobial peptides from amphibian skin. A NMR spectroscopy and differential scanning calorimetry study. *Biochemistry*, 47 (40), pp.10513–10525.

Abbassi, F., Lequin, O., Piesse, C., Goasdoue, N., Foulon, T., Nicolas, P. & Ladram, A. (2010) Temporin-SHf, a New Type of Phe-rich and Hydrophobic Ultrashort Antimicrobial Peptide. *Journal of Biological Chemistry*, 285 (22), pp.16880–16892.

Abbassi, F., Oury, B., Blasco, T. & Sereno, D. (2008) Isolation, characterization and molecular cloning of new temporins from the skin of the North African ranid Pelophylax saharica. *Peptides*, 29 (9), pp.1526–1533.

Abdel-Wahab, Y.H. a & Marenah, L. (2007) Insulin releasing properties of the temporin family of antimicrobial peptides. *Protein and peptide ...*, 14 (7), pp.702–707.

Abdel-Wahab, Y.H. a, Patterson, S., Flatt, P.R. & Conlon, J.M. (2010) Brevinin-2-related Peptide and its [D4K] Analogue Stimulate Insulin Release In Vitro and Improve Glucose Tolerance in Mice Fed a High Fat Diet. *Hormone and Metabolic Research*, 42 (9), pp.652–656.

Abdel-Wahab, Y.H. a, Power, G., Flatt, P.R., Woodhams, D.C., Rollins-Smith, L.A. & Conlon, J.M. (2008) A peptide of the phylloseptin family from the skin of the frog Hylomantis lemur (Phyllomedusinae) with potent in vitro and in vivo insulin-releasing activity. *Peptides*, 29 (12), pp.2136–2143.

Abdel-Wahab, Y.H. a, Power, G. & Ng, M. (2008) Insulin-releasing properties of the frog skin peptide pseudin-2 and its -substituted analogue. *Biological ...*, 389 (2), pp.143–148.

Abramo, M.D., Rinaldi, A.C., Nola, A. Di, Chimica, D., La, R., D'Abramo, M., Bozzi, A., Amadei, A., Mignogna, G., Di Nola, A. & Aschi, M. (2006) Conformational Behavior of Temporin A and Temporin L in Aqueous Solution : A Computational / Experimental Study. *Biopolymers*, 81 (3), pp.215–224.

Ali, M.H., Moghaddam, B., Kirby, D.J., Mohammed, A.R. & Perrie, Y. (2013) The role of lipid geometry in designing liposomes for the solubilisation of poorly water soluble drugs. *International journal of pharmaceutics*, 453 (1), pp.225–32.

Almeida, M.S., Cabral, K.M.S., Kurtenbach, E., Almeida, F.C.L. & Valente, A.P. (2002) Solution structure of Pisum sativum defensin 1 by high resolution NMR: plant defensins, identical backbone with different mechanisms of action. *Journal of molecular biology*, 315 (4), pp.749–57.

Ambroggio, E.E., Separovic, F., Bowie, J.H. & Fidelio, G.D. (2004) Surface behaviour and peptide-lipid interactions of the antibiotic peptides, Maculatin and Citropin. *Biochimica Et Biophysica Acta-Biomembranes*, 1664 (1), pp.31–37.

Ambroggio, E.E., Separovic, F., Bowie, J.H., Fidelio, G.D. & Bagatolli, L.A. (2005) Direct visualization of membrane leakage induced by the antibiotic peptides: maculatin, citropin, and aurein. *Biophysical journal*, 89 (3), pp.1874–81.

Amiche, M., Ladram, A. & Nicolas, P. (2008) A consistent nomenclature of antimicrobial peptides isolated from frogs of the subfamily Phyllomedusinae. *Peptides*, 29 (11), pp.2074–2082.

Andersson, M., Ulmschneider, J.P., Ulmschneider, M.B. & White, S.H. (2013) Conformational States of Melittin at a Bilayer Interface. *Biophysical Journal*, 104 (6), pp.L12–L14.

Andreu, D., Aschauer, H., Kreil, G. & Merrifield, R.B. (1985) Solid-phase synthesis of PYLa and isolation of its natural counterpart, PGLa [PYLa-(4-24)] from skin secretion of Xenopus laevis. *European journal of biochemistry / FEBS*, 149 (3), pp.531–5.

Avitabile, C., Netti, F. & Orefice, G. (2013) Design, structural and functional characterization of a Temporin-1b analogue active against Gram negative bacteria. *... et Biophysica Acta (BBA ...*, 18, pp.S60–S61.

Babich, H. & Stotzky, G. (1983) *ADVANCES IN APPLIED MICROBIOLOGY, Volume 29*. Academic Press.

Baker, M.A., Maloy, W.L., Zasloff, M. & Jacob, L.S. (1993) Anticancer efficacy of Magainin2 and analogue peptides. *Cancer Research*, 53 (13), pp.3052–3057.

Balaraman, G.S., Park, I.-H., Jain, A. & Vaidehi, N. (2011) Folding of small proteins using constrained molecular dynamics. *The journal of physical chemistry. B*, 115 (23), pp.7588–96.

Balla, M.S., Bowie, J.H. & Separovic, F. (2004) Solid-state {NMR} study of antimicrobial peptides from Australian frogs in phospholipid membranes. *European Biophysics Journal with Biophysics Letters*, 33 (2), pp.109–116.

Batista, C.V.., Scaloni, A., Rigden, D.J., Silva, L.R., Rodrigues Romero, A., Dukor, R., Sebben, A., Talamo, F. & Bloch, C. (2001) A novel heterodimeric antimicrobial peptide from the tree-frog Phyllomedusa distincta. *FEBS Letters*, 494 (1-2), pp.85–89.

Batista, C.V.F., Rosendo da Silva, L., Sebben, A., Scaloni, A., Ferrara, L., Paiva, G.R., Olamendi-Portugal, T., Possani, L.D. & BlochJr., C. (1999) Antimicrobial peptides from the Brazilian frog Phyllomedusa distincta. *Peptides*, 20 (6), pp.679–686.

Bechinger, B., Ruysschaert, J.M. & Goormaghtigh, E. (1999) Membrane helix orientation from linear dichroism of infrared attenuated total reflection spectra. *Biophysical journal*, 76 (January), pp.552–563.

Bechinger, B., Zasloff, M. & Opella, S.J. (1998) Structure and dynamics of the antibiotic peptide PGLa in membranes by solution and solid-state nuclear magnetic resonance spectroscopy. *Biophysical journal*, 74 (2 Pt 1), pp.981–7.

Becucci, L., Papini, M., Mullen, D., Scaloni, A., Veglia, G. & Guidelli, R. (2011) Probing membrane permeabilization by the antimicrobial peptide distinctin in mercury-supported biomimetic membranes. *Biochimica Et Biophysica Acta-Biomembranes*, 1808 (11), pp.2745–2752.

Belaid, A., Aouni, M., Khelifa, R., Trabelsi, A., Jemmali, M. & Hani, K. (2002) In vitro antiviral activity of dermaseptins against herpes simplex virus type-1. *Journal of Medical Virology*, 66 (2), pp.229–234.

Bernstein, F.C., Koetzle, T.F., Williams, G.J., Meyer, E.F., Brice, M.D., Rodgers, J.R., Kennard, O., Shimanouchi, T. & Tasumi, M. (1977) The Protein Data Bank: a computer-based archival file for macromolecular structures. *Journal of molecular biology*, 112 (3), pp.535–42.

Bertelsen, K., Dorosz, J., Hansen, S.K., Nielsen, N.C. & Vosegaard, T. (2012) Mechanisms of peptide-induced pore formation in lipid bilayers investigated by oriented 31P solid-state NMR spectroscopy. *PloS one*, 7 (10), p.e47745.

Boakes, S., Ayala, T., Herman, M., Appleyard, A.N., Dawson, M.J. & Cortés, J. (2012) Generation of an actagardine A variant library through saturation mutagenesis. *Applied microbiology and biotechnology*, 95 (6), pp.1509–17.

Bond, P.J., Parton, D.L., Clark, J.F. & Sansom, M.S.P. (2008) Coarse-grained simulations of the membrane-active antimicrobial Peptide maculatin 1.1. *Biophysical journal*, 95 (8), pp.3802–15.

Brooks, B.R., Brooks, C.L., Mackerell, A.D., Nilsson, L., Petrella, R.J., Roux, B., Won, Y., Archontis, G., Bartels, C., Boresch, S., Caflisch, A., Caves, L., Cui, Q., Dinner, A.R., Feig, M., Fischer, S., Gao, J., Hodoscek, M., Im, W., Kuczera, K., Lazaridis, T., Ma, J., Ovchinnikov, V., Paci, E., Pastor, R.W., Post, C.B., Pu, J.Z., Schaefer, M., Tidor, B., Venable, R.M., Woodcock, H.L., Wu, X., Yang, W., York, D.M. & Karplus, M. (2009) CHARMM: the biomolecular simulation program. *Journal of computational chemistry*, 30 (10), pp.1545–614.

Brooks, B.R., Bruccoleri, R.E., Olafson, B.D., States, D.J., Swaminathan, S. & Karplus, M. (1983) CHARMM: A program for macromolecular energy, minimization, and dynamics calculations. *Journal of Computational Chemistry*, 4 (2), pp.187–217.

Brunton, L., Lazo, J. & Parker, K. (2005) *Goodman & Gilman's The Pharmacological Basis of Therapeutics, Eleventh Edition (Goodman and Gilman"S the Pharmacological Basis of Therapeutics)*. McGraw-Hill Medical.

Carotenuto, A., Malfi, S., Saviello, M.R., Campiglia, P., Gomez-Monterrey, I., Mangoni, M.L., Gaddi, L.M.H., Novellino, E. & Grieco, P. (2008) A different molecular mechanism underlying antimicrobial and hemolytic actions of temporins A and L. *Journal of medicinal ...*, 51 (8), pp.2354–2362.

Chakrabarti, N., Tajkhorshid, E., Roux, B. & Pomès, R. (2004) Molecular basis of proton blockage in aquaporins. *Structure (London, England : 1993)*, 12 (1), pp.65–74.

Chaudhury, S., Olson, M.A., Tawa, G., Wallqvist, A. & Lee, M.S. (2012) Efficient Conformational Sampling in Explicit Solvent Using a Hybrid Replica Exchange Molecular Dynamics Method. *Journal of Chemical Theory and Computation*, 8 (2), pp.677–687.

Chen, R. & Mark, A.E. (2011) The effect of membrane curvature on the conformation of antimicrobial peptides: implications for binding and the mechanism of action. *European Biophysics Journal with Biophysics Letters*, 40 (4), pp.545–553.

Cheng, J., Hale, J. & Elliot, M. (2009) Effect of membrane composition on antimicrobial peptides aurein 2.2 and 2.3 from Australian southern bell frogs. *Biophysical journal*, 96 (2), pp.552–565.

Cheng, J., Hale, J., Kindrachuk, J. & Jessen, H. (2010) Importance of Residue 13 and the C-Terminus for the Structure and Activity of the Antimicrobial Peptide Aurein 2.2. *Biophysical journal*, 99 (9), pp.2926–2935.

Cheng, J.T.J., Hale, J.D., Elliott, M., Hancock, R.E.W. & Straus, S.K. (2011) The importance of bacterial membrane composition in the structure and function of aurein 2.2 and selected variants. *Biochimica et biophysica acta*, 1808 (3), pp.622–33.

Chi, S., Kim, J., Kim, D. & Lee, S. (2007) Solution structure and membrane interaction mode of an antimicrobial peptide gaegurin 4. ... *and biophysical research* ..., 352 (3), pp.592–597.

Chia, B., Carver, J. & Lindner, R. (2000) Caerin 4.1, an Antibiotic Peptide from the Australian Tree Frog, Litoria caerulea. The NMR-Derived Solution Structure. *Australian Journal of* ..., 53 (4), pp.257–265.

Chia, B.C.S., Lam, Y.-H.H., Dyall-Smith, M., Separovic, F. & Bowie, J.H. (2000) A31p {NMR} study of the interaction of amphibian antimicrobial peptides with the membranes of live bacteria. *Letters in Peptide Science*, 7 (3), pp.151–156.

Chia, C.S.B., Gong, Y., Bowie, J.H., Zuegg, J. & Cooper, M. a (2011) Membrane binding and perturbation studies of the antimicrobial peptides caerin, citropin, and maculatin. *Biopolymers*, 96 (2), pp.147–57.

Chia, C.S.B., Torres, J., Cooper, M.A., Arkin, I.T. & Bowie, J.H. (2002) The orientation of the antibiotic peptide maculatin 1.1 in {DMPG} and {DMPC} lipid bilayers. Support for a pore-forming mechanism. *Febs Letters*, 512 (1-3), pp.47–51.

Conlon, J.M. (2008) Reflections on a systematic nomenclature for antimicrobial peptides from the skins of frogs of the family Ranidae. *Peptides*, 29 (9), pp.1815–1819.

Conlon, J.M., Ahmed, E. & Condamine, E. (2009) Antimicrobial Properties of Brevinin-2-Related Peptide and its Analogs: Efficacy Against Multidrug-Resistant Acinetobacter baumannii. *Chemical Biology & Drug Design*, 74 (5), pp.488–493.

Conlon, J.M., Al-Kharrge, R., Ahmed, E., Raza, H., Galadari, S. & Condamine, E. (2007) Effect of aminoisobutyric acid (Aib) substitutions on the antimicrobial and cytolytic activities of the frog skin peptide, temporin-1DRa. *Peptides*, 28 (10), pp.2075–2080.

Conlon, J.M., Power, G., Abdel-Wahab, Y.H. a, Flatt, P.R., Jiansheng, H., Coquet, L., Leprince, J., Jouenne, T. & Vaudry, H. (2008) A potent, non-toxic insulin-releasing peptide isolated from an extract of the skin of the Asian frog, Hylarana guntheri (Anura:Ranidae). *Regulatory Peptides*, 151 (1-3), pp.153–159.

Daubner, S.C., Avila, A., Bailey, J.O., Barrera, D., Bermudez, J.Y., Giles, D.H., Khan, C.A., Shaheen, N., Thompson, J.W., Vasquez, J., Oxley, S.P. & Fitzpatrick, P.F. (2013) Mutagenesis of a specificity-determining residue in tyrosine hydroxylase establishes that the enzyme is a robust phenylalanine hydroxylase but a fragile tyrosine hydroxylase. *Biochemistry*, 52 (8), pp.1446–55.

David, J. (1992) The structure of caerin 1.1, a novel antibiotic peptide from Australian tree frogs. *Journal of the Chemical Society, Chemical* ..., (17), pp.1224–1225.

Dennison, S. (2012) Effect of Amidation on the Antimicrobial Peptide Aurein 2.5 from Australian Southern Bell Frogs. *Protein and Peptide …*, 19 (6), pp.586–591.

Dickson, J.S. & Koohmaraie, M. (1989) Cell surface charge characteristics and their relationship to bacterial attachment to meat surfaces. *Applied and environmental microbiology*, 55 (4), pp.832–6.

Dodge, J.T. & Phillips, G.B. (1967) Composition of phospholipids and of phospholipid fatty acids and aldehydes in human red cells. *Journal of lipid research*, 8 (6), pp.667–75.

Domingues, T.M., Riske, K.A. & Miranda, A. (2010) Revealing the lytic mechanism of the antimicrobial peptide gomesin by observing giant unilamellar vesicles. *Langmuir : the ACS journal of surfaces and colloids*, 26 (13), pp.11077–84.

Doyle, J., Brinkworth, C.S., Wegener, K.L., Carver, J. a., Llewellyn, L.E., Olver, I.N., Bowie, J.H., Wabnitz, P. a. & Tyler, M.J. (2003) nNOS inhibition, antimicrobial and anticancer activity of the amphibian skin peptide, citropin 1.1 and synthetic modifications. The solution structure of a modified citropin 1.1. *European Journal of Biochemistry*, 270 (6), pp.1141–1153.

Eleftheriou, M., Germain, R.S., Royyuru, A.K. & Zhou, R. (2006) Thermal denaturing of mutant lysozyme with both the OPLSAA and the CHARMM force fields. *Journal of the American Chemical Society*, 128 (41), pp.13388–95.

Ennaceur, S.M., Hicks, M.R., Pridmore, C.J., Dafforn, T.R., Rodger, A. & Sanderson, J.M. (2009) Peptide adsorption to lipid bilayers: slow processes revealed by linear dichroism spectroscopy. *Biophysical journal*, 96 (4), pp.1399–407.

Enrique Islas-Rodriguez, A., Marcellini, L., Orioni, B., Barra, D., Stella, L. & Mangoni, M.L. (2009) Esculentin 1-21: a linear antimicrobial peptide from frog skin with inhibitory effect on bovine mastitis-causing bacteria. *Journal of Peptide Science*, 15 (9), pp.607–614.

Eun, S.Y., Jang, H.K., Han, S.K., Ryu, P.D., Lee, B.J., Han, K.H. & Kim, S.J. (2006) A helix-induced oligomeric transition of gaegurin 4, an antimicrobial peptide isolated from a Korean frog. *Molecules and Cells*, 21 (2), pp.229–236.

Falk, H., Vormayr, G., Margulies, L., Metz, S. & Mazur, Y. (1986) A linear dichroism study of pyrromethene-, pyrromethenone- and bilatriene-abc-derivatives. *Monatshefte für Chemie Chemical Monthly*, 117 (6-7), pp.849–858.

Feig, M., Karanicolas, J. & Brooks, C.L. (2004) MMTSB Tool Set: enhanced sampling and multiscale modeling methods for applications in structural biology. *Journal of molecular graphics & modelling*, 22 (5), pp.377–95.

Ferber, M., Zoete, V. & Michielin, O. (2012) T-cell receptors binding orientation over peptide/MHC class I is driven by long-range interactions. *PloS one*, 7 (12), p.e51943.

Fernandez, D.I., Le Brun, A.P., Lee, T.-H., Bansal, P., Aguilar, M.-I., James, M. & Separovic, F. (2013) Structural effects of the antimicrobial peptide maculatin 1.1 on supported lipid bilayers. *European Biophysics Journal with Biophysics Letters*, 42 (1), pp.47–59.

Fernandez, D.I., Le Brun, A.P., Whitwell, T.C., Sani, M.-A., James, M. & Separovic, F. (2012) The antimicrobial peptide aurein 1.2 disrupts model membranes via the carpet mechanism. *Physical chemistry chemical physics : PCCP*, 14 (45), pp.15739–51.

Fernandez, D.I., Sani, M.-A., Miles, A.J., Wallace, B. a & Separovic, F. (2013) Membrane defects enhance the interaction of antimicrobial peptides, aurein 1.2 versus caerin 1.1. *Biochimica et biophysica acta*, 1828 (8), pp.1863–1872.

Gehman, J., Luc, F., Hall, K. & Lee, T. (2008) Effect of Antimicrobial Peptides from Australian Tree Frogs on Anionic Phospholipid Membranes†. *Biochemistry*, pp.8557–8565.

Gesell, J., Zasloff, M. & Opella, S.J. (1997) Two-dimensional 1H NMR experiments show that the 23-residue magainin antibiotic peptide is an alpha-helix in dodecylphosphocholine micelles, sodium dodecylsulfate micelles, and trifluoroethanol/water solution. *Journal of biomolecular NMR*, 9 (2), pp.127–35.

Ghiselli, R., Silvestri, C. & Cirioni, O. (2011) Protective Effect of Citropin 1.1 and Tazobactam-Piperacillin Against Oxidative Damage and Lethality in Mice Models of Gram-Negative Sepsis. *Journal of Surgical …*, 171 (2), pp.726–733.

Giacometti, A. & Cirioni, O. (2005) In vitro activity of citropin 1.1 alone and in combination with clinically used antimicrobial agents against Rhodococcus equi. *… of Antimicrobial …*, 56 (2), pp.410–412.

Giacometti, A., Cirioni, O., Ghiselli, R., Mocchegiani, F., Orlando, F., Silvestri, C., Bozzi, A., Di Giulio, A., Luzi, C., Mangoni, M.L., Barra, D., Saba, V., Scalise, G. & Rinaldi, A.C. (2006) Interaction of antimicrobial peptide temporin L with lipopolysaccharide in vitro and in experimental rat models of septic shock caused by gram-negative bacteria. *Antimicrobial agents and chemotherapy*, 50 (7), pp.2478–86.

Goraya, J., Knoop, F.C. & Conlon, J.M. (1998) Ranatuerins: Antimicrobial peptides isolated from the skin of the American bullfrog, Rana catesbeiana. *Biochemical and Biophysical Research Communications*, 250 (3), pp.589–592.

Gordon, Y.J., Romanowski, E.G. & McDermott, A.M. (2005) A review of antimicrobial peptides and their therapeutic potential as anti-infective drugs. *Current eye research*, 30 (7), pp.505–15.

Green, B.D., Mooney, M.H., Gault, V.A., Irwin, N., Bailey, C.J., Harriott, P., Greer, B., O'Harte, F.P.M. & Flatt, P.R. (2004) N-terminal His(7)-modification of glucagon-like peptide-1(7-36) amide generates dipeptidyl peptidase IV-stable analogues with potent antihyperglycaemic activity. *The Journal of Endocrinology*, 180 (3), pp.379–388.

Greenfield, N.J. & Fasman, G.D. (1969) Computed circular dichroism spectra for the evaluation of protein conformation. *Biochemistry*, 8 (10), pp.4108–4116.

Grieco, P., Luca, V., Auriemma, L., Carotenuto, A., Saviello, M.R., Campiglia, P., Barra, D., Novellino, E. & Mangoni, M.L. (2011) Alanine scanning analysis and structure-function relationships of the frog-skin antimicrobial peptide temporin-1Ta. *Journal of peptide science : an official publication of the European Peptide Society*, 17 (5), pp.358–65.

Guerrero, E. & Saugar, J. (2004) Role of positional hydrophobicity in the leishmanicidal activity of magainin 2. *Antimicrobial agents and …*, 48 (8), pp.2980–2986.

Hancock, R.E. (1997) Peptide antibiotics. *The Lancet*, 349 (9049), pp.418–422.

Hang, X. & Kang, W.J. (2004) Sequence analysis and membrane partitioning energies of alpha-helical antimicrobial peptides. *Bioinformatics*, 20 (6), pp.970–973.

Hicks, M.R., Dafforn, T.R., Damianoglou, A., Wormell, P., Rodger, A. & Hoffmann, S. V (2009) Synchrotron radiation linear dichroism spectroscopy of the antibiotic peptide gramicidin in lipid membranes. *The Analyst*, 134 (8), pp.1623–8.

Hossain, M. & Guilhaudis, L. (2011) Synthesis, conformational analysis and biological properties of a dicarba derivative of the antimicrobial peptide, brevinin-1BYa. *European Biophysics ...*, 40 (4), pp.555–564.

Hu, J., Ma, A. & Dinner, A.R. (2006) Monte Carlo simulations of biomolecules: The MC module in CHARMM. *Journal of computational chemistry*, 27 (2), pp.203–16.

Huang, Z. & Tajkhorshid, E. (2008) Dynamics of the extracellular gate and ion-substrate coupling in the glutamate transporter. *Biophysical journal*, 95 (5), pp.2292–300.

Huang, Z. & Tajkhorshid, E. (2010) Identification of the third Na+ site and the sequence of extracellular binding events in the glutamate transporter. *Biophysical journal*, 99 (5), pp.1416–25.

Humphrey, W., Dalke, A. & Schulten, K. (1996) VMD: visual molecular dynamics. *Journal of molecular graphics*, 14 (1), pp.33–8, 27–8.

Hwang, P.M., Zhou, N., Shan, X., Arrowsmith, C.H. & Vogel, H.J. (1998) Three-dimensional solution structure of lactoferricin B, an antimicrobial peptide derived from bovine lactoferrin. *Biochemistry*, 37 (12), pp.4288–98.

Im, W. & Brooks, C.L. (2005) Interfacial folding and membrane insertion of designed peptides studied by molecular dynamics simulations. *Proceedings of the National Academy of Sciences of the United States of America*, 102 (19), pp.6771–6.

Isaacson, T., Soto, A., Iwamuro, S., Knoop, F.C. & Conlon, J.M.M. (2002) Antimicrobial peptides with atypical structural features from the skin of the Japanese brown frog Rana japonica. *Peptides*, 23 (3), pp.419–425.

Iwakoshi-Ukena, E., Ukena, K., Okimoto, A., Soga, M., Okada, G., Sano, N., Fujii, T., Sugawara, Y. & Sumida, M. (2011) Identification and characterization of antimicrobial peptides from the skin of the endangered frog Odorrana ishikawae. *Peptides*, 32 (4), pp.670–676.

Jakoblinnert, A., Wachtmeister, J., Schukur, L., Shivange, A. V, Bocola, M., Ansorge-Schumacher, M.B. & Schwaneberg, U. (2013) Reengineered carbonyl reductase for reducing methyl-substituted cyclohexanones. *Protein engineering, design & selection : PEDS*, 26 (4), pp.291–8.

Jani, V., Sonavane, U.B. & Joshi, R. (2011) Microsecond scale replica exchange molecular dynamic simulation of villin headpiece: an insight into the folding landscape. *Journal of biomolecular structure & dynamics*, 28 (6), pp.845–60.

Jas, G.S. & Kuczera, K. (2004) Equilibrium structure and folding of a helix-forming peptide: circular dichroism measurements and replica-exchange molecular dynamics simulations. *Biophysical journal*, 87 (6), pp.3786–98.

Kang, S., Son, W., Han, K. & Mishig-Ochir, T. (2010) Solution structure of antimicrobial peptide esculentin-1c from skin secretion of Rana esculenta. *Molecules and ...*, 30 (5), pp.435–441.

Kim, H., Han, S. & Park, J. (1999) Gaegurin 4, a peptide antibiotic of frog skin, forms voltage-dependent channels in planar lipid bilayers. ... *Journal of peptide ...*, 53 (1), pp.1–7.

Kim, H., Kim, S. & Lee, M. (2004) Role of C-terminal heptapeptide in pore-forming activity of antimicrobial agent, gaegurin 4. *The Journal of peptide ...*, 64 (4), pp.151–158.

Kim, H., Lee, B. & Lee, M. (2009) Mechanisms of selective antimicrobial activity of Gaegurin 4. *The Korean Journal of ...*, 13 (1), pp.39–47.

Kim, J., Lee, J., Jung, J., Lee, S. & You, G. (2010) Gaegurin-6 stimulates insulin secretion through calcium influx in pancreatic β Rin5mf cells. *Regulatory peptides*, 159 (1-3), pp.123–128.

Kim, J., Lee, S., Park, H., Park, Y. & Hahm, K. (2007) Antimicrobial Mechanism of an Antimicrobial Peptide, Pseudin-2, Derived from the Skin of the Paradoxical Frog in Various Membrane Lipid Compositions.

Kim, J.M., Jang, S.A., Yu, B.J., Sung, B.H., Cho, J.H. & Kim, S.C. (2008) High-level expression of an antimicrobial peptide histonin as a natural form by multimerization and furin-mediated cleavage. *Applied microbiology and biotechnology*, 78 (1), pp.123–30.

Kumari, V. & Nagaraj, R. (2001) – function studies on the amphibian peptide brevinin 1E: translocating the cationic segment from the C-terminal end to a central position favors selective antibacterial. *The Journal of Peptide Research*, 58 (5), pp.433–441.

Kyte, J. & Doolittle, R.F. (1982) A simple method for displaying the hydropathic character of a protein. *Journal of Molecular Biology*, 157 (1), pp.105–132.

Lacroix, E., Viguera, A.R. & Serrano, L. (1998) Elucidating the folding problem of alpha-helices: local motifs, long-range electrostatics, ionic-strength dependence and prediction of NMR parameters. *Journal of molecular biology*, 284 (1), pp.173–91.

Laver, D.R. (1994) The barrel-stave model as applied to alamethicin and its analogs reevaluated. *Biophysical Journal*, 66 (2), pp.355–359.

Lee, H., Jang, I.H., Ryu, S.H. & Park, T.G. (2003) N-Terminal Site-Specific Mono-PEGylation of Epidermal Growth Factor. *Pharmaceutical Research*, 20 (5), pp.818–825.

Lee, K., Hong, S., Oh, J., Lee, B. & Choi, B. (1998) Antimicrobial activity and conformation of gaegurin-6 amide and its analogs. *Peptides*, 19 (10), pp.1653–1658.

Lee, M.-T., Sun, T.-L., Hung, W.-C. & Huang, H.W. (2013) Process of inducing pores in membranes by melittin. *Proceedings of the National Academy of Sciences of the United States of America*, 110 (35), pp.14243–8.

Lee, T.-H., Heng, C., Swann, M.J., Gehman, J.D., Separovic, F. & Aguilar, M.-I. (2010) Real-time quantitative analysis of lipid disordering by aurein 1.2 during membrane adsorption, destabilisation and lysis. *Biochimica et biophysica acta*, 1798 (10), pp.1977–86.

Leontiadou, H., Mark, A.E. & Marrink, S.J. (2006) Antimicrobial Peptides in Action. *Journal of the American Chemical Society*, 128 (37), pp.12156–12161.

Liu, B. & Pop, M. (2009) ARDB--Antibiotic Resistance Genes Database. *Nucleic acids research*, 37 (Database issue), pp.D443–7.

Lobley, A., Whitmore, L. & Wallace, B.A. (2002) DICHROWEB: an interactive website for the analysis of protein secondary structure from circular dichroism spectra. *Bioinformatics*, 18 (1), pp.211–212.

Lohner, K. & Prossnigg, F. (2009) Biological activity and structural aspects of PGLa interaction with membrane mimetic systems. *Biochimica Et Biophysica Acta-Biomembranes*, 1788 (8), pp.1656–1666.

Lorenzon, E.N., Sanches, P.R.S., Nogueira, L.G., Bauab, T.M., Cilli, E.M. & Lorenzón, E.N. (2013) Dimerization of aurein 1.2: effects in structure, antimicrobial activity and aggregation of Cândida albicans cells. *Amino acids*, 44 (6), pp.1521–8.

Ludtke, S., He, K., Heller, W. & Harroun, T. (1996) Membrane pores induced by magainin. *Biochemistry*, 35 (43), pp.13723–13728.

Ma, B. & Nussinov, R. (2003) Molecular dynamics simulations of the unfolding of beta(2)-microglobulin and its variants. *Protein engineering*, 16 (8), pp.561–75.

Ma, N., Chung, Y.-H. & van der Vaart, A. (2013) Free energy simulation of helical transitions. *Journal of computational chemistry*, 34 (8), pp.640–5.

Macholz, R. (1990) Microbiallipids, Vol. 1. Herausgegeben von C. Ratledge und S. G. Wilkinson. 963 Seiten, zahlr. Tab. Academic Press, London, San Diego, New York u. a. 1988. Preis: 110,— £. *Food / Nahrung*, 34 (6), pp.574–574.

Maddox, M.W. & Longo, M.L. (2002) A Monte Carlo Study of Peptide Insertion into Lipid Bilayers: Equilibrium Conformations and Insertion Mechanisms. *Biophysical Journal*, 82 (1), pp.244–263.

Maisetta, G., Mangoni, M.L., Esin, S., Pichierri, G., Capria, A.L., Brancatisano, F.L., Di Luca, M., Barnini, S., Barra, D., Campa, M. & Batoni, G. (2009) In vitro bactericidal activity of the N-terminal fragment of the frog peptide esculentin-1b (Esc 1-18) in combination with conventional antibiotics against Stenotrophomonas maltophilia. *Peptides*, 30 (9), pp.1622–1626.

Mangoni, M., Papo, N. & Barra, D. (2004) Effects of the antimicrobial peptide temporin L on cell morphology, membrane permeability and viability of Escherichia coli. *Biochemical ...*, 380, pp.859–865.

Mangoni, M. & Rinaldi, A. (2000) Structure–function relationships of temporins, small antimicrobial peptides from amphibian skin. *European Journal of ...*, 267 (5), pp.1447–1454.

Mangoni, M.L., Carotenuto, A., Auriemma, L., Saviello, M.R., Campiglia, P., Gomez-Monterrey, I., Malfi, S., Marcellini, L., Barra, D., Novellino, E. & Grieco, P. (2011) Structure-Activity Relationship, Conformational and Biological Studies of Temporin L Analogues. *Journal of Medicinal Chemistry*, 54 (5), pp.1298–1307.

Mangoni, M.L., Maisetta, G., Di Luca, M., Gaddi, L.M.H., Esin, S., Florio, W., Brancatisano, F.L., Barra, D., Campy, M. & Batoni, G. (2008) Comparative analysis of the bactericidal activities of amphibian peptide analogues against multidrug-resistant nosocomial bacterial strains. *Antimicrobial Agents and Chemotherapy*, 52 (1), pp.85–91.

Marcotte, I., Wegener, K.L., Lam, Y.H., Chia, B.C.S., de Planque, M.R.R., Bowie, J.H., Auger, M. & Separovic, F. (2003) Interaction of antimicrobial peptides from Australian amphibians with lipid membranes. *Chemistry and Physics of Lipids*, 122 (1-2), pp.107–120.

Marenah, L., Flatt, P.R. & Orr, D. (2005) Isolation and structural characterization of novel Rugosin A-like insulinotropic peptide from the skin secretions of Rana saharica frog. *Peptides*, 26 (11), pp.2117–2123.

Marenah, L., Flatt, P.R., Orr, D. F., McClean, S., Shaw, C. & Abdel-Wahab, Y.H. a (2004) Brevinin-1 and multiple insulin-releasing peptides in the skin of the frog Rana palustris. *Journal of Endocrinology*, 181 (2), pp.347–354.

Marenah, L., Flatt, P.R., Orr, David F., McClean, S., Shaw, C. & Abdel-Wahab, Y.H. a (2004) Skin secretion of the toad Bombina variegata contains multiple insulin-releasing peptides including bombesin and entirely novel insulinotropic structures. *Biological Chemistry*, 385 (3-4), pp.315–321.

Marenah, L., Flatt, P.R., Orr, D.F., Shaw, C. & Abdel-Wahab, Y.H. a (2005) Characterization of naturally occurring peptides in the skin secretion of Rana pipiens frog reveal pipinin-1 as the novel insulin-releasing agent. *The Journal of Peptide Research: Official Journal of the American Peptide Society*, 66 (4), pp.204–210.

Marenah, L., Flatt, P.R., Orr, D.F., Shaw, C. & Abdel-Wahab, Y.H. a (2006) Skin secretions of Rana saharica frogs reveal antimicrobial peptides esculentins-1 and-1B and brevinins-1E and-2EC with novel insulin releasing activity. *Journal of Endocrinology*, 188 (1), pp.1–9.

Marenah, L., McClean, S., Flatt, P.R., Orr, D.F., Shaw, C. & Abdel-Wahab, Y.H. a (2004) Novel insulin-releasing peptides in the skin of Phyllomedusa trinitatis frog include 28 amino acid peptide from dermaseptin BIV precursor. *Pancreas*, 29 (2), pp.110–115.

Marenah, L., Shaw, C., Orr, D. & McClean, S. (2004) Isolation and characterisation of an unexpected class of insulinotropic peptides in the skin of the frog Agalychnis litodryas. ... *peptides*, 120 (1-3), pp.33–38.

Marion, D., Zasloff, M. & Bax, A. (1988) A two-dimensional NMR study of the antimicrobial peptide magainin 2. *FEBS Letters*, 227 (1), pp.21–26.

Marrington, R., Dafforn, T.R., Halsall, D.J., MacDonald, J.I., Hicks, M. & Rodger, A. (2005) Validation of new microvolume Couette flow linear dichroism cells. *The Analyst*, 130 (12), pp.1608–16.

Marx, P.F., Havik, S.R., Marquart, J.A., Bouma, B.N. & Meijers, J.C.M. (2004) Generation and characterization of a highly stable form of activated thrombin-activable fibrinolysis inhibitor. *The Journal of biological chemistry*, 279 (8), pp.6620–8.

Matsuzaki, K., Mitani, Y. & Akada, K. (1998) Mechanism of synergism between antimicrobial peptides magainin 2 and PGLa. *Biochemistry*, 37 (43), pp.15144–15153.

Mechkarska, M., Ahmed, E. & Coquet, L. (2010) Antimicrobial peptides with therapeutic potential from skin secretions of the Marsabit clawed frog Xenopus borealis(Pipidae). *... and Physiology Part C: ...*, 152 (4), pp.467–472.

Mechkarska, M., Ojo, O. & Meetani, M. (2011) Peptidomic analysis of skin secretions from the bullfrog Lithobates catesbeianus(Ranidae) identifies multiple peptides with potent insulin-releasing activity. *Peptides*, 32 (2), pp.203–208.

Mechler, A., Praporski, S., Atmuri, K., Boland, M., Separovic, F. & Martin, L.L. (2007) Specific and selective peptide-membrane interactions revealed using quartz crystal microbalance. *Biophysical Journal*, 93 (11), pp.3907–3916.

Mehrnejad, F., Naderi-Manesh, H., Ranjbar, B., Maroufi, B., Asoodeh, A. & Doustdar, F. (2008) PCR-based gene synthesis, molecular cloning, high level expression, purification, and characterization of novel antimicrobial peptide, Brevinin-2R, in Escherichia coli. *Applied Biochemistry and Biotechnology*, 149 (2), pp.109–118.

Meng, P., Wei, L., Yang, S., Liu, H., Liu, R. & Lai, R. (2012) A novel frog skin peptide containing function to induce muscle relaxation. *Biochimie*, 94 (12), pp.2508–2513.

Menz, W.J., Penna, M.J. & Biggs, M.J. (2010) TNAMD: Implementation of TIGER2 in NAMD. *Computer Physics Communications*, 181 (12), pp.2082–2085.

Mihajlovic, M. & Lazaridis, T. (2012) Charge distribution and imperfect amphipathicity affect pore formation by antimicrobial peptides. *Biochimica et biophysica acta*, 1818 (5), pp.1274–83.

Molloy, E.M., Field, D., Connor, P.M.O., Cotter, P.D., Hill, C. & Ross, R.P. (2013) Saturation mutagenesis of lysine 12 leads to the identification of derivatives of nisin a with enhanced antimicrobial activity. *PloS one*, 8 (3), p.e58530.

Morikawa, N., Hagiwara, K. & Nakajima, T. (1992) Brevinin-1 and -2, unique antimicrobial peptides from the skin of the frog Rana brevipoda porsa. *Biochemical and Biophysical Research Communications*, 189 (1), pp.184–190.

Morin, K.M., Arcidiacono, S., Beckwitt, R. & Mello, C.M. (2006) Recombinant expression of indolicidin concatamers in Escherichia coli. *Applied microbiology and biotechnology*, 70 (6), pp.698–704.

Morrissey, J.H., Davis-Harrison, R.L., Tavoosi, N., Ke, K., Pureza, V., Boettcher, J.M., Clay, M.C., Rienstra, C.M., Ohkubo, Y.Z., Pogorelov, T. V & Tajkhorshid, E. (2010) Protein-phospholipid interactions in blood clotting. *Thrombosis research*, 125 Suppl , pp.S23–5.

Morrissey, J.H., Pureza, V., Davis-Harrison, R.L., Sligar, S.G., Ohkubo, Y.Z. & Tajkhorshid, E. (2008) Blood clotting reactions on nanoscale phospholipid bilayers. *Thrombosis research*, 122 Suppl , pp.S23–6.

Muller, L.M.A.J., Gorter, K.J., Hak, E., Goudzwaard, W.L., Schellevis, F.G., Hoepelman, A.I.M. & Rutten, G.E.H.M. (2005) Increased risk of common infections in patients with type 1 and type 2 diabetes mellitus. *Clinical infectious diseases : an official publication of the Infectious Diseases Society of America*, 41 (3), pp.281–8.

Muñoz, V. & Serrano, L. (1997) Development of the multiple sequence approximation within the AGADIR model of α-helix formation: Comparison with Zimm-Bragg and Lifson-Roig formalisms. *Biopolymers*, 41 (5), pp.495–509.

Muñoz, Victor & Serrano, L. (1995) Elucidating the Folding Problem of Helical Peptides using Empirical Parameters. II†. Helix Macrodipole Effects and Rational Modification of the Helical Content of Natural Peptides. *Journal of Molecular Biology*, 245 (3), pp.275–296.

Muñoz, V & Serrano, L. (1995) Elucidating the folding problem of helical peptides using empirical parameters. III. Temperature and pH dependence. *Journal of molecular biology*, 245 (3), pp.297–308.

Muñoz, V., Serrano, L. & Munoz, V. (1994) Elucidating the folding problem of helical peptides using empirical parameters. *Nature Structural Biology*, 1 (6), pp.399–409.

Münster, C., Spaar, A., Bechinger, B. & Salditt, T. (2002) Magainin 2 in phospholipid bilayers: peptide orientation and lipid chain ordering studied by x-ray diffraction. *Biochimica et Biophysica Acta (…*, 1562 (1-2), pp.37–44.

Mura, M. & Dennison, S. (2012) Aurein 2.3 functionality is supported by oblique orientated α-helical formation. *Biochimica et Biophysica …*, 1828 (2), pp.586–594.

Mustafa, M. & Busath, D.D. (2009) The gramicidin channel ion permeation free-energy profile: direct and indirect effects of CHARMM force field improvements. *Interdisciplinary sciences, computational life sciences*, 1 (2), pp.113–27.

Niidome, T., Kobayashi, K., Arakawa, H., Hatakeyama, T. & Aoyagi, H. (2004) Structure-activity relationship of an antibacterial peptide, maculatin 1.1, from the skin glands of the tree frog, Litoria genimaculata. *Journal of Peptide Science*, 10 (7), pp.414–422.

Obst, S. & Bradaczek, H. (1997) Molecular Dynamics Simulations of Zinc Ions in Water Using CHARMM. *Journal of Molecular Modeling*, 3 (6), pp.224–232.

Ohkubo, Y.Z. & Brooks, C.L. (2003) Exploring Flory's isolated-pair hypothesis: statistical mechanics of helix-coil transitions in polyalanine and the C-peptide from RNase A. *Proceedings of the National Academy of Sciences of the United States of America*, 100 (24), pp.13916–21.

Ojo, O.O., Abdel-Wahab, Y.H. a, Flatt, P.R., Mechkarska, M. & Conlon, J.M. (2011) Tigerinin-1R: a potent, non-toxic insulin-releasing peptide isolated from the skin of the Asian frog, Hoplobatrachus rugulosus. *Diabetes, obesity & metabolism*, 13 (12), pp.1114–22.

Olson, L., Soto, A., Knoop, F. & Conlon, J. (2001) Pseudin-2: an antimicrobial peptide with low hemolytic activity from the skin of the paradoxical frog. *Biochemical and biophysical …*, 288 (4), pp.1001–1005.

Pal, T., Sonnevend, A., Galadari, S. & Conlon, J.M.M. (2005) Design of potent, non-toxic antimicrobial agents based upon the structure of the frog skin peptide, pseudin-2. *Regulatory peptides*, 129 (1-3), pp.85–91.

PARK, J., Jung, J. & Lee, B. (1994) Antimicrobial Peptides from the Skin of a Korean Frog, Rana rugosa. *Biochemical and biophysical research …*, 205 (1), pp.948–954.

Park, S., Kim, J., Jeong, C. & Yoo, S. (2011) A plausible mode of action of pseudin-2, an antimicrobial peptide from Pseudis paradoxa. *Biochimica et Biophysica*.

Park, S., Park, S.-H., Ahn, H.-C., Kim, S., Kim, S.S., Lee, B.J. & Lee, B.-J. (2001) Structural study of novel antimicrobial peptides, nigrocins, isolated from Rana nigromaculata. *FEBS Letters*, 507 (1), pp.95–100.

Park, S., Son, W., Kim, Y., Kwon, A. & Lee, B. (2007) NMR spectroscopic assessment of the structure and dynamic properties of an amphibian antimicrobial peptide (Gaegurin 4) bound to SDS micelles. *Journal of biochemistry and …*, 40 (2), pp.261–269.

Park, S.H., Kim, Y.K., Park, J.W. & Lee, B.J. (2000) Solution structure of the antimicrobial peptide gaegurin 4 by H-1 and N-15 nuclear magnetic resonance spectroscopy. *European Journal of Biochemistry*, 267 (9), pp.2695–2704.

Parton, D.L., Akhmatskaya, E. V & Sansom, M.S.P. (2012) Multiscale Simulations of the Antimicrobial Peptide Maculatin 1.1: Water Permeation through Disordered Aggregates. *Journal of Physical Chemistry B*, 116 (29), pp.8485–8493.

Peng, X.-Q. (2013) Improved thermostability of lipase B from Candida antarctica by directed evolution and display on yeast surface. *Applied biochemistry and biotechnology*, 169 (2), pp.351–8.

Perez-Iratxeta, C. & Andrade-Navarro, M.A. (2008) K2D2: estimation of protein secondary structure from circular dichroism spectra. *BMC structural biology*, 8, p.25.

Phillips, J.C., Braun, R., Wang, W., Gumbart, J., Tajkhorshid, E., Villa, E., Chipot, C., Skeel, R.D., Kalé, L. & Schulten, K. (2005) Scalable molecular dynamics with NAMD. *Journal of computational chemistry*, 26 (16), pp.1781–802.

De Planque, M.R.R., Goormaghtigh, E., Greathouse, D. V., Koeppe, R.E., Kruijtzer, J.A.W., Liskamp, R.M.J., de Kruijff, B. & Killian, J.A. (2001) Sensitivity of Single Membrane-Spanning α-Helical Peptides to Hydrophobic Mismatch with a Lipid Bilayer: Effects on Backbone Structure, Orientation, and Extent of Membrane Incorporation †. *Biochemistry*, 40 (16), pp.5000–5010.

Ponti, D., Mignogna, G., Mangoni, M.L., De Biase, D., Simmaco, M. & Barra, D. (1999) Expression and activity of cyclic and linear analogues of esculentin-1, an anti-microbial peptide from amphibian skin. *European Journal of Biochemistry*, 263 (3), pp.921–927.

Pouny, Y., Rapaport, D., Mor, A., Nicolas, P. & SHAI, Y. (1992) Interaction of antimicrobial dermaseptin and its fluorescently labeled analogues with phospholipid membranes. *Biochemistry*, 31 (49), pp.12416–12423.

Prabhu, N. V, Panda, M., Yang, Q. & Sharp, K.A. (2008) Explicit ion, implicit water solvation for molecular dynamics of nucleic acids and highly charged molecules. *Journal of computational chemistry*, 29 (7), pp.1113–30.

Pukala, T., Brinkworth, C., Carver, J. & Bowie, J.H. (2004) Investigating the importance of the flexible hinge in caerin 1.1: solution structures and activity of two synthetically modified caerin peptides. *Biochemistry*, 43 (4), pp.937–944.

Ramamoorthy, A., Lee, D.-K., Narasimhaswamy, T. & Nanga, R.P.R. (2010) Cholesterol reduces pardaxin's dynamics-a barrel-stave mechanism of membrane disruption investigated by solid-state NMR. *Biochimica et biophysica acta*, 1798 (2), pp.223–7.

Reed, J. & Reed, T.A. (1997) A set of constructed type spectra for the practical estimation of peptide secondary structure from circular dichroism. *Analytical biochemistry*, 254 (1), pp.36–40.

Resende, J. (2009) Membrane structure and conformational changes of the antibiotic heterodimeric peptide distinctin by solid-state NMR spectroscopy. *Proceedings of the …*, 106 (39), pp.16639–16644.

Rinaldi, A.C., Di Giulio, A., Liberi, M., Gualtieri, G., Oratore, A., Bozzi, A., Schininà, M.E., Simmaco, M. & Schinina, M.E. (2001) Effects of temporins on molecular dynamics and membrane permeabilization in lipid vesicles. *The journal of peptide research : official journal of the American Peptide Society*, 58 (3), pp.213–20.

Rozek, A., Friedrich, C.L. & Hancock, R.E. (2000) Structure of the bovine antimicrobial peptide indolicidin bound to dodecylphosphocholine and sodium dodecyl sulfate micelles. *Biochemistry*, 39 (51), pp.15765–74.

Rozek, T., Bowie, J.H., Wallace, J.C. & Tyler, M.J. (2000) The antibiotic and anticancer active aurein peptides from the Australian Bell Frogs Litoria aurea and Litoria raniformis. Part 2. Sequence determination using electrospray mass spectrometry. *Rapid communications in mass spectrometry : RCM*, 14 (21), pp.2002–11.

Rozek, T., Wegener, K.L., Bowie, J.H., Olver, I.N., Carver, J.A., Wallace, J.C. & Tyler, M.J. (2000) The antibiotic and anticancer active aurein peptides from the Australian Bell Frogs Litoria aurea and Litoria raniformis the solution structure of aurein 1.2. *European journal of biochemistry / FEBS*, 267 (17), pp.5330–41.

Sani, M.-A., Whitwell, T.C., Gehman, J.D., Robins-Browne, R.M., Pantarat, N., Attard, T.J., Reynolds, E.C., O'Brien-Simpson, N.M. & Separovic, F. (2013) Maculatin 1.1 disrupts Staphylococcus aureus lipid membranes via a pore mechanism. *Antimicrobial agents and chemotherapy*, 57 (8), pp.3593–600.

Sani, M.-A., Whitwell, T.C. & Separovic, F. (2012) Lipid composition regulates the conformation and insertion of the antimicrobial peptide maculatin 1.1. *Biochimica et biophysica acta*, 1818 (2), pp.205–11.

Sarzyńska, J., Réblová, K., Sponer, J. & Kuliński, T. (2008) Conformational transitions of flanking purines in HIV-1 RNA dimerization initiation site kissing complexes studied by CHARMM explicit solvent molecular dynamics. *Biopolymers*, 89 (9), pp.732–46.

Saviello, M., Malfi, S. & Campiglia, P. (2010) New insight into the mechanism of action of the temporin antimicrobial peptides. *Biochemistry*, 49 (7), pp.1477–1485.

Schägger, H. (2006) Tricine-SDS-PAGE. *Nature protocols*, 1 (1), pp.16–22.

Serra, M.D., Cirioni, O. & Vitale, R. (2008) Structural Features of Distinctin Affecting Peptide Biological and Biochemical Properties†. *Biochemistry*, 47 (30), pp.7888–7899.

Seto, G.W.J., Marwaha, S., Kobewka, D.M., Lewis, R.N.A.H., Separovic, F. & McElhaney, R.N. (2007) Interactions of the Australian tree frog antimicrobial peptides aurein 1.2, citropin 1.1 and maculatin 1.1 with lipid model membranes: Differential scanning calorimetric and Fourier transform infrared spectroscopic studies. *Biochimica Et Biophysica Acta-Biomembranes*, 1768 (11), pp.2787–2800.

Shang, D., Li, X., Sun, Y., Wang, C., Sun, L., Wei, S. & Gou, M. (2012) Design of Potent, Non-Toxic Antimicrobial Agents Based upon the Structure of the Frog Skin Peptide, Temporin-1CEb from Chinese Brown Frog, Rana chensinensis. *Chemical Biology & Drug Design*, 79 (5), pp.653–662.

Shental-Bechor, D., Haliloglu, T. & Ben-Tal, N. (2007) Interactions of cationic-hydrophobic peptides with lipid bilayers: A Monte Carlo simulation method. *Biophysical Journal*, 93 (6), pp.1858–1871.

Sikorska, E. & Greber, K. (2009) Synthesis and antimicrobial activity of truncated fragments and analogs of citropin 1.1: The solution structure of the SDS micelle-bound citropin-like peptides. *Journal of structural ...*, 168 (2), pp.250–258.

Simmaco, M. & Mignogna, G. (1996) Temporins, antimicrobial peptides from the European red frog Rana temporaria. *European Journal of ...*, 242 (3), pp.788–792.

Simmaco, M., Mignogna, G., Barra, D. & Bossa, F. (1993) Novel antimicrobial peptides from skin secretion of the European frog Rana esculenta. *FEBS letters*, 324 (2), pp.159–161.

Skosyrev, V.S., Kulesskiy, E.A., Yakhnin, A. V., Temirov, Y. V. & Vinokurov, L.M. (2003) Expression of the recombinant antibacterial peptide sarcotoxin IA in Escherichia coli cells. *Protein Expression and Purification*, 28 (2), pp.350–356.

Son, W.S., Kim, J.S., Kim, H.E., Park, S.H. & Lee, B.J. (2003) Structural studies on the antimicrobial peptide Brevinin 1E by spectroscopic methods. *Spectroscopy-an International Journal*, 17 (2-3), pp.127–138.

Sonnevend, A., Knoop, F., Patel, M. & Pál, T. (2004) Antimicrobial properties of the frog skin peptide, ranatuerin-1 and its -substituted analog. *peptides*, 25 (1), pp.29–36.

Soufian, S. & Hassani, L. (2011) Study of structure-activity relationship in Aurein 1.2 analogs. *Pakistan journal of biological sciences: {PJBS}*, 14 (14), pp.729–735.

Strandberg, E., Zerweck, J., Wadhwani, P. & Ulrich, A.S. (2013) Synergistic Insertion of Antimicrobial Magainin-Family Peptides in Membranes Depends on the Lipid Spontaneous Curvature. *Biophysical Journal*, 104 (6), pp.L09–L11.

Subasinghage, A., Conlon, J. & Hewage, C. (2008) Conformational analysis of the broad-spectrum antibacterial peptide, ranatuerin-2CSa: identification of a full length helix–turn–helix motif. *Biochimica et Biophysica …*, 1784 (6), pp.924–929.

Sun, Y., Li, Q., Li, Z., Zhang, Y., Zhao, J. & Wang, L. (2012) Molecular Cloning, Expression, Purification, and Functional Characterization of Palustrin-2CE, an Antimicrobial Peptide of Rana chensinensis. *Bioscience Biotechnology and Biochemistry*, 76 (1), pp.157–162.

Suomalainen, H. & Nurminen, T. (1970) The lipid composition of cell wall and plasma membrane of baker's yeast. *Chemistry and Physics of Lipids*, 4 (3), pp.247–256.

Svensson, F.R., Lincoln, P., Nordén, B. & Esbjörner, E.K. (2011) Tryptophan orientations in membrane-bound gramicidin and melittin-a comparative linear dichroism study on transmembrane and surface-bound peptides. *Biochimica et biophysica acta*, 1808 (1), pp.219–28.

Tachi, T., Epand, RF, Epand, RM & Matsuzaki, K. (2002) Position-dependent hydrophobicity of the antimicrobial magainin peptide affects the mode of peptide-lipid interactions and selective toxicity. *Biochemistry*, 41 (34), pp.10723–10731.

Tamba, Y. & Yamazaki, M. (2009) Magainin 2-induced pore formation in the lipid membranes depends on its concentration in the membrane interface. *The Journal of Physical Chemistry B*, 113 (14), pp.4846–4852.

Tavoosi, N., Davis-Harrison, R.L., Pogorelov, T. V, Ohkubo, Y.Z., Arcario, M.J., Clay, M.C., Rienstra, C.M., Tajkhorshid, E. & Morrissey, J.H. (2011) Molecular determinants of phospholipid synergy in blood clotting. *The Journal of biological chemistry*, 286 (26), pp.23247–53.

Thomas, P., Kumar, T., Reshmy, V., Vineeth Kumar, T. V., Kumar, K.S. & George, S. (2012) A mini review on the antimicrobial peptides isolated from the genus Hylarana (Amphibia: Anura) with a proposed nomenclature for amphibian skin peptides. *Molecular Biology Reports*, 39 (6), pp.6943–6947.

Törnroth-Horsefield, S., Wang, Y., Hedfalk, K., Johanson, U., Karlsson, M., Tajkhorshid, E., Neutze, R. & Kjellbom, P. (2006) Structural mechanism of plant aquaporin gating. *Nature*, 439 (7077), pp.688–94.

Tremouilhac, P. & Strandberg, E. (2006) Synergistic transmembrane alignment of the antimicrobial heterodimer PGLa/magainin. *Journal of Biological …*, 281 (43), pp.32089–32094.

Unneberg, P., Merelo, J.J., Chacón, P. & Morán, F. (2001) SOMCD: method for evaluating protein secondary structure from UV circular dichroism spectra. *Proteins*, 42 (4), pp.460–70.

Varadarajan, N., Gam, J., Olsen, M.J., Georgiou, G. & Iverson, B.L. (2005) Engineering of protease variants exhibiting high catalytic activity and exquisite substrate selectivity. *Proceedings of the National Academy of Sciences of the United States of America*, 102 (19), pp.6855–60.

Verardi, R., Traaseth, N. & Shi, L. (2011) Probing membrane topology of the antimicrobial peptide distinctin by solid-state NMR spectroscopy in zwitterionic and charged lipid bilayers. *… et Biophysica Acta (BBA …*, 1808 (1), pp.34–40.

Verkleij, A.., Zwaal, R.F.., Roelofsen, B., Comfurius, P., Kastelijn, D. & van Deenen, L.L.. (1973) The asymmetric distribution of phospholipids in the human red cell membrane. A combined study using phospholipases and freeze-etch electron microscopy. *Biochimica et Biophysica Acta (BBA) - Biomembranes*, 323 (2), pp.178–193.

Verly, R.M., Moraes, C.M. de, Resende, J.M., Aisenbrey, C., Bemquerer, M.P., Piló-Veloso, D., Valente, A.P., Almeida, F.C.L. & Bechinger, B. (2009) Structure and Membrane Interactions of the Antibiotic Peptide Dermadistinctin K by Multidimensional Solution and Oriented 15N and 31P Solid-State NMR Spectroscopy. *Biophysical Journal*, 96 (6), pp.2194–2203.

Vojcic, L., Despotovic, D., Maurer, K.-H., Zacharias, M., Bocola, M., Martinez, R. & Schwaneberg, U. (2013) Reengineering of subtilisin Carlsberg for oxidative resistance. *Biological chemistry*, 394 (1), pp.79–87.

Wade, D., Silberring, J., Soliymani, R., Heikkinen, S., Kilpelainen, I., Lankinen, H. & Kuusela, P. (2000) Antibacterial activities of temporin A analogs. *Febs Letters*, 479 (1-2), pp.6–9.

Wakiec, R., Gabriel, I., Prasad, R., Becker, J.M., Payne, J.W. & Milewski, S. (2008) Enhanced susceptibility to antifungal oligopeptides in yeast strains overexpressing ABC multidrug efflux pumps. *Antimicrobial agents and chemotherapy*, 52 (11), pp.4057–63.

Wang, G. & Li, X. (2004) {1VM5:} Solution structure of micelle-bound aurein 1.2, an antimicrobial and anticancer peptide from an Australian frog. *Protein Data Bank*.

Wang, G., Li, X. & Wang, Z. (2009) APD2: the updated antimicrobial peptide database and its application in peptide design. *Nucleic acids research*, 37 (Database issue), pp.D933–7.

Wang, M., Wang, Y., Wang, A., Song, Y., Ma, D., Yang, H., Ma, Y. & Lai, R. (2010) Five novel antimicrobial peptides from skin secretions of the frog, Amolops loloensis. *Comparative biochemistry and physiology. Part B, Biochemistry & molecular biology*, 155 (1), pp.72–6.

Wang, Y. & Tajkhorshid, E. (2007) Molecular mechanisms of conduction and selectivity in aquaporin water channels. *The Journal of nutrition*, 137 (6 Suppl 1), p.1509S–1515S; discussion 1516S–1517S.

Wang, Y. & Tajkhorshid, E. (2010) Nitric oxide conduction by the brain aquaporin AQP4. *Proteins*, 78 (3), pp.661–70.

Wegener, K.L., Carver, J.A. & Bowie, J.H. (2003) The solution structures and activity of caerin 1.1 and caerin 1.4 in aqueous trifluoroethanol and dodecylphosphocholine micelles. *Biopolymers*, 69 (1), pp.42–59.

Wegener, K.L., Wabnitz, P.A., Carver, J.A., Bowie, J.H., Chia, B.C.S., Wallace, J.C. & Tyler, M.J. (1999) Host defence peptides from the skin glands of the Australian Blue Mountains tree-frog Litoria citropa. *European Journal of …*, 265 (2), pp.627–637.

Westerhoff, H. (1989) Magainins and the disruption of membrane-linked free-energy transduction. *Proceedings of the …*, 86 (17), pp.6597–6601.

Williams, A.B., Nguyen, B., Li, L., Brown, P., Levis, M., Leahy, D. & Small, D. (2013) Mutations of FLT3/ITD confer resistance to multiple tyrosine kinase inhibitors. *Leukemia*, 27 (1), pp.48–55.

Won, H., Kim, S., Jung, S. & Son, W. (2004) Structure-activity relationships of antimicrobial peptides from the skin of Rana esculenta inhabiting in Korea. *Molecules and ...*, 17 (3), pp.469–476.

Won, H.-S., Jung, S.-J., Kim, H.E., Seo, M.-D. & Lee, B.-J. (2004) Systematic peptide engineering and structural characterization to search for the shortest antimicrobial peptide analogue of gaegurin 5. *The Journal of biological chemistry*, 279 (15), pp.14784–91.

Wong, H., Bowie, J.H. & Carver, J.A. (1997) The solution structure and activity of caerin 1.1, an antimicrobial peptide from the Australian green tree frog, Litoria splendida. *European journal of biochemistry / FEBS*, 247 (2), pp.545–57.

Xie, Y.-G., Luan, C., Zhang, H.-W., Han, F.-F., Feng, J., Choi, Y.-J., Groleau, D. & Wang, Y.-Z. (2013) Effects of Thioredoxin: SUMO and Intein on Soluble Fusion Expression of an Antimicrobial Peptide OG2 in Escherichia coli. *Protein and Peptide Letters*, 20 (1), pp.54–60.

Xu, X., Jin, F., Yu, X., Ji, S., Wang, J., Cheng, H., Wang, C. & Zhang, W. (2007) Expression and purification of a recombinant antibacterial peptide, cecropin, from Escherichia coli. *Protein expression and purification*, 53 (2), pp.293–301.

Yedavalli, P. & Madhusudhana Rao, N. (2013) Engineering the loops in a lipase for stability in DMSO. *Protein engineering, design & selection : PEDS*, 26 (4), pp.317–24.

Yeh, I.-C. & Hummer, G. (2002) Peptide loop-closure kinetics from microsecond molecular dynamics simulations in explicit solvent. *Journal of the American Chemical Society*, 124 (23), pp.6563–8.

Yu, F., Wang, J., Zhang, P., Hong, Y. & Liu, W. (2010) Fusion expression of cecropin B-like antibacterial peptide in Escherichia coli and preparation of its antiserum. *Biotechnology letters*, 32 (5), pp.669–73.

Zahid, O.K., Mechkarska, M., Ojo, O.O., Abdel-Wahab, Y.H. a, Flatt, P.R., Meetani, M.A. & Conlon, J.M. (2011) Caerulein-and xenopsin-related peptides with insulin-releasing activities from skin secretions of the clawed frogs, Xenopus borealis and Xenopus amieti (Pipidae). *General and Comparative Endocrinology*, 172 (2), pp.314–320.

Zasloff, M. (1987) Magainins, a class of antimicrobial peptides from Xenopus skin: isolation, characterization of two active forms, and partial cDNA sequence of a precursor. *Proceedings of the National Academy of ...*, 84 (15), pp.5449–5453.

Zhou, Q., Li, M. & Li, C. (2009) Cloning and expression of a novel insulin-releasing peptide, brevinin-2GU from Escherichia coli. *Journal of Bioscience and Bioengineering*, 107 (4), pp.460–463.

Zhou, Y.X., Cao, W., Luo, Q.P., Ma, Y.S., Wang, J.Z. & Wei, D.Z. (2005) Production and purification of a novel antibiotic peptide, adenoregulin, from a recombinant Escherichia coli. *Biotechnology Letters*, 27 (10), pp.725–730.

Appendix A: Expression constructs

pMAL-c5x expression construct

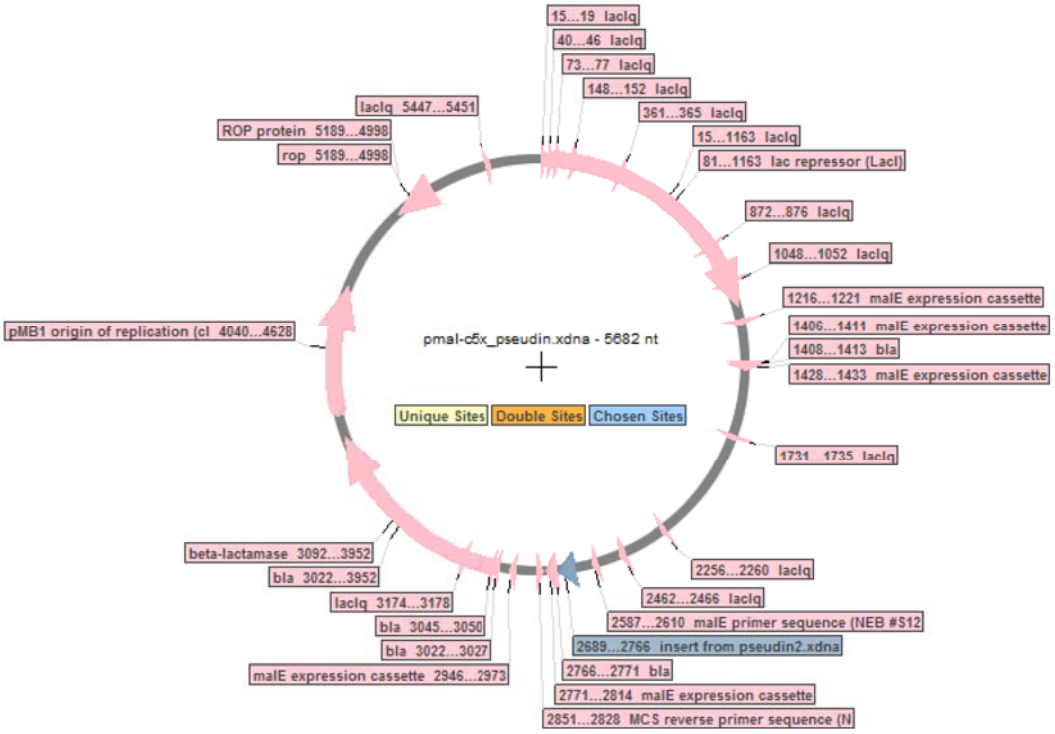

pMAL-p5x pseudin-2 expression construct

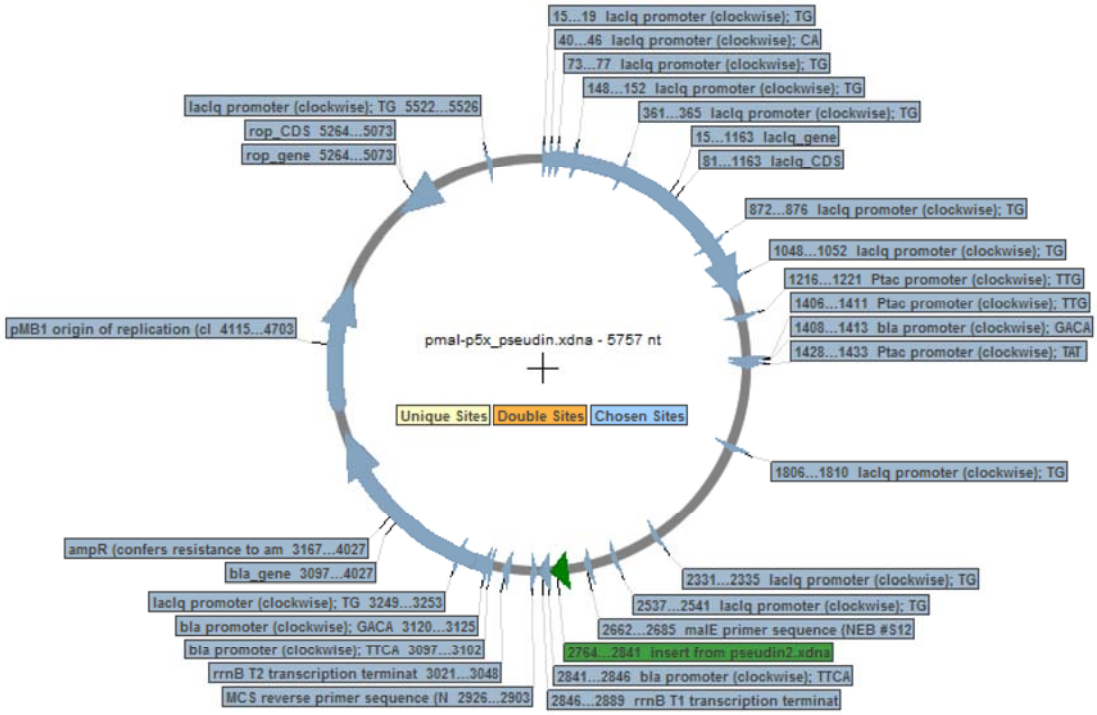

pET45b pseudin-2 expression construct

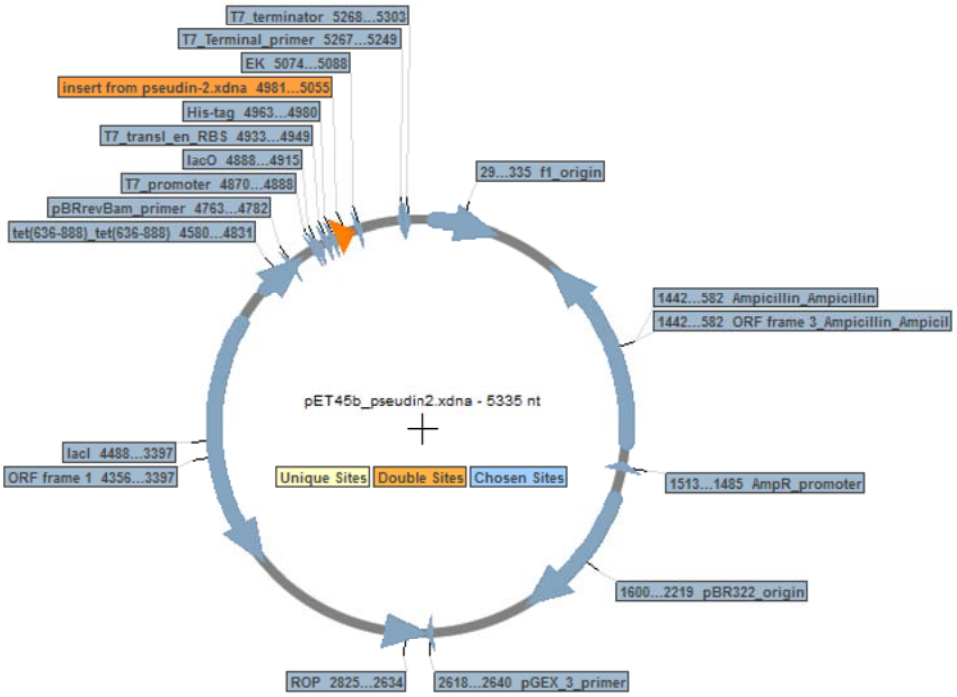

Appendix B: Protein and DNA Ladders

Massruler DNA Ladder, Low Range

Thermo Scientific, SM0383

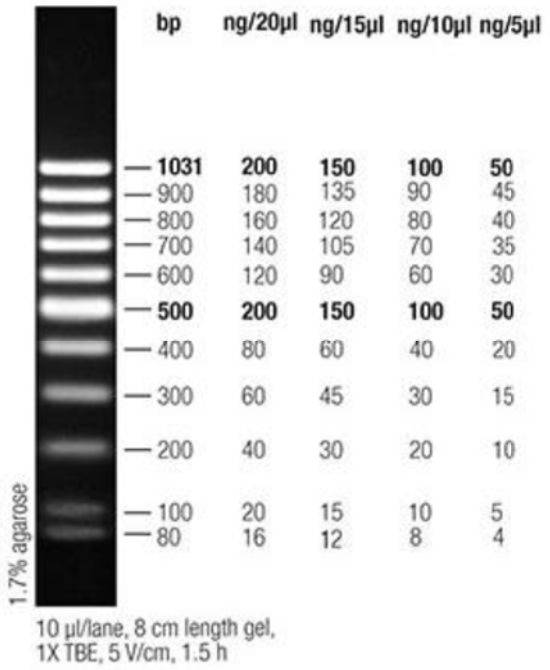

Massruler DNA Ladder, High Range

Thermo Scientific, SM0393

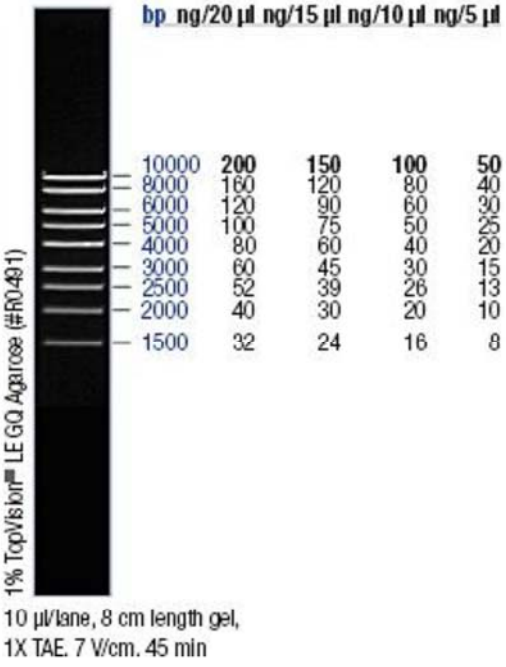

Spectra LR protein ladder

Thermo Scientific, 26628

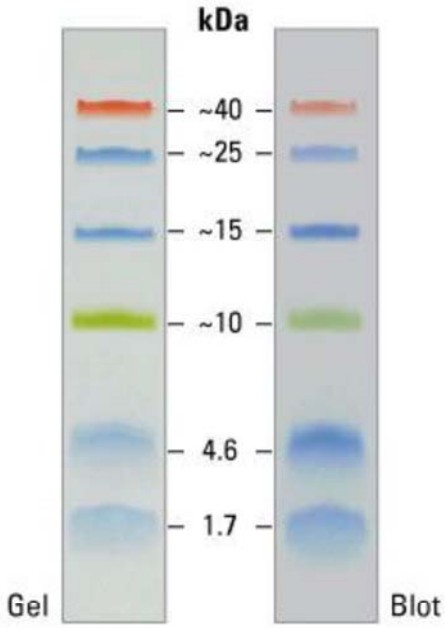

Pageruler prestained protein ladder

Thermo Scientific, 26619

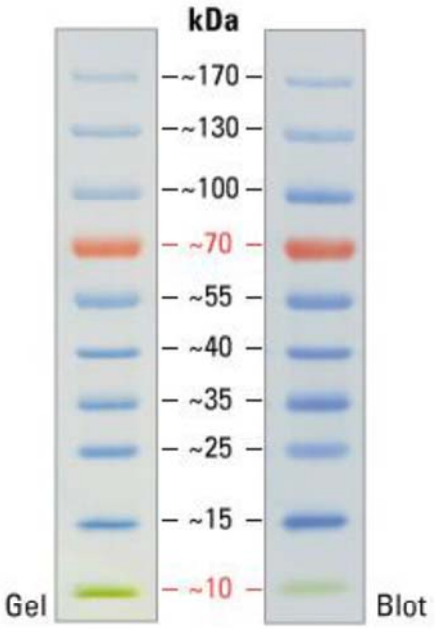

Appendix C: Sequence data of crude peptides

Peptide code	Sequence	C-terminus
M2612-A 1	GLNALKKVFCGIHTAIKHINNHVQ	2653
M2612-A 2	GLNALKKVFYGIHKAIKIINNHVQ	2716
M2612-A 3	GLNALKKVFWGIHVAIKDINNHVQ	2712
M2612-A 4	GLNALKKVFSGIHGAIKMINNHVQ	2587
M2612-A 5	GLNALKKVFWGIHGAIKSINNHVQ	2642
M2612-A 6	GLNALKKVFHGIHRAIKVINNHVQ	2704
M2612-A 7	GLNALKKVFKGIHTAIKNINNHVQ	2655
M2612-A 8	GLNALKKVFSGIHGAIKIINNHVQ	2569
M2612-A 9	GLNALKKVFTGIHRAIKIINNHVQ	2682
M2612-A10	GLNALKKVFFGIHGAIKAINNHVQ	2587
M2612-A11	GLNALKKVFNGIHPAIKLINNHVQ	2636
M2612-A12	GLNALKKVFFGIHPAIKIINNHVQ	2669
M2612-B 1	GLNALKKVFTGIHWAIKPINNHVQ	2696
M2612-B 2	GLNALKKVFTGIHVAIKAINNHVQ	2583
M2612-B 3	GLNALKKVFTGIHSAIKAINNHVQ	2571
M2612-B 4	GLNALKKVFSGIHNAIKVINNHVQ	2612
M2612-B 5	GLNALKKVFNGIHQAIKIINNHVQ	2667
M2612-B 6	GLNALKKVFQGIHTAIKLINNHVQ	2654
M2612-B 7	GLNALKKVFNGIHQAIKFINNHVQ	2701
M2612-B 8	GLNALKKVFSGIHSAIKWINNHVQ	2672
M2612-B 9	GLNALKKVFTGIHNAIKFINNHVQ	2674
M2612-B10	GLNALKKVFQGIHTAIKFINNHVQ	2688
M2612-B11	GLNALKKVFTGIHQAIKIINNHVQ	2654
M2612-B12	GLNALKKVFSGIHNAIKAINNHVQ	2584
M2612-C 1	GLNALKKVFRGIHSAIKAINNHVQ	2626
M2612-C 2	GLNALKKVFHGIHQAIKLINNHVQ	2690
M2612-C 3	GLNALKKVFKGIHTAIKIINNHVQ	2654
M2612-C 4	GLNALKKVFRGIHNAIKVINNHVQ	2681
M2612-C 5	GLNALKKVFKGIHTAIKFINNHVQ	2688

Peptide code	Sequence	C-terminus
M2612-C 6	GLNALKKVFHGIHQAIKVINNHVQ	2676
M2612-C 7	GLNALKKVFHGIHSAIKWINNHVQ	2722
M2612-C 8	GLNALKKVFRGIHNAIKIINNHVQ	2695
M2612-C 9	GLNALKKVFKGIHTAIKAINNHVQ	2612
M2612-C10	GLNALKKVFKGIHSAIKFINNHVQ	2674
M2612-C11	GLNALKKVFDGIHSAIKAINNHVQ	2585
M2612-C12	GLNALKKVFEGIHNAIKVINNHVQ	2654
M2612-D 1	GLNALKKVFDGIHTAIKIINNHVQ	2641
M2612-D 2	GLNALKKVFEGIHQAIKLINNHVQ	2682
M2612-D 3	GLNALKKVFDGIHSAIKFINNHVQ	2661
M2612-D 4	GLNALKKVFRGIHRAIKAINNHVQ	2695
M2612-D 5	GLNALKKVFHGIHKAIKVINNHVQ	2676
M2612-D 6	GLNALKKVFKGIHRAIKIINNHVQ	2709
M2612-D 7	GLNALKKVFRGIHHAIKLINNHVQ	2718
M2612-D 8	GLNALKKVFKGIHHAIKFINNHVQ	2724

Appendix D: Sequence, mass spectroscopy and HPLC traces of purified peptides